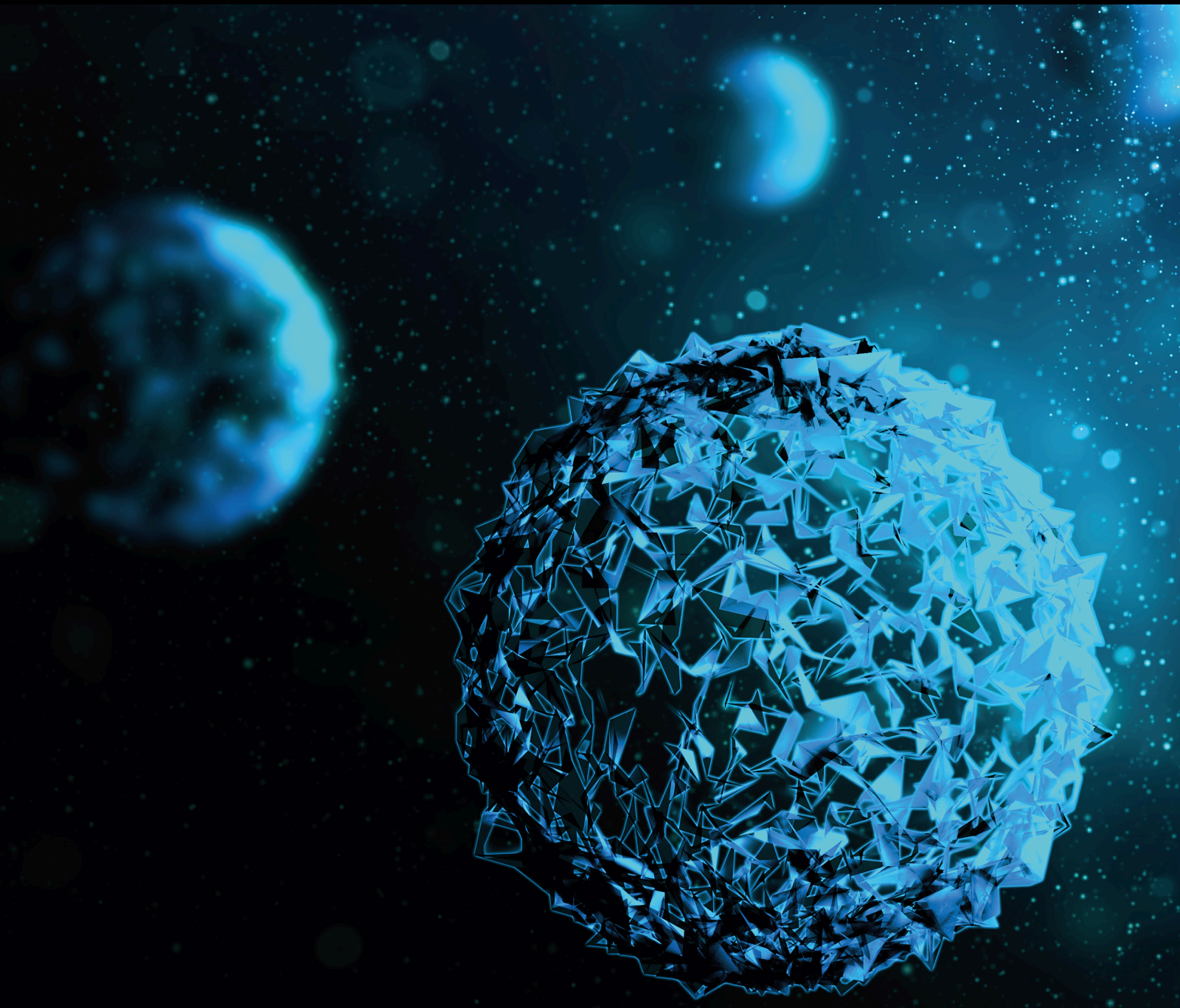


# Oxidative Stress and Cardiometabolic Disorders

Lead Guest Editor: Roland E. Akhigbe

Guest Editors: Ayodeji F. Ajayi and Ram K. Sahu





---

# **Oxidative Stress and Cardiometabolic Disorders**

BioMed Research International

---

## **Oxidative Stress and Cardiometabolic Disorders**

Lead Guest Editor: Roland E. Akhigbe

Guest Editors: Ayodeji F. Ajayi and Ram K. Sahu



---

Copyright © 2021 Hindawi Limited. All rights reserved.

This is a special issue published in "BioMed Research International." All articles are open access articles distributed under the Creative Commons Attribution License, which permits unrestricted use, distribution, and reproduction in any medium, provided the original work is properly cited.

## Editorial Board

Ahmed Abdel-Latif, USA  
Ramazan Akdemir, Turkey  
Pablo Avanzas, Spain  
Dirk Bandorski, Germany  
Andras Bikov, Hungary  
Raffaella Bloise, Italy  
Roberto Cangemi, Italy  
Nazario Carrabba, Italy  
Cheng-I Cheng, Taiwan  
Dragos Cretoiu, Romania  
Claudio de Lucia, Italy  
Gianluca Di Bella, Italy  
Nicola Gaibazzi, Italy  
Nicola Galea, Italy  
Natig Gassanov, Germany  
Inna Gladysheva, USA  
Michael Gotzmann, Germany  
Ernesto Greco, Italy  
Andrea I. Guaricci, Italy  
Marco Guglielmo, Italy  
Miklos Illyes, Hungary  
Ruxandra Jurcut, Romania  
Christof Kolb, Germany  
Mitja Lainscak, Slovenia  
Tong Liu, China  
Ping-Yen Liu, Taiwan  
Claudia Loardi, Italy  
Zaid H. Maayah, Canada  
Shinro Matsuo, Japan  
Rocco Antonio Montone, United Kingdom  
Giuseppe Muscogiuri, Italy  
Francesco Nappi, France  
Ionut Nistor, Romania, Romania  
David Platts, Australia  
Raffaella Rastaldo, Italy  
Vincenzo Russo, Italy  
Matthias Thielmann, Germany  
Kimimasa Tobita, USA  
Jörn Tongers, Germany  
Kazunori Uemura, Japan  
Gurpreet S. Wander, India  
Suowen Xu, USA

Utako Yokoyama, Japan  
Xinhua Yu, USA  
Jose L. Zamorano, Spain

## Contents




### **Oxidative Stress and Cardiometabolic Disorders**

Roland E. Akhigbe , Ayodeji F. Ajayi , and Sahu K. Ram  
Editorial (3 pages), Article ID 9872109, Volume 2021 (2021)

### **Orosomucoid 1 Attenuates Doxorubicin-Induced Oxidative Stress and Apoptosis in Cardiomyocytes via Nrf2 Signaling**

Xiaoli Cheng, Dan Liu, Ruinan Xing, Haixu Song, Xiaoxiang Tian, Chenghui Yan, and Yaling Han   
Research Article (13 pages), Article ID 5923572, Volume 2020 (2020)






### **The Free Radical Scavenging and Anti-Isolated Human LDL Oxidation Activities of *Pluchea indica* (L.) Less. Tea Compared to Green Tea (*Camellia sinensis*)**

Kittipot Sirichaiwetchakoon , Gordon Matthew Lowe , and Griangsak Eumkeb   
Research Article (12 pages), Article ID 4183643, Volume 2020 (2020)



### **Role of Oxidation-Dependent CaMKII Activation in the Genesis of Abnormal Action Potentials in Atrial Cardiomyocytes: A Simulation Study**

Na Zhao , Qince Li , Haibo Sui , and Henggui Zhang   
Research Article (13 pages), Article ID 1597012, Volume 2020 (2020)



### **Qiliqiangxin Improves Cardiac Function through Regulating Energy Metabolism via HIF-1 $\alpha$ -Dependent and Independent Mechanisms in Heart Failure Rats after Acute Myocardial Infarction**

Yanyan Wang , Mingqiang Fu, Jingfeng Wang , Jingjing Zhang, Xueting Han, Yu Song, Yuyuan Fan, Kai Hu , Jingmin Zhou , and Junbo Ge   
Research Article (16 pages), Article ID 1276195, Volume 2020 (2020)

### ***Dracocephalum moldavica* L. Extracts Protect H9c2 Cardiomyocytes against H<sub>2</sub>O<sub>2</sub>-Induced Apoptosis and Oxidative Stress**

Min Jin, Hui Yu, Xia Jin, Lailai Yan, Jingyu Wang , and Zhanli Wang   
Research Article (12 pages), Article ID 8379358, Volume 2020 (2020)

### **Multimodal $\alpha$ -Glucosidase and $\alpha$ -Amylase Inhibition and Antioxidant Effect of the Aqueous and Methanol Extracts from the Trunk Bark of *Ceiba pentandra***

Telesphore Benoit Nguelefack , Christian Kuete Fofie, Elvine Pami Nguelefack-Mbuyo , and Adeline Kaptue Wuyt  
Research Article (13 pages), Article ID 3063674, Volume 2020 (2020)

## Editorial

# Oxidative Stress and Cardiometabolic Disorders

**Roland E. Akhigbe** <sup>1,2,3</sup>, **Ayodeji F. Ajayi** <sup>1</sup> and **Sahu K. Ram**<sup>4</sup>

<sup>1</sup>Reproductive Physiology and Bioinformatics Research Unit, Department of Physiology, College of Medicine, Ladoko Akintola University of Technology, Ogbomoso, Oyo State, Nigeria

<sup>2</sup>Reproductive Biology and Toxicology Research Laboratories, Oasis of Grace Hospital, Osogbo, Osun State, Nigeria

<sup>3</sup>Department of Chemical Sciences, Kings University, Ode Omu, Osun, Nigeria

<sup>4</sup>University College of Pharmacy, Naya Raipur (CG), India

Correspondence should be addressed to Roland E. Akhigbe; [akhigberoland@gmail.com](mailto:akhigberoland@gmail.com)

Received 28 July 2021; Accepted 28 July 2021; Published 5 November 2021

Copyright © 2021 Roland E. Akhigbe et al. This is an open access article distributed under the Creative Commons Attribution License, which permits unrestricted use, distribution, and reproduction in any medium, provided the original work is properly cited.

Cardiometabolic disorders (CMD) are a cluster of metabolic derangements that increases the susceptibility to insulin resistance and type II diabetes mellitus, systemic hypertension, central obesity, and dyslipidaemia [1, 2]. The rise in the prevalence of CMD is a global phenomenon involving developed nations and underdeveloped and developing countries, leading to a double burden of disease in the tropics. CMD is a multifactorial disorder caused by an intricate interaction between genetics and environmental factors, which lead to increased insulin resistance and circulatory free fatty acids (FFA), lipid and glucose dysmetabolism, and elevated levels of adipokines and cytokines [1, 3–7].

Studies have linked OS with incident CMD [8]. The observed dwindling antioxidant level in advanced age has been shown to reduce cardiometabolic tolerance [9]. This is accompanied by arterial thickening, atherosclerosis, vascular damage, and remodeling [10, 11]. These contribute to the development of CMD. In-depth knowledge of the impact of OS in the development of CMD will help to identify possible effective treatment modalities to improve cardiometabolic status.

The purpose of this special issue is to illuminate the effect of OS in the etiopathogenesis of CMD and open new management opportunities. This special issue, oxidative stress and cardiometabolic disorders, contains contributions from 34 reputable scientists from 17 different institutions across the globe.

The first article, “Orosomucoid 1 Attenuates Doxorubicin-Induced OS and Apoptosis in Cardiomyocytes via Nrf2 Signaling,” by X. Cheng et al. documents the rescue effect of orosomucoid 1 on doxorubicin-induced cardiotoxicity. The authors clearly demonstrated that orosomucoid 1, an acute-phase protein, attenuated inflammation and ischemic stroke in an animal model via upregulation of nuclear factor-like 2 (Nrf2) and suppression of heme oxygenase 1 (HO-1) [12]. In addition, there was a reversal of the impact of ORM1 on doxorubicin-induced OS and apoptosis in cardiac muscles when Nrf2 was silenced. Their study lends credence to the use of orosomucoid as a therapeutic strategy for doxorubicin-induced cardiotoxicity.

In the second article, “The Free Radical Scavenging and Anti-Isolated Human LDL Oxidation Activities of *Pluchea indica* (L.) Less. Tea Compared to Green Tea (*Camellia sinensis*),” K. Sirichaiwetchakoon et al. challenged isolated human low-density lipoproteins (LDL) with either 2,2'-azobis (2-amidinopropane) dihydrochloride (AAPH), copper, or 3-morpholinopyrrolidine hydrochloride (SIN-1) to induce LDL oxidation [13]. *Pluchea indica* (L.) Less. Tea (PIT) showed antioxidant potential in all test systems and its capacity to mop off peroxynitrite. PIT performed significantly better than the green tea, *Camellia sinensis* tea (CST), in DPPH and peroxynitrite scavenging assays. Although the antioxidant activities of flavonols and polyphenol catechins

in CST have reported earlier [14–17], the study of K. Sirichaiwetchakoon et al. opens a new opportunity for a novel nutraceutical.

N. Zhao et al., in the third article, “Role of Oxidation-Dependent CaMKII Activation in the Genesis of Abnormal Action Potentials in Atrial Cardiomyocytes: A Simulation Study,” probed the influence of oxidation-dependent  $\text{Ca}^{2+}$ -calmodulin-dependent protein kinase II (CaMKII) activation in the genesis of abnormal atrial action potentials (AP) [18]. Zhao and his colleagues explored the intrinsic pathophysiology of OS-induced arrhythmia in the atria. They observed that OS triggered early after depolarizations of AP by modifying the dynamics of transmembrane currents and intracellular calcium cycling. OS caused a rise in cytoplasmic calcium ions via enhancement of L-type  $\text{Ca}^{2+}$  current and calcium release by the sarcoplasmic reticulum. The resultant increases in intracellular calcium level, elevated  $\text{Na}^+/\text{Ca}^{2+}$  exchange current, and reduced repolarization of the action potential. This culminated in prolonged AP and consequent early after depolarizations.

The study in the fourth article “*Qiliqiangxin* Improves Cardiac Function through Regulating Energy Metabolism via HIF-1 $\alpha$ -Dependent and Independent Mechanisms in Heart Failure Rats after Acute Myocardial Infarction,” authored by Y. Wang et al. was designed to evaluate the influence of *Qiliqiangxin*, QL, on energy metabolism in experimental myocardial infarction and the role of hypoxia-inducible factor 1 $\alpha$  (HIF-1 $\alpha$ ) signaling [19]. Acute myocardial infarction (AMI) was established by ligating the left anterior descending coronary artery in adult male Sprague Dawley rats, and animals with an ejection fraction < 50% at two weeks postoperation were considered animals with heart failure. They randomized rats into sham, MI-induced, MI + QL, and MI + QL+2-MeOEt<sub>2</sub> groups. They found out that QL significantly improved cardiac function and myocardial capillary density, reduced serum NT-proBNP, and attenuated myocardial fibrosis. This was accompanied by enhanced glucose and free fatty acid uptake, glycolysis, and ATP production, as well as upregulation of the protein expression of vascular endothelial growth factor (VEGF), myocardial glucose oxidation enzyme expression, and CD 31 via regulation of HIF-1 $\alpha$ /VEGF signaling.

The fifth article, “*Dracocephalum moldavica* L. Extracts Protect H9c2 Cardiomyocytes against H<sub>2</sub>O<sub>2</sub>-Induced Apoptosis and OS,” evaluated the cardioprotective potential of *Dracocephalum moldavica* L., a phytomedicinal plant used in the management of cardiovascular diseases in China against H<sub>2</sub>O<sub>2</sub>-induced apoptosis and OS in H9c2 cells. M. Jin et al. pretreated H9c2 cells with *Dracocephalum moldavica* L. before challenging with H<sub>2</sub>O<sub>2</sub> [20]. *Dracocephalum moldavica* L. therapy was found to attenuate H<sub>2</sub>O<sub>2</sub>-induced decline in cell viability, SOD activity, and mitochondrial membrane potential. The phenol- and flavonoid-rich *Dracocephalum moldavica* L. also abrogated H<sub>2</sub>O<sub>2</sub>-induced elevations in ROS generation and concentrations of MDA and lactate dehydrogenase. *Dracocephalum moldavica* L. cardioprotective activities were revealed to be mediated through upregulation of the Bcl-2 expression and downregulation of the Bax and caspase 3 expression.

In the sixth article, “Multimodal  $\alpha$ -Glucosidase and  $\alpha$ -Amylase Inhibition and Antioxidant Effect of the Aqueous and Methanol Extracts from the Trunk Bark of *Ceiba pentandra*,” T.B. Nguelefack et al. explored the postprandial modulatory activities and antioxidant potentials of *Ceiba pentandra* aqueous and methanolic stem bark extracts [21]. They demonstrated that the phenol- and flavonoid-rich extracts of *Ceiba pentandra* significantly reduced postprandial hyperglycemia by inhibiting protein oxidation,  $\alpha$ -amylase, and  $\alpha$ -glucosidase through scavenging reactive oxygen species. These findings are extensions of their previous studies that revealed that *Ceiba pentandra* promotes glucose utilization and reduces hepatic glucose release [22], upregulates glycogen synthesis, and impairs gluconeogenesis [23], inhibits lipid peroxidation and shows antioxidant activity against DPPH and hydroxyl radical [22], and demonstrated antidiabetic properties in dexamethasone-treated rats [24] and high-fat diet/streptozotocin-treated rats [25].

We hope our readers will find these articles interesting and stimulating. The articles and recommendations of the contributing experts will hopefully spur further discussion and expand research in these biomedical areas.

## Conflicts of Interest

The authors declare that there are no competing interests.

Roland E. Akhigbe  
Ayodeji F. Ajayi  
Sahu K. Ram

## References

- [1] S. M. Grundy, J. I. Cleeman, S. R. Daniels et al., “Diagnosis and management of the metabolic syndrome: an American Heart Association/National Heart, Lung, and Blood Institute Scientific Statement,” *Circulation*, vol. 112, no. 17, pp. 2735–2752, 2005.
- [2] R. Akhigbe and A. Ajayi, “The impact of reactive oxygen species in the development of cardiometabolic disorders: a review,” *Lipids in Health and Disease*, vol. 20, no. 1, p. 23, 2021.
- [3] K. Esposito, F. Giugliano, E. Martedì et al., “High proportions of erectile dysfunction in men with the metabolic syndrome,” *Diabetes Care*, vol. 28, no. 5, pp. 1201–1203, 2005.
- [4] R. E. Akhigbe, L. O. Ajayi, and A. F. Ajayi, “Codeine exerts cardiorenal injury via upregulation of adenine deaminase/xanthine oxidase and caspase 3 signaling,” *Life Sciences*, vol. 273, p. 118717, 2021.
- [5] N. Méndez-Sánchez, N. C. Chavez-Tapia, D. Motola-Kuba et al., “Metabolic syndrome as a risk factor for gallstone disease,” *World Journal of Gastroenterology*, vol. 11, no. 11, pp. 1653–1657, 2005.
- [6] A. F. Ajayi, R. E. Akhigbe, and L. O. Ajayi, “Activation of cardiac TNF- $\alpha$  in altered thyroid state-induced cardiometabolic disorder,” *Journal of Cardiovascular Disease Research*, vol. 8, no. 4, pp. 151–156, 2017.
- [7] S. F. Ige and R. E. Akhigbe, “Common onion (*Allium cepa*) extract reverses cadmium-induced organ toxicity and dyslipidaemia via redox alteration in rats,” *Pathophysiology*, vol. 20, no. 4, pp. 269–274, 2013.



- [8] M. A. Hamed, G. O. Aremu, and R. E. Akhigbe, "Concomitant administration of HAART aggravates anti-Koch-induced oxidative hepatorenal damage via dysregulation of glutathione and elevation of uric acid production," *Biomedicine and Pharmacotherapy*, vol. 137, p. 111309, 2021.
- [9] P. Abete, C. Napoli, G. Santoro et al., "Age-related decrease in cardiac tolerance to oxidative stress," *Journal of Molecular and Cellular Cardiology*, vol. 31, no. 1, pp. 227–236, 1999.
- [10] T. E. Brinkley, B. J. Nicklas, A. M. Kanaya et al., "Plasma oxidized low-density lipoprotein levels and arterial stiffness in older adults," *Hypertension*, vol. 53, no. 5, pp. 846–852, 2009.
- [11] D. Gradinaru, C. Borsa, C. Ionescu, and G. I. Prada, "Oxidized LDL and NO synthesis—biomarkers of endothelial dysfunction and ageing," *Mechanisms of Ageing and Development*, vol. 151, pp. 101–113, 2015.
- [12] X. Cheng, D. Liu, R. Xing et al., "Orosomucoid 1 Attenuates Doxorubicin-Induced Oxidative Stress and Apoptosis in Cardiomyocytes via Nrf2 Signaling," *BioMed Research International*, vol. 2020, Article ID 5923572, 13 pages, 2020.
- [13] K. Sirichaiwetchakoon, G. M. Lowe, and G. Eumkeb, "The free radical scavenging and anti-isolated human LDL oxidation activities of *Pluchea indica* (L.) Less. Tea compared to green tea (*Camellia sinensis*)," *BioMed Research International*, vol. 2020, Article ID 4183643, 12 pages, 2020.
- [14] L. K. Leung, Y. Su, R. Chen, Z. Zhang, Y. Huang, and Z. Y. Chen, "Theaflavins in black tea and catechins in green tea are equally effective antioxidants," *The Journal of Nutrition*, vol. 131, no. 9, pp. 2248–2251, 2001.
- [15] C. Folch-Cano, C. Jullian, H. Speisky, and C. Olea-Azar, "Antioxidant activity of inclusion complexes of tea catechins with  $\beta$ -cyclodextrins by ORAC assays," *Food Research International*, vol. 43, no. 8, pp. 2039–2044, 2010.
- [16] K. Yamagata, "Protective effect of epigallocatechin gallate on endothelial disorders in atherosclerosis," *Journal of Cardiovascular Pharmacology*, vol. 75, no. 4, pp. 292–298, 2020.
- [17] S. Kongkiatpaiboon, S. Chewchinda, and B. Vongsak, "Optimization of extraction method and HPLC analysis of six caffeoylquinic acids in *Pluchea indica* leaves from different provenances in Thailand," *Revista Brasileira de Farmacognosia*, vol. 28, no. 2, pp. 145–150, 2018.
- [18] N. Zhao, Q. Li, H. Sui, and H. Zhang, "Role of oxidation-dependent CaMKII activation in the genesis of abnormal action potentials in atrial cardiomyocytes: a simulation study," *BioMed Research International*, vol. 2020, Article ID 1597012, 13 pages, 2020.
- [19] Y. Wang, M. Fu, J. Wang et al., "Qiliqiangxin improves cardiac function through regulating energy metabolism via HIF-1 $\alpha$ -dependent and independent mechanisms in heart failure rats after acute myocardial infarction," *BioMed Research International*, vol. 2020, Article ID 1276195, 16 pages, 2020.
- [20] M. Jin, H. Yu, X. Jin, L. Yan, J. Wang, and Z. Wang, "Dracocephalum moldavica L. Extracts Protect H9c2 Cardiomyocytes against H<sub>2</sub>O<sub>2</sub>-Induced Apoptosis and Oxidative Stress," *BioMed Research International*, vol. 2020, Article ID 8379358, 12 pages, 2020.
- [21] T. B. Nguefack, C. K. Fofie, E. P. Nguefack-Mbuyo, and A. K. Wuyt, "Multimodal  $\alpha$ -glucosidase and  $\alpha$ -amylase inhibition and antioxidant effect of the aqueous and methanol extracts from the trunk bark of *Ceiba pentandra*," *BioMed Research International*, vol. 2020, Article ID 3063674, 13 pages, 2020.
- [22] C. K. Fofie, S. L. Wansi, E. P. Nguefack-Mbuyo et al., "In vitro anti-hyperglycemic and antioxidant properties of extracts from the stem bark of *Ceiba pentandra*," *Journal of Complementary and Integrative Medicine*, vol. 11, no. 3, pp. 185–193, 2014.
- [23] K. S. Fofie, K. S. Nguefack-mbuyo et al., "Insulin sensitizing effect as possible mechanism of the antidiabetic properties of the methanol and the aqueous extracts from the trunk bark of *Ceiba pentandra*," *Diabetes Updates*, vol. 5, no. 1, 2018.
- [24] C. K. Fofie, E. P. Nguefack-Mbuyo, N. Tsabang, A. Kamanyi, and T. B. Nguefack, "Hypoglycemic properties of the aqueous extract from the stem bark of *Ceiba pentandra* in dexamethasone-induced insulin resistant rats," *Evidence-based Complementary and Alternative Medicine*, vol. 2018, Article ID 4234981, 11 pages, 2018.
- [25] C. K. Fofie, S. Katekhaye, S. Borse et al., "Antidiabetic properties of aqueous and methanol extracts from the trunk bark of *Ceiba pentandra* type 2 diabetic rat," *Cell Biochemistry*, vol. 120, no. 7, pp. 11573–11581, 2019.

## Research Article

# Orosomucoid 1 Attenuates Doxorubicin-Induced Oxidative Stress and Apoptosis in Cardiomyocytes via Nrf2 Signaling

Xiaoli Cheng,<sup>1</sup> Dan Liu,<sup>2</sup> Ruinan Xing,<sup>2</sup> Haixu Song,<sup>2</sup> Xiaoxiang Tian,<sup>2</sup> Chenghui Yan,<sup>2</sup> and Yaling Han <sup>1</sup>

<sup>1</sup>Department of Cardiology, Shengjing Hospital of China Medical University, Shenyang, Liaoning Province 110004, China

<sup>2</sup>Department of Cardiology and Cardiovascular Research Institute of PLA, General Hospital of Northern Theater Command, Shenyang, Liaoning Province 110016, China

Correspondence should be addressed to Yaling Han; [yaling.han1953@gmail.com](mailto:yaling.han1953@gmail.com)

Received 16 June 2020; Revised 22 August 2020; Accepted 8 October 2020; Published 19 October 2020

Academic Editor: Roland E. Akhigbe

Copyright © 2020 Xiaoli Cheng et al. This is an open access article distributed under the Creative Commons Attribution License, which permits unrestricted use, distribution, and reproduction in any medium, provided the original work is properly cited.

Doxorubicin (DOX) is an effective anticancer drug, but its therapeutic use is limited by its cardiotoxicity. The principal mechanisms of DOX-induced cardiotoxicity are oxidative stress and apoptosis in cardiomyocytes. Orosomucoid 1 (ORM1), an acute-phase protein, plays important roles in inflammation and ischemic stroke; however, the roles and mechanisms of ORM1 in DOX-induced cardiotoxicity remain unknown. Therefore, in the present study, we aimed to investigate the function of ORM1 in cardiomyocytes experiencing DOX-induced oxidative stress and apoptosis. A DOX-induced cardiotoxicity animal model was established in C57BL/6 mice by administering an intraperitoneal injection of DOX (20 mg/kg), and the control group was intraperitoneally injected with the same volume of sterilized saline. The effects were assessed after 7 d. Additionally, H9c2 cells were stimulated with DOX (10  $\mu$ M) for 24 h. The results showed decreased ORM1 and increased oxidative stress and apoptosis after DOX stimulation in vivo and in vitro. ORM1 overexpression significantly reduced DOX-induced oxidative stress and apoptosis in H9c2 cells. ORM1 significantly increased the expression of nuclear factor-like 2 (Nrf2) and its downstream protein heme oxygenase 1 (HO-1) and reduced the expression of the lipid peroxidation end product 4-hydroxynonenal (4-HNE) and the level of cleaved caspase-3. In addition, Nrf2 silencing reversed the effects of ORM1 on DOX-induced oxidative stress and apoptosis in cardiomyocytes. In conclusion, ORM1 inhibited DOX-induced oxidative stress and apoptosis in cardiomyocytes by regulating the Nrf2/HO-1 pathway, which might provide a new treatment strategy for DOX-induced cardiotoxicity.

## 1. Introduction

Heart failure is a prevalent disease worldwide, representing a severe manifestation and end stage of most heart diseases. The number of patients with heart failure in China has reached 1-2% of the total population. Heart failure not only significantly decreases the quality of life of patients and causes a substantial economic burden on patient families and society but is also associated with a high mortality rate. Over 50% of patients with chronic heart failure die within five years of diagnosis. Therefore, heart failure is also known as “the final battlefield of cardiovascular disease of the 21st century”.

The incidence rate of cancer is more than one-third worldwide, and cardiovascular disease is the two causes of

death in developed countries. Doxorubicin (DOX), a cardiotoxic anthracycline chemotherapy drug, was first isolated from *Streptomyces peucetius caesius* in 1967 [1, 2]. DOX plays an important role in the treatment of many cancers, as 32% of patients with breast cancer, 57-70% of elderly patients with lymphoma, and 50-60% of children with cancer have been treated with anthracycline drugs [3-6]. DOX has been included in the World Health Organization (WHO) model list of essential medicines, as a milestone of cancer therapy development and one of the most commonly used antitumor anthracycline antibiotics.

However, the cardiotoxic effects of DOX limit its use in cancer patients with irreversible degenerative cardiomyopathy and heart failure. More than half of the elderly patients and children who survive lymphoma and other cancers,

respectively, show a high risk of cardiotoxicity after DOX treatment [7]. Therefore, it is essential to study DOX-induced myocardial injury to increase survival rates and improve the quality of life of patients. Numerous studies have shown that oxidative stress and apoptosis are important mechanisms of DOX-induced myocardial injury [8, 9]. Therefore, an effective antioxidant and antiapoptotic agent that improves DOX-induced myocardial injury is urgently needed.

Orosomucoid 1 (ORM1) is an acute-phase protein that was first discovered by Tokita and Schmid more than 100 years ago. It is mainly synthesized in the liver, but many extrahepatic tissues have also been reported to produce ORM1 under various conditions [10, 11]. ORM1 performs various activities, acting as an acute-phase reactant and disease marker, regulating immunity, maintaining the capillary barrier function, regulating sphingomyelin metabolism, and scavenging reactive oxygen species (ROS) [12–14]. However, the current understanding of ORM1 is limited [15, 16], and its role in cardiovascular disease is not clear.

Nuclear factor-like 2 (Nrf2) is an important member of the cap collar family of basic leucine zipper transcription factors; it plays a role in the antioxidant defense system by regulating the expression of antioxidant enzymes [17, 18]. During conditions of oxidative stress, Nrf2 is activated, translocated to the nuclear region, and combined with the antioxidant response element located in the promoter region of phase II antioxidant enzyme genes, such as heme oxygenase 1 (*HO-1*). It results in the detoxification of 4-hydroxynonenal (4-HNE) and a decrease in ROS level, which releases the level of apoptosis [19, 20]. In previous studies, it was found that DOX decreases the expression of Nrf2, resulting in an increase in oxidative stress and cell apoptosis [21]. However, it is not clear whether ORM1 plays a protective role during oxidative stress and cell apoptosis by regulating Nrf2.

In our study, we aimed to investigate the potential relationship between ORM1 and Nrf2 and clarify the roles of ORM1 in the oxidative stress and cell apoptosis resulting from DOX-induced cardiomyocyte toxicity.

## 2. Materials and Methods

**2.1. Animals and In Vivo Experimental Design.** Eight-week-old male C57BL/6J mice were acquired from Southern Animal Model Co., Ltd. (Nanjing, China) and housed in a non-pathogenic animal facility at an ambient temperature of  $23 \pm 2^\circ\text{C}$  and on a 12 h dark/light cycle for 2 wk. DOX (Sigma, USA) was dissolved in sterilized saline to a final concentration of <2%. Forty mice were randomly divided into the following two groups with 20 mice in each group: control (saline) and DOX (20 mg/kg DOX). Mice in the DOX group were intraperitoneally injected with 10 mg/kg DOX on the first and fourth days, leading to a cumulative DOX dose of 20 mg/kg. Mice in the control group were intraperitoneally injected with the same volume of saline at the same times. These doses of DOX and sterilized saline were selected based on previous studies [22]. Seven days after the first DOX injection, all mice were euthanized. All animal experiments

complied with the “Guiding Principles for the Care of Experimental Animals” and “Guidelines for the Care and Use of Experimental Animals” (NIH publication 86-23, revised 1985). Animal care and procedures were approved by the Committee on the Care and Use of Laboratory Animals of the General Hospital of Northern Theater Command.

**2.2. Cell Culture, Transfection, and In Vitro Experimental Design.** The H9c2 cell line was purchased from the Chinese Academy of Sciences, Shanghai Institute for the Cell Resource Center and cultured in 5%  $\text{CO}_2$  at  $37^\circ\text{C}$ . Adenoviral vectors (Ad-control and Ad-ORM1) were purchased from Hanbio Biotechnology (China). Nrf2 siRNA and control siRNA were purchased from Thermo Scientific (USA). H9c2 cells were seeded onto 6-well plates ( $2 \times 10^5$  cells per well), and fetal bovine serum (FBS, USA) was added to 2 mL of normal culture medium without antibiotics. After the cells reached a confluence of 60-70%, they were transfected using Lipo iMAX (Thermo Scientific, USA) to control siRNA or target siRNA double strands (100 pM). After 48 h of transfection, the cells were collected for further experiments. DOX was dissolved in sterile saline.

Before the experiment, sterile saline was used as a control. In the preliminary in vitro experiment, the cells were divided into the following four groups: (1) control, (2) ORM1 (100 MOI) treated (ORM1), (3) DOX (10  $\mu\text{M}$ ) treated (DOX), and (4) DOX+ORM1 treated (DOX+ORM1). In the subsequent in vitro experiments, the cells were divided into the following groups: (1) control, (2) Nrf2 siRNA treated (Nrf2), (3) DOX treated (DOX), (4) DOX+Nrf2 siRNA treated, (5) DOX+ORM1 treated, and (6) DOX+ORM1+Nrf2 siRNA treated. After treatment, the cells were collected for further analyses.

**2.3. Echocardiography.** Seven days after the first DOX injection, the mice were anesthetized with 1.5% isoflurane to stabilize the heart rate at 400-500 bpm. The size and function of the hearts were measured by M-mode echocardiography using the ms-400 linear transducer echocardiography system (Visual Sonics Vevo 2100, Toronto, CA). All measurements are the average of five consecutive heartbeat cycles.

**2.4. Measurement of Plasma Levels of Lactate Dehydrogenase (LDH) and Creatine Kinase Isoenzyme (CKMB).** Blood samples were taken from mice in the control and DOX groups and poured into EDTA tubes to prevent clotting. Plasma was separated by centrifugation. LDH and CKMB levels in plasma were determined using the standard enzyme-linked immunosorbent assay (ELISA) kit (Roche, Switzerland) and presented in U/l. All procedures were performed according to the manufacturer’s instructions.

**2.5. Wheat Germ Agglutinin (WGA) Staining.** Hearts were collected from five mice in the control and DOX groups, respectively, and then fresh-frozen heart tissues were stained with WGA (Sigma, USA) according to the manufacturer’s instructions (200 cross-sectional areas per mouse). Fluorescence images were examined using a Zeiss Axio Imager 2 microscope (Zeiss, Germany).

**2.6. Terminal Deoxynucleotidyl Transferase dUTP Nick End Labeling (TUNEL) Assay.** Hearts were collected from five mice in the control and DOX groups, respectively. Frozen heart tissues were cut into 5  $\mu\text{m}$  thick sections, and H9c2 cells were cultured on cover glass. H9c2 cells were transfected with ORM1 virus, Nrf2 siRNA, or the corresponding control. After 48 h of transfection, cells were stimulated with DOX for 24 h and fixed with 4% paraformaldehyde. Apoptosis in myocardial tissues was analyzed using a TUNEL staining kit (Roche, Switzerland), and H9c2 cells were analyzed using a different TUNEL staining kit (Abcam, UK) according to the manufacturer's instructions. Fluorescence images were examined using a Zeiss Axio Imager 2 microscope (Zeiss, Germany).

**2.7. Liquid Chromatography-Tandem Mass Spectrometry (LC/MS).** The hearts were collected from mice in the control and DOX groups, and three mice from each group were sent to Bio Miao Biological and processed according to the corresponding procedure. The peptide mixtures in each group of samples were labeled with different isobaric tags for relative and absolute quantification (iTRAQ) reagents; equal amounts of the labeled peptides in each sample were prepared. Finally, LC/MS detection and analysis were performed.

**2.8. Immunohistochemical Staining.** Mouse hearts were fixed in 4% paraformaldehyde (pH 7.4) overnight, embedded in paraffin, and continuously sectioned at a thickness of 5  $\mu\text{m}$ . For dewaxing, sections were sealed with phosphate-buffered saline (PBS) containing 5% normal target serum and 1% bovine serum albumin (BSA) and then incubated overnight at 4°C under humidified conditions with anti-ORM1 (Abcam, UK), anti-Nrf2 (Abcam, UK), anti-HO-1 (Abcam, UK), anti-4-HNE (Abcam, UK), and anticlaved caspase-3 (Cell Signaling Technology, USA). A routine histological examination was performed using light microscopy. Images were examined with a Zeiss Axio Imager 2 microscope (Zeiss, Germany).

**2.9. Analysis of Cell Viability.** Cell survival rate was determined using the Cell Counting Kit-8 (CCK-8, Beyotime, China) according to the manufacturer's instructions. H9c2 cells ( $1 \times 10^4$ ) were seeded onto 96-well plates and subjected to the treatments described above. CCK-8 solution (10  $\mu\text{L}$ ) was added to 100  $\mu\text{L}$  of culture medium in each well and incubated for 2 h at 37°C, before the optical density (OD) was measured at 450 nm with a Thermo Multiskan FC microplate reader (Thermo, USA). Cell survival rates were expressed as the ratio of the OD value of the experimental well to that of the control well. Each treatment was performed six times. Cell survival rates were expressed as the ratio of the OD value of the experimental well to that of the control well.

**2.10. Malondialdehyde (MDA) Determination.** To analyze oxidative stress parameters, we examined the MDA content. H9c2 cells ( $1 \times 10^4$ ) were seeded onto 96-well plates and subjected to the treatments described above. Blood samples were collected from mice in the control and DOX groups.

We determined the MDA content using a commercially available MDA detection kit (Beyotime, China) according to the manufacturer's instructions.

**2.11. Dichlorodihydrofluorescein Diacetate (DCFH-DA) Assay.** The production of ROS was established using a DCFH-DA staining kit (Beyotime, China). H9c2 cells were seeded onto 96-well plates and subjected to the treatments described above, then incubated with 10  $\mu\text{M}$  DCFH-DA for 30 min in the dark at 37°C. Fluorescence intensities were immediately measured by spectrophotometry using a microplate reader; the excitation and emission wavelengths were 488 and 522 nm, respectively. The fluorescence intensity of the control group was set to 100%. The accumulation of ROS in H9c2 cells was analyzed by confocal microscopy (red staining), and the fluorescence intensity of DCFH-DA was quantified using the Image Pro Plus software (Media Cybernetics Inc., USA).

**2.12. Polymerase Chain Reaction (PCR) Analysis.** Trizol (Invitrogen, USA) was used to extract total RNA from heart tissues and cells, and the concentration and purity of RNA were determined by spectrophotometry. The PrimeScript RT Kit (Takara, Japan) was used to synthesize cDNA according to the manufacturer's instructions. Quantitative PCR was performed using the CFX96 Real-Time System (Bio-Rad) to detect differences in gene expression. Relative gene expression of each protein of interest was calculated using the  $2^{-\Delta\Delta\text{CT}}$  method and normalized to GAPDH expression. All reactions were performed in triplicate, and the specificity was monitored by melting curve analysis. The primers were purchased from RiboBio (China) (see S-Fig4 for the PCR primers used).

**2.13. Western Blot Analysis.** After collecting cells and heart samples from the different treatment groups and extracting proteins, the protein concentrations were determined using a bicinchoninic acid (BCA) protein assay (Thermo Scientific, USA). The samples from each group were separated by sodium dodecyl sulfate polyacrylamide gel electrophoresis (SDS-PAGE) and transferred to a polyvinylidene fluoride (PVDF) membrane. The membrane was blocked by incubation with 5% skimmed milk (containing 0.1% Tween-20) for 2 h at room temperature. After incubation, the membrane was further incubated with the primary antibodies anti-ORM1 (Abcam, UK), anti-Nrf2 (Abcam, UK), anti-HO-1 (Abcam, UK), anti-4-HNE (Abcam, UK), and anticlaved caspase-3 (Cell Signaling Technology, USA). Next, the membrane was washed in Tris-buffered saline Tween (TBST) and incubated with the corresponding secondary antibody (Abcam; at a dilution of 1 : 5000) for 2 h at room temperature. The Amersham Imager 680 (GE, USA) was used to detect the bands, and the signal was quantified.

**2.14. Statistical Analysis.** The data are expressed as the mean  $\pm$  standard error of the mean (SEM). Data were analyzed using the SPSS 19.0 statistical software (SPSS Inc., USA). Differences between two groups were calculated using the *t*-test, and one-way analysis of variance (ANOVA) with Tukey's post hoc test was used when comparing multiple

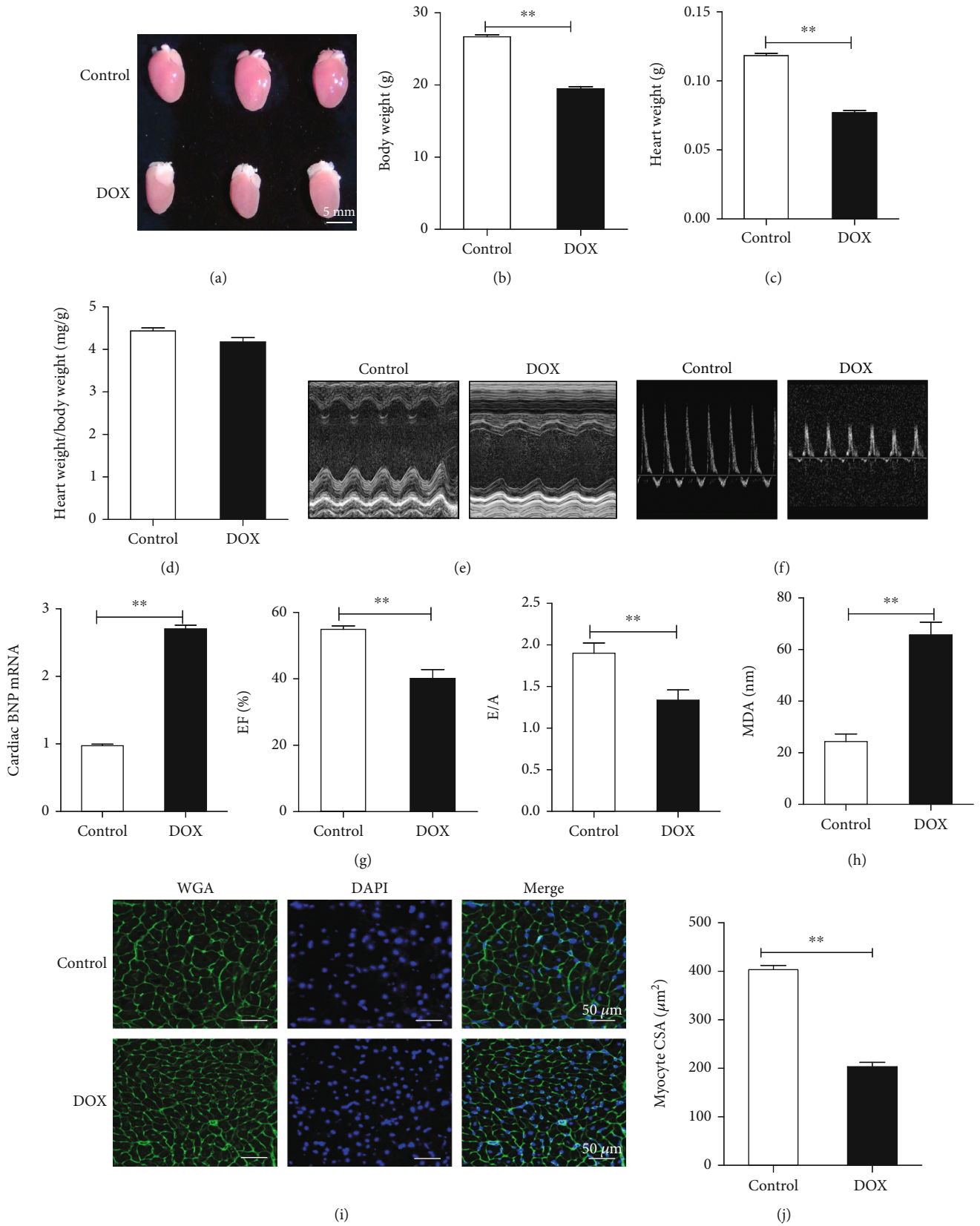


FIGURE 1: Continued.

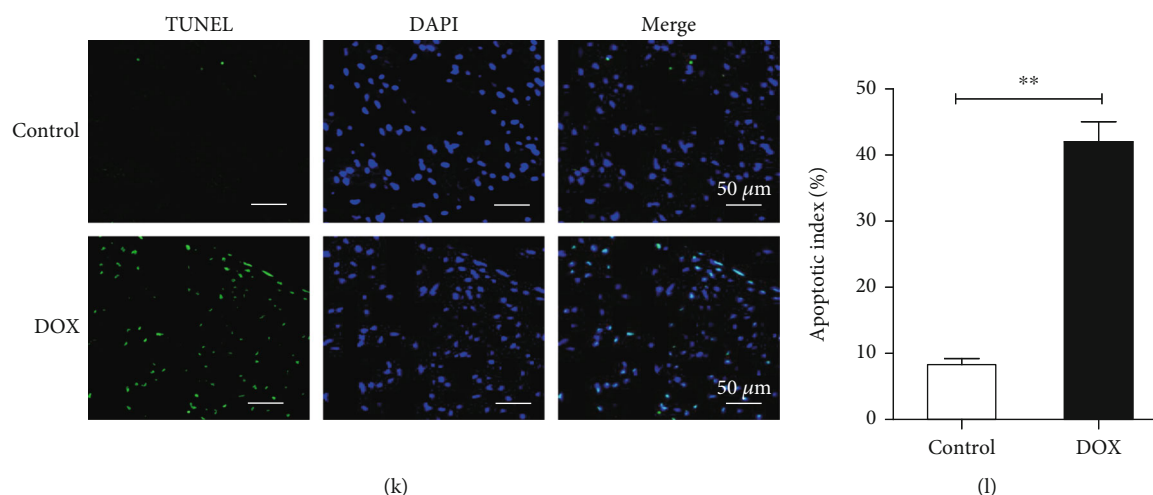


FIGURE 1: Effects of doxorubicin (DOX) on C57BL/6 mice. (a) General pictures of the heart. (b) Body weight. (c) Heart weight. (d) Heart weight/body weight. (e, f) Systolic and diastolic functions in both groups ( $n = 20$ ). (g) B-type natriuretic peptide (BNP) levels in mice detected using polymerase chain reaction (PCR) ( $n = 10$ ). (h) Malondialdehyde (MDA) levels in both groups ( $n = 10$ ). (i, j) Myocardial cell size evaluated using wheat germ agglutinin (WGA) staining ( $n = 5$ ). (k, l) Terminal deoxynucleotidyl transferase dUTP nick end labeling (TUNEL) staining ( $n = 5$ ). Data are expressed as the mean  $\pm$  standard error of the mean (SEM). \*\* $P < 0.01$ .

groups. Differences with a  $P$  value  $< 0.05$  were considered significant.

### 3. Results

**3.1. DOX Caused Cardiac Dysfunction and Heart Injury in C57BL/6 Mice.** All experimental mice were weighed to determine weight loss during each treatment. The results showed that the weight of DOX-treated mice was higher than that of the control group. After sacrificing, it was found that the hearts of DOX-treated mice were significantly atrophic, and the heart weight was significantly reduced compared to that of the normal group, indicating DOX-induced cardiac atrophy (Figures 1(a)–1(d)). DOX caused acute cardiac dysfunction in male mice, leading to a significant decrease in systolic and diastolic functions relative to those of the control group (Figures 1(e) and 1(f), Supplementary Figure 1a). To determine the levels of myocardial injury caused by DOX, we tested the serum LDH and CKMB levels and found that the difference was statistically significant between the DOX-treated and control groups (Supplementary Figure 1b-c). To evaluate cell damage induced by DOX, we measured the B-type natriuretic peptide (BNP) and A-type natriuretic peptide (ANP) levels 7 d after DOX administration and found that the mRNA levels of BNP and ANP were significantly increased in DOX-treated mice, indicating obvious heart failure (Figure 1(g), Supplementary Figure 1d).

According to previous studies, one of the main mechanisms of DOX-mediated myocardial injury is oxidative stress injury. Therefore, we examined the serum MDA levels in the mice and found that the level in the DOX group was significantly higher than that in the control group (Figure 1(h)). To evaluate the DOX-induced damage to cardiomyocytes, we stained murine heart sections with WGA and found that cardiomyocytes from DOX-treated mice were significantly

reduced, which is in accordance with the observed atrophy (Figures 1(i) and 1(j)). To evaluate the level of cardiomyocyte apoptosis, we conducted TUNEL staining of the myocardial tissues of the mice. The results showed that compared with the control group, the DOX group exhibited a significantly higher apoptosis index (Figures 1(k) and 1(l)).

**3.2. DOX Treatment Evoked the Downregulation of ORM1 and Upregulation of Oxidative Stress and Apoptosis in Murine Myocardial Tissue.** First, we collected the hearts from control and DOX-treated mice and performed LC/MS analysis. The heat map shows differentially expressed genes between the cardiac tissues of control and DOX-treated mice. Low expression is depicted in green, and high expression is depicted in red. We found that ORM1 levels were significantly decreased in DOX-treated mice (Figure 2(a)). We then examined the mRNA levels of ORM1, Nrf2, and HO-1 in vivo. Compared with those in the control group, the mRNA levels of ORM1, Nrf2, and HO-1 were significantly reduced in the DOX group (Figure 2(b)). The protein levels of ORM1, Nrf2, and HO-1 were also significantly reduced in the DOX group, which was consistent with the effect on the mRNA levels (Figures 2(c) and 2(d)). In addition, 4-HNE is the downstream molecule of HO-1, which can cause extensive oxidative damage and cell apoptosis, and cleaved caspase-3 is a marker of cell apoptosis. Therefore, we chose to examine 4-HNE and cleaved caspase-3 to evaluate the effects of DOX on the level of oxidative stress and cell apoptosis. Compared with those in the control group, the protein levels of 4-HNE and cleaved caspase-3 were significantly increased in the DOX group (Figures 2(c) and 2(d)). The results of immunohistochemical staining of the myocardia from DOX-treated and control mice confirmed the above findings (Figures 2(e) and 2(f)).

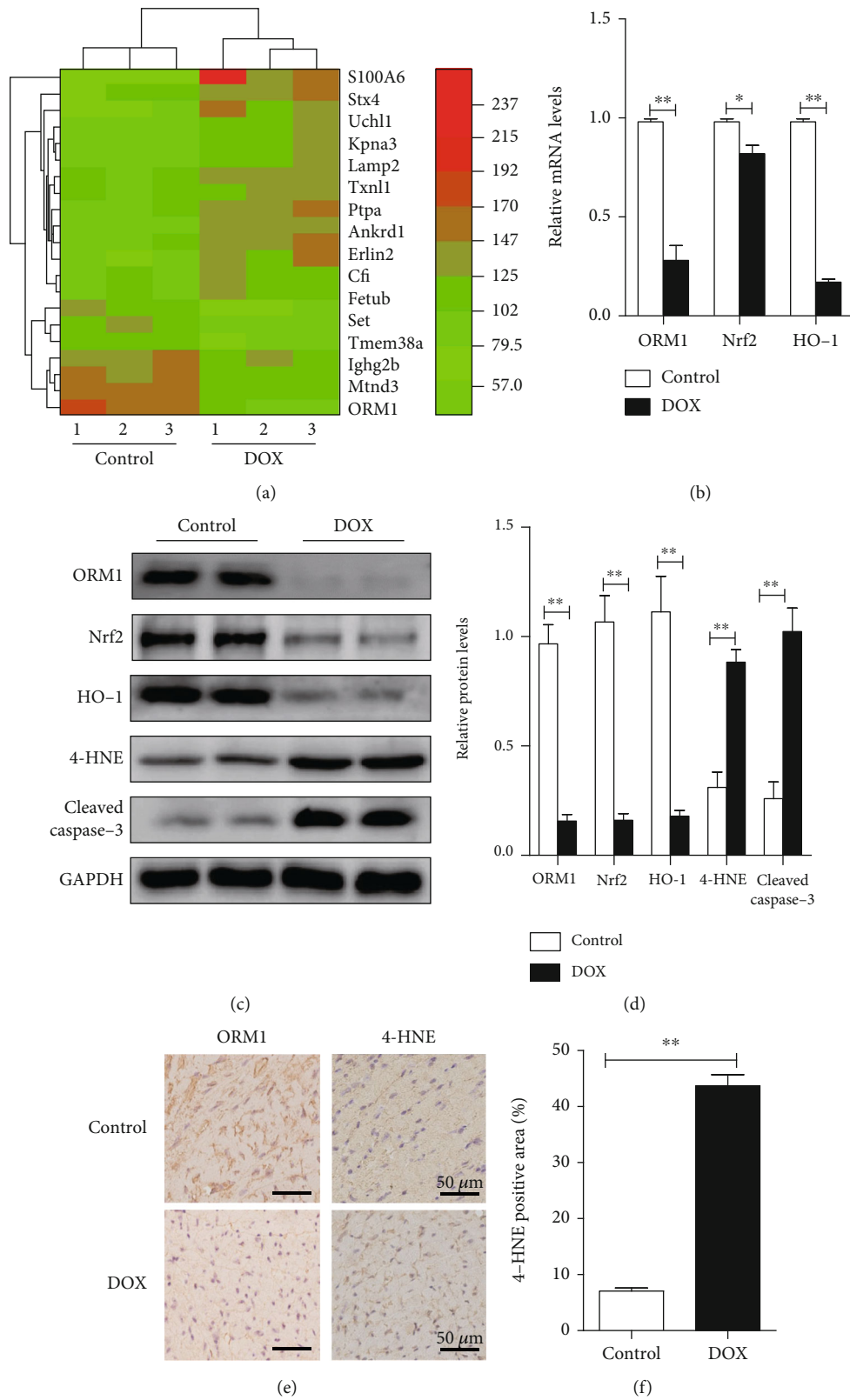


FIGURE 2: Continued.

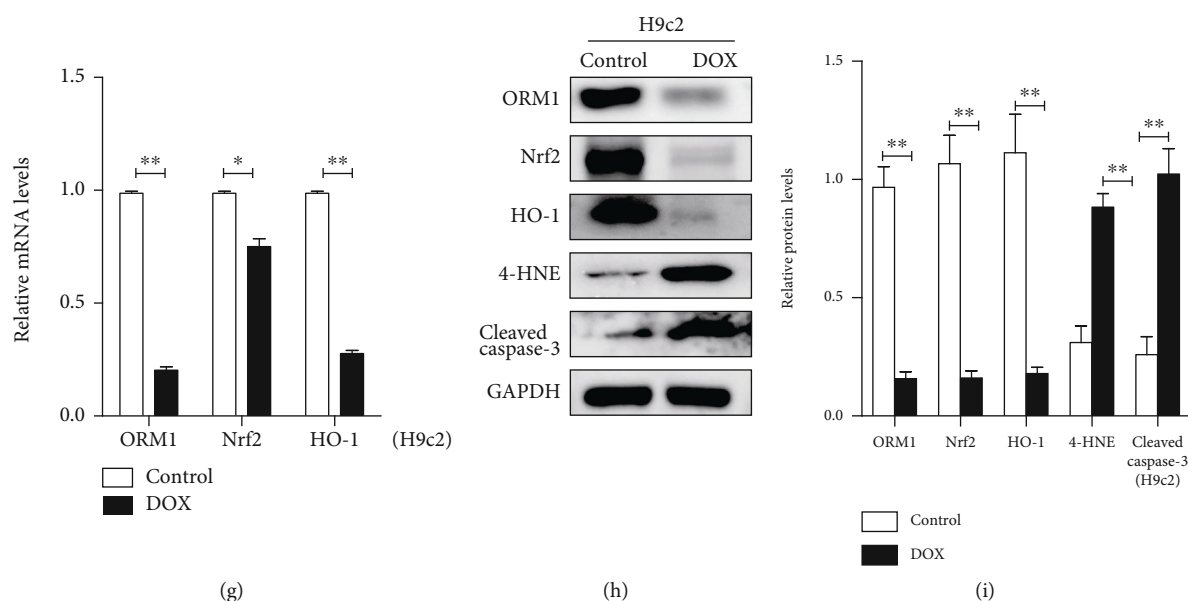


FIGURE 2: Downregulation of ORM1 and upregulation of oxidative stress and apoptosis in the DOX-induced cardiomyopathy model in vitro and in vivo. (a) Differentially expressed candidate proteins in control and DOX-treated mice analyzed using LC/MS technology. Low expression is depicted in green, and high expression is depicted in red. (b) mRNA levels of ORM1, Nrf2, and HO-1 in the hearts of mice in the DOX-treated groups ( $n = 6$ ). (c, d) Western blot analysis of ORM1, Nrf2, HO-1, 4-HNE, and cleaved caspase-3 ( $n = 6$ ). (e, f) Immunohistochemical staining images of ORM1- and 4-HNE-stained heart sections from control and DOX-treated mice ( $n = 6$ ). (g) mRNA levels of ORM1, Nrf2, and HO-1 in DOX-treated H9c2 cells ( $10 \mu\text{M}$  and 24 h) and the control group ( $n = 3$ ). (h, i) Western blot analysis of ORM1, Nrf2, HO-1, 4-HNE, and cleaved caspase-3 in DOX-treated H9c2 cells ( $10 \mu\text{M}$  and 24 h) and the control group ( $n = 3$ ). Data are expressed as the mean  $\pm$  standard error of the mean (SEM). \*\* $P < 0.01$  and \* $P < 0.05$ .

**3.3. DOX Treatment Produced the Downregulation of ORM1 and Upregulation of Oxidative Stress and Apoptosis in H9c2 Cells.** In H9c2 cells, different concentrations of DOX (0, 2, 5, and  $10 \mu\text{M}$ ) were used to examine the effect of DOX on cell viability. The results showed that DOX significantly reduced cell viability in a concentration-dependent manner; the effect was most obvious when the concentration was  $10 \mu\text{M}$  (Supplementary Figure 2). Therefore,  $10 \mu\text{M}$  DOX was used in subsequent experiments.

The mRNA and protein levels of ORM1, Nrf2, and HO-1 in H9c2 cells treated with DOX were significantly decreased (Figures 2(g)–2(i)). In addition, the levels of 4-HNE and cleaved caspase-3 were significantly increased in H9c2 cells after DOX stimulation (Figures 2(h) and 2(i)). These results were consistent with the in vivo results and indicated that decreased levels of ORM1 might play an important role in DOX-induced cardiotoxicity.

**3.4. ORM1 Reduced DOX-Induced Oxidative Stress and Apoptosis in H9c2 Cells.** To explore the protective effect of ORM1 against DOX in H9c2 cells in vitro, the effect of ORM1 on the viability of H9c2 cells was measured. A concentration of ORM1 below 100 MOI produced no cytotoxic effects. However, a higher concentration slightly reduced the viability of H9c2 cells (Supplementary Figure 3a). Cotreatment of  $10 \mu\text{M}$  DOX and either 10, 30, 50, or 100 MOI ORM1 caused a concentration-dependent increase in cell viability compared to that of the control group (Supplementary Figure 3b). Further experiments were carried out using  $10 \mu\text{M}$  DOX.

Next, we more closely examined the effects of 100 MOI ORM1 on H9c2 cells treated with DOX. Western blot analysis demonstrated that the addition of exogenous ORM1 reduced the oxidative level and apoptosis index in cardiomyocytes, reversing the DOX-induced effects (Figures 3(a) and 3(b)). The CCK-8 assay was utilized to further examine the protective effects of ORM1 in H9c2 cells. The results showed that the cell survival rate significantly increased in DOX+ORM1-treated cells compared with that in cells treated with DOX only (Figure 3(c)).

MDA is a parameter of oxidative stress, and its content in cells was significantly upregulated by DOX (Figure 3(d)). Under various pathological conditions, the initiation of oxidative stress and the overproduction of ROS play a key role in the development of cardiac dysfunction. A DCFH-DA assay was utilized to analyze the production of cellular ROS, and the fluorescence intensity increased with the production of reactive metabolites. The combination of ORM1 and DOX effectively inhibited ROS production (Figures 3(e) and 3(f)). A subsequent TUNEL assay of H9c2 cells showed that DOX significantly increased apoptosis, while ORM1 produced the opposite effect (Figures 3(g) and 3(h)).

**3.5. Nrf2 Knockdown Reversed the Protective Effects of ORM1 in DOX-Treated H9c2 Cells.** To study the role of the Nrf2-mediated transcription network in the DOX-induced cardioprotective effects of ORM1, Nrf2 was knocked down by specific Nrf2 siRNA. Western blot analysis showed that Nrf2 knockdown did not affect the ORM1 level, it downregulated



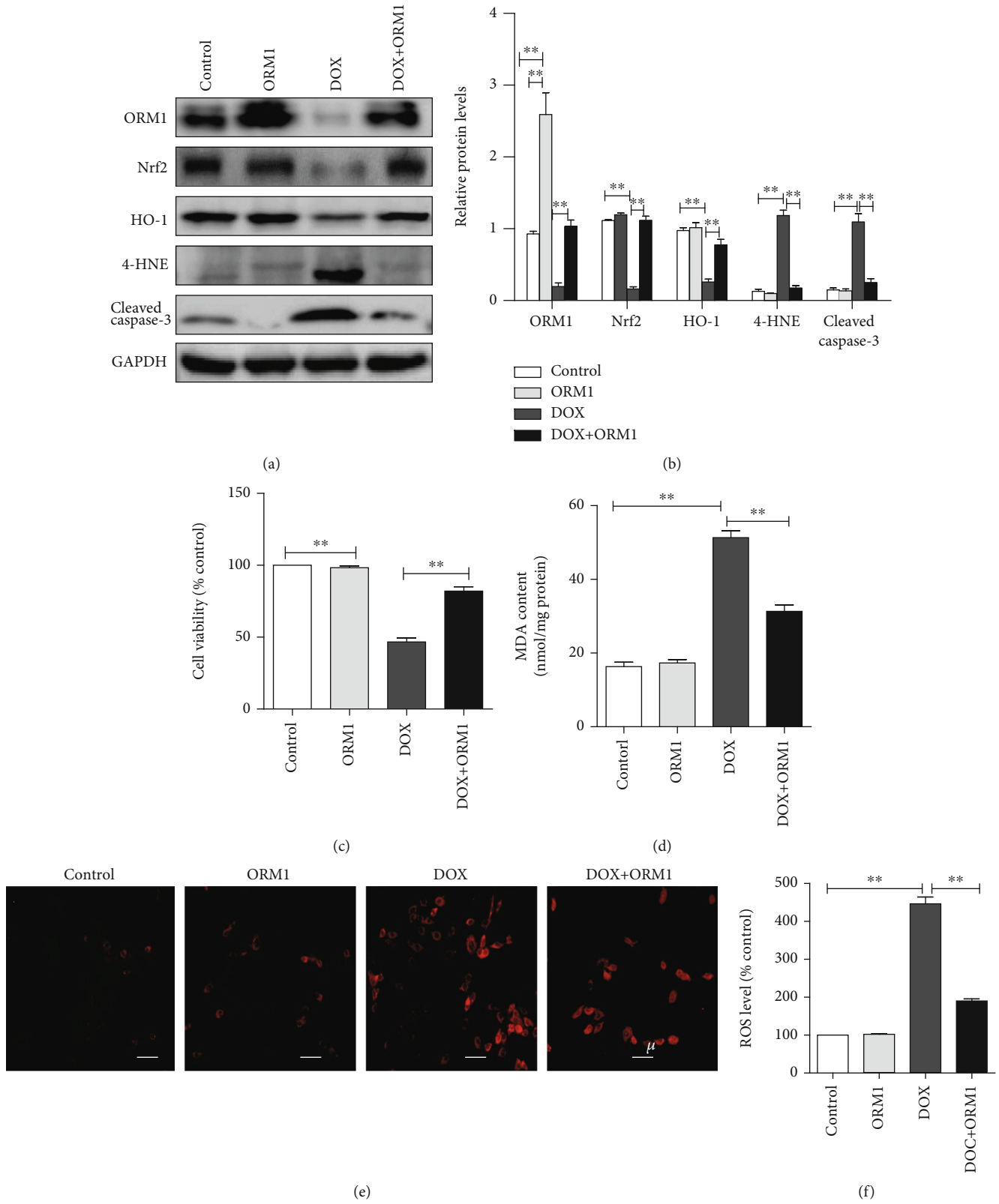


FIGURE 3: Continued.

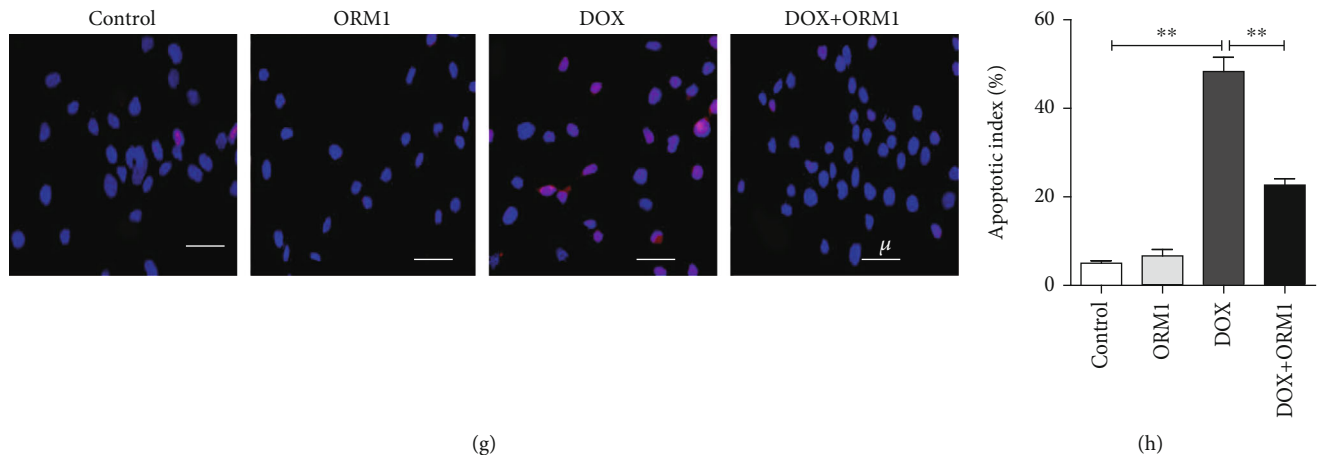


FIGURE 3: ORM1 reduces doxorubicin- (DOX-) induced oxidative stress and apoptosis in H9c2 cells. (a, b) Western blot analysis of ORM1, Nrf2, HO-1, 4-HNE, and cleaved caspase-3. (c) Cell survival rate analysis using the Cell Counting Kit 8 (CCK-8). Cell survival rate is expressed as the optical density (OD) value (% control). (d) Cellular malondialdehyde (MDA) content. (e, f) Fluorescence image (red fluorescence) of reactive oxygen species (ROS) measured using dichlorodihydrofluorescein diacetate (DCFH-DA). (g, h) Terminal deoxynucleotidyl transferase dUTP nick end labeling (TUNEL) staining images with calculated apoptosis indices. Data are expressed as the mean  $\pm$  standard error of the mean (SEM);  $n = 6$ . \*\* $P < 0.01$ .

HO-1 expression and upregulated 4-HNE and cleaved caspase-3 levels in the DOX+ORM1+Nrf2 siRNA group compared to the corresponding levels in the DOX+ORM1 group (Figures 4(a) and 4(b)). CCK-8 analysis showed that compared with cells expressing Nrf2, Nrf2-knockdown cells exhibited an aggravated reduction of cell viability in DOX group, while silencing Nrf2 significantly reduced cell viability in the DOX+ORM1+Nrf2 siRNA group compared to the corresponding levels in the DOX+ORM1 group in H9c2 cells (Figure 4(c)). Similarly, silencing Nrf2 significantly promoted the production of ROS and MDA in DOX-treated H9c2 cells, and Nrf2 knockdown reversed the protection of ORM1 in DOX-treated H9c2 cells. In conclusion, inhibition of Nrf2 activation reversed the antioxidative effects of ORM1 against DOX-induced myocardial toxicity in H9c2 cells (Figures 4(d)–4(f)). TUNEL analysis showed that Nrf2 siRNA reversed the protective effects of ORM1 in DOX-treated H9c2 cells (Figures 4(g) and 4(h)). These findings confirmed that the Nrf2 pathway was involved in the protective function of ORM1 in cardiomyocytes affected by DOX-induced oxidative stress and apoptosis.

#### 4. Discussion

DOX has been used for more than half a century as an anti-cancer drug and is the cornerstone of chemotherapy in children and adults; however, its cardiotoxicity poses a serious threat. Accumulating evidence shows that oxidative stress and cell apoptosis play key roles in the pathogenesis of DOX-induced myocardial injury [23, 24], which is caused by the elevated production of ROS and 4-HNE (the final product of lipid peroxidation [25, 26]) and leads to cardiomyocyte apoptosis.

In our study, LC/MS technology was used to identify and quantify candidate proteins that are differentially expressed in response to DOX-induced cardiotoxicity. We found that

ORM1 levels were significantly decreased, and analyses of in vivo and in vitro DOX-induced myocardial injury models confirmed this result. We also found that the levels of oxidative stress and apoptosis were increased and that ORM1 inhibited oxidative stress and apoptosis in H9c2 cells via Nrf2 signaling. Many studies have shown that various molecular mechanisms and signaling pathways can regulate oxidative stress and cardiomyocyte apoptosis; for example, activation of the Nrf2/HO-1 pathway can affect DOX-induced myocardial injury [19–21]; our study produced consistent findings and showed that the Nrf2/HO-1 pathway also participates in the antiapoptotic action of ORM1 in DOX-treated H9c2 cells.

Nrf2 is the master regulator of cellular redox homeostasis and is also involved in maintaining mitochondrial redox homeostasis by providing reduced forms of glutathione (GSH) and mitochondrial antioxidant enzymes such as GSH peroxidase, superoxide dismutase, and peroxiredoxin. Nrf2 deficiency results in impaired mitochondrial fatty acid oxidation, respiration, and adenosine triphosphate (ATP) production. Recent studies have shown that Nrf2 also affects mitochondrial function in cardiomyocyte regeneration and neural stem/progenitor cell survival [27–29]. However, the function of Nrf2 in myocardial injury caused by DOX is not completely understood. In future studies, we intend to further analyze the function of Nrf2 in the mitochondria of DOX-treated mice.

The addition of exogenous ORM1 reduced both the oxidative stress and apoptosis caused by DOX. DOX-induced oxidative stress was significantly reversed when H9c2 cells were treated with a combination of ORM1 and DOX, confirming the antioxidative power of ORM1. Cardiomyocyte apoptosis is another hallmark of acute DOX-induced cardiotoxicity, and ORM1 reportedly exhibits protective effects against apoptosis under various pathogenic conditions [12–14]. The results from the TUNEL assay confirmed the antiapoptotic effect of ORM1, as the protein significantly inhibited DOX-

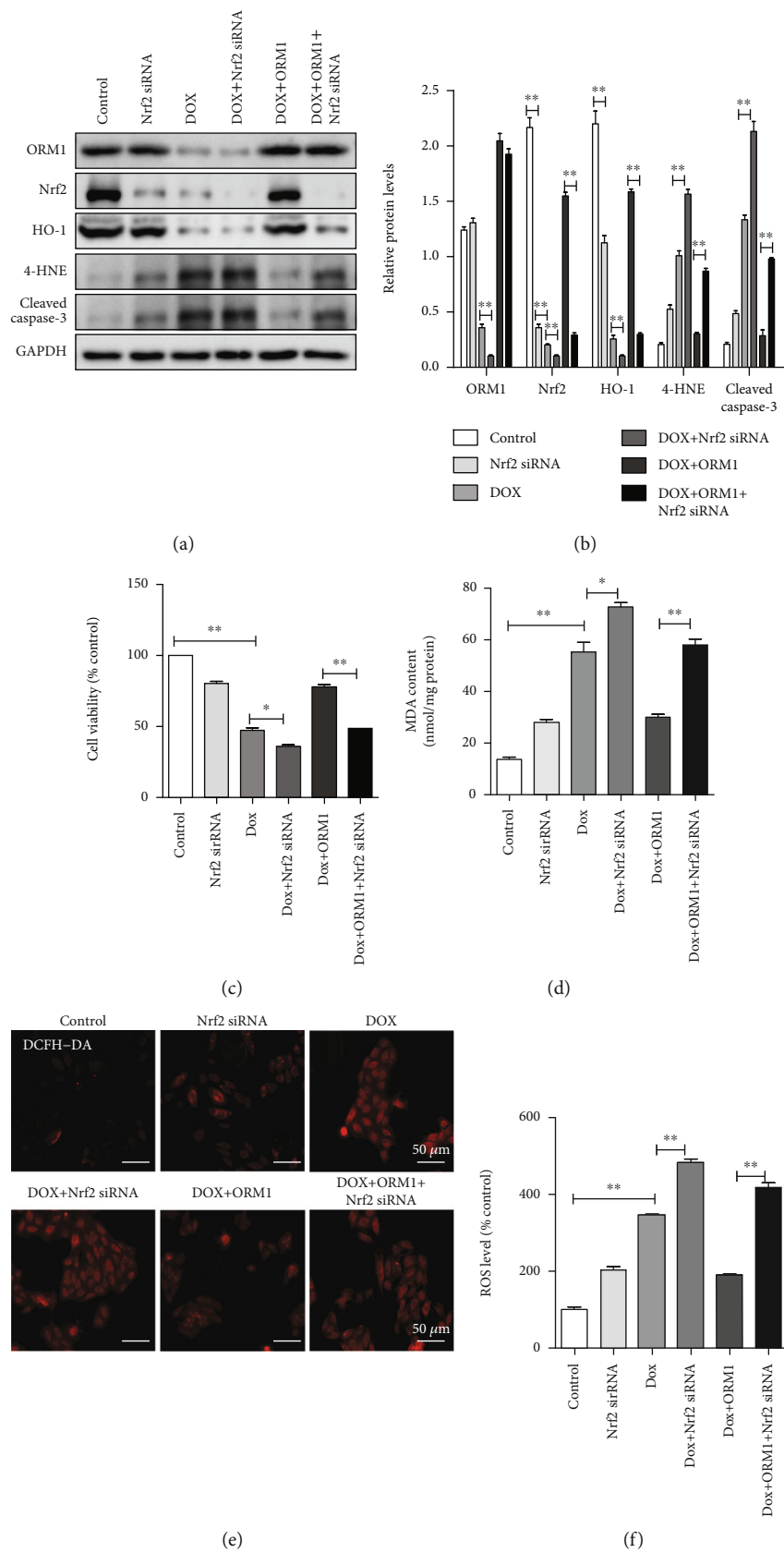


FIGURE 4: Continued.

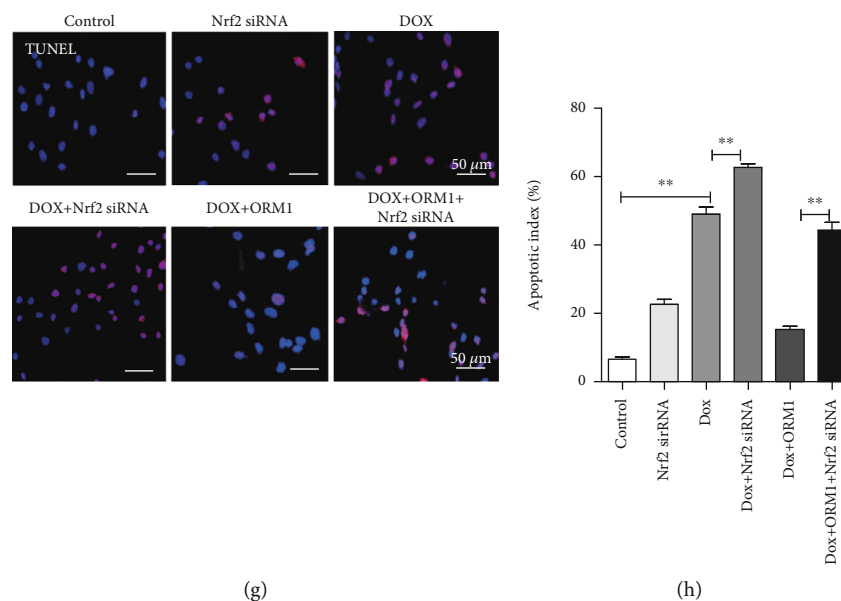


FIGURE 4: Nrf2 knockdown reverses the protective effects of ORM1 in doxorubicin- (DOX-) treated H9c2 cells. (a, b) Western blot analysis of ORM1, Nrf2, HO-1, 4-HNE, and cleaved caspase-3. (c) Cell survival analysis using the Cell Counting Kit 8 (CCK-8). (d) Cellular malondialdehyde (MDA) content. (e, f) Fluorescence image (red fluorescence) of reactive oxygen species (ROS) measured using dichlorodihydrofluorescein diacetate (DCFH-DA). (g, h) Terminal deoxynucleotidyl transferase dUTP nick end labeling (TUNEL) staining images with calculated apoptosis indices. Data are expressed as the mean  $\pm$  standard error of the mean (SEM);  $n = 6$ . \*\* $P < 0.01$  and \* $P < 0.05$ .

induced apoptosis in vitro. Nrf2 silencing negated the protective effects of ORM1 against DOX-induced cardiomyocyte injury, suggesting that ORM1 regulates DOX-induced cardiomyocyte oxidation and apoptosis by upregulating Nrf2/HO-1 signaling and other important antioxidative Nrf2-related pathways that influence cell apoptosis [30, 31].

There were several limitations to this study. First, the effects of ORM1 on DOX-induced oxidative stress and apoptosis in cardiomyocytes were only examined in vitro. ORM1 cardiac-specific transgenic mice or knockout mice will be considered in future studies to clarify the key role of ORM1 in vivo. Moreover, it is not clear whether there was an Nrf2 binding site in the promoter region of the ORM1 gene. Chromatin immunoprecipitation and luciferase reporter gene assays will be used to clarify the details of the relationship between ORM1 and Nrf2.

## 5. Conclusions

In summary, our study showed that ORM1 could attenuate DOX-induced oxidative stress and apoptosis in cardiomyocytes via Nrf2 signaling, suggesting that ORM1 might be an effective therapeutic target for the treatment of DOX-induced cardiotoxicity. This finding provides novel insights that may contribute to significant advances in the field of oncology.

## Data Availability

The data used in this study are available upon request from the corresponding author.

## Conflicts of Interest

The authors declare that there is no conflict of interest regarding the publication of this paper.

## Acknowledgments

This work was supported by the National Natural Science Foundation of China (81670276, 81870553, 81770303, and 91739118), Natural Science Foundation of Liaoning Province (20180550368), Science and Technology Project of Shenyang (19-112-4-056), and Military Science and Technology Youth Talents Entrustment Project (17-JCJQ-QT-028).

## Supplementary Materials

Fig. S1: DOX causes heart failure on C57BL/6 mice. (a) The level of FS valve ( $n = 20$ ). (b) Serum LDH ( $n = 10$ ). (c) Serum CK/MB ( $n = 10$ ). (d) Relative ANP mRNA levels of hearts ( $n = 10$ ). Data are expressed as the mean  $\pm$  standard error of the mean (SEM); \*\* $P < 0.01$ . Fig S2: DOX causes a dose-dependent inhibition of cell viability in H9c2 cells ( $n = 3$ ). Data are expressed as the mean  $\pm$  standard error of the mean (SEM); \* $P < 0.05$  and \*\* $P < 0.01$ . Fig. S3: ORM1 upregulated cell viability in DOX-induced cardiomyocytes. (a) The cell viability with different dose ORM1 ( $n = 3$ ). (b) ORM1 upregulated cell viability in DOX-induced cardiomyocytes ( $n = 3$ ). Data are expressed as the mean  $\pm$  standard error of the mean (SEM); \*\* $P < 0.01$ . Fig S4: sequences of the primers used for real-time RT-PCR analysis. (Supplementary Materials)

## References

- [1] P. Guo, R. Harding, and I. J. Higginson, "Palliative care needs of heart failure patients in China: putting people first," *Current Opinion in Supportive and Palliative Care*, vol. 12, no. 1, pp. 10–15, 2018.
- [2] J. R. Teerlink, B. A. Davison, G. Cotter et al., "Effects of serelaxin in patients admitted for acute heart failure: a meta-analysis," *European Journal of Heart Failure*, vol. 22, no. 2, pp. 315–329, 2020.
- [3] A. Carbone and A. Gloghini, "Subclassifying peripheral T-cell lymphoma NOS," *Blood*, vol. 134, no. 24, pp. 2120–2121, 2019.
- [4] H. Babaei, N. Razmaraii, G. Assadnassab et al., "Ultrastructural and echocardiographic assessment of chronic doxorubicin-induced cardiotoxicity in rats," *Archives of Razi Institute*, vol. 75, no. 1, pp. 55–62, 2020.
- [5] V. K. Todorova, I. Makhoul, J. Wei, and V. S. Klimberg, "Circulating miRNA profiles of doxorubicin-induced cardiotoxicity in breast cancer patients," *Annals of Clinical and Laboratory Science*, vol. 47, no. 2, pp. 115–119, 2017.
- [6] J. Sui, M. Zhao, Y. Yang et al., "Acid-labile polysaccharide pro-drug via lapatinib-sensitizing effect substantially prevented metastasis and postoperative recurrence of triple-negative breast cancer," *Nanoscale*, vol. 12, no. 25, pp. 13567–13581, 2020.
- [7] J. Wen, L. Zhang, J. Wang et al., "Therapeutic effects of higenamine combined with [6]-gingerol on chronic heart failure induced by doxorubicin via ameliorating mitochondrial function," *Journal of Cellular Molecular Medicine*, vol. 24, no. 7, pp. 4036–4050, 2020.
- [8] C. Nabhan, M. Byrtek, A. Rai et al., "Disease characteristics, treatment patterns, prognosis, outcomes and lymphoma-related mortality in elderly follicular lymphoma in the United States," *British Journal of Haematology*, vol. 170, no. 1, pp. 85–95, 2015.
- [9] L. Zhao, Y. Qi, L. Xu et al., "MicroRNA-140-5p aggravates doxorubicin-induced cardiotoxicity by promoting myocardial oxidative stress via targeting Nrf2 and Sirt2," *Redox Biology*, vol. 15, pp. 284–296, 2018.
- [10] D. Chihara, J. R. Westin, Y. Oki et al., "Management strategies and outcomes for very elderly patients with diffuse large B-cell lymphoma," *Cancer*, vol. 122, no. 20, pp. 3145–3151, 2016.
- [11] M. M. McGuckin, S. L. Giesy, A. N. Davis et al., "The acute phase protein orosomucoid 1 is upregulated in early lactation but does not trigger appetite-suppressing STAT3 signaling via the leptin receptor," *Journal of Dairy Science*, vol. 103, no. 5, pp. 4765–4776, 2020.
- [12] R. Fandiño-Vaquero, A. Fernández-Trasancos, E. Álvarez et al., "Orosomucoid secretion levels by epicardial adipose tissue as possible indicator of endothelial dysfunction in diabetes mellitus or inflammation in coronary artery disease," *Atherosclerosis*, vol. 235, no. 2, pp. 281–288, 2014.
- [13] F. Ren, Y. Chen, Y. Wang et al., "Comparative serum proteomic analysis of patients with acute-on-chronic liver failure: alpha-1-acid glycoprotein maybe a candidate marker for prognosis of hepatitis B virus infection," *Journal of Viral Hepatitis*, vol. 17, no. 11, pp. 816–824, 2010.
- [14] H. Z. Zhu, W. J. Zhou, Y. F. Wan, K. Ge, J. Lu, and C. K. Jia, "Downregulation of orosomucoid 2 acts as a prognostic factor associated with cancer-promoting pathways in liver cancer," *World Journal of Gastroenterology*, vol. 26, no. 8, pp. 804–817, 2020.
- [15] H. Higuchi, D. Kamimura, J. J. Jiang et al., "Orosomucoid 1 is involved in the development of chronic allograft rejection after kidney transplantation," *International Immunology*, vol. 32, no. 5, pp. 335–346, 2020.
- [16] J. J. Wan, P. Y. Wang, Y. Zhang et al., "Role of acute-phase protein ORM in a mice model of ischemic stroke," *Journal of Cellular Physiology*, vol. 234, no. 11, pp. 20533–20545, 2019.
- [17] X. Fang, H. Wang, D. Han et al., "Ferroptosis as a target for protection against cardiomyopathy," *Proceedings of the National Academy of Sciences of the United States of America*, vol. 116, no. 7, pp. 2672–2680, 2019.
- [18] H. Lin, J. Zhang, T. Ni et al., "Yellow wine polyphenolic compounds prevents doxorubicin-induced cardiotoxicity through activation of the Nrf2 signalling pathway," *Journal of Cellular Molecular Medicine*, vol. 23, no. 9, pp. 6034–6047, 2019.
- [19] S. N. S. Ahmad, D. Sanajou, A. Kalantary-Charvadeh et al., "β-LAPachone ameliorates doxorubicin-induced cardiotoxicity via regulating autophagy and Nrf2 signalling pathways in mice," *Basic Clinical Pharmacology Toxicology*, vol. 126, no. 4, pp. 364–373, 2020.
- [20] M. Chen, V. P. Samuel, Y. Wu et al., "Nrf2/HO-1 mediated protective activity of genistein against doxorubicin-induced cardiac toxicity," *Journal of Environmental Pathology, Toxicology and Oncology*, vol. 38, no. 2, pp. 143–152, 2019.
- [21] L. Rochette, C. Guenancia, A. Gudjoncik et al., "Anthracyclines/trastuzumab: new aspects of cardiotoxicity and molecular mechanisms," *Trends in Pharmacological Sciences*, vol. 36, no. 6, pp. 326–348, 2015.
- [22] D. Liu, Z. Ma, S. di et al., "AMPK/PGC1α activation by melatonin attenuates acute doxorubicin cardiotoxicity via alleviating mitochondrial oxidative damage and apoptosis," *Free Radical Biology & Medicine*, vol. 129, pp. 59–72, 2018.
- [23] M. C. Sunitha, R. Dhanyakrishnan, B. PrakashKumar, and K. G. Nevin, "p-Coumaric acid mediated protection of H9c2 cells from doxorubicin-induced cardiotoxicity: involvement of augmented Nrf2 and autophagy," *Biomedicine & Pharmacotherapy*, vol. 102, pp. 823–832, 2018.
- [24] M. Räsänen, J. Degerman, T. A. Nissinen et al., "VEGF-B gene therapy inhibits doxorubicin-induced cardiotoxicity by endothelial protection," *Proceedings of the National Academy of Sciences of the United States of America*, vol. 113, no. 46, pp. 13144–13149, 2016.
- [25] L. Zhou, R. Li, C. Liu et al., "Foxo3a inhibits mitochondrial fission and protects against doxorubicin-induced cardiotoxicity by suppressing MIEF2," *Free Radical Biology & Medicine*, vol. 104, pp. 360–370, 2017.
- [26] L. Bharathi Priya, R. Baskaran, C. Y. Huang, and V. Vijaya Padma, "Neferine modulates IGF-1R/Nrf2 signaling in doxorubicin treated H9c2 cardiomyoblasts," *Journal of Cellular Biochemistry*, vol. 119, no. 2, pp. 1441–1452, 2018.
- [27] A. T. Dinkova-Kostova and A. Y. Abramov, "The emerging role of Nrf2 in mitochondrial function," *Free Radical Biology & Medicine*, vol. 88, Part B, pp. 179–188, 2015.
- [28] K. M. Holmström, R. V. Kostov, and A. T. Dinkova-Kostova, "The multifaceted role of Nrf2 in mitochondrial function," *Current Opinion in Toxicology*, vol. 1, pp. 80–91, 2016.
- [29] I. G. Ryoo and M. K. Kwak, "Regulatory crosstalk between the oxidative stress-related transcription factor Nfe2l2/Nrf2 and mitochondria," *Toxicology and Applied Pharmacology*, vol. 359, pp. 24–33, 2018.

- [30] R. Dhingra, V. Margulets, S. R. Chowdhury et al., “Bnip3 mediates doxorubicin-induced cardiac myocyte necrosis and mortality through changes in mitochondrial signaling,” *Proceedings of the National Academy of Sciences of the United States of America*, vol. 111, no. 51, pp. E5537–E5544, 2014.
- [31] T. Zhang, Y. Zhang, M. Cui et al., “CaMKII is a RIP3 substrate mediating ischemia and oxidative stress induced myocardial necroptosis,” *Nature Medicine*, vol. 22, no. 2, pp. 175–182, 2016.

## Research Article

# The Free Radical Scavenging and Anti-Isolated Human LDL Oxidation Activities of *Pluchea indica* (L.) Less. Tea Compared to Green Tea (*Camellia sinensis*)

Kittipot Sirichaiwetchakoon <sup>1</sup>, Gordon Matthew Lowe <sup>2</sup>, and Griangsak Eumkeb <sup>1</sup>

<sup>1</sup>School of Preclinic, Institute of Science, Suranaree University of Technology, 111 University Avenue, Suranaree Subdistrict, Muang District, Nakhonratchasima 30000, Thailand

<sup>2</sup>School of Pharmacy and Biomolecular Sciences, Liverpool John Moores University, James Parsons Building, Byrom Street, Liverpool, UK

Correspondence should be addressed to Gordon Matthew Lowe; [g.m.lowe@ljmu.ac.uk](mailto:g.m.lowe@ljmu.ac.uk) and Griangsak Eumkeb; [griang@sut.ac.th](mailto:griang@sut.ac.th)

Received 21 July 2020; Revised 26 August 2020; Accepted 15 September 2020; Published 25 September 2020

Academic Editor: Roland E. Akhigbe

Copyright © 2020 Kittipot Sirichaiwetchakoon et al. This is an open access article distributed under the Creative Commons Attribution License, which permits unrestricted use, distribution, and reproduction in any medium, provided the original work is properly cited.

Tea is one of the most popular beverages in the world. *Camellia sinensis* tea (CST) or green tea is widely regarded as a potent antioxidant. In Thailand, *Pluchea indica* (L.) Less. tea (PIT) has been commercially available as a health-promoting drink. This study focused on free radical scavenging activities of PIT, and its ability to protect isolated human low-density lipoproteins (LDL) from oxidation by chemical agents. A preliminary study to investigate the antioxidant nature of PIT was undertaken. These included common antioxidant assays involving 2,2-Diphenyl-1-picrylhydrazyl (DPPH), 2,2-azinobis-(3-ethylbenzothiazoline)-6-sulfonic acid (ABTS), hypochlorous acid (HOCl), and its potential to scavenge peroxynitrite. In separated experiments, isolated human LDL was challenged with either 2,2'-azobis(2-amidinopropane) dihydrochloride (AAPH), copper ( $\text{Cu}^{2+}$ ), or 3-Morpholinopyridone hydrochloride (SIN-1) to induce LDL oxidation. PIT exhibited antioxidant activity in all test systems and performed significantly better than CST in both DPPH ( $P < 0.05$ ;  $\text{IC}_{50}\text{PIT} = 245.85 \pm 15.83$  and  $\text{CST} = 315.41 \pm 24.18 \mu\text{g/ml}$ ) and peroxynitrite scavenging assays. PIT at  $75 \mu\text{g/ml}$  almost fully prevented the peroxynitrite over a 5 h period. Moreover, it displayed similar properties to CST during the antioxidantation of isolated human LDL using AAPH,  $\text{Cu}^{2+}$ , SIN-1, and hypochlorous acid scavenging assays. However, it revealed a significantly lower ABTS scavenging activity than CST ( $P < 0.05$ ;  $\text{IC}_{50}\text{PIT} = 30.47 \pm 2.20$  and  $\text{CST} = 21.59 \pm 0.67 \mu\text{g/ml}$ ). The main constituents of the PIT were identified using LC-MS/MS. It contained 4-O-caffeoylquinic acid (4-CQ), 5-O-caffeoylquinic acid (5-CQ), 3,4-O-dicaffeoylquinic acid (3,4-CQ), 3,5-O-dicaffeoylquinic acid (3,5-CQ), and 4,5-O-dicaffeoylquinic acid (4,5-CQ). In conclusion, caffeoyl derivatives in PIT could play an important role in potent antioxidant properties. So, it may be further developed to be antioxidant beverages for preventing atherosclerosis and cardiovascular diseases associated with oxidative stress.

## 1. Introduction

Oxidative stress is defined as the imbalance between the production of free radicals and defense mechanisms, which are natural physiological processes in biological systems [1]. The excesses of intracellular reactive oxygen species (ROS) and reactive nitrogen species (RNS) is the major causes of oxidative stress that is associated with the development of

chronic and degenerative diseases such as cancer, arthritis, aging, autoimmune disorders, cardiovascular, and neurodegenerative diseases [2–5]. Moreover, oxidative stress may also modify the structure and function of certain biomolecules, including proteins, lipids, and DNA [6].

Oxidative stress may also result in the oxidation of human LDL. LDL oxidation may result in lipid peroxidation or the direct oxidation of apolipoprotein. Oxidized LDL is

thought to have a vital role in the etiology of atherosclerosis, which ultimately has a profound effect on cardiovascular function [7–9].

Herbal supplements derived from fruit and vegetables tend to be rich in both water and lipid-soluble antioxidants [10]. One of the most popular herbal supplements is a beverage, such as a tea infusion. Many herbal tea infusions have a strong antioxidant capacity [11–14], and it has the potential to prevent diseases associated with oxidative stress such as atherosclerosis [15, 16].

Tea is the most widely consumed beverage in the world, second only to water [17], and one of the most popular beverages in Southeast Asia. Green tea is derived from the tea plant *Camellia sinensis*. It has been demonstrated that some of the components of green tea have potent antioxidative properties and have free radical scavenging properties towards the DPPH, ABTS, and Fluorescence Recovery After Photobleaching (FRAP) assays [18]. Also, flavonols from green tea have potent antioxidant capacities and reduced oxidative stress [19]. Moreover, green tea can prevent lipid oxidation induced by copper ions [20]. The main active ingredients of green tea are polyphenol catechins. The major catechins present in green tea are Epicatechin (EC), Epigallocatechin gallate (EGCG), Epicatechin gallate (ECG), Epigallocatechin (EGC), and Gallic catechin gallate (GCG) [21]. EGCG, which acts as an antioxidant, might exert a preventive effect against cardiovascular disease [22].

The plant *Pluchea indica* (L.) Less. (*P. indica*) is a large evergreen shrub found abundantly in salt marshes. It is widely distributed in India, Southern China, and Southeast Asia. In Thailand, The PIT has been commercially available for approximately ten years as a health-promoting drink [23]. The various biological activities of *P. indica* leaves have been widely reported. Several studies revealed that its methanolic extract had diuretic [24], hypoglycemic, and antihyperglycemic effects [25]. Moreover, the ethyl acetate fraction from an ethanolic extract of *P. indica* in lipopolysaccharide (LPS-) stimulated RAW 264.7 macrophages displayed anti-inflammatory activities [26]. Besides, the volatile oil of *P. indica* exhibited antioxidant activity [27]. Although some biological activities of *P. indica* have been reported, there is little information published on the antioxidative properties of the aqueous tea.

The aim of this study was to examine the free radical scavenging potential of PIT with regard to established antioxidant assays and its potential to inhibit the oxidation of isolated human LDL by  $\text{Cu}^{2+}$ , AAPH, or SIN-1. The antioxidant properties of PIT were compared to a commercially available green tea.

## 2. Materials and Methods

**2.1. Tea Materials.** PIT was supplied by the Crystal Biotechnology Company, Thailand. Commercial green tea was purchased from a supermarket in the United Kingdom. The tea samples were kept in the dark, dry place until required. Beverages were prepared by brewing ground tea leaves in 80°C 1x phosphate buffer saline (PBS) for 5 min and filtered by What-

man No. 1 filter paper. The concentration of PIT was calculated from the ground tea leaves dry weight in PBS volume ( $\mu\text{g}/\text{ml}$ ). Tea samples were kept at -20°C until used.

**2.2. Chemicals and Reagents.** 2,2-Diphenyl-1-picrylhydrazyl (DPPH), 2,2-azinobis-(3-ethylbenzothiazoline)-6-sulfonic acid (ABTS), potassium persulfate, sodium hypochlorite (NaOCl), catalase, sulfanilamide, naphthylethylenediamine dihydrochloride (NED), 3-Morpholinopyridone hydrochloride (SIN-1), Diethylene-triamine-pentaacetic acid (DTPA), Evans blue, iodixanol (Optiprep™), 2,2'-azobis (2-amidinopropane) dihydrochloride (AAPH), copper sulfate ( $\text{Cu}_2\text{SO}_4$ ), trichloroacetic acid (TCA), thiobarbituric acid were purchased from Sigma-Aldrich Chemical Co. (St. Louis, MO, USA). 4-O-caffeoylquinic acid (4-CQ), 5-O-caffeoylquinic acid (5-CQ), 3,4-O-dicaffeoylquinic acid (3,4-CQ), 3,5-O-dicaffeoylquinic acid (3,5-CQ), and 4,5-O-dicaffeoylquinic acid (4,5-CQ) were purchased from Chengdu Biopurify Phytochemicals Ltd., China. Other reagents used were all analytical grade.

**2.3. DPPH Scavenging Assay.** The %DPPH scavenging activity of PIT and CST were evaluated by the method of Brand-Williams et al. [28] with slight modifications. In brief, 0–300  $\mu\text{g}/\text{ml}$  of the tea extracts was prepared using 0.002% DPPH reagent in a 96-well plate. The samples were suitably mixed prior to incubation in the dark at room temperature for 30 min. PBS was used as a negative control. The absorbance of all samples was measured at 515 nm. Radical scavenging activity was repeated for six times and expressed as a DPPH scavenging percentage as,

$$\% \text{DPPH scavenging} = \left( 1 - \frac{\text{OD}_{\text{sample}} - \text{OD}_{\text{sample blank}}}{\text{OD}_{\text{control}} - \text{OD}_{\text{sample blank}}} \right) \times 100. \quad (1)$$

**2.4. ABTS Scavenging Assay.** The ABTS scavenging activity of PIT was measured and compared with CST. The  $\text{ABTS}^+$  radical cation was prepared by mixing 7 mM ABTS stock solution with 2.45 mM potassium persulfate (final concentration) in methanol and kept them in the dark at room temperature for 16 h. The solution was adjusted to an absorbance of 0.70 ( $\pm 0.02$ ) with ethanol. The reaction was performed in a 96-well plate by mixing and shaking 90  $\mu\text{l}$   $\text{ABTS}^+$  radical cation solution with 10  $\mu\text{l}$  of the test sample at various concentrations (0–40  $\mu\text{g}/\text{ml}$  final concentration) for 45 seconds. The absorbance was measured at 734 nm. The assay was repeated six times, and the percentage inhibition of absorbance was reported as an ABTS scavenging percentage as

$$\% \text{ABTS scavenging} = \left( 1 - \frac{\text{OD}_{\text{sample}} - \text{OD}_{\text{sample blank}}}{\text{OD}_{\text{control}} - \text{OD}_{\text{sample blank}}} \right) \times 100. \quad (2)$$

**2.5. Hypochlorous Acid (HOCl) Scavenging Assay.** This assay was performed as previously described by Aruoma and Halliwell [29] with minor modifications. HOCl was generated by



adjusting the pH of a 10% (*v/v*) solution of NaOCl to 6.2% with 0.6 M H<sub>2</sub>SO<sub>4</sub>. The HOCl was mixed with 50 mM phosphate buffer (pH 6.8), catalase (7.2 μM), and tea samples at various concentrations (0–300 μg/ml) in 96 well-plate. The mixture was incubated at 25°C for 20 min. The scavenging activity was measured by the decrease in absorbance of catalase at 404 nm. The assay was performed in triplicate. %HOCl scavenging was calculated as

$$\%HOCl \text{ scavenging} = \left( 1 - \frac{OD_{\text{sample blank}} - OD_{\text{sample}}}{OD_{\text{sample blank}} - OD_{\text{control}}} \right) \times 100. \quad (3)$$

**2.6. Nitric Oxide (NO) Scavenging Assay.** SIN-1 was used for generating RNS in this experiment. One of the end products of RNS chemistry is nitrite. Nitrite concentration was determined using the Griess assay. The test solution was prepared in a 96-well plate by mixing 0.25 mM SIN-1 with PBS (pH 7.4) and various doses of tea samples (0–100 μg/ml final concentration). The test solutions were incubated at 25°C for 30 min. Then, 80 μl of 0.33% sulfanilamide in 20% glacial acetic acid was added to the produced solution and was suitably shaken for 5 min before adding 80 μl of 0.1% NED and incubated at 25°C for 15 min. The nitric oxide scavenging was measured spectrophotometrically at 540 nm against a blank sample. All tests were repeated six times, and %Nitric oxide radical scavenging was expressed as

$$\%Nitric \text{ oxide radical scavenging} = \left( 1 - \frac{OD_{\text{sample}} - OD_{\text{sample blank}}}{OD_{\text{control}} - OD_{\text{sample blank}}} \right) \times 100. \quad (4)$$

**2.7. Peroxynitrite Scavenging Assay.** SIN-1 was used as a peroxynitrite donor, and peroxynitrite scavenging activity was measured by an Evans blue bleaching assay. Briefly, the reaction mixture comprised of 50 mM phosphate buffer (pH 7.4), 0.1 mM DTPA, 90 mM NaCl, 5 mM KCl, 12.5 μM Evans blue, 1 mM SIN-1, 37.5, and 75 μg/ml of

either PIT or CST in a 96-well plate. The mixture was incubated at 37°C for 300 min, and the absorbance was measured at 611 nm every 30 min. The assay was performed six times. The percentage scavenging of peroxynitrite at various times was calculated by the %Optical density of Evans blue as;

$$\%Optical \text{ density of Evans blue} = \left( 1 - \frac{OD_{\text{sample blank}} - OD_{\text{sample}}}{OD_{\text{sample blank}} - OD_{\text{control}}} \right) \times 100. \quad (5)$$

**2.8. LDL Isolation by Ultracentrifugation Technique.** The Liverpool John Moores University (LJMU) ethics committee approved the use of human blood and the preparation of LDL. Whole blood was obtained from the vein of healthy volunteers aged between 24 and 70 years who were normolipidemic, nonsmoking, had not taken any medications or supplements within the last two weeks. Whole blood was added to 3.8% (*w/v*) sodium citrate at a ratio of blood against anticoagulant as 9:1. The whole blood was centrifuged at 1500 x g for 20 min, and the platelet-poor plasma was transferred to a separate plastic tube. LDL was isolated by density gradient ultracentrifugation using a method developed by Graham et al. (1996) with minor modifications [30]. In brief, 0.5 ml of 60% (*v/v*) iodixanol (Optiprep™) was mixed with 4.5 ml of plasma and transferred to an 11.2 ml capacity Optiseal tube. Then, it was overlaid with 5 ml of 12% *v/v* iodixanol prepared with human plasma, and PBS was used to fill the rest of the tube. The tubes were centrifuged in a Beckman L8-80 ultracentrifuge using a vertical rotor V65.1 at 350,000 x g for 3 h. An Auto Densi-Flow gradient fractionator (Labconco, UK) was used for fractionating

the gradient by unloading the gradient from the top to the bottom of the tube. Each tube of 11.2 ml was fractionated into 0.5 ml aliquots per tube. All fractions were measured for triglycerides, cholesterol, LDL, and apoB100 components by using reagents and standards from Randox (Eire). Pooled LDL fraction was measured protein concentration by Bradford assay and stored at -20°C until required.

**2.9. AAPH Induce LDL Oxidation Assay.** AAPH is a reactive oxygen species generator. The sample solution was prepared by adding 20 mM AAPH to 50 μg/ml of LDL protein. Either 50 μg/ml or 75 μg/ml of PIT or CST was added in the test samples. The control sample was 50 μg/ml of LDL protein added with PBS. The LDL protein was added with AAPH 20 mM. All samples were incubated at 37°C. At this temperature, AAPH produces a range of ROS. At a specific time point (0, 30, 60, 90, 120, 150, and 180 min), sample aliquots were removed and placed at -20°C prior to thiobarbituric acid reactive substances (TBARS) measurements. The first stage of the TBARS assay was to precipitate protein by the addition of 20% *v/v* TCA. The samples were then spun at

10,000 rpm for 10 min at 4°C. The supernatant was collected and treated with 1% *w/v* thiobarbituric acid. The samples were heated at 95°C for 20 min. TBARS concentration was determined by UV absorption at 532 nm. The malondialdehyde (MDA) concentration was determined by a calibration curve. The assay was performed in triplicate.

**2.10. Copper Induce LDL Oxidation Assay.** LDL protein was challenged with  $\text{Cu}^{2+}$  by adding  $\text{Cu}_2\text{SO}_4$  at a final concentration of 40  $\mu\text{M}$  to 50  $\mu\text{g/ml}$  of LDL protein. The negative control sample was 50  $\mu\text{g/ml}$  of LDL protein with PBS. The positive control was 50  $\mu\text{g/ml}$  of LDL protein incubated with 40  $\mu\text{M}$   $\text{Cu}_2\text{SO}_4$ . The 15  $\mu\text{g/ml}$  of PIT or CST was added in the test samples that contained 50  $\mu\text{g/ml}$  LDL protein plus 40  $\mu\text{M}$   $\text{Cu}_2\text{SO}_4$ . All samples were incubated at 37°C for 3 h. At various time points, the samples were assessed for MDA equivalence as TBARS products. The assay was performed in triplicate.

**2.11. SIN-1 Induce LDL Oxidation Assay.** SIN-1, which is a peroxynitrite donor, has been used to investigate RNS-mediated LDL oxidation. In this assay, 50  $\mu\text{g/ml}$  of LDL protein was challenged with 1 mM of SIN-1. In test samples, 15  $\mu\text{g/ml}$  of PIT or CST was mixed with 50  $\mu\text{g/ml}$  of LDL protein and 1 mM of SIN-1. The samples were incubated at 37°C for 18 h. Finally, the samples were stored at -20°C before further analysis by TBARS assay. The assay was repeated three times.

**2.12. LC-MS/MS Instrument and Conditions.** LC-MS/MS technique has been used for identifying the main chemical constituents of PIT as previously described by Kongkiatpaiboon et al. [23]. The combination of chromatographic separation of LC-MS/MS system was combined by Agilent HPLC 1290 Infinity and mass analyzer 6490 Triple Quad LC/MS Agilent Technologies, which equipped with an electrospray ionization (ESI) source system. Agilent ZORBAX Rapid Resolution High Definition (RRHD) SB-C18, 2.1 mm id  $\times$  150 mm (1.8  $\mu\text{m}$ ) was used for chromatographic separation. The mobile phase system used 1% formic acid in water as solvent A and 1% formic acid in acetonitrile as solvent B. The gradient of the mobile phase was set at a ratio of solvent A : solvent B, 100 : 0, with gradient elution, from 30% solvent B at 10 min and 100% solvent B at 30 min at a flow-rate of 0.2 ml/min. The sample injection volume was 5  $\mu\text{L}$ , and the column was set at 25°C. 4-CQ, 5-CQ, 3,4-CQ, 3,5-CQ, and 4,5-CQ were used as standard.

**2.13. Statistical Analysis.** All the data were presented as a mean  $\pm$  standard deviation (S.D.) or standard error of the mean (S.E.M.). Statistical analysis was performed using SPSS version 18.0. The significant statistical differences between groups of DPPH, ABTS, HOCl, and NO scavenging assay were analyzed by an independent *t*-test, whereas peroxynitrite,  $\text{Cu}^{2+}$ , AAPH, and SIN-1 scavenging assay were compared by one-way analysis of variance (ANOVA) with a Tukey's HSD post hoc test. Values were considered statistically significant when  $P < 0.05$ , and data were the representative of at least three independent experiments.

### 3. Results

**3.1. DPPH Scavenging Assay.** The activities of both teas were investigated using the DPPH radical scavenging assay. The antioxidant activity was calculated spectrophotometrically at 515 nm. The result indicated that PIT generated significantly stronger antioxidant capacity than CST at a concentration of 75  $\mu\text{g/ml}$  to 300  $\mu\text{g/ml}$  CST ( $P < 0.05$ ) (Figure 1). At a concentration of 300  $\mu\text{g/ml}$ , the %DPPH scavenging value of PIT and CST was  $51.19 \pm 4.02$  and  $41.46 \pm 3.83$ , respectively. The  $\text{IC}_{50}$  value of PIT was determined at  $245.85 \pm 15.83$   $\mu\text{g/ml}$ , which was lower than CST at  $315.41 \pm 24.18$   $\mu\text{g/ml}$ .

**3.2. ABTS Scavenging Assay.** This assay shows the abilities of the extract to quench the  $\text{ABTS}^+$  radical. The extracts interacted with  $\text{ABTS}^+$ , which decreased the absorbance of the solution. The absorbance was measured spectrophotometrically at 734 nm. Figure 2 displays %ABTS radical scavenging of PIT and CST. CST significantly inhibited  $\text{ABTS}^+$  radical stronger than PIT at 5-40  $\mu\text{g/ml}$  ( $P < 0.05$ ). The  $\text{IC}_{50}$  of PIT and CST was  $30.47 \pm 2.20$  and  $21.59 \pm 0.67$   $\mu\text{g/ml}$ , respectively.

**3.3. Hypochlorous Acid Scavenging Assay.** The hypochlorous acid scavenging activity of the PIT and CST are shown in Figure 3. The results showed that PIT significantly scavenged more hypochlorous acid than CST at a concentration of 18.75  $\mu\text{g/ml}$  ( $P < 0.05$ ). Nevertheless, the other strengths of PIT inhibited more hypochlorous acid than CST but not significantly.

**3.4. Nitric Oxide Scavenging Assay.** Nitric oxide scavenging could be detected by determining the nitrite concentration using the decolorization by the Griess reaction method. Figure 4 shows % inhibition of nitric oxide of PIT and CST. The result indicated that the %nitric oxide scavenging activity of PIT was significantly higher than CST ( $P < 0.01$ ). The  $\text{IC}_{50}$  of PIT was  $116.48 \pm 5.08$   $\mu\text{g/ml}$ , while the  $\text{IC}_{50}$  of CST was  $178.42 \pm 15.52$   $\mu\text{g/ml}$ .

**3.5. Peroxynitrite Scavenging Assay.** Evans blue assay is used to measure peroxynitrite scavenging, which is generated by SIN-1. The peroxynitrite is thought to bleach the Evans blue dye. The results are shown in Figure 5. At higher concentrations, PIT (75  $\mu\text{g/ml}$ ) almost fully prevented the peroxynitrite bleaching the dye over a 5 h period. Whereas at 37.5  $\mu\text{g/ml}$ , the %peroxynitrite scavenging was  $64.50 \pm 8.07\%$  at 2 h. In contrast, a higher concentration of CST (75  $\mu\text{g/ml}$ ) exhibited significantly lower peroxynitrite scavenging activity compared to PIT.

**3.6. AAPH Induce LDL Oxidation Assay.** The ROS induce LDL oxidation scavenging effect has been investigated by challenging isolated human LDL with AAPH, which is ROS. PIT and CST at 50 and 75  $\mu\text{g/ml}$  were used for the experiment. The samples were incubated for 3 h, and aliquots were collected at various times for analysis using the TBARS assay. The result indicated that after 60 min of AAPH activity, both teas could significantly decrease the TBARS formation (Figure 6). Furthermore, a stronger effect was observed

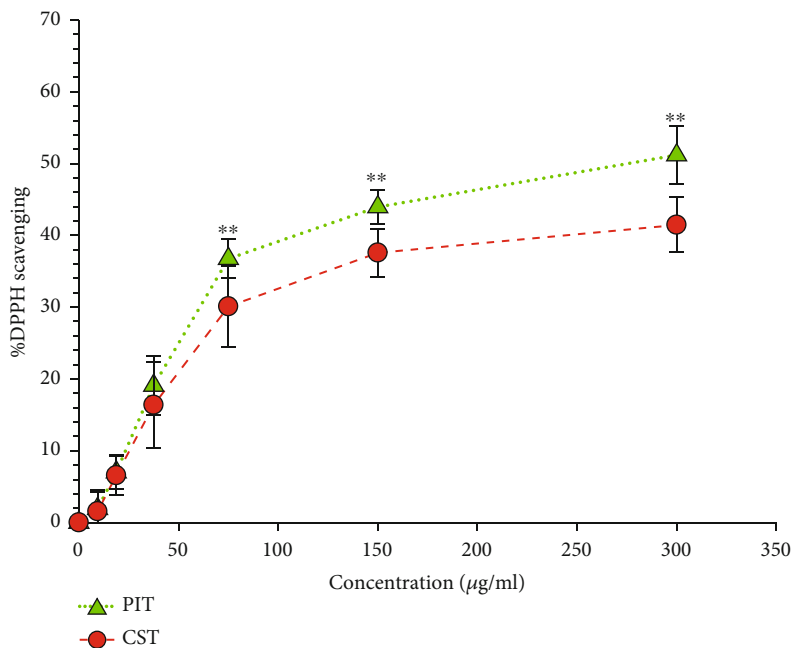


FIGURE 1: The DPPH radical scavenging activity. PIT: *P. indica* (L.) Less. tea; CST: *C. sinensis* tea at concentrations ranging from 0-300 µg/ml. The data represent the percentage of DPPH inhibition. Each value represents mean ± S.D. (n = 6). \*\* indicates a significant difference between groups at P < 0.01.

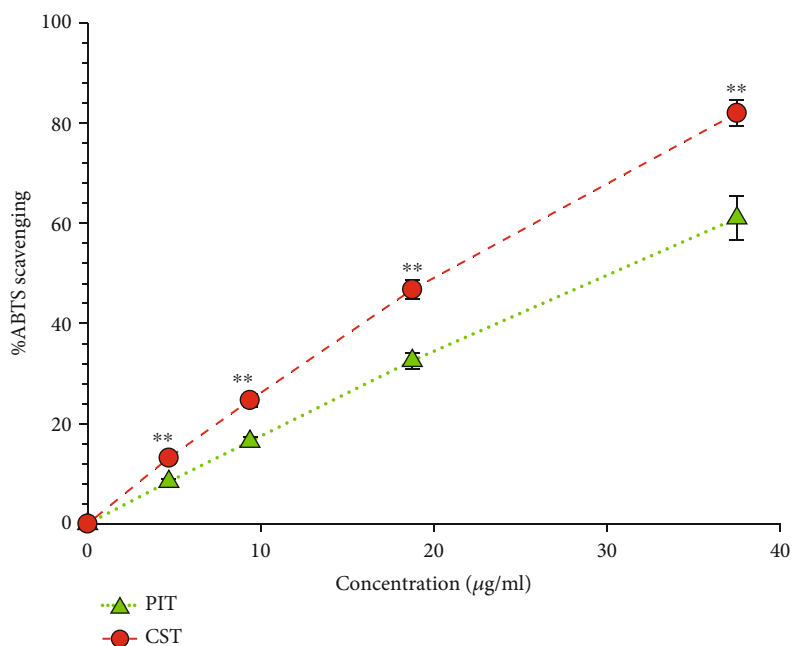


FIGURE 2: The ABTS radical scavenging activity. PIT: *P. indica* (L.) Less. tea; CST: *C. sinensis* tea at concentrations ranging from 0-40 µg/ml. The data represent the percentage of ABTS inhibition. Each value represents mean ± S.D. (n = 6). \*\* indicates a significant difference between groups at P < 0.01.

at higher concentrations of both teas. The lag time of LDL oxidation was increased from 40 to 70 min at all strengths of testing teas. These results suggest that both teas have approximately similar LDL oxidation scavenging properties.

3.7. *Copper Induce LDL Oxidation Assay.* Isolated human LDL was incubated with either PIT or CST at 15 µg/ml and

challenged with Cu<sup>2+</sup>. The result was presented as MDA equivalence (nmol/mgprotein), which was calculated from the MDA calibration standard curve. Figure 7 showed that in the Cu<sup>2+</sup>-treated group, the MDA equivalence was continually increased by 210 min at 222.73 ± 2.22 nmol/mgprotein, while the PIT and CST treated group could almost entirely prevent Cu<sup>2+</sup> oxidation of human LDL.

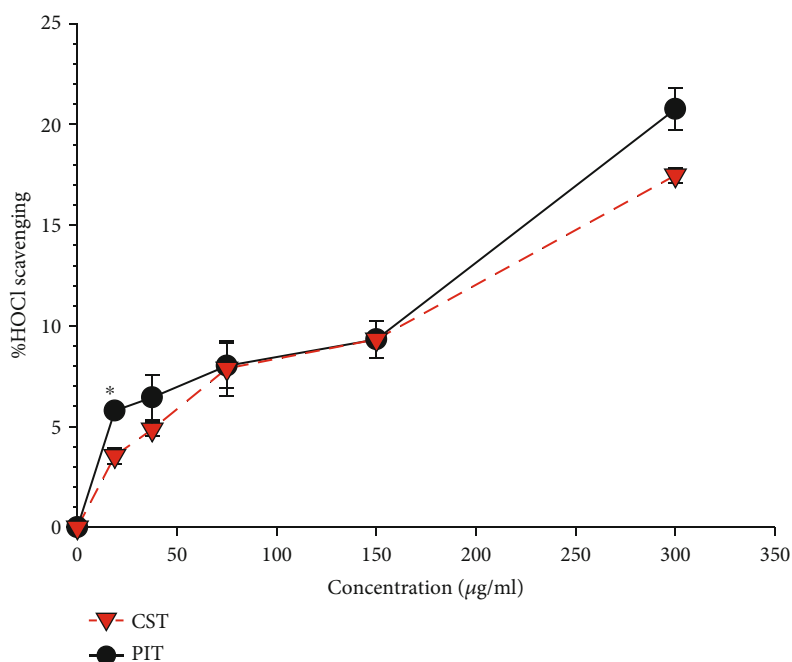


FIGURE 3: The hypochlorous acid radical scavenging activity. PIT: *P. indica* (L.) Less. tea; CST: *C. sinensis* tea at concentrations ranging from 0-300 µg/ml. The data represent the percentage of HOCl inhibition. Each value represents mean  $\pm$  S.E.M ( $n = 3$ ). \* indicates a significant difference between groups at  $P < 0.05$ .

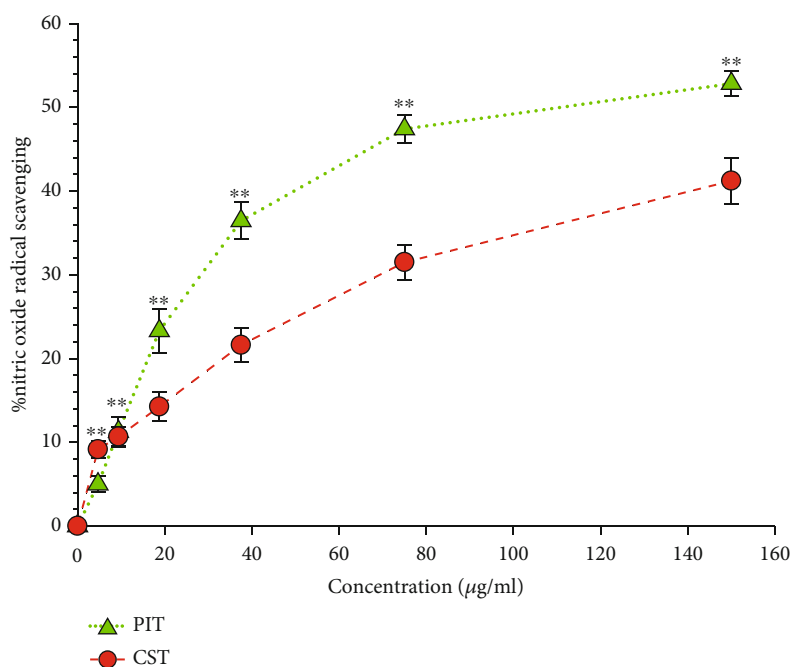


FIGURE 4: The nitric oxide radical scavenging activity. PIT: *P. indica* (L.) Less. tea; CST: *C. sinensis* tea at concentrations ranging from 0-150 µg/ml in various concentrations. The data represent the percentage of nitric oxide inhibition. Each value represents mean  $\pm$  S.D. ( $n = 6$ ). \*\* indicates a significant difference between groups at  $P < 0.01$ .

3.8. *SIN-1 Induce LDL Oxidation Assay.* SIN-1, which is an RNS generator, is used to induce LDL oxidation. Isolated human LDL was incubated with SIN-1 and tea extracts. The result expressed the RNS scavenging effect of both

PIT and CST at a dose of 15 µg/ml (Figure 8). PIT and CST displayed nearly similar properties and could decrease MDA concentration from  $86.73 \pm 2.55$  to  $20.41 \pm 2.55$  and  $23.81 \pm 3.90$  nmol/mgprotein, respectively.

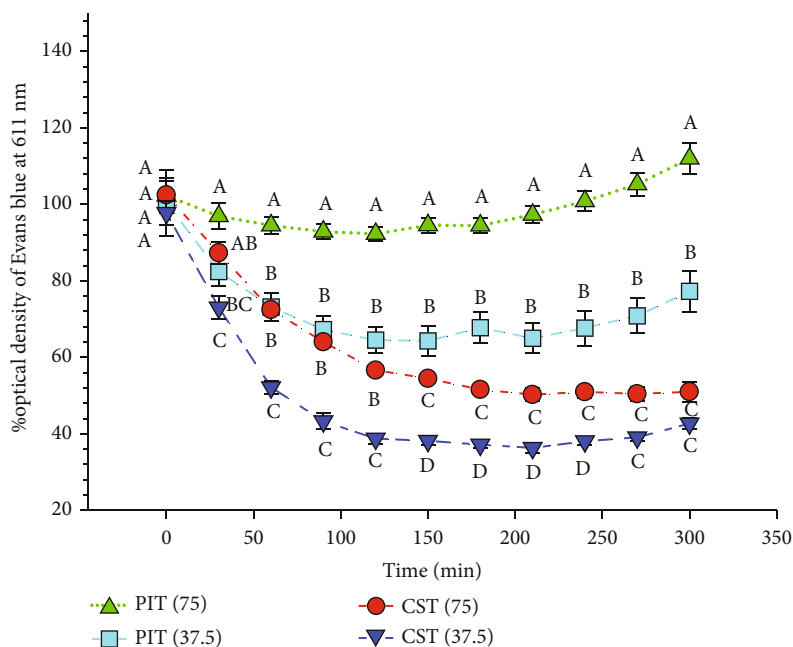


FIGURE 5: The peroxynitrite radical scavenging activity. PIT(75): *P. indica* (L.) Less. tea at 75  $\mu\text{g/ml}$ ; CST(75): *C. sinensis* tea at 75  $\mu\text{g/ml}$ . The data represent the percentage of the optical density of Evans blue at 611 nm at various times over 5 h. Means  $\pm$  S.E.M is illustrated for six replicates. Means with the same superscript are not significantly different from each other (Tukey's HSD test,  $P < 0.05$ ).

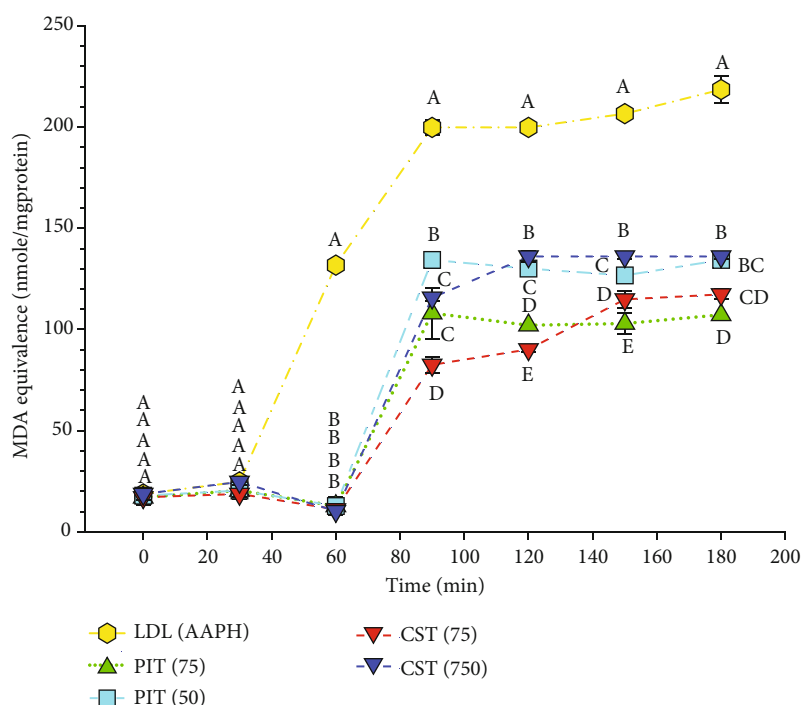


FIGURE 6: The AAPH induces LDL oxidation scavenging activity. LDL(AAPH): LDL-treated with 20 mM of AAPH; PIT(75): *P. indica* (L.) Less. tea at 75  $\mu\text{g/ml}$ ; CST(75): *C. sinensis* tea at 75  $\mu\text{g/ml}$ . The data represent the MDA equivalence at various times over 3 h. Means  $\pm$  S.D. is illustrated for three replicates. Means with the same superscript are not significantly different from each other (Tukey's HSD test,  $P < 0.05$ ).

3.9. LC-MS/MS Analysis of PIT. In this experiment, ESI-MS analysis used negative ion mode and identified the chemical constituents by comparing the profiles with authentic stan-

dards using the Multiple Reaction Monitoring (MRM) modes. Two pairs of MRM transitions were selected at  $m/z$  353.1  $\rightarrow$  191.0 and 515  $\rightarrow$  353. Table 1 displayed that 4-CQ,

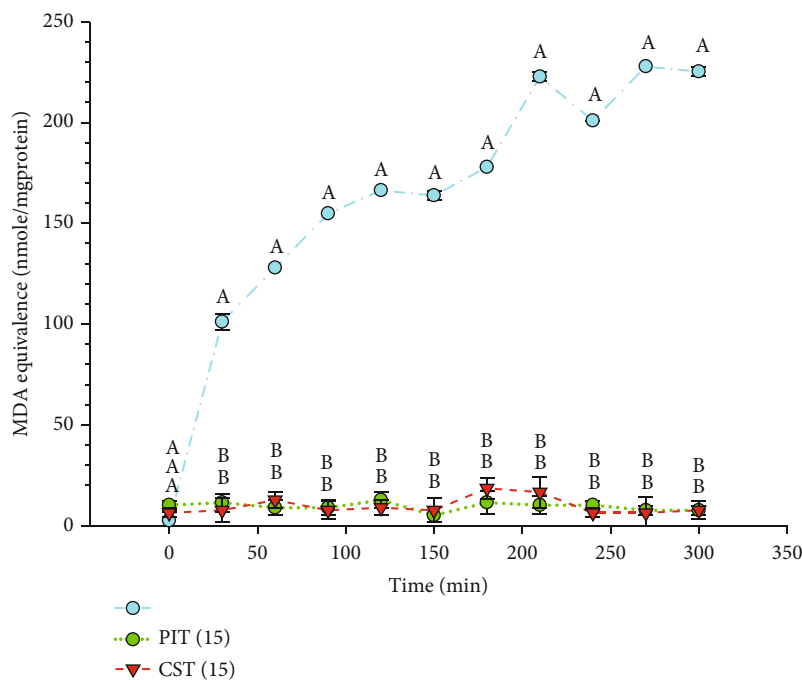


FIGURE 7: The copper induces LDL oxidation scavenging activity. LDL(Cu<sup>2+</sup>): LDL-treated with 40  $\mu$ M of copper sulfate; PIT(15): *P. indica* (L.) Less. tea at 15  $\mu$ g/ml; CST(15): *C. sinensis* tea at 15  $\mu$ g/ml. The data represent the MDA equivalence at various times over 5 h. Means  $\pm$  S.D. is illustrated for three replicates. Means with the same superscript are not significantly different from each other (Tukey's HSD test,  $P < 0.05$ ).

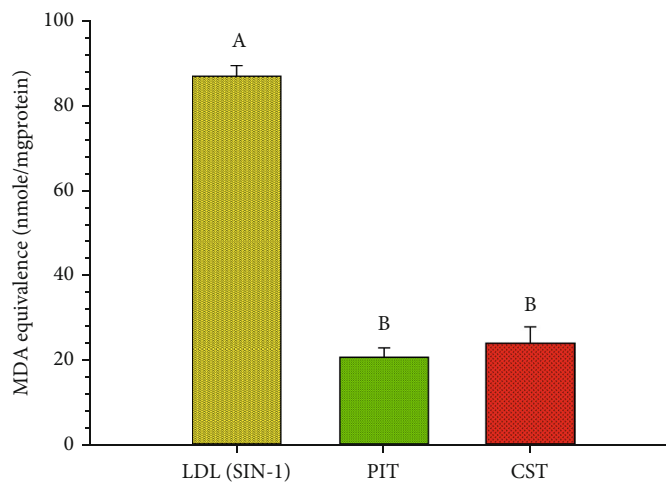


FIGURE 8: The SIN-1 induces LDL oxidation scavenging activity. LDL(SIN-1): LDL-treated with 1 mM of SIN-1; PIT: *P. indica* (L.) Less. tea at 15  $\mu$ g/ml; CST: *C. sinensis* tea at 15  $\mu$ g/ml. The data represent the MDA equivalence at 18 h. Means  $\pm$  S.D. is illustrated for three replicates. Means with the same superscript are not significantly different from each other (Tukey's HSD test,  $P < 0.05$ ).

5-CQ, 3,4-CQ, 3,5-CQ, and 4,5-CQ were detected in the PIT (Table 1). Moreover, the results showed a concentration of 3,5-CQ, which was the highest peak of the chromatogram at 169.93  $\mu$ g/ml of 1,500  $\mu$ g/ml PIT (data not showed).

#### 4. Discussion

Free radicals encompassing the ROS and RNS are derived from both endogenous sources (mitochondria, peroxisomes, endoplasmic reticulum, phagocytic cells, etc.) and exogenous sources (pollution, alcohol, tobacco smoke, heavy metals,

transition metals, industrial solvents, pesticides, certain drugs like halothane, paracetamol, and radiation) [31]. The imbalance between free radical and antioxidant systems can cause extensive damage to tissues and biomolecules [32], leading to various diseases especially degenerative diseases of aging such as cancer, immune-system decline, brain dysfunction, and cardiovascular [33]. Antioxidants derived from the diet assist physiological protective mechanisms in preventing damage from ROS or RNS. Dietary antioxidants can be derived from either supplements, fruit, vegetables, or herbal beverages, including teas. These are popular with

TABLE 1: The main chemical constituent of *P. indica* tea. was analyzed by Liquid Chromatography-Mass Spectrometer/Mass Spectrometer (LC-MS/MS).

Main chemical constituent	Detection
4-O-caffeoylquinic acid (4-CQ)	+
5-O-caffeoylquinic acid (5-CQ)	+
3,4-O-dicaffeoylquinic acid (3,4-CQ)	+
3,5-O-dicaffeoylquinic acid (3,5-CQ)	+
4,5-O-dicaffeoylquinic acid (4,5-CQ)	+

consumers and are widely used to prevent the diseases generated by free radicals [34, 35].

PIT has been used for health-promoting tea, but its antioxidative properties have not been fully explored. In this study, the antioxidative properties of PIT were compared with a well-known and commercially available green tea. The properties were investigated using well-established techniques, including DPPH and ABTS. The properties of the tea to scavenge peroxynitrite, RNS, and hypochlorous acid and prevent the oxidation of isolated human LDL were also undertaken.

DPPH radical scavenging assay has been widely used in the determination of the antioxidant activity of natural antioxidants from plant sources [28, 36]. This assay determines the reduction of DPPH radical by measuring the color changing from the violet color of DPPH radical to yellow of the nonradical DPPH derivative at 515 nm. Several studies indicated that CST scavenged the DPPH radical [37, 38]. Interestingly, PIT showed significantly stronger antioxidant activity in this assay than CST at all concentrations. These results are in substantial agreement with Srisook et al. [39] that hot water extract of *P. indica* leaves shows the DPPH radical scavenging activity ( $EC_{50}$  value =  $23.8 \pm 1.0 \mu\text{g/ml}$ ).

ABTS<sup>+</sup> radical cation decolorization assay was used to measure the antioxidant capacity of PIT compared to CST. These results provide evidence that CST could significantly reduce ABTS<sup>+</sup> radical better than PIT. This higher action of CST may come from various classes of polyphenols in CST, which act as a potent antioxidant for the ABTS<sup>+</sup> radical [40, 41].

Hypochlorous acid is a weak acid that could inactivate the antioxidant enzyme catalase by breaking down the heme prosthetic group [42]. Our results demonstrated that PIT was a higher potent hypochlorous acid scavenger than CST, which has been previously reported its hypochlorous acid scavenging capacity [43, 44].

Nitric oxide has an important role in several physiological processes like neural signal transmission, immune response, control vasodilation, and control of blood pressure [45, 46]. Nevertheless, the elevation of the nitric oxide causes inflammation and sustained levels of nitric oxide results in tissue toxicity and several pathological, including in vascular disease [47]. The present study examined the nitric oxide scavenging effect of PIT. Tsai et al. reported that CST had  $IC_{50}$  values of nitric oxide scavenging less than  $500 \mu\text{g/ml}$  and was proven to be a good nitric oxide suppressor [48].

Interestingly, our findings provide evidence that PIT displays significantly higher nitric oxide scavenging activity than CST.

Peroxynitrite, which is one of the nitrogen-containing species, is indicated as RNS. Excess peroxynitrite represents a crucial pathogenic mechanism in conditions, such as stroke, myocardial infarction, chronic heart failure, diabetes, circulatory shock, chronic inflammatory diseases, cancer, and neurodegenerative disorders [49]. PIT at a concentration of  $75 \mu\text{g/ml}$  had the capacity to fully inhibit the ability of peroxynitrite to bleach the color of Evan blue dye. Noticeably, PIT demonstrated significantly better peroxynitrite scavenging activity than the green tea preparation at the same concentration of  $75 \mu\text{g/ml}$ . Chung et al. reported that catechins, a galloyl group containing in green tea, inhibited peroxynitrite formation by both SIN-1 and scavenged peroxynitrite itself [50]. These findings lead us to believe that the effect of PIT on DPPH, ABTS, hypochlorous acid, nitric oxide, and peroxynitrite scavenging is better than CST.

LDL lipid oxidation is considered to be essential in the pathogenesis of atherosclerotic vascular diseases [51]. Several lines of evidence suggest that the important mechanisms of LDL lipid oxidation occur by ROS, RNS, and  $\text{Cu}^{2+}$  [52]. The natural compounds with anti-LDL oxidation activity could have some beneficial effects in the prevention of the disease [53, 54]. The investigation of anti-LDL oxidation activity *in vivo* can be measured *in vitro* by using whole plasma/serum [55]. In this study, we measured the LDL oxidation in AAPH,  $\text{Cu}^{2+}$ , and SIN-1 challenged isolated human LDL using the TBARS assay and presented the results by MDA equivalence. AAPH is a ROS generator that can initiate lipid peroxidation and protein oxidation in isolated LDL particles. One measure of antioxidative protection in LDL is the lag-time. The inclusion of both PIT and CST extended the lag time compared to the control. From the results, the antioxidative properties of CST observed toward AAPH activity are consistent with those of Liu et al. reported that the polyphenolic components derived from green tea leaves are effective antioxidants against AAPH-initiated photosensitized LDL oxidation [56]. Noticeably, our studies found that PIT demonstrated better AAPH scavenging activity than green tea from 150 min onward. Besides, the  $\text{Cu}^{2+}$  scavenging activity effect of both PIT and CST was also investigated. The results expressed that PIT could favorably inhibit  $\text{Cu}^{2+}$  induced LDL oxidation compared to CST. It was reported by Yokozawa et al. that green tea extract markedly delayed  $\text{Cu}^{2+}$  induced LDL oxidation with a dose-dependent pattern [57]. Green tea contains a rich array of polyphenols, and these may chelate the copper ions from solution, the same may be true for PIT. Moreover, SIN-1, which is an RNS generator, was also used to investigate LDL oxidation. The RNS, which is generated by SIN-1, was scavenged by both teas. This result is consistent with the Evan blue dye study presented in this study. These results suggest that PIT may have a role in preventing the initial stages of atherogenic events by inhibiting ROS, RNS, and  $\text{Cu}^{2+}$  induce lipid peroxidation.

The PIT has been investigated as the main chemical constituent by using LC-MS/MS technique. The result expressed that caffeoylquinic acid derivatives were the main chemical compositions of PIT. This result is in correspondence with

the study from Kongkiatpaiboon et al. [23], which reported that PIT contained six caffeoylquinic acid derivatives. Interestingly, caffeoylquinic acid derivatives were reported that they had potent antioxidant properties [58]. Caffeoylquinic acid derivatives from *Dipsacus asper* Wall (Dipsacaceae) showed antioxidant activity against free radical and Cu<sup>2+</sup>-mediated LDL oxidation. They may have an essential role in preventing the development and progression of atherosclerotic disease [58]. Furthermore, these derivatives also showed high DPPH-radical and peroxynitrite scavenging activity [59, 60]. These findings provide evidence that the antioxidative nature, which is free radical scavenging activities and anti-LDL oxidation, of PIT, is better than or approximately equal CST. These effects may be acted by caffeoylquinic acid derivatives rather than polyphenolic catechins found in CST [12].

## 5. Conclusion

The results of the present work show free radical scavenging activities and anti-LDL oxidation effects of PIT. The PIT has the potential to be developed as a health supplement product to provide antioxidants for atherosclerosis or other diseases associated with oxidative stress prevention. Further studies should focus on *in vivo* investigation, including pharmacokinetics, pharmacodynamic, efficacious, and safe dose in humans.

## Data Availability

The data used and analyzed in this study are available from the corresponding author on reasonable request.

## Conflicts of Interest

The authors declare that there is no conflict of interest regarding the publication of this paper.

## Authors' Contributions

KS performed the experiments and wrote the report. GE and GL designed the project, supervised the experiments, analyzed data, gave comments, and wrote the full manuscript. All authors have read and approved the final manuscript.

## Acknowledgments

The authors are indebted and grateful to the Thailand Research Fund, Newton Fund (PhD Placement grant for Scholars), and the Crystal Biotechnology Co., Ltd for the assistance in research fund support through The Research and Researchers for Industries Ph.D. scholarships (Grant No. PHD58I0015 Code 5712035). Commenting on the report's findings is responsible for a grant recipient; the Thailand Research Fund, Newton Fund, and the Crystal Biotechnology Co., Ltd. are not necessarily always agreeing.

## References

- [1] V. Dhawan, "Reactive oxygen and nitrogen species: general considerations," in *Studies on Respiratory Disorders*, pp. 27–47, Humana press, New York, 2014.
- [2] L. A. Pham-Huy, H. He, and C. Pham-Huy, "Free radicals, antioxidants in disease and health," *International Journal of Biomedical Science*, vol. 4, no. 2, p. 89, 2008.
- [3] H. Bartsch and J. Nair, "Chronic inflammation and oxidative stress in the genesis and perpetuation of cancer: role of lipid peroxidation, DNA damage, and repair," *Langenbeck's Archives of Surgery*, vol. 391, no. 5, pp. 499–510, 2006.
- [4] P. P. Tak, N. J. Zvaifler, D. R. Green, and G. S. Firestein, "Rheumatoid arthritis and p53: how oxidative stress might alter the course of inflammatory diseases," *Immunology Today*, vol. 21, no. 2, pp. 78–82, 2000.
- [5] E. R. Stadtman, "Role of oxidant species in aging," *Current Medicinal Chemistry*, vol. 11, no. 9, pp. 1105–1112, 2004.
- [6] S. Toyokuni, "Reactive oxygen species-induced molecular damage and its application in pathology," *Pathology International*, vol. 49, no. 2, pp. 91–102, 2002.
- [7] T. Bahorun, M. Soobrattee, V. Luximon-Ramma, and O. Aruoma, "Free radicals and antioxidants in cardiovascular health and disease," *Internet Journal of Medical Update*, vol. 1, no. 2, pp. 25–41, 2006.
- [8] P. Marchio, S. Guerra-Ojeda, J. M. Vila, M. Aldasoro, V. M. Victor, and M. D. Mauricio, "Targeting early atherosclerosis: a focus on oxidative stress and inflammation," *Oxidative Medicine and Cellular Longevity*, vol. 2019, 32 pages, 2019.
- [9] T. Yuan, T. Yang, H. Chen et al., "New insights into oxidative stress and inflammation during diabetes mellitus-accelerated atherosclerosis," *Redox Biology*, vol. 20, pp. 247–260, 2019.
- [10] J. L. Slavin and B. Lloyd, "Health benefits of fruits and vegetables," *Advances in Nutrition*, vol. 3, no. 4, pp. 506–516, 2012.
- [11] S. Li, S. K. Li, H. B. Li, X. R. Xu, G. F. Deng, and D. P. Xu, "Antioxidant capacities of herbal infusions," in *Processing and Impact on Antioxidants in Beverages*, pp. 41–50, 2014.
- [12] A. K. Atoui, A. Mansouri, G. Boskou, and P. Kefalas, "Tea and herbal infusions: their antioxidant activity and phenolic profile," *Food Chemistry*, vol. 89, no. 1, pp. 27–36, 2005.
- [13] B. Dimitrios, "Sources of natural phenolic antioxidants," *Trends in Food Science & Technology*, vol. 17, no. 9, pp. 505–512, 2006.
- [14] E. W. C. Chan, Y. Y. Lim, K. L. Chong, J. B. L. Tan, and S. K. Wong, "Antioxidant properties of tropical and temperate herbal teas," *Journal of Food Composition and Analysis*, vol. 23, no. 2, pp. 185–189, 2010.
- [15] A. Babu, V. Pon, and D. Liu, "Green tea catechins and cardiovascular health: an update," *Current Medicinal Chemistry*, vol. 15, no. 18, pp. 1840–1850, 2008.
- [16] Y. Miura, T. Chiba, I. Tomita et al., "Tea catechins prevent the development of atherosclerosis in apoprotein E-deficient mice," *The Journal of Nutrition*, vol. 131, no. 1, pp. 27–32, 2001.
- [17] S. I. Koo and S. K. Noh, "Green tea as inhibitor of the intestinal absorption of lipids: potential mechanism for its lipid-lowering effect," *The Journal of Nutritional Biochemistry*, vol. 18, no. 3, pp. 179–183, 2007.
- [18] S. Yan, H. Shao, Z. Zhou, Q. Wang, L. Zhao, and X. Yang, "Non-extractable polyphenols of green tea and their antioxidant, anti- $\alpha$ -glucosidase capacity, and release during *in vitro*



- digestion," *Journal of Functional Foods*, vol. 42, pp. 129–136, 2018.
- [19] C.-S. Rha, H. W. Jeong, S. Park, S. Lee, Y. S. Jung, and D.-O. Kim, "Antioxidative, anti-inflammatory, and anticancer effects of purified flavonol glycosides and aglycones in green tea," *Antioxidants*, vol. 8, no. 8, p. 278, 2019.
- [20] L. K. Leung, Y. Su, R. Chen, Z. Zhang, Y. Huang, and Z. Y. Chen, "Theaflavins in black tea and catechins in green tea are equally effective antioxidants," *The Journal of Nutrition*, vol. 131, no. 9, pp. 2248–2251, 2001.
- [21] C. Folch-Cano, C. Jullian, H. Speisky, and C. Olea-Azar, "Antioxidant activity of inclusion complexes of tea catechins with  $\beta$ -cyclodextrins by ORAC assays," *Food Research International*, vol. 43, no. 8, pp. 2039–2044, 2010.
- [22] K. Yamagata, "Protective effect of epigallocatechin gallate on endothelial disorders in atherosclerosis," *Journal of Cardiovascular Pharmacology*, vol. 75, no. 4, pp. 292–298, 2020.
- [23] S. Kongkiatpaiboon, S. Chewchinda, and B. Vongsak, "Optimization of extraction method and HPLC analysis of six caffeoylquinic acids in *Pluchea indica* leaves from different provenances in Thailand," *Revista Brasileira de Farmacognosia*, vol. 28, no. 2, pp. 145–150, 2018.
- [24] K. C. Pramanik, R. Biswas, A. Mitra, D. Bandyopadhyay, M. Mishra, and T. K. Chatterjee, "Tissue culture of the plant *Pluchea indica* (L.) Less. and evaluation of diuretic potential of its leaves," *Oriental Pharmacy and Experimental Medicine*, vol. 7, no. 2, pp. 197–204, 2007.
- [25] K. C. Pramanik, P. Bhattacharya, R. Biswas, D. Bandyopadhyay, M. Mishra, and T. Chatterjee, "Hypoglycemic and antihyperglycemic activity of leaf extract of *Pluchea indica* Less.," *Oriental Pharmacy and Experimental Medicine*, vol. 6, pp. 232–236, 2006.
- [26] D. Buapool, N. Mongkol, J. Chantimal, S. Roytrakul, E. Srisook, and K. Srisook, "Molecular mechanism of anti-inflammatory activity of *Pluchea indica* leaves in macrophages RAW 264.7 and its action in animal models of inflammation," *Journal of Ethnopharmacology*, vol. 146, no. 2, pp. 495–504, 2013.
- [27] P. S. Widyawati, C. H. Wijaya, P. S. Hardjosworo, and D. Sajuthi, "Volatile compounds of *Pluchea indica* Less and *Ocimum basilicum* Linn essential oil and potency as antioxidant," *Journal of Biosciences*, vol. 20, no. 3, pp. 117–126, 2013.
- [28] W. Brand-Williams, M.-E. Cuvelier, and C. Berset, "Use of a free radical method to evaluate antioxidant activity," *LWT-Food Science and Technology*, vol. 28, no. 1, pp. 25–30, 1995.
- [29] O. I. Aruoma and B. Halliwell, "Action of hypochlorous acid on the antioxidant protective enzymes superoxide dismutase, catalase and glutathione peroxidase," *Biochemical Journal*, vol. 248, no. 3, pp. 973–976, 1987.
- [30] J. M. Graham, J. A. Higgins, T. Gillott et al., "A novel method for the rapid separation of plasma lipoproteins using self-generating gradients of iodixanol," *Atherosclerosis*, vol. 124, no. 1, pp. 125–135, 1996.
- [31] A. Phaniendra, D. B. Jestadi, and L. Periyasamy, "Free radicals: properties, sources, targets, and their implication in various diseases," *Indian Journal of Clinical Biochemistry*, vol. 30, no. 1, pp. 11–26, 2015.
- [32] B. Halliwell and J. M. Gutteridge, *Free Radicals in Biology and Medicine*, Oxford university press, USA, 2015.
- [33] B. N. Ames, M. K. Shigenaga, and T. M. Hagen, "Oxidants, antioxidants, and the degenerative diseases of aging," *Proceedings of the National Academy of Sciences*, vol. 90, no. 17, pp. 7915–7922, 1993.
- [34] M. Wojcik, I. Burzynska-Pedziwiatr, and L. Wozniak, "A review of natural and synthetic antioxidants important for health and longevity," *Current Medicinal Chemistry*, vol. 17, no. 28, pp. 3262–3288, 2010.
- [35] Y. Fukushima, T. Ohie, Y. Yonekawa et al., "Coffee and green tea as a large source of antioxidant polyphenols in the Japanese population," *Journal of Agricultural and Food Chemistry*, vol. 57, no. 4, pp. 1253–1259, 2009.
- [36] G. C. Yen and P. D. Duh, "Scavenging effect of methanolic extracts of peanut hulls on free-radical and active-oxygen species," *Journal of Agricultural and Food Chemistry*, vol. 42, no. 3, pp. 629–632, 1994.
- [37] D. Bastos, L. Saldanha, R. Catharino et al., "Phenolic antioxidants identified by ESI-MS from yerba maté (*Ilex paraguariensis*) and green tea (*Camellia sinensis*) extracts," *Molecules*, vol. 12, no. 3, pp. 423–432, 2007.
- [38] R. Manian, N. Anusuya, P. Siddhuraju, and S. Manian, "The antioxidant activity and free radical scavenging potential of two different solvent extracts of *Camellia sinensis* (L.) O. Kuntz, *Ficus bengalensis* L. and *Ficus racemosa* L.," *Food Chemistry*, vol. 107, no. 3, pp. 1000–1007, 2008.
- [39] K. Srisook, D. Buapool, R. Boonbai, P. Simmasut, Y. Charoensuk, and E. Srisook, "Antioxidant and anti-inflammatory activities of hot water extract from *Pluchea indica* Less. herbal tea," *Journal of Medicinal Plants Research*, vol. 6, no. 23, pp. 4077–4408, 2012.
- [40] R. Tsao, "Chemistry and biochemistry of dietary polyphenols," *Nutrients*, vol. 2, no. 12, pp. 1231–1246, 2010.
- [41] L. S. Lee, S. H. Kim, Y. B. Kim, and Y. C. Kim, "Quantitative analysis of major constituents in green tea with different plucking periods and their antioxidant activity," *Molecules*, vol. 19, no. 7, pp. 9173–9186, 2014.
- [42] R. Sarkar, B. Hazra, S. Mandal, S. Biswas, and N. Mandal, "Assessment of *in vitro* antioxidant and free radical scavenging activity of *Cajanus cajan*," *Journal of Complementary and Integrative Medicine*, vol. 6, no. 1, p. 1248, 2009.
- [43] P. Valentão, E. Fernandes, F. Carvalho, P. Andrade, R. Seabra, and M. Bastos, "Hydroxyl radical and hypochlorous acid scavenging activity of small centaury (*Centaureum erythraea*) infusion. A comparative study with green tea (*Camellia sinensis*)," *Phytomedicine*, vol. 10, no. 6-7, pp. 517–522, 2003.
- [44] C. Cabrera, R. Artacho, and R. Giménez, "Beneficial effects of green tea—a review," *Journal of the American College of Nutrition*, vol. 25, no. 2, pp. 79–99, 2006.
- [45] D. Rees, R. Palmer, and S. Moncada, "Role of endothelium-derived nitric oxide in the regulation of blood pressure," *Proceedings of the National Academy of Sciences*, vol. 86, no. 9, pp. 3375–3378, 1989.
- [46] R. M. Palmer, A. Ferrige, and S. Moncada, "Nitric oxide release accounts for the biological activity of endothelium-derived relaxing factor," *Nature*, vol. 327, no. 6122, pp. 524–526, 1987.
- [47] H. Li and U. Förstermann, "Nitric oxide in the pathogenesis of vascular disease," *The Journal of Pathology*, vol. 190, no. 3, pp. 244–254, 2000.
- [48] P. J. Tsai, T. H. Tsai, C. H. Yu, and S. C. Ho, "Comparison of NO-scavenging and NO-suppressing activities of different herbal teas with those of green tea," *Food Chemistry*, vol. 103, no. 1, pp. 181–187, 2007.

- [49] P. Pacher, J. S. Beckman, and L. Liaudet, "Nitric oxide and peroxynitrite in health and disease," *Physiological Reviews*, vol. 87, no. 1, pp. 315–424, 2007.
- [50] H. Y. Chung, T. Yokozawa, D. Y. Soung, I. S. Kye, J. K. No, and B. S. Baek, "Peroxynitrite-scavenging activity of green tea tannin," *Journal of Agricultural and Food Chemistry*, vol. 46, no. 11, pp. 4484–4486, 1998.
- [51] H. Yoshida and R. Kisugi, "Mechanisms of LDL oxidation," *Clinica Chimica Acta*, vol. 411, no. 23-24, pp. 1875–1882, 2010.
- [52] R. Govindarajan, M. Vijayakumar, and P. Pushpangadan, "Antioxidant approach to disease management and the role of 'Rasayana' herbs of Ayurveda," *Journal of Ethnopharmacology*, vol. 99, no. 2, pp. 165–178, 2005.
- [53] B. Fuhrman and M. Aviram, "Flavonoids protect LDL from oxidation and attenuate atherosclerosis," *Current Opinion in Lipidology*, vol. 12, no. 1, pp. 41–48, 2001.
- [54] W. J. Craig, "Health-promoting properties of common herbs," *The American Journal of Clinical Nutrition*, vol. 70, no. 3, pp. 491s–499s, 1999.
- [55] T. Spranger, B. Finckh, R. Fingerhut, A. Kohlschütter, U. Beisiegel, and A. Kontush, "How different constituents of human plasma and low density lipoprotein determine plasma oxidizability by copper," *Chemistry and Physics of Lipids*, vol. 91, no. 1, pp. 39–52, 1998.
- [56] Z. Q. Liu, L. P. Ma, B. Zhou, L. Yang, and Z. L. Liu, "Antioxidative effects of green tea polyphenols on free radical initiated and photosensitized peroxidation of human low density lipoprotein," *Chemistry and Physics of Lipids*, vol. 106, no. 1, pp. 53–63, 2000.
- [57] T. Yokozawa and E. Dong, "Influence of green tea and its three major components upon low-density lipoprotein oxidation," *Experimental and Toxicologic Pathology*, vol. 49, no. 5, pp. 329–335, 1997.
- [58] T. M. Hung, M. Na, P. T. Thuong et al., "Antioxidant activity of caffeoyl quinic acid derivatives from the roots of *Dipsacus asper* Wall," *Journal of Ethnopharmacology*, vol. 108, no. 2, pp. 188–192, 2006.
- [59] M. S. Islam, M. Yoshimoto, and O. Yamakawa, "Distribution and physiological functions of caffeoylquinic acid derivatives in leaves of sweetpotato genotypes," *Journal of Food Science*, vol. 68, no. 1, pp. 111–116, 2003.
- [60] H. J. Park, A. Nugroho, J. H. Lee et al., "HPLC analysis of caffeoylquinic acids in the extract of *Cacalia firma* and peroxynitrite scavenging effect," *Korean Journal of Pharmacognosy*, vol. 40, no. 4, pp. 365–369, 2009.

## Research Article

# Role of Oxidation-Dependent CaMKII Activation in the Genesis of Abnormal Action Potentials in Atrial Cardiomyocytes: A Simulation Study

Na Zhao <sup>1</sup>, Qince Li <sup>1,2</sup>, Haibo Sui <sup>1</sup> and Henggui Zhang <sup>1,2,3</sup>

<sup>1</sup>School of Computer Science and Technology, Harbin Institute of Technology, Harbin 150000, China

<sup>2</sup>Peng Cheng Laboratory, Shenzhen 518000, China

<sup>3</sup>School of Physics and Astronomy, University of Manchester, Manchester M13 9PL, UK

Correspondence should be addressed to Qince Li; [qinceli@hit.edu.cn](mailto:qinceli@hit.edu.cn) and Henggui Zhang; [henggui.zhang@manchester.ac.uk](mailto:henggui.zhang@manchester.ac.uk)

Received 25 October 2019; Revised 20 May 2020; Accepted 2 June 2020; Published 22 June 2020

Guest Editor: Roland E. Akhigbe

Copyright © 2020 Na Zhao et al. This is an open access article distributed under the Creative Commons Attribution License, which permits unrestricted use, distribution, and reproduction in any medium, provided the original work is properly cited.

Atrial fibrillation is a common cardiac arrhythmia with an increasing incidence rate. Particularly for the aging population, understanding the underlying mechanisms of atrial arrhythmia is important in designing clinical treatment. Recently, experiments have shown that atrial arrhythmia is associated with oxidative stress. In this study, an atrial cell model including oxidative-dependent  $\text{Ca}^{2+}$ /calmodulin- (CaM-) dependent protein kinase II (CaMKII) activation was developed to explore the intrinsic mechanisms of atrial arrhythmia induced by oxidative stress. The simulation results showed that oxidative stress caused early afterdepolarizations (EADs) of action potentials by altering the dynamics of transmembrane currents and intracellular calcium cycling. Oxidative stress gradually elevated the concentration of calcium ions in the cytoplasm by enhancing the L-type  $\text{Ca}^{2+}$  current and sarcoplasmic reticulum (SR) calcium release. Owing to increased intracellular calcium concentration, the inward  $\text{Na}^+/\text{Ca}^{2+}$  exchange current was elevated which slowed down the repolarization of the action potential. Thus, the action potential was prolonged and the L-type  $\text{Ca}^{2+}$  current was reactivated, resulting in the genesis of EAD. Furthermore, based on the atrial single-cell model, a two-dimensional (2D) ideal tissue model was developed to explore the effect of oxidative stress on the electrical excitation wave conduction in 2D tissue. Simulation results demonstrated that, under oxidative stress conditions, EAD hindered the conduction of electrical excitation and caused an unstable spiral wave, which could disrupt normal cardiac rhythm and cause atrial arrhythmia. This study showed the effects of excess reactive oxygen species on calcium cycling and action potential in atrial myocytes and provided insights regarding atrial arrhythmia induced by oxidative stress.

## 1. Introduction

Atrial fibrillation (AF) is the most common cardiac arrhythmia [1–3]. To design optimal treatment of AF, the mechanisms underlying AF need to be better understood. Both reactive oxygen species (ROS) and  $\text{Ca}^{2+}$ /calmodulin- (CaM-) dependent protein kinase II (CaMKII) have been shown to be associated with the development of cardiac arrhythmias [4, 5]. The kinase CaMKII is ubiquitously expressed in the cardiomyocytes [4, 6]. It is involved in numerous cellular signaling cascades, such as phosphorylation of L-type  $\text{Ca}^{2+}$  channels [7–9],  $\text{Na}^+$  channels [10, 11], ryanodine receptors

(RyRs) [12–18], and phospholamban (PLB) [12, 17, 19, 20]. Overexpression of CaMKII increases fractional sarcoplasmic reticulum (SR)  $\text{Ca}^{2+}$  release [13] and SR  $\text{Ca}^{2+}$  leakage [16], enhancing the activation of RyRs during both systole and diastole. As mentioned, it has been reported that CaMKII can also phosphorylate PLB [20]. In its unphosphorylated state, PLB acts as an endogenous inhibitor of sarco/endoplasmic reticulum  $\text{Ca}^{2+}$ -ATPase (SERCA). Therefore, phosphorylation of PLB by CaMKII will enhance SERCA activity [21]. In addition to SR  $\text{Ca}^{2+}$  dynamics, many ion channels show CaMKII-dependent phosphorylation. Phosphorylation of L-type  $\text{Ca}^{2+}$  channels induced by CaMKII is associated with

Ca<sup>2+</sup>-dependent Ca<sup>2+</sup> current facilitation [22, 23]; CaMKII-dependent phosphorylation of Na<sup>+</sup> channels may cause an increase in the late sodium current, which predisposes cardiomyocytes to arrhythmias [10, 11].

Conventionally, CaMKII is activated by Ca<sup>2+</sup>-bound calmodulin (Ca-CaM). Recently, a novel mechanism of CaMKII activation, which is ROS dependent, has been revealed [19, 24]. Previous studies have demonstrated that oxidative stress is closely associated with cardiac arrhythmias through alteration of the electrical activity and intracellular calcium dynamics of cardiac myocytes [25–27]. Oxidative stress is the main manifestation of cell metabolism disorders with excessive ROS. This oxidation-induced CaMKII activation is in relation to apoptosis [28], sinus node dysfunction [29], heart injury [30], and arrhythmias [31]. Although both ROS and CaMKII are associated with cardiac arrhythmias, the role of oxidative-dependent CaMKII activation in the development of atrial arrhythmias is not yet well understood.

In previous studies of cardiac arrhythmias, *in vivo* and *in vitro* experiments provide insights into mechanisms underlying arrhythmogenesis [5, 31]. However, these approaches have several limitations. For example, it is difficult to record the electrophysiological properties at different physical scales (from subcellular level to organ level) at the same time in one experiment. The electrophysiological properties recorded from different experiments, such as patch clamp and optical mapping, might be affected by gradual changes in cell or tissue properties. In addition to *in vivo* and *in vitro* experiments, a common method widely used in cardiac arrhythmia studies is *in silico* modeling. In this study, to simulate the effects of ROS-dependent CaMKII activation on regulations of intracellular Ca<sup>2+</sup> and ionic currents, we first developed a Markov chain model of CaMKII, including both the autophosphorylation and oxidation pathways. Then, the effect of CaMKII on related proteins and ion channels was integrated to establish a computational model of the atrial cell to simulate changes in the electrophysiology under oxidative stress conditions, including ion currents, ion concentrations, calcium cycling, and transmembrane potential. Finally, the two-dimensional (2D) spiral wave was induced and the electrical excitation propagation was analyzed under normal and oxidative stress conditions.

## 2. Methods

**2.1. CaMKII Model, including Both Autophosphorylation and Oxidation-Dependent Activation.** A six-state Markov chain model of CaMKII developed by our previous study of Zhang et al. [32] was incorporated into a human atrial model developed by Grandi et al. [33] to simulate autophosphorylation- and oxidation-dependent CaMKII activation.

The CaMKII monomer consists of three domains (an association domain, a regulatory domain, and a catalytic domain). When CaMca4 (one calmodulin bound with four Ca<sup>2+</sup>) binds to the regulatory domain, the catalytic domain will be exposed, leading to CaMKII activation. In this state, CaMKII can be further autophosphorylated or oxidized, producing a long-lasting activation, even if CaMca4 dissociates from CaMKII. Finally, CaMKII is fully deactivated by

dephosphorylation with protein phosphatases, or reduction with methionine sulfoxide reductases (MsrA). Based on the four-state model of CaMKII developed by Chiba et al. [34], two oxidized states, with and without CaMca4 binding with CaMKII, were added (see Figure S1 in the Supplementary Material for illustration), corresponding to the conformational change of oxidation-dependent CaMKII activation. Since there is no evidence to show that oxidation and autophosphorylation can occur at the same time, in this study, autophosphorylation and oxidation of CaMKII were treated as two independent processes [24]. The CaMKII autophosphorylation was based on the model developed by Chiba et al. [34]. The parameters of CaMKII oxidation were fitted to the experimental data recorded by Erickson et al. [24]. The detailed parameters of the CaMKII model are listed in Table S1 in the Supplementary Material.

**2.2. Effects of CaMKII on Ion Channels.** Previous studies showed that the ion channels influenced by CaMKII included the fast Na<sup>+</sup> current ( $I_{Na}$ ) and the L-type Ca<sup>2+</sup> current ( $I_{CaL}$ ) [7–11]. According to the method developed by O'Hara et al. [35], the current of each ion channel ( $I$ ) was divided into two parts:

$$I = (1 - \Phi)I_{base} + \Phi I_{CaMK}, \quad (1)$$

where  $I_{base}$  is the part of ion channel current not affected by CaMKII,  $I_{CaMK}$  is the part of ion channel current affected by CaMKII, and  $\Phi$  is the proportion affected by CaMKII using the following equations:

$$\Phi = \frac{CaMK_{active}}{CaMK_{active} + K_{CaMK}}, \quad (2)$$

where  $CaMK_{active}$  is the fraction of CaMKII activation and  $K_{CaMKII}$  is the Michaelis constant with the same value in O'Hara et al. [35]. For  $I_{Na}$ , the time constant of gate  $j$  was slowed down by 1.46-fold [32]. And for  $I_{CaL}$ , experimental data showed that CaMKII activation produced an increased amplitude and a slowed inactivation of  $I_{CaL}$  [36]. Therefore, in this study, the time constant of gate  $f$  was slowed down by 1.5-fold and the part of  $I_{CaL}$  affected by CaMKII was increased by  $\Delta I_{CaL,CaMK}$  shown in Equation (3).

$$\Delta I_{CaL,CaMK} = \frac{CaMKII_{active}^7}{CaMKII_{active}^7 + K_{CaMK}}. \quad (3)$$

**2.3. Effects of CaMKII on Ca<sup>2+</sup> Cycling.** Both RyR and PLB are primary regulatory proteins, controlling SR Ca<sup>2+</sup> release and uptake; these are crucial processes, maintaining the balance of intracellular Ca<sup>2+</sup>. CaMKII activation-induced RyR phosphorylation can increase RyR opening probability and SR Ca<sup>2+</sup> release. CaMKII activation-induced PLB phosphorylation can reduce SERCA inhibition, increasing SR Ca<sup>2+</sup> uptake during diastole. The RyR and PLB models developed by Soltis and Saucerman [37] were used to simulate the effects of CaMKII activation on intracellular Ca<sup>2+</sup> cycling. The rate constants controlling RyR opening ( $k_{oSRCa}$ ) and SR leakage

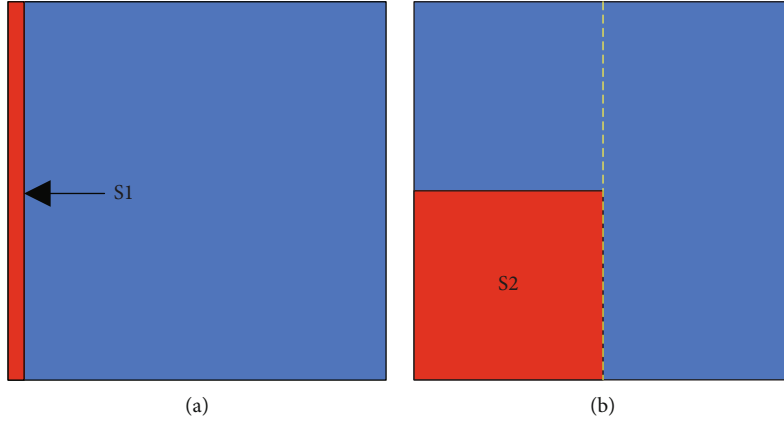


FIGURE 1: The S1–S2 protocol used in 2D simulations. The red bar in (a) and the red square in (b) represent the regions where S1 and S2 stimuli were applied.

( $k_{leak}$ ) were modified (Equations (4) and (5)) under CaMKII activation to increase RyR opening in both systolic and diastolic conditions. Meanwhile, the half maximal saturation constant of SERCA ( $K_{mf}$ ) was modified (Equation (6)) to mimic the phenomenon of increased SERCA pump calcium sensitivity, which is induced by Thr17 phosphorylation of PLB under CaMKII activation.

$$k_{oSRCa} = \left( \frac{[RyR_{2815p}]}{[RyR_{Tot}]} \frac{20}{3} - \frac{1}{3} \right) \frac{k_{oCa}}{k_{CaSR}}, \quad (4)$$

$$k_{leak} = 2.5 \frac{[RyR_{2815p}]}{[RyR_{Tot}]} + 0.5, \quad (5)$$

$$K_{mf} = K_{mf} \left( 1 - 0.5 \frac{[PLB_{T17p}]}{[PLB_{Tot}]} \right). \quad (6)$$

**2.4. Single Atrial Cell Model.** The cell membrane of an atrial myocyte was mimicked as an electrical circuit. The AP in a human atrial cell was calculated using the following ordinary differential equation [33]:

$$C_m \frac{dV_m}{dt} = -I_{ion} + I_{stim}, \quad (7)$$

where  $C_m$  is the cell capacitance,  $V_m$  is the transmembrane voltage,  $t$  is time,  $I_{ion}$  is the total transmembrane ionic current, and  $I_{stim}$  is the stimulus current.  $I_{ion}$  was calculated as

$$I_{ion} = I_{Na} + I_{Nabk} + I_{to} + I_{Kur} + I_{Kr} + I_{Ks} + I_{K1} + I_{NaK} + I_{CaL} + I_{Cabk} + I_{pCa} + I_{NCX} + I_{ClCa} + I_{Clbk}, \quad (8)$$

where  $I_{Na}$  is the fast  $Na^+$  current,  $I_{Nabk}$  is the background  $Na^+$  current,  $I_{to}$  is the transient outward  $K^+$  current,  $I_{Kur}$  is the ultrarapid delayed rectifier  $K^+$  current,  $I_{Kr}$  is the rapid activating  $K^+$  current,  $I_{Ks}$  is the slowly activating  $K^+$  current,  $I_{K1}$  is the inward rectifier  $K^+$  current,  $I_{NaK}$  is the  $Na^+/K^+$  pump current,  $I_{CaL}$  is the L-type  $Ca^{2+}$  current,  $I_{Cabk}$  is the

background  $Ca^{2+}$  current,  $I_{pCa}$  is the sarcolemmal  $Ca^{2+}$  pump current,  $I_{NCX}$  is the  $Na^+/Ca^{2+}$  exchange current,  $I_{ClCa}$  is the  $Ca^{2+}$ -activated  $Cl^-$  current, and  $I_{Clbk}$  is the background  $Cl^-$  current.

In this study, 0.5, 1, and 2 Hz stimulation frequencies were used to investigate the frequency dependency of CaMKII activation. Action potentials of atrial cells were produced by applying a stimulus current with an amplitude of  $-12.5$  pA/pF and a duration of 5 ms. The time step used in the simulation was 0.1 ms using the CVODE solver of the SUite of Nonlinear and Differential/ALgebraic equation Solvers (SUNDIALS) to solve initial value problems for ordinary differential equation systems. These simulation results were consistent with the ones using forward Euler with a time step of 0.005 ms. Under the control condition, the value of  $H_2O_2$  in the CaMKII model was  $0 \mu M$ , and the one was  $200 \mu M$  under the oxidative stress condition. To ensure that the model reached a quasistable steady state, the simulations were carried out for more than 50 s under the control condition and 150 s under the oxidative stress condition.

**2.5. Excitation Wave Conduction in 2D Tissue.** In this study, a monodomain model was used for 2D simulations in an ideal square tissue. The excitation wave propagation was simulated using the following equation:

$$\frac{\partial V_m}{\partial t} = -\frac{I_{ion}}{C_m} + \nabla \cdot (\mathbf{D} \nabla V_m), \quad (9)$$

where  $\mathbf{D}$  is the diffusion tensor describing the conductivity of the tissue and  $\nabla$  is the spatial gradient operator.

In 2D simulations, the 2D ideal isotropic tissue was constructed as a sheet of  $1000 \times 1000$  nodes to investigate the stability of the spiral waves, as used in [38]. The time step  $\Delta t$  was set at 0.005 ms, and the space step  $\Delta x$  was 0.1 mm along both direction axes, as used in [39]. The S1–S2 stimulation protocol was used to produce spiral waves. An S1 stimulus was applied to the five column nodes on the left side to induce a plane wave (Figure 1(a)). After the nodes in the middle line (the dashed line in Figure 1(b)) reached the end point of

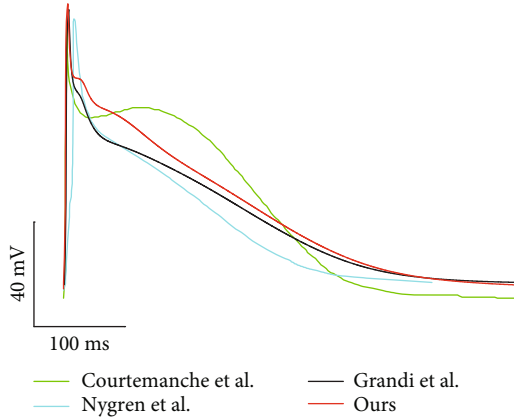


FIGURE 2: Action potential traces produced by our simulation and previous mathematical models and experiments at 1 Hz. Traces labeled “Courtemanche et al.,” “Nygren et al.,” and “Grandi et al.” were reproduced from mathematical models [33, 43, 44].

the refractory period, an S2 stimulus was applied in the left lower quadrant to induce a spiral wave (Figure 1(b)).

The conduction velocity (CV) was measured using the following equation:

$$CV = \frac{x_2 - x_1}{t_2 - t_1}, \quad (10)$$

where  $x_1$  and  $x_2$  are the positions and  $t_1$  and  $t_2$  are the times when the excitation reaches the two recording points. In 2D simulation, the tissue was isotropic and the diffusion tensor ( $D$ ) along both direction axes was set to  $0.029 \text{ mm}^2/\text{ms}$  to produce a CV of  $69 \text{ cm/s}$  in control conditions, which was consistent with the CV ( $70 \text{ cm/s}$ ) previously used for human atrial tissue simulation [40–42].

### 3. Results

**3.1. Electrophysiological Properties of a Single Atrial Cell under Control Conditions.** The action potential (AP) in a single-cell model was generated by applying a series of 1 Hz stimuli. The time trace of the simulated AP is presented in Figure 2, along with other AP traces from previous mathematical models [33, 43, 44]. The resting membrane potential (RMP), maximum upstroke velocity ( $dV/dt_{\max}$ ), action potential amplitude (APA), and action potential duration at 90% repolarization ( $APD_{90}$ ) were measured as  $-75.2 \text{ mV}$ ,  $160 \text{ mV/ms}$ ,  $110 \text{ mV}$ , and  $312 \text{ ms}$ , respectively. These parameters were consistent with previous models developed by Grandi et al. [33], Courtemanche et al. [43], and Nygren et al. [44], and  $APD_{90}$  was within the scope of previously reported experimental data [45–48], as listed in Table 1.

To further validate the model, the ionic currents and intracellular calcium cycling process were investigated and compared with those from the model of Grandi et al. [33] at 1 Hz, as shown in Figure 3. These results demonstrated an elevation in the repolarization phase of the AP and, therefore, a longer action potential duration (APD) in our model (Figure 3(a)). This was attributed to the change in  $I_{\text{CaL}}$ . In our model,  $I_{\text{CaL}}$  showed a larger amplitude and a slowed

TABLE 1: Comparison of action potential characteristics.

Model and experimental data	RMP (mV)	$dV/dt_{\max}$ (mV/ms)	APA (mV)	$APD_{90}$ (ms)
Courtemanche et al. [43]	-79.5	216	106	297
Nygren et al. [44]	-76.4	116	103.8	245
Grandi et al. [33]	-74.5	135	105	294
Our model	-75.2	160	110	312
Dawodu et al. [45]	—	—	—	$361 \pm 71$
Katoh et al. [46]	—	—	—	$255 \pm 39$
Bosch et al. [47]	—	—	—	$255 \pm 45$
Kim et al. [48]	—	—	—	$258 \pm 25$

inactivation (Figure 3(b)), which was consistent with the effect of CaMKII activation on  $I_{\text{CaL}}$  [36]. In addition to the AP, the variation in  $I_{\text{CaL}}$  altered intracellular calcium regulation, as  $I_{\text{CaL}}$  was the main influx of intracellular  $\text{Ca}^{2+}$ . The increase in  $I_{\text{CaL}}$  caused a larger  $\text{Ca}^{2+}$  influx, leading to a larger SR  $\text{Ca}^{2+}$  release (Figure 3(c)) and thus a larger intracellular  $\text{Ca}^{2+}$  concentration (Figure 3(d)). The accumulation of intracellular  $\text{Ca}^{2+}$  finally caused an elevation in the concentration of SR  $\text{Ca}^{2+}$  (Figure 3(e)). Interestingly, the peak inward  $I_{\text{NCX}}$  in our model declined even when the intracellular  $\text{Ca}^{2+}$  concentration increased (Figure 3(f)). This may be explained by the fact that the elevation of the membrane potential during the repolarization phase suppressed the inward  $\text{Na}^+$  flux and decreased  $I_{\text{NCX}}$ .

To justify the increase of intracellular  $\text{Ca}^{2+}$  concentration in our model, the  $\text{Ca}^{2+}$  concentration was compared with previous studies. The calcium transient amplitude in our model was  $\sim 0.53 \mu\text{M}$ , which was consistent with the studies of Courtemanche et al. and Colman et al. ( $0.45\text{--}0.55 \mu\text{M}$ ) [43, 49], although the  $\text{Ca}^{2+}$  transient amplitude in the study of Nygren et al. was reported to be even larger ( $\sim 1.2 \mu\text{M}$ ) [44].

The variations in  $I_{\text{CaL}}$  and intracellular calcium cycling were caused by adding the effect of CaMKII activation in our model. Previous studies demonstrated that CaMKII activation was significantly influenced by pacing frequencies. In our simulation, CaMKII activation and intracellular  $\text{Ca}^{2+}$  dynamics were investigated at 0.5, 1, and 2 Hz. Figure 4(a) shows that the fraction of CaMKII activation increased with increasing pacing rate. Meanwhile, the time required for CaMKII activation was also decreased, indicating a faster activation at a higher pacing rate (Figure 4(a)). The frequency-dependent activation of CaMKII was mainly due to the intracellular  $\text{Ca}^{2+}$  concentration. With increasing pacing rate, both RyR  $\text{Ca}^{2+}$  release and intracellular  $\text{Ca}^{2+}$  concentration increased (Figure 4(b)), causing an increase in CaMCA4 and, therefore, augmenting CaMKII activation.

**3.2. Electrophysiological Properties of a Single Atrial Cell under Oxidative Stress Conditions.** The simulation results showed that an EAD was induced in the AP under conditions of oxidative stress at a pacing rate of 1 Hz (Figure 5(a)). In this case, the elevated ROS concentration ( $0.2 \text{ mM}$ ) induced a significant increase in CaMKII activation (Figure 5(b)).

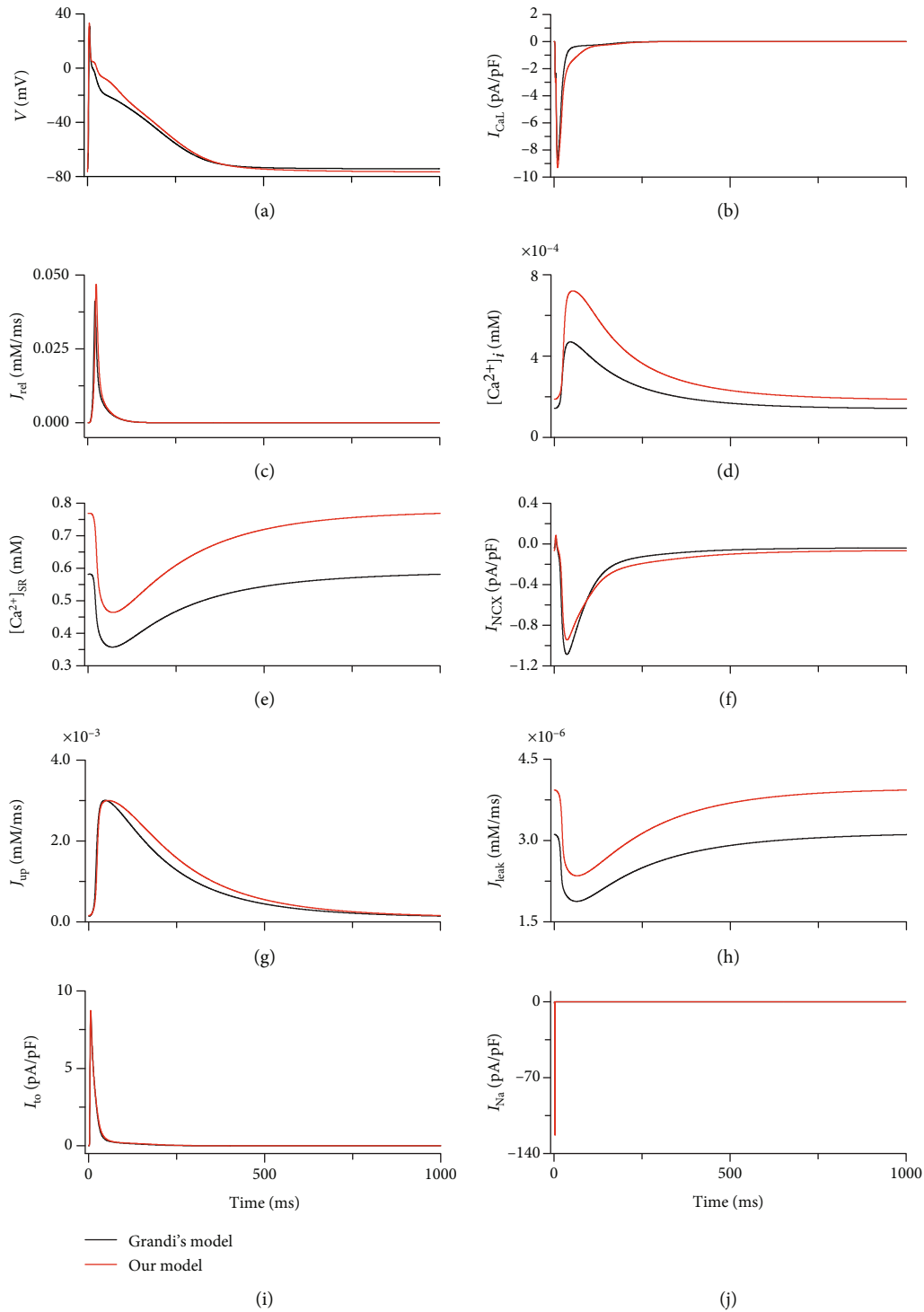


FIGURE 3: Traces of AP, ionic currents, and calcium cycling produced by our model (red) and the model of Grandi et al. [33] (black). (a) AP. (b)  $I_{CaL}$ . (c) SR  $Ca^{2+}$  release ( $J_{rel}$ ). (d) intracellular  $Ca^{2+}$  concentration ( $[Ca^{2+}]_i$ ). (e) SR  $Ca^{2+}$  concentration ( $[Ca^{2+}]_{SR}$ ). (f)  $I_{NCX}$ . (g) SR  $Ca^{2+}$  reuptake ( $J_{up}$ ). (h) SR  $Ca^{2+}$  leakage ( $J_{leak}$ ). (i)  $I_{to}$ . (j)  $I_{Na}$ .

ROS-enhanced CaMKII activation further enlarged  $I_{CaL}$ ,  $I_{NCX}$ , fraction of RyR phosphorylation, and fraction of PLB phosphorylation (Figures 5(c)–5(f)). Under oxidative stress conditions, the intracellular  $Ca^{2+}$  dynamics were remarkably changed. Enhanced RyR and PLB phosphorylation caused significant increases in  $J_{rel}$ ,  $J_{up}$ , and  $J_{leak}$  (Figures 5(g)–5(i)),

which further induced a dramatic increase in intracellular  $Ca^{2+}$  concentration (Figure 5(j)) and a decrease in minimum SR  $Ca^{2+}$  (Figure 5(k)). However, there was no obvious change in the intracellular  $Na^+$  concentration (Figure 5(l)).

As CaMKII activation showed frequency-dependent behavior, ROS-induced EADs are rate dependent as well.

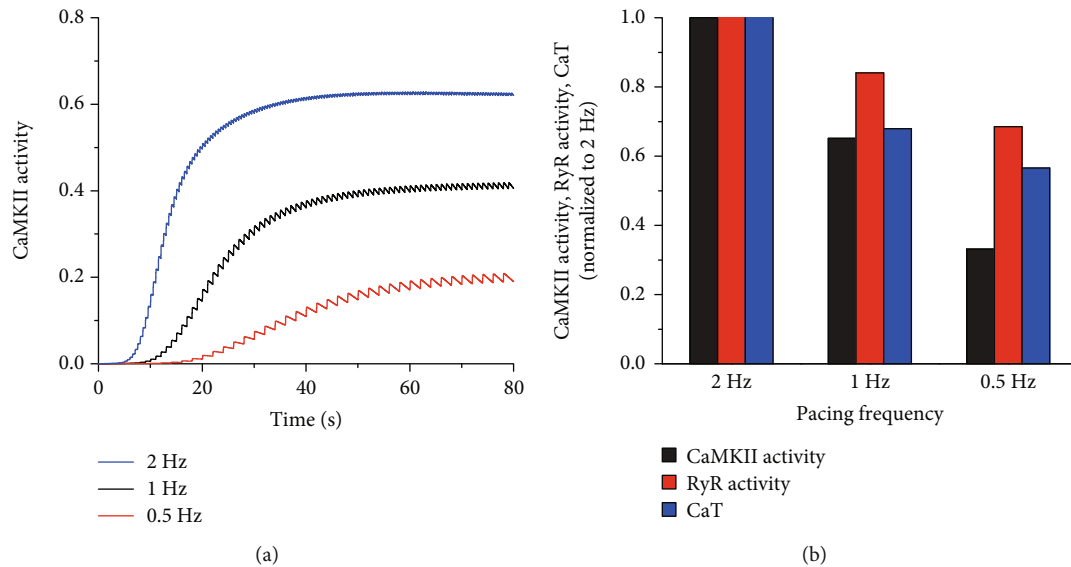


FIGURE 4: Frequency-dependent activation of CaMKII. (a) CaMKII activation curves at 0.5, 1, and 2 Hz in 80 s. (b) Normalized CaMKII activation, RyR calcium release (RyR Activity), and intracellular  $\text{Ca}^{2+}$  transient (CaT) to 2 Hz at 0.5, 1, and 2 Hz.

Under oxidative stress conditions, the occurrence of EADs in 50 s became more prominent with decreasing pacing rate, as shown in Figure 6. Under control conditions, the CaMKII activation (without ROS-induced activation) gradually decreased with decreasing pacing rate (Figure 4(b)). This meant that more CaMKII could be activated by ROS under oxidative conditions at low pacing rates. Consequently, the CaMKII activation induced by ROS gradually increased with decreasing pacing rate (green bars in Figure 6). Therefore, under oxidative stress conditions, more EADs were induced at low pacing rates.

**3.3. Mechanisms Underlying the Genesis of EAD under Oxidative Stress Conditions.** In the case of EAD,  $I_{\text{CaL}}$  and  $I_{\text{NCX}}$  were the main currents significantly influenced by oxidative stress. Blocking  $I_{\text{CaL}}$  at the point of  $I_{\text{CaL}}$  reactivation abolished EAD (data not shown), implying that  $I_{\text{CaL}}$  was a main factor contributing to the genesis of EAD. However, blocking  $I_{\text{NCX}}$  did not guarantee elimination of EAD. Figure 7 indicated the effects of blocking  $I_{\text{NCX}}$  at different times from the point of  $I_{\text{CaL}}$  reactivation (70 ms) to the time of the peak of EAD (350 ms). With the delay in blocking  $I_{\text{NCX}}$  (Figure 7(a)), the reactivation of  $I_{\text{CaL}}$  became more prominent (Figure 7(b)) and the APD gradually increased (Figure 7(c)). When blocking  $I_{\text{NCX}}$  in the interval 70–210 ms, the reactivation of  $I_{\text{CaL}}$  did not induce AP depolarization and therefore abolished EAD. On blocking  $I_{\text{NCX}}$  during the interval 210–280 ms, the enlarged reactivation of  $I_{\text{CaL}}$  started to transfer AP repolarization to depolarization. However, in this time interval, AP depolarization was not obvious and no EAD was induced. When blocking  $I_{\text{NCX}}$  during the interval 280–350 ms, the reactivation of  $I_{\text{CaL}}$  was able to induce AP depolarization. Consequently, in this time interval, blocking  $I_{\text{NCX}}$  could not eliminate EAD (Figure 7(c)). Therefore,  $I_{\text{NCX}}$  played an important role in  $I_{\text{CaL}}$  reactivation and thus in triggering EAD.

In our model,  $I_{\text{NCX}}$  was not directly regulated by ROS. As the main efflux of intracellular  $\text{Ca}^{2+}$ ,  $I_{\text{NCX}}$  was regulated by intracellular  $\text{Ca}^{2+}$  concentration;  $\text{Ca}^{2+}$  cycling was another important process affected by ROS-induced CaMKII activation. Three factors associated with intracellular cycling in our model were directly regulated by ROS-induced CaMKII activation, namely,  $I_{\text{CaL}}$ ,  $J_{\text{rel}}$ , and  $J_{\text{up}}$ . Under oxidative stress conditions, intracellular  $\text{Ca}^{2+}$  concentration significantly increased (Figure 5(j)). To investigate the role of  $[\text{Ca}^{2+}]_i$  regulation in the genesis of EAD, decreased  $I_{\text{CaL}}$ , reduced  $J_{\text{rel}}$ , and enhanced  $J_{\text{up}}$  were independently applied to reduce the  $[\text{Ca}^{2+}]_i$  under oxidative stress conditions, as shown in Figure 8. Figure 8(a) shows that decreasing  $I_{\text{CaL}}$  by 10% abolished EAD. This was due not only to  $[\text{Ca}^{2+}]_i$  decline but also to a decrease in  $I_{\text{CaL}}$  reactivation. Reducing SR  $\text{Ca}^{2+}$  release postponed the occurrence of EAD but did not successfully eliminate EAD (Figure 8(b)). Although a reduction in SR  $\text{Ca}^{2+}$  release temporarily reduced  $[\text{Ca}^{2+}]_i$ , it caused  $\text{Ca}^{2+}$  accumulation in SR, which finally induced  $[\text{Ca}^{2+}]_i$  elevation (data not shown) and EAD. Increasing SR  $\text{Ca}^{2+}$  uptake by 10% had a similar effect to that of reducing SR calcium release (Figure 8(c)). Nonetheless, further increasing  $J_{\text{up}}$  by 20%–30% abolished EAD. In these two cases, the SR  $\text{Ca}^{2+}$  uptake and release reached a new balance and maintained  $[\text{Ca}^{2+}]_i$  and  $[\text{Ca}^{2+}]_{\text{SR}}$  at a steady state (data not shown).

**3.4. Effect of Oxidative Stress on Excitation Wave Propagation in 2D Tissue.** The excitation wave propagation was investigated in 2D ideal tissue under control and oxidative stress conditions. Spiral waves were induced using the S1–S2 protocol. Under control conditions with the S1–S2 interval of 550 ms, a stationary spiral wave was produced, with its tip anchored in the central region of the square tissue, as shown in Figure 9. Under oxidative stress conditions, the ROS concentration was set to 0.2 mM for all nodes in the tissue. In this



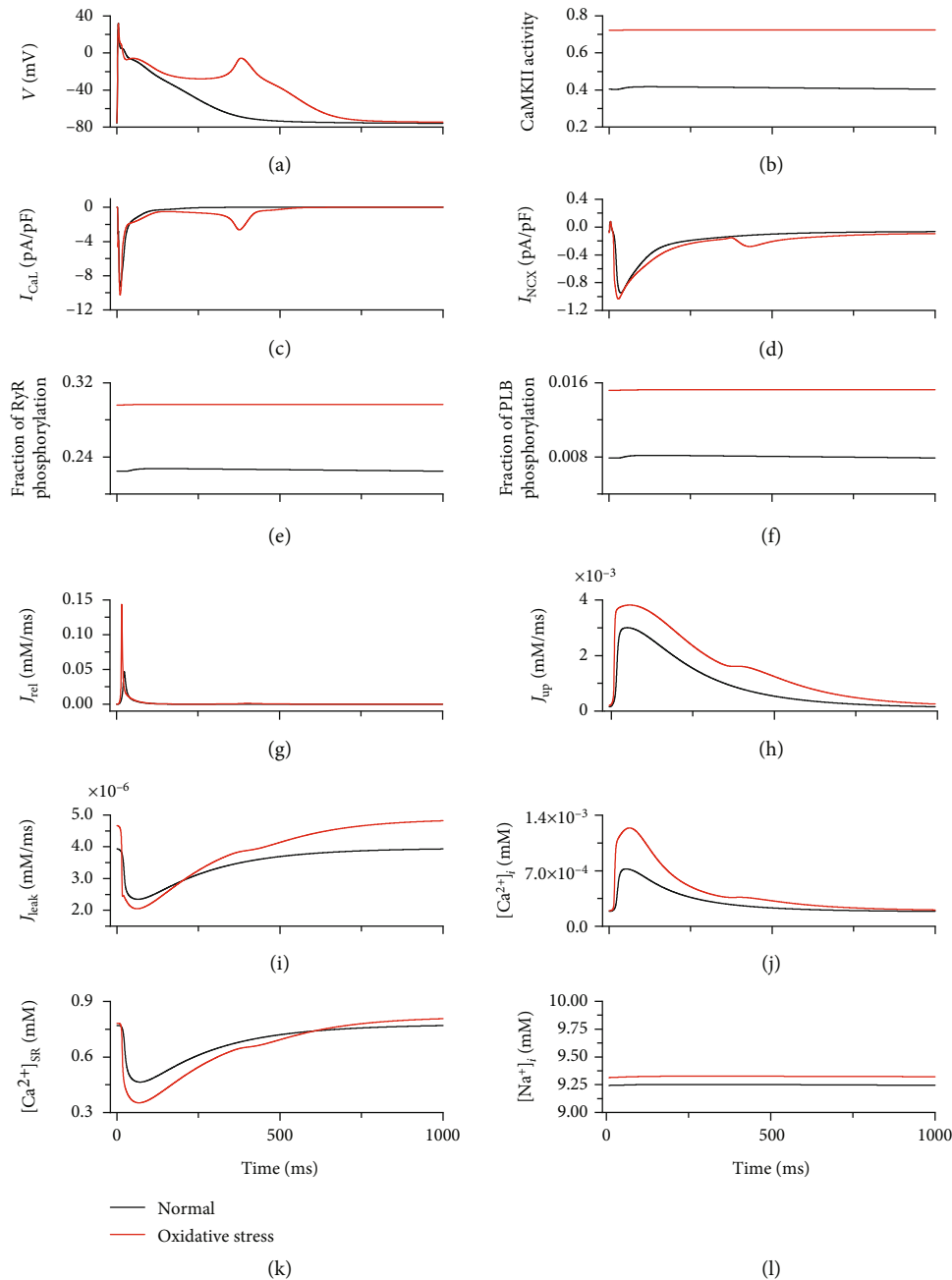


FIGURE 5: Traces of AP, ionic currents, and calcium cycling under normal (black) and oxidative stress (red) conditions. (a) AP. (b) CaMKII activity. (c)  $I_{CaL}$ . (d)  $I_{NCX}$ . (e) Fraction of RyR phosphorylation. (f) Fraction of PLB phosphorylation. (g)  $J_{rel}$ . (h)  $J_{up}$ . (i)  $J_{leak}$ . (j)  $[Ca^{2+}]_i$ . (k)  $[Ca^{2+}]_{SR}$ . (l) Intracellular  $Na^+$  concentration ( $[Na^+]_i$ ).

case with the S1–S2 interval of 730 ms, a nonstationary spiral wave was induced. As the EAD was induced under this condition, the region to which the S2 stimulus was applied showed a prolonged depolarization (Figure 10, 1125 ms) and a second wavefront was induced at 1450 ms, as shown in Figure 10. When the wavefronts reached the region to which the S2 stimulus was applied (Figure 10, 1650 ms), the nodes were not fully repolarized, owing to the prolonged APD induced by EAD. Therefore, the excitation wave propagation was suppressed (Figure 10, 1650 ms). Finally, the tip of the spiral wave wandered across the tissue and pro-

duced a nonstationary spiral wave. When oxidative stress only occurred in the right third of the tissue, the spatial heterogeneity further aggravated the instability of the nonstationary spiral wave and gave rise to a breakup of the spiral wave (data not shown).

#### 4. Discussion

In this study, the effects of ROS-dependent CaMKII activation on regulations of intracellular  $Ca^{2+}$  and ionic currents were investigated *in silico* using the updated human atrial cell

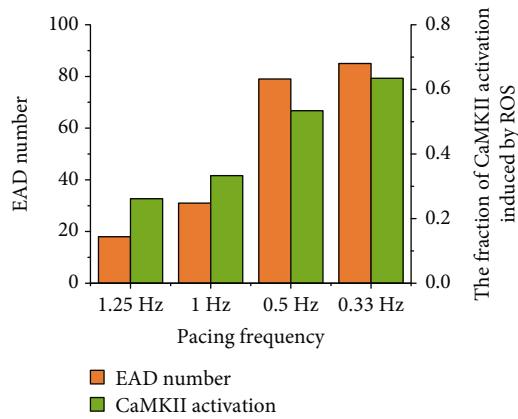


FIGURE 6: Number of EAD occurring in the same duration (orange) and the fraction of CaMKII activation induced by ROS (green) at different pacing rates under oxidative stress conditions.

model including the CaMKII model with autophosphorylation- and oxidation-dependent activation at the single-cell level and 2D tissue model. Our major findings follow: (i) A new Markov chain model of CaMKII, including both the autophosphorylation and oxidation pathways, was developed, and the effects of CaMKII on ion channels and  $\text{Ca}^{2+}$  cycling were incorporated into the computational model of the atrial myocyte. (ii) The mechanisms of oxidative stress-induced EADs in atrial cells were thoroughly examined which are helpful to further understand or investigate the mechanisms underlying oxidative stress-induced AF. The simulation results at the single-cell level illustrated that oxidative stress resulted in EADs of the AP at the normal pacing rate of 1 Hz. It was contributed by reactivation of  $I_{\text{CaL}}$  and intracellular  $\text{Ca}^{2+}$  elevation induced by CaMKII activation under oxidative stress conditions. (iii) The 2D simulations provide insights into reentry in atrial tissue under the oxidative stress condition, which plays significant roles in AF mechanisms. In 2D simulation, oxidative stress aggravated the instability of the excitation wave and gave rise to a non-stationary spiral wave, owing to the EAD induced by oxidative stress hindering the electrical conduction.

**4.1. Model Development of ROS-Dependent CaMKII Activation.** Previous experimental studies have revealed that both ROS and CaMKII are associated with the development of atrial arrhythmia [4, 5]. In addition, it has recently been reported that CaMKII can keep persistent activity by oxidation [24]. However, the role of ROS-dependent CaMKII activation in the genesis of atrial fibrillation is not yet well understood. In this study, we developed a computational model of human atrial cell including both ROS-dependent and autophosphorylation-dependent CaMKII activation to investigate effects of CaMKII activation on atrial electrophysiology under oxidative stress condition. In this CaMKII model, a pathway of ROS-dependent CaMKII activation was introduced which was different from previous CaMKII models only including the autophosphorylation-dependent CaMKII activation [34, 35, 50]. Christensen et al. [39] also developed a model of CaMKII activity including oxidation and autophosphorylation activation pathways. However, dif-

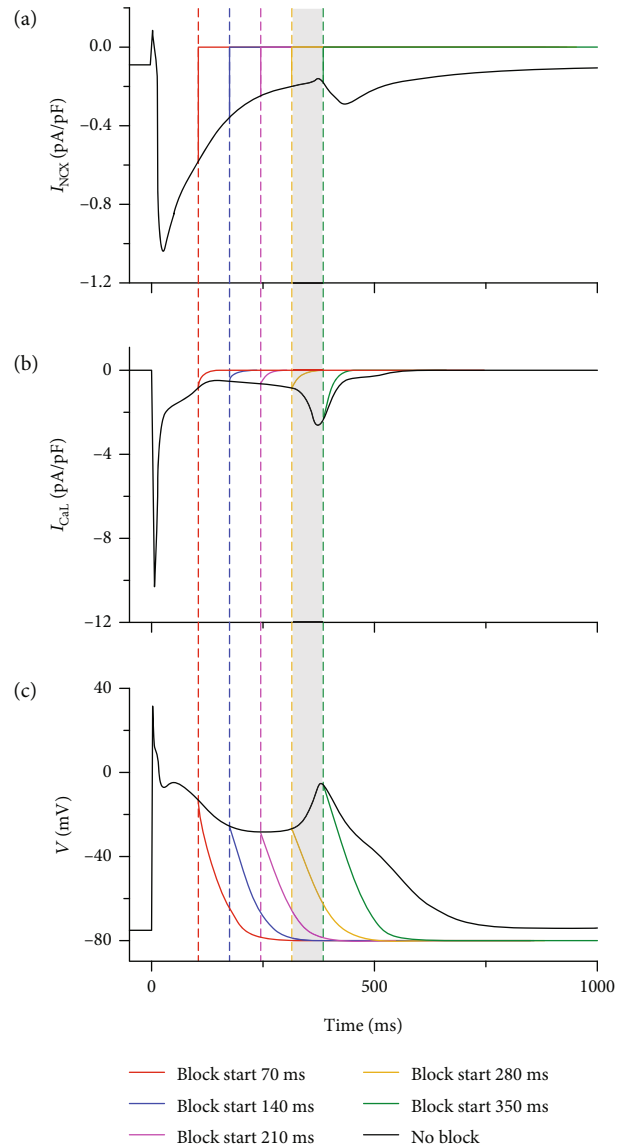


FIGURE 7: Effects of blocking  $I_{\text{NCX}}$  at different times on the genesis of EAD under oxidative stress condition: (a)  $I_{\text{NCX}}$ . (b)  $I_{\text{CaL}}$ . (c) AP. The gray box represents the time interval during which EAD can occur while blocking  $I_{\text{NCX}}$ .

ferent from their model, the oxidation and autophosphorylation activation pathways in our six-state CaMKII are mutual independence, implying that there is no such a state with both oxidation and autophosphorylation activation simultaneously. This fact is consistent with the experimental observations reported in [24].

The effect of CaMKII on  $I_{\text{Na}}$ ,  $I_{\text{CaL}}$ , RyR, and PLB was integrated into the human atrial myocyte model, producing action potential characteristics (such as RMP,  $dV/dt_{\text{max}}$ , APA,  $\text{APD}_{90}$ , and the calcium transient amplitude) consistent with previous models and experimental data of human atrial myocytes [33, 43–49] (Figure 2 and Table 1).

**4.2. Mechanisms Underlying the Genesis of EAD under Oxidative Stress Conditions.** The generation of EADs

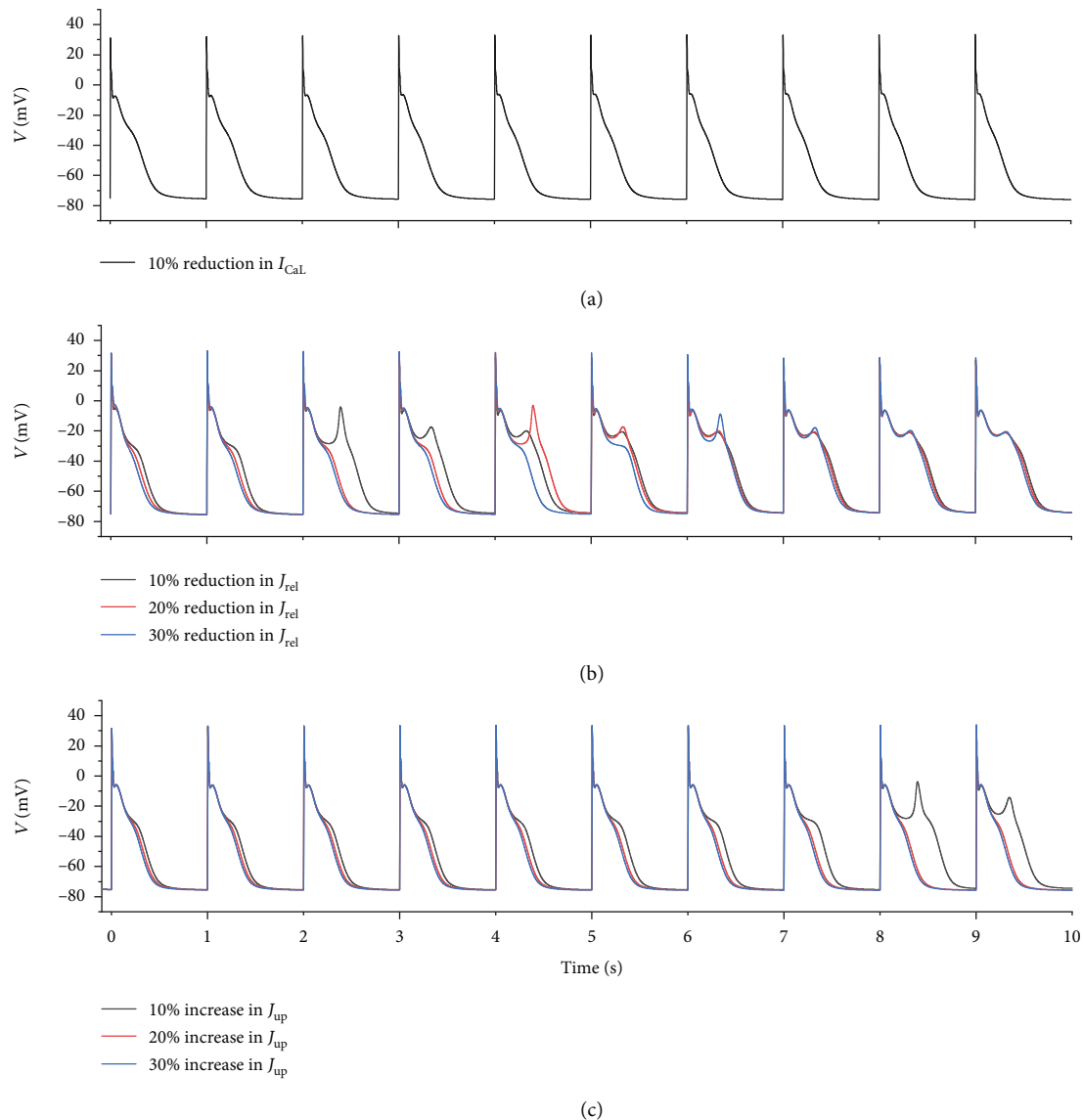


FIGURE 8: Effect of (a) reducing  $I_{CaL}$  by 10%, (b) reducing  $J_{rel}$  by 10%, 20%, and 30%, and (c) increasing  $J_{up}$  by 10%, 20%, and 30% on the genesis of EAD under oxidative stress conditions.

associated with ectopic (triggered) activity can be contributed by CaMKII activation [51–55]. Animal experiments have shown that oxidative stress can promote EADs in the ventricle of guinea pigs and rabbits [56]. Therefore, this study explored the intrinsic mechanisms of EADs associated with atrial arrhythmia induced by oxidative stress, using the developed CaMKII model.

First, simulation results demonstrated that the characteristics of AP and calcium cycling generated by our model were consistent with previous computational and experimental studies [43–49]. After model validation, the role of oxidation-dependent CaMKII activation on the AP was investigated in a single atrial cell model. The simulation results demonstrated that, under oxidative stress conditions, increasing ROS concentrations in the cytoplasm enhanced CaMKII activation and consequently augmented  $I_{CaL}$ , RyR phosphorylation, and PLB phosphorylation (Figures 5(c),

5(e), and (f)), inducing an enhanced  $Ca^{2+}$  influx, a larger SR  $Ca^{2+}$  release, and a promoted SR  $Ca^{2+}$  uptake (Figures 5(g) and 5(h)). These effects generated a remarkable elevation in intracellular  $Ca^{2+}$  concentration and therefore enlarged  $I_{NCX}$  via promoted  $Ca^{2+}$  extrusion (Figure 5(d)).  $I_{NCX}$  augmentation provided a depolarization component to counterbalance the repolarization reserve and prolong the APD. The elevated and prolonged AP in phase 3 gradually caused reactivation of  $I_{CaL}$  (Figure 5(c)), which ultimately induced action potential depolarization and produced EAD (Figure 5(a)), consistent with previous studies [57–59].

In this process, as  $I_{CaL}$  was the direct depolarization current inducing EAD, blocking  $I_{CaL}$  completely abolished EAD. However, blocking  $I_{NCX}$  at different time points had different effects on EAD. If  $I_{NCX}$  was blocked before  $I_{CaL}$  reactivation could induce AP depolarization, EAD was eliminated (Figure 7). This phenomenon suggested that  $I_{NCX}$

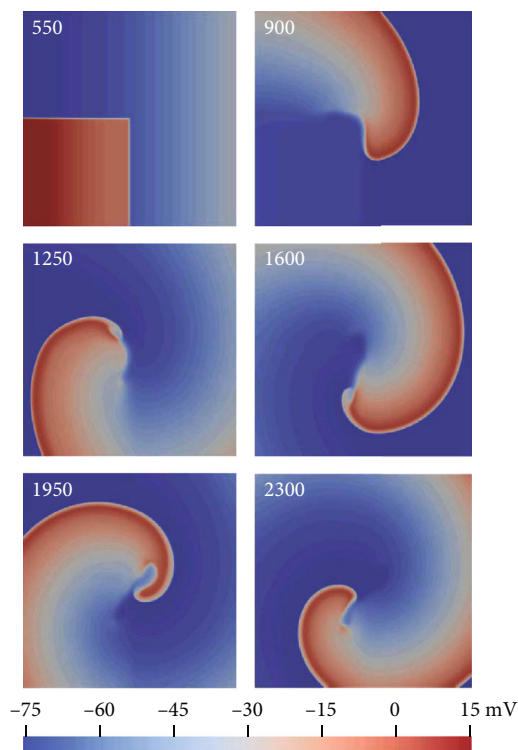


FIGURE 9: Spiral wave induced under control conditions using the S1–S2 protocol. The number in each panel represents the recording time.

augmentation acted as a trigger of  $I_{CaL}$  reactivation. EAD can be induced only when the trigger is large enough. Under oxidative stress condition, ROS elevation did not affect  $I_{NCX}$  directly and the increase of  $[Ca^{2+}]_i$  primarily accounted for  $I_{NCX}$  augmentation. Therefore, the effects of ROS-induced CaMKII activation on intracellular calcium cycling also played a crucial role in the genesis of EAD.

To examine the role of ROS-induced  $[Ca^{2+}]_i$  elevation in the genesis of EAD,  $Ca^{2+}$  influx and SR  $Ca^{2+}$  release and uptake were modified to reduce ROS-induced  $[Ca^{2+}]_i$  elevation. First,  $I_{CaL}$  was reduced by 10% to inhibit  $Ca^{2+}$  influx, causing a decline of  $[Ca^{2+}]_i$ . Together with the decreased reactivation of  $I_{CaL}$ , the  $[Ca^{2+}]_i$  decline caused by reducing  $I_{CaL}$  abolished EAD (Figure 8(a)). Second, partial inhibition of SR  $Ca^{2+}$  release (by 10%–30%) temporarily reduced  $[Ca^{2+}]_i$ . However, inhibition of SR  $Ca^{2+}$  release gradually caused SR  $Ca^{2+}$  accumulation and ultimately gave rise to further  $[Ca^{2+}]_i$  elevation, which accounted for the fact that partial inhibition of SR  $Ca^{2+}$  release could only postpone the occurrence of EAD but could not abolish EAD (Figure 8(b)). Increasing SR  $Ca^{2+}$  uptake by 10% had a similar effect to partial inhibition of SR  $Ca^{2+}$  release. Interestingly, on further increasing SR  $Ca^{2+}$  uptake by 20% and 30%,  $[Ca^{2+}]_i$  declined and EAD was abolished. This phenomenon might be attributed to a new balance of increased SR  $Ca^{2+}$  uptake and ROS-induced  $[Ca^{2+}]_i$  release (Figure 8(c)). Therefore, the dynamic balance between SR  $Ca^{2+}$  release and uptake is the key factor in maintaining  $[Ca^{2+}]_i$  at a steady state.

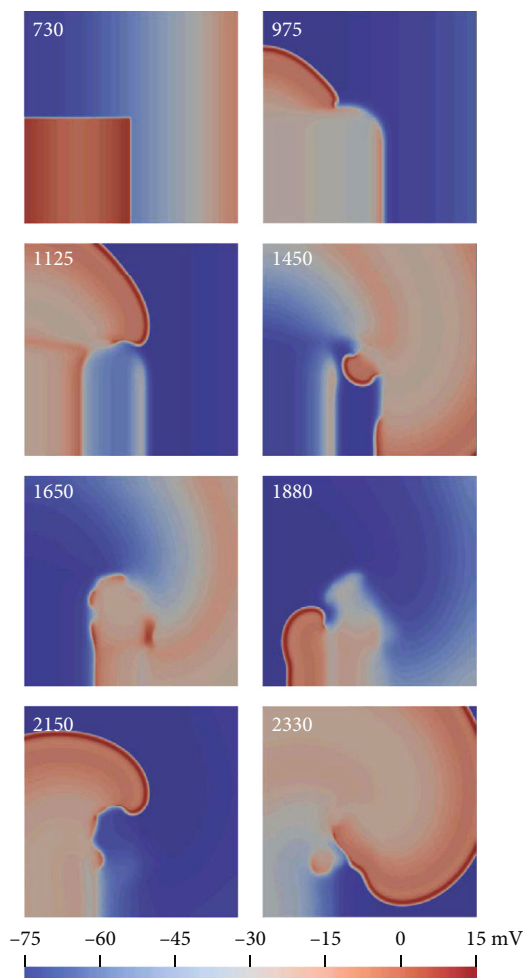


FIGURE 10: Spiral wave induced under oxidative stress conditions using the S1–S2 protocol. The number in each panel represents the recording time.

**4.3. Effect of Rate-Dependent CaMKII Activation on EAD under Oxidative Stress Conditions.** Under control conditions, CaMKII activation gradually decreased with a decrease in the pacing rate, as  $Ca^{2+}$  concentration gradually decreased at low pacing rates. However, under oxidative stress conditions, once CaMKII was activated, the high ROS concentration tended to maintain CaMKII activation. Therefore, under oxidative stress conditions, fractions of CaMKII activation at different pacing rates were similar and maintained at a high level (about 75%). This indicated that, at low pacing rates, ROS-induced CaMKII activation played a more important role. At low pacing rates, intracellular  $Ca^{2+}$  concentration could be dramatically increased by ROS-induced CaMKII activation and therefore could induce more EADs (Figure 6). Although the heart rate is not so slow such as 0.5 Hz and 0.33 Hz under normal conditions, it may be such slow under some pathological conditions, such as bradycardia [60]. The purpose of exploring up to such slow pacing frequencies is to investigate whether the occurrence of EAD is linear with the decrease of pacing frequency or not. The results showed that the occurrence of EAD was more

dependent on ROS-induced CaMKII activation rather than the pacing frequencies.

**4.4. Effect of Oxidative Stress on Excitation Wave Propagation in 2D Tissue.** The spiral wave is a well-known approach to understanding reentry in cardiac tissue, which plays significant roles in AF mechanisms [61]. This study investigated the stability of the spiral wave in 2D ideal tissue under control and oxidative stress conditions. In tissue with a uniform distribution of oxidative stress (Figure 10), the region to which the S2 stimulus was applied had a prolonged depolarization phase, owing to the ROS-induced EAD, forming a spiral wave barrier. In addition, the ROS-induced EAD produced a second excitation wavefront during wave propagation. These effects finally produced a nonstationary spiral wave. In the case of nonuniform distribution of oxidative stress, a breakup of the spiral wave was induced, which might disrupt normal cardiac rhythm and cause atrial arrhythmia [62–64].

**4.5. Model Limitations and Future Directions.** The present model was based on models of Grandi et al. [33] and O'Hara et al. [35] and thus inherited the same limitations of both models. The main limitation of the current model, which will be addressed in the future, is that the ROS concentration is constant. In future versions, pathways of ROS production and scavenging should be added. Another issue for model development is to expand the model into real 2D heart tissue and 3D organ models, to explore electrical wave propagation induced by abnormal action potentials, and electrocardiography in real heart geometry.

Although the S1–S2 interval in 2D simulation to produce the spiral wave was dependent on the tissue size, it is reasonable to investigate the difference in the stability of the spiral wave using the same tissue size under control and oxidative stress conditions. Further work is required to measure the range of S1–S2 intervals for producing the spiral wave (vulnerable window) varying from control to oxidative stress conditions to further determine the proarrhythmic effect of oxidative stress.

## 5. Conclusions

In this study, we have investigated the role of oxidation-dependent CaMKII activation in the genesis of abnormal action potentials in atria. It was shown that, at the atrial cell level, oxidation-dependent CaMKII activation-induced  $I_{CaL}$  reactivation and  $[Ca^{2+}]_i$  elevation contributed to EAD generation. Moreover, at the 2D tissue level, oxidative stress-induced EAD contributed to the instability of excitation waves, facilitating atrial arrhythmia. This study investigated the role of ROS-dependent CaMKII activation in the development of atrial arrhythmias, shedding light on the genesis of atrial arrhythmias under oxidative stress conditions.

## Data Availability

The data used to support the findings of this study are available from the corresponding author upon request.

## Conflicts of Interest

The authors declare that there is no conflict of interest regarding the publication of this paper.

## Authors' Contributions

Qince Li, Henggui Zhang, and Na Zhao conceived the study and designed the simulations. Na Zhao and Haibo Sui developed the model and conducted the simulations. The paper was written by Qince Li. Qince Li and Henggui Zhang analyzed the simulation results. Qince Li and Na Zhao contributed equally to this work. All the authors read and approved the final manuscript.

## Acknowledgments

This work was supported by the National Natural Science Foundation of China (grant numbers 61601143, 81770328, and 61572152) and the Heilongjiang and China Postdoctoral Science Foundation (grant number 2015M581448).

## Supplementary Materials

Figure S1: The CaMKII model. B, CaMKII-CaM $Ca_4$  (bound state); BO, CaMKII $Ox$ -CaM $Ca_4$  (oxidized and bound state); BP, CaMKIIP-CaM $Ca_4$  (phosphorylated and bound state); I, CaMKII (inactive state); O, CaMKII $Ox$  (oxidized state); P, CaMKIIP (phosphorylated state). Table S1: Parameters of CaMKII model (*Supplementary Materials*)

## References

- [1] C. R. Wyndham, "Atrial fibrillation: the most common arrhythmia," *Texas Heart Institute Journal*, vol. 27, no. 3, pp. 257–267, 2000.
- [2] M. C. E. F. Wijffels, C. J. H. J. Kirchhof, R. Dorland, J. Power, and M. A. Allesie, "Electrical remodeling due to atrial fibrillation in chronically instrumented conscious goats," *Circulation*, vol. 96, no. 10, pp. 3710–3720, 1997.
- [3] M. A. Allesie, "Atrial electrophysiologic remodeling: another vicious circle?," *Journal of Cardiovascular Electrophysiology*, vol. 9, no. 12, pp. 1378–1393, 1998.
- [4] S. Wagner, A. G. Rokita, M. E. Anderson, and L. S. Maier, "Redox regulation of sodium and calcium handling," *Antioxidants & Redox Signaling*, vol. 18, no. 9, pp. 1063–1077, 2013.
- [5] P. D. Swaminathan, A. Purohit, T. J. Hund, and M. E. Anderson, "Calmodulin-dependent protein kinase II: linking heart failure and arrhythmias," *Circulation Research*, vol. 110, no. 12, pp. 1661–1677, 2012.
- [6] T. Zhang and J. H. Brown, "Role of  $Ca^{2+}$ /calmodulin-dependent protein kinase II in cardiac hypertrophy and heart failure," *Cardiovascular Research*, vol. 63, no. 3, pp. 476–486, 2004.
- [7] A. Hudmon, H. Schulman, J. Kim, J. M. Maltez, R. W. Tsien, and G. S. Pitt, "CaMKII tethers to L-type  $Ca^{2+}$  channels, establishing a local and dedicated integrator of  $Ca^{2+}$  signals for facilitation," *The Journal of Cell Biology*, vol. 171, no. 3, pp. 537–547, 2005.
- [8] I. Dzshura, Y. Wu, R. J. Colbran, J. R. Balsler, and M. E. Anderson, "Calmodulin kinase determines calcium-dependent

- facilitation of L-type calcium channels," *Nature Cell Biology*, vol. 2, no. 3, pp. 173–177, 2000.
- [9] A. Blaich, A. Welling, S. Fischer et al., "Facilitation of murine cardiac L-type Cav1.2 channel is modulated by calmodulin kinase II-dependent phosphorylation of S1512 and S1570," *Proceedings of the National Academy of Sciences*, vol. 107, no. 22, pp. 10285–10289, 2010.
- [10] S. Wagner, N. Dybkova, E. C. L. Rasenack et al., "Ca<sup>2+</sup>/calmodulin-dependent protein kinase II regulates cardiac Na<sup>+</sup> channels," *The Journal of Clinical Investigation*, vol. 116, no. 12, pp. 3127–3138, 2006.
- [11] S. Wagner, H. M. Ruff, S. L. Weber et al., "Reactive oxygen species-activated Ca/calmodulin kinase II $\delta$  is required for Late INa augmentation leading to cellular Na and Ca overload," *Circulation Research*, vol. 108, no. 5, pp. 555–565, 2011.
- [12] L. S. Maier and D. M. Bers, "Role of Ca<sup>2+</sup>/calmodulin-dependent protein kinase (CaMK) in excitation-contraction coupling in the heart," *Cardiovascular Research*, vol. 73, no. 4, pp. 631–640, 2007.
- [13] L. S. Maier, T. Zhang, L. Chen, J. DeSantiago, J. H. Brown, and D. M. Bers, "Transgenic CaMKII $\delta$ CO overexpression uniquely alters cardiac myocyte Ca<sup>2+</sup> handling," *Circulation Research*, vol. 92, no. 8, pp. 904–911, 2003.
- [14] X. H. T. Wehrens, S. E. Lehnart, S. R. Reiken, and A. R. Marks, "Ca<sup>2+</sup>/calmodulin-dependent protein kinase II phosphorylation regulates the cardiac ryanodine receptor," *Circulation Research*, vol. 94, no. 6, pp. e61–e70, 2004.
- [15] T. Guo, T. Zhang, R. Mestral, and D. M. Bers, "Ca<sup>2+</sup>/calmodulin-dependent protein kinase II phosphorylation of ryanodine receptor does affect calcium sparks in mouse ventricular myocytes," *Circulation Research*, vol. 99, no. 4, pp. 398–406, 2006.
- [16] M. Kohlhaas, T. Zhang, T. Seidler et al., "Increased sarcoplasmic reticulum calcium leak but unaltered contractility by acute CaMKII overexpression in isolated rabbit cardiac myocytes," *Circulation Research*, vol. 98, no. 2, pp. 235–244, 2006.
- [17] C. M. Sag, H. A. Wolff, K. Neumann et al., "Ionizing radiation regulates cardiac Ca handling via increased ROS and activated CaMKII," *Basic research in cardiology*, vol. 108, no. 6, p. 385, 2013.
- [18] H.-T. Ho, B. Liu, J. S. Snyder et al., "Ryanodine receptor phosphorylation by oxidized CaMKII contributes to the cardiotoxic effects of cardiac glycosides," *Cardiovascular Research*, vol. 101, no. 1, pp. 165–174, 2014.
- [19] J. R. Erickson, B. J. He, I. M. Grumbach, and M. E. Anderson, "CaMKII in the cardiovascular system: sensing redox states," *Physiological Reviews*, vol. 91, no. 3, pp. 889–915, 2011.
- [20] H. K. Simmerman, J. H. Collins, J. L. Theibert, A. D. Wegener, and L. R. Jones, "Sequence analysis of phospholamban. Identification of phosphorylation sites and two major structural domains," *Journal of Biological Chemistry*, vol. 261, no. 28, pp. 13333–13341, 1986.
- [21] A. G. Brittsan and E. G. Kranias, "Phospholamban and cardiac contractile function," *Journal of Molecular and Cellular Cardiology*, vol. 32, no. 12, pp. 2131–2139, 2000.
- [22] M. E. Anderson, A. P. Braun, H. Schulman, and B. A. Premack, "Multifunctional Ca<sup>2+</sup>/calmodulin-dependent protein kinase mediates Ca(2+)-induced enhancement of the L-type Ca<sup>2+</sup> current in rabbit ventricular myocytes," *Circulation Research*, vol. 75, no. 5, pp. 854–861, 1994.
- [23] W. Yuan and D. M. Bers, "Ca-dependent facilitation of cardiac Ca current is due to Ca-calmodulin-dependent protein kinase," *American Journal of Physiology-Heart and Circulatory Physiology*, vol. 267, no. 3, pp. H982–H993, 1994.
- [24] J. R. Erickson, M.-I. A. Joiner, X. Guan et al., "A dynamic pathway for calcium-independent activation of CaMKII by methionine oxidation," *Cell*, vol. 133, no. 3, pp. 462–474, 2008.
- [25] Q. Li, D. Su, B. O'Rourke, S. M. Pogwizd, and L. Zhou, "Mitochondria-derived ROS bursts disturb Ca<sup>2+</sup> cycling and induce abnormal automaticity in guinea pig cardiomyocytes: a theoretical study," *American Journal of Physiology-Heart and Circulatory Physiology*, vol. 308, no. 6, pp. H623–H636, 2015.
- [26] Q. Li, S. M. Pogwizd, S. D. Prabhu, and L. Zhou, "Inhibiting Na<sup>+</sup>/K<sup>+</sup> ATPase can impair mitochondrial energetics and induce abnormal Ca<sup>2+</sup> cycling and automaticity in guinea pig cardiomyocytes," *PLoS One*, L.-H. Xie, Ed., vol. 9, no. 4, p. e93928, 2014.
- [27] D. B. Zorov, M. Juhaszova, and S. J. Sollott, "Mitochondrial ROS-induced ROS release: an update and review," *Biochimica et Biophysica Acta (BBA)-Bioenergetics*, vol. 1757, no. 5–6, pp. 509–517, 2006.
- [28] J. Palomeque, O. V. Rueda, L. Sapia et al., "Angiotensin II-induced oxidative stress resets the Ca<sup>2+</sup> dependence of Ca<sup>2+</sup>-calmodulin protein kinase II and promotes a death pathway conserved across different species," *Circulation Research*, vol. 105, no. 12, pp. 1204–1212, 2009.
- [29] P. D. Swaminathan, A. Purohit, S. Soni et al., "Oxidized CaMKII causes cardiac sinus node dysfunction in mice," *The Journal of Clinical Investigation*, vol. 121, no. 8, pp. 3277–3288, 2011.
- [30] B. J. He, M.-I. A. Joiner, M. V. Singh et al., "Oxidation of CaMKII determines the cardiotoxic effects of aldosterone," *Nature Medicine*, vol. 17, no. 12, pp. 1610–1618, 2011.
- [31] L.-H. Xie, F. Chen, H. S. Karagueuzian, and J. N. Weiss, "Oxidative stress-induced afterdepolarizations and calmodulin kinase II signaling," *Circulation Research*, vol. 104, no. 1, pp. 79–86, 2009.
- [32] S. Zhang, Q. Li, L. Zhou, K. Wang, and H. Zhang, "Development of a novel Markov chain model for oxidative-dependent CaMKII $\delta$  activation," in *2015 Computing in Cardiology Conference (CinC)*, pp. 881–884, Nice, France, September, 2015, IEEE.
- [33] E. Grandi, S. V. Pandit, N. Voigt et al., "Human atrial action potential and Ca<sup>2+</sup> model," *Circulation Research*, vol. 109, no. 9, pp. 1055–1066, 2011.
- [34] H. Chiba, N. S. Schneider, S. Matsuoka, and A. Noma, "A Simulation Study on the Activation of Cardiac CaMKII $\delta$  -Isoform and Its Regulation by Phosphatases," *Biophysical Journal*, vol. 95, no. 5, pp. 2139–2149, 2008.
- [35] T. O'Hara, L. Virág, A. Varró, and Y. Rudy, "Simulation of the undiseased human cardiac ventricular action potential: model formulation and experimental validation," *PLoS computational biology*, vol. 7, no. 5, article e1002061, 2011.
- [36] T. Christ, P. Boknik, S. Wöhrle et al., "L-type Ca<sup>2+</sup> current downregulation in chronic human atrial fibrillation is associated with increased activity of protein phosphatases," *Circulation*, vol. 110, no. 17, pp. 2651–2657, 2004.
- [37] A. R. Soltis and J. J. Saucerman, "Synergy between CaMKII substrates and  $\beta$ -adrenergic signaling in regulation of cardiac myocyte Ca<sup>2+</sup> handling," *Biophysical Journal*, vol. 99, no. 7, pp. 2038–2047, 2010.

- [38] K. H. W. J. ten Tusscher and A. V. Panfilov, "Alternans and spiral breakup in a human ventricular tissue model," *American Journal of Physiology-heart and Circulatory Physiology*, vol. 291, no. 3, pp. H1088–H1100, 2006.
- [39] M. D. Christensen, W. Dun, P. A. Boyden, M. E. Anderson, P. J. Mohler, and T. J. Hund, "Oxidized calmodulin kinase II regulates conduction following myocardial infarction: a computational analysis," *PLOS Computational Biology*, vol. 5, no. 12, article e1000583, 2009.
- [40] H. Ni, D. G. Whittaker, W. Wang, W. R. Giles, S. M. Narayan, and H. Zhang, "Synergistic anti-arrhythmic effects in human atria with combined use of sodium blockers and acacetin," *Frontiers in Physiology*, vol. 8, 2017.
- [41] H. Ni, I. Adeniran, and H. Zhang, "In-silico investigations of the functional impact of *CaMKII* mutations on atrial mechanical dynamics," *Journal of Molecular and Cellular Cardiology*, vol. 111, pp. 86–95, 2017.
- [42] D. G. Whittaker, M. A. Colman, H. Ni, J. C. Hancox, and H. Zhang, "Human atrial arrhythmogenesis and sinus bradycardia in *CaMKII*-linked short QT syndrome: insights from computational modelling," *Frontiers in Physiology*, vol. 9, article 1402, 2018.
- [43] M. Courtemanche, R. J. Ramirez, and S. Nattel, "Ionic mechanisms underlying human atrial action potential properties: insights from a mathematical model," *American Journal of Physiology-Heart and Circulatory Physiology*, vol. 275, no. 1, pp. H301–H321, 1998.
- [44] A. Nygren, C. Fiset, L. Firek et al., "Mathematical model of an adult human atrial cell," *Circulation research*, vol. 82, no. 1, pp. 63–81, 1998.
- [45] A. A. Dawodu, F. Monti, K. Iwashiro, M. Schiariti, R. Chiavarelli, and P. E. Puddu, "The shape of human atrial action potential accounts for different frequency-related changes in vitro," *International Journal of Cardiology*, vol. 54, no. 3, pp. 237–249, 1996.
- [46] H. Katoh, T. Shinozaki, S. Baba et al., "Monophasic action potential duration at the crista terminalis in patients with sinus node disease," *Circulation*, vol. 69, no. 11, pp. 1361–1367, 2005.
- [47] R. F. Bosch, X. Zeng, J. B. Grammer, K. Popovic, C. Mewis, and V. Kühnkamp, "Ionic mechanisms of electrical remodeling in human atrial fibrillation," *Cardiovascular Research*, vol. 44, no. 1, pp. 121–131, 1999.
- [48] B.-S. Kim, Y.-H. Kim, G.-S. Hwang et al., "Action potential duration restitution kinetics in human atrial fibrillation," *Journal of the American College of Cardiology*, vol. 39, no. 8, pp. 1329–1336, 2002.
- [49] M. A. Colman, O. V. Aslanidi, S. Khariche et al., "Pro-arrhythmic effects of atrial fibrillation-induced electrical remodeling: insights from the three-dimensional virtual human atria," *The Journal of Physiology*, vol. 591, no. 17, pp. 4249–4272, 2013.
- [50] T. J. Hund and Y. Rudy, "Rate dependence and regulation of action potential and calcium transient in a canine cardiac ventricular cell model," *Circulation*, vol. 110, no. 20, pp. 3168–3174, 2004.
- [51] M. E. Anderson, A. P. Braun, Y. Wu et al., "KN-93, an inhibitor of multifunctional  $Ca^{++}$ /calmodulin-dependent protein kinase, decreases early afterdepolarizations in rabbit heart," *Journal of Pharmacology and Experimental Therapeutics*, vol. 287, no. 3, pp. 996–1006, 1999.
- [52] Y. Wu, L. B. MacMillan, R. B. McNeill, R. J. Colbran, and M. E. Anderson, "CaM kinase augments cardiac L-type  $Ca^{2+}$  current: a cellular mechanism for long Q-T arrhythmias," *American Journal of Physiology-heart and Circulatory Physiology*, vol. 276, no. 6, pp. H2168–H2178, 1999.
- [53] Y. Wu, J. Temple, R. Zhang et al., "Calmodulin kinase II and arrhythmias in a mouse model of cardiac hypertrophy," *Circulation*, vol. 106, no. 10, pp. 1288–1293, 2002.
- [54] D. M. Bers and S. Morotti, " $Ca^{2+}$  current facilitation is CaMKII-dependent and has arrhythmogenic consequences," *Frontiers in Pharmacology*, vol. 5, article 144, 2014.
- [55] J. Heijman, N. Voigt, X. H. T. Wehrens, and D. Dobrev, "Calcium dysregulation in atrial fibrillation: the role of CaMKII," *Frontiers in Pharmacology*, vol. 5, article 30, 2014.
- [56] Y. Song, J. C. Shryock, S. Wagner, L. S. Maier, and L. Belardinelli, "Blocking late sodium current reduces hydrogen peroxide-induced arrhythmogenic activity and contractile dysfunction," *Journal of Pharmacology and Experimental Therapeutics*, vol. 318, no. 1, pp. 214–222, 2006.
- [57] X. Y. Qi, Y.-H. Yeh, D. Chartier et al., "The calcium/calmodulin/kinase system and arrhythmogenic afterdepolarizations in bradycardia-related acquired long-QT syndrome," *Circulation. Arrhythmia and Electrophysiology*, vol. 2, no. 3, pp. 295–304, 2009.
- [58] A. Burashnikov and C. Antzelevitch, "Reinduction of atrial fibrillation immediately after termination of the arrhythmia is mediated by late phase 3 early afterdepolarization-induced triggered activity," *Circulation*, vol. 107, no. 18, pp. 2355–2360, 2003.
- [59] E. Patterson, R. Lazzara, B. Szabo et al., "Sodium-calcium exchange initiated by the  $Ca^{2+}$  transient," *Journal of the American College of Cardiology*, vol. 47, no. 6, pp. 1196–1206, 2006.
- [60] F. M. Kusumoto, M. H. Schoenfeld, C. Barrett et al., "2018 ACC/AHA/HRS guideline on the evaluation and management of patients with bradycardia and cardiac conduction delay: a report of the American College of Cardiology/American Heart Association task force on clinical practice guidelines and the Heart Rhythm Society," *Journal of the American College of Cardiology*, vol. 74, no. 7, pp. e51–e156, 2019.
- [61] S. Nattel, F. Xiong, and M. Aguilar, "Demystifying rotors and their place in clinical translation of atrial fibrillation mechanisms," *Nature Reviews Cardiology*, vol. 14, no. 9, pp. 509–520, 2017.
- [62] J. Jalife, O. Berenfeld, and M. Mansour, "Mother rotors and fibrillatory conduction: a mechanism of atrial fibrillation," *Cardiovascular Research*, vol. 54, no. 2, pp. 204–216, 2002.
- [63] J. Kneller, R. Zou, E. J. Vigmond, Z. Wang, L. J. Leon, and S. Nattel, "Cholinergic atrial fibrillation in a computer model of a two-dimensional sheet of canine atrial cells with realistic ionic properties," *Circulation Research*, vol. 90, no. 9, pp. E73–E87, 2002.
- [64] J. Kneller, J. Kalifa, R. Zou et al., "Mechanisms of atrial fibrillation termination by pure sodium channel blockade in an ionically-realistic mathematical model," *Circulation Research*, vol. 96, no. 5, pp. e35–e47, 2005.

## Research Article

# ***Qiliqiangxin* Improves Cardiac Function through Regulating Energy Metabolism via HIF-1 $\alpha$ -Dependent and Independent Mechanisms in Heart Failure Rats after Acute Myocardial Infarction**

Yanyan Wang <sup>1</sup>, Mingqiang Fu,<sup>1</sup> Jingfeng Wang <sup>1</sup>, Jingjing Zhang,<sup>2</sup> Xueting Han,<sup>1</sup> Yu Song,<sup>1</sup> Yuyuan Fan,<sup>3</sup> Kai Hu <sup>1</sup>, Jingmin Zhou <sup>1</sup>, and Junbo Ge <sup>1</sup>

<sup>1</sup>Department of Cardiology, Shanghai Institute of Cardiovascular Diseases, Zhongshan Hospital, Fudan University, Shanghai, China

<sup>2</sup>Department of Cardiology, Zoucheng Hospital, Affiliated Hospital of Jining Medical University, Jining, Shandong, China

<sup>3</sup>North Sichuan Medical College, Nanchong, Sichuan, China

Correspondence should be addressed to Jingmin Zhou; [zhou.jingmin@zs-hospital.sh.cn](mailto:zhou.jingmin@zs-hospital.sh.cn) and Junbo Ge; [jbge@zs-hospital.sh.cn](mailto:jbge@zs-hospital.sh.cn)

Received 19 February 2020; Revised 22 April 2020; Accepted 16 May 2020; Published 12 June 2020

Guest Editor: Roland E. Akhigbe

Copyright © 2020 Yanyan Wang et al. This is an open access article distributed under the Creative Commons Attribution License, which permits unrestricted use, distribution, and reproduction in any medium, provided the original work is properly cited.

The present study is aimed at investigating whether *Qiliqiangxin* (QL) could regulate myocardial energy metabolism in heart failure rats after acute myocardial infarction (AMI) and further exploring the underlying mechanisms. AMI was established by ligating the left anterior descending coronary artery in adult male SD rats. AMI rats with ejection fraction (EF) < 50% at two weeks after the operation were chosen as heart failure rats for the main study. Rats were randomized into the sham, MI, MI+QL, and MI+QL+2-MeOE2 groups. The results showed that compared with the MI group, QL significantly improved cardiac function, reduced serum NT-proBNP level, and alleviated myocardial fibrosis. QL also increased myocardial capillary density by upregulated protein expressions of vascular endothelial growth factor (VEGF) and CD31 by regulating the HIF-1 $\alpha$ /VEGF pathway. Moreover, QL promoted ATP production, glucose uptake, and glycolysis by upregulating HIF-1 $\alpha$  and a series of glycolysis-relevant enzymes in a HIF-1 $\alpha$ -dependent manner. QL also improved myocardial glucose oxidation enzyme expression and free fatty acid uptake by a HIF-1 $\alpha$ -independent pathway. Our results indicate that QL treatment improves cardiac function through regulating glucose uptake, FFA uptake, and key enzymes of energy metabolism via HIF-1 $\alpha$ -dependent and independent mechanisms.

## 1. Introduction

Heart failure (HF) is one of the most important cardiovascular diseases (CVD) that is associated with high morbidity and mortality [1]. Myocardial ischemia is one of the major causes of heart failure. Although reperfusion therapy has improved the prognosis of ST-elevation myocardial infarction (STEMI), the progression to HF can still occur in 30% of patients post myocardial infarction (MI) [1]. Despite recent advances in medical and surgical therapy, patients with HF have a 5-year mortality rate of around 50% [2, 3]. Thus, new approaches for HF treatments are needed. Targeting myocardial metabolism might be an attractive therapeutic option for HF. There is

a vicious metabolic circle in heart failure as the activated adrenergic system could lead to an increase in the serum free fatty acid (FFA), which inhibits mitochondrial function at the level of acyl carnitine transferase (ACT), thus inhibiting fatty acid (FA) oxidation and synthesis of ATP [4, 5]. Furthermore, this increase in the serum FFA also inhibits pyruvate dehydrogenase (PDH) activity via the Randle cycle to promote anaerobic glycolysis rather than oxidative metabolism [6]. Previous studies have shown that the metabolic shift from oxidative metabolism (including FA and glucose oxidative metabolism) to glycolysis and the substrate shift from primarily fatty acids to glucose could result in decreased myocardial ATP production, which might play a crucial role



in the development of heart failure [7, 8]. Accordingly, there is accumulating evidence that modulating cardiac energy metabolism, either by increasing glucose oxidation or by decreasing serum FFA concentrations and FA oxidation, can improve cardiac function [9, 10].

Hypoxia-inducible factor 1 $\alpha$  (HIF-1 $\alpha$ ) is an important cellular adaptation mediator against hypoxia, which can regulate the delivery of oxygen by promoting vascular endothelial growth factor (VEGF) expression and angiogenesis [11]. Furthermore, HIF-1 $\alpha$  can also modulate energy metabolism by activating the expression of glucose metabolic key enzymes (e.g., hexokinase 2 (HK2), pyruvate dehydrogenase K1 (PDK1), lactic dehydrogenase (LDHA)), and glucose transporter vectors 1/4 (GLUT1/4) and mitochondrial proteins [12]. Recent studies have suggested that upregulated HIF-1 $\alpha$  activity is closely linked with cardioprotective effects induced by myocardial infarction; the related mechanism promotes angiogenesis [13] and improves metabolism [14]. Another study also showed that the HIF-1 $\alpha$  activity in endothelial cells was required for the cardioprotective effects induced by ischemic preconditioning (IPC), while in HIF-1 $\alpha$ -/- mice, the cardioprotective effect of IPC was diminished [15]. This evidence suggested that the upregulation of HIF-1 $\alpha$  might be a potential therapeutic option for treating heart failure post AMI.

*Qiliqiangxin* is a compound preparation of traditional Chinese medicine, which is extracted from 11 types of Chinese herbs, including Radix Astragali, Aconite Root, Ginseng, Salvia miltiorrhiza, Semen Lepidii Apetali, Cortex Periplocae Sepii Radicis, Rhizoma Alismatis, Carthamus tinctorius, Polygonatum Odorati, Seasoned Orange Peel, and Rumulus Ginnamomi. The 17 chemical constituents of QL mainly include ginsenoside Rg1, phenolic acids, flavonoids and alkaloids, astragaloside, calycosin-7-glucoside, and sinapine [16]. QL has shown satisfactory efficacy in the treatment of HF patients in China [17]. Previous studies found that QL improved cardiac metabolism and mitochondrial function in heart failure induced by pressure overload, while QL also enhanced the metabolism of H9C2 cardiomyocytes by regulating peroxisome proliferator-activated receptor gamma (PPAR $\gamma$ ) coactivator-1 $\alpha$  (PGC-1 $\alpha$ ) expression [18, 19]. Our previous studies also demonstrated that QL could increase cardiac angiogenesis both in rats post MI and in hypoxic cardiac microvascular endothelial cells [16, 20]. However, it remains unknown to what extent the changes in energy metabolism contributed to the beneficial effects of QL in MI rats.

The present study is aimed at investigating the effects of QL on energy metabolism in rats with experimental MI and exploring whether HIF-1 $\alpha$  signaling is actively involved in these effects.

## 2. Materials and Methods

**2.1. Experimental Animals.** Adult male SD rats (with an average weight of 200  $\pm$  20 g) were purchased from the Shanghai SLAC Laboratory Animal Co., Ltd. (Shanghai, China). Rats were housed in a temperature-controlled laboratory animal center (22–24°C) under circadian conditions with free access

to standard chow and tap water. The study was approved by the ethical committees of the Zhongshan Hospital Affiliated to Fudan University, and all the experimental procedures were performed in accordance with the Guide for the Care and Use of Laboratory Animals published by the US National Institutes of Health (NIH Publication No. 85-23, revised 1996).

**2.2. Induction of Myocardial Infarction in Rats.** After 1 week of adaptive feeding, the rats were anesthetized with sodium pentobarbital (30 mg/kg, intraperitoneally), intubated, and connected to a SAR-830/A Small Animal Ventilator (CWE, Inc., Weston, WI, USA). Thereafter, MI was created by exteriorizing the heart through a left thoracic incision, placing a 6-0 silk 3–4 mm below the tip of the left auricle, and making a slipknot. The complete occlusion of the vessel was confirmed by the presence of myocardial blanching in the perfusion bed. After ligation, the chest of the animal was closed with three 5-0 prolene sutures, which was followed by 4-0 polyester sutures to close the skin. For the sham group, the needle was passed around the artery without ligation.

Two weeks later, the rats that survived after the MI operation (the survival rate was 65%) were subjected to an echocardiographic examination and those with left ventricular ejection fraction (EF) of <50% were chosen for subsequent studies. The distribution of EF in MI rats before treatment was 35%–45%, and there was no significant difference between groups; those rats whose EF was not at this range were excluded.

**2.3. Experimental Groups.** Rats were randomly divided into the following groups ( $n=7$  per group). The sham group and the MI group both received the same volume of 0.5% sodium carboxymethyl cellulose (CMC-Na). The other two groups were the MI+QL group and the MI+QL+2-MeOE2 group. QL at 0.5 g/kg was given daily by gavage, while 2-MeOE2 (HIF-1 $\alpha$  inhibitor) at 30 mg/kg was given daily by gavage. According to our previous study [16], we planned to give this medicine for 6 weeks.

The QL compound was supplied by Yiling Pharmaceutical Corporation (Shijiazhuang, China); the compound was suspended in 0.5% sodium carboxymethyl cellulose (CMC-Na) at a 10% concentration before administration.

**2.4. Small-Animal Positron Emission Tomography Imaging Analysis.** Micro-PET/CT (Metis PET, Madic, Shandong, China) was performed before and 6 weeks after various interventions to evaluate the changes in the myocardial glucose metabolism. After anesthesia with sodium pentobarbital (30 mg/kg, IP), 2-deoxy-2-fluoro-D-glucose (<sup>18</sup>F-FDG) (approximately 1250  $\mu$ Ci/kg) was injected via the tail vein of the rats. One hour later, the myocardial glucose metabolism level was examined. The emission scan was acquired in one bed position with a total acquisition time of 30 minutes. During the entire PET examination process, anesthesia was maintained with 1.5% isoflurane delivered in pure oxygen at a rate of 1.2 l/min via a face mask and the rats were placed within the aperture of the tomography in a prone position. The Metis Viewer Version 1.0 for Windows was used for

TABLE 1: Primer sequences for HIF-1 $\alpha$  and glucose metabolism-related genes.

Genes	Forward primer	Reverse primer
HIF-1 $\alpha$	5'-CTCCCTTTTCAAGCAGCAG-3'	5'-GCTCCATTCCATCCTGTTCA-3'
GLUT4	5'-AGGCACCTCACTACCCTTT-3'	5'-AGCATAGCCCTTTTCCTTCC-3'
HK2	5'-CTCTGGGTTTCACCTTCTCG-3'	5'-ACCACATCTCTGCCTTCCAC-3'
PFK1	5'-GTTCTGGGGATGCGTAAGAG-3'	5'-CCTCAGTTTCAGCCACCACT-3'
PKM2	5'-TCCCATTCTCTACCGACCTG-3'	5'-TTCAGTGTGGCTCCCTTCTT-3'
LDHA	5'-GTCAGCAAGAGGGAGAGAGC-3'	5'-CACTGGGTTTGAGACGATGA-3'
$\beta$ -Actin	5'-GAAGTGTGACGTTGACATCCG-3'	5'-TGCTGATCCACATCTGCTGGA-3'

image analysis. After this, the standardized uptake value (SUV), which is equal to the PET count/injected radioactivity per body weight (Bq/g), was calculated and normalized according to body weight and the injected dose of  $^{18}\text{F}$ -FDG. Finally, the mean standardized  $^{18}\text{F}$ -FDG-uptake values (SUV<sub>mean</sub>) were obtained by a professional observer.

**2.5. Echocardiography and Blood and Myocardial Sample Collection.** Echocardiography was performed under anesthesia 6 weeks after the interventions. The rats were placed in the proper posture after the precordial region was shaved. M-mode images of LV long axis were obtained at the level of the papillary muscle tips using an animal specific instrument (VisualSonics Vevo770; VisualSonics Inc., Toronto, ON, Canada) as previously described [21–23]. Left ventricular internal diameter at end diastole (LVIDd) and left ventricular internal diameter at end systole (LVIDs), fractional shortening (FS), and EF were measured. Parameters were obtained and averaged from three consecutive cardiac cycles and performed by one experienced echocardiographer who was blinded to the treatment protocol.

Blood samples were collected by cardiac puncture and centrifuged at 3000 rpm/min for 20 minutes at 4°C. After this, the serum was collected and stored at -80°C. The heart was immediately excised after euthanasia, which was irrigated clean with cold saline. The ventricular transection was separated into 2 equal parts. The top half of the transversely dissected heart tissue was fixed in 4% paraformaldehyde, while the other half of the tissue was divided into the infarct border zone and noninfarcted left ventricular myocardium, which was stored at -80°C. After 6 hours, the tissues fixed in 4% paraformaldehyde were divided into 2 equal parts again: the top part was made into frozen embedded tissues immediately, while the other part was fixed for 48 hours and made into paraffin-embedded tissues used for hematoxylin/eosin (H&E) and Sirius red staining.

**2.6. Serum Concentrations of NT-proBNP and Free Fatty Acid (FFA) Level.** The serum NT-proBNP level was measured using the enzyme-linked immunosorbent assay (ELISA) according to the manufacturer's instructions (Cloud-Clone Corp., USA). The serum FFA level was measured by a commercial assay kit according to the manufacturer's instructions (BioSino Bio-Technology & Science Inc., Beijing, China).

**2.7. Detection of ATP Production and Citrate Synthase (CS) Activity.** The ATP level was measured using an ATPlite assay kit (Beyotime Biotechnology, Shanghai, China). The tissues around the border zone (20 mg) were homogenized in 200  $\mu\text{l}$  of the ATP assay buffer before being centrifuged at 12,000 g for 5 min at 4°C. A total of 100  $\mu\text{l}$  of samples or standards was mixed with 100  $\mu\text{l}$  of the ATP Reaction Mix in duplicate wells of a 96-well plate. Luminescence was detected using a fluorescent plate reader (Synergy™ H4, BioTek Instruments, Inc., USA).

In the present study, we detected the CS activity to evaluate the effect of QL on glucose oxidative metabolism according to the manufacturer's instructions (Sigma-Aldrich Co. LLC., USA). Briefly, the border zone tissue samples (10 mg) were homogenized in 100  $\mu\text{l}$  of the CS Assay Buffer, kept on ice for 10 minutes, and centrifuged at 10,000 g for 5 minutes at 4°C. We added 50  $\mu\text{l}$  of the samples (containing 20  $\mu\text{l}$  of supernatants and 30  $\mu\text{l}$  of CS Assay Buffer) or 50  $\mu\text{l}$  of the standard buffer to the 96-well plate. After this, we added 50  $\mu\text{l}$  of the reaction mix, which includes the CS Assay Buffer, CS Developer, and CS Substrate Mix, to each well. We incubated the plate at 25°C, before both the initial and final absorbance at 412 nm was measured. Finally, we calculated the CS activity according to the following mathematical formula: CS activity (nmol/min/ $\mu\text{l}$ ) = Sa/(reaction time)  $\times$  Sv, where Sa represents the amount of GSH (nmol) generated in the sample wells between T<sub>initial</sub> and T<sub>final</sub> from the standard curve and Sv is the sample volume. Finally, we used the following formula: reactive time = T<sub>final</sub> – T<sub>initial</sub>.

**2.8. Histology and Fibrosis Assessment.** After 6 weeks of the intervention, hearts were excised, cut into 2 mm thick transverse sections, and fixed in 4% phosphate-buffered formalin. After this, the paraffin-embedded tissues were cut into 5  $\mu\text{m}$  slices and stained with hematoxylin/eosin (H&E) and Sirius red. Sections were examined by light microscopy, and the images were analyzed with ImageJ software to quantify the collagen percentage as previously described [24]. Images of five randomly chosen fields round the border zone were photographed under a microscope (Leica, Germany). The myocardial collagen volume fraction (CVF) was obtained by calculating the ratio of fibrotic area (red) to the total myocardial area using ImageJ software (NIH, Bethesda, MD, USA).

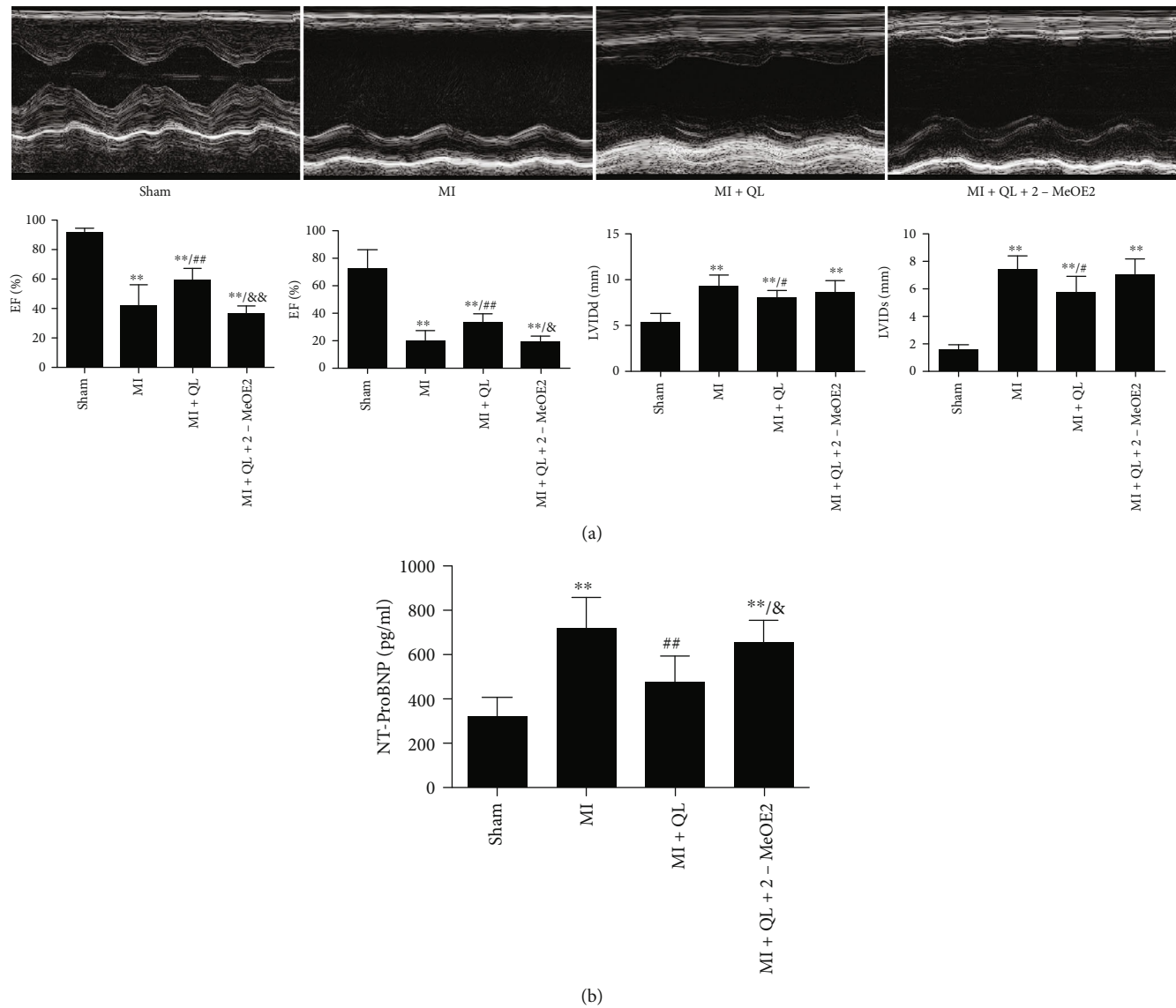


FIGURE 1: Qiliqiangxin (QL) improved cardiac function and decreased serum NT-proBNP levels via the HIF-1 $\alpha$  signaling pathway. (a) QL improved cardiac function with preserved left ventricular ejection fraction (EF), left ventricular fractional shortening (FS), left ventricular internal diameter at end-diastole (LVIDd), and left ventricular internal diameter at end systole (LVIDs), while the HIF-1 $\alpha$  inhibitor partly suppressed these protective effects of QL ( $n = 7$ /group). (b) QL decreased serum NT-proBNP levels in a HIF-1 $\alpha$ -dependent manner ( $n = 7$ /group). Data are expressed as means  $\pm$  SEM. \* $p < 0.05$  and \*\* $p < 0.01$  compared with the sham group; # $p < 0.05$  and ## $p < 0.01$  compared with the MI group; & $p < 0.05$  and && $p < 0.01$  compared with the MI+QL group.

2.9. *Detection of Myocardial Microvessel Density by Immunofluorescence Staining.* CD31 was used to evaluate the level of angiogenesis. The frozen embedded tissues were cut into 8  $\mu\text{m}$  frozen slices. Frozen tissue sections were placed at room temperature for 30 minutes and washed with phosphate-buffered saline (PBS) three times before immunofluorescence staining. After blocking with goat serum for 30 min, the sections were incubated with rabbit anti-rat CD31 (1:20 dilution, Santa Cruz Biotechnology, Inc., USA) primary antibody overnight at 4 $^{\circ}\text{C}$ . On the next day, after being washed with PBS four times (10 min for each), the slides were incubated with goat anti-rabbit secondary antibodies (Alexa Fluor 555, Invitrogen, Carlsbad, CA, USA) for 1.5 hour at 37 $^{\circ}\text{C}$  in the dark. Nuclei were counterstained

with DAPI. Images of five randomly chosen fields round the border zone were photographed under a microscope (Leica, Germany), and the vessel density was analyzed by ImageJ software (NIH, Bethesda, MD, USA).

2.10. *Fluorescent Quantitative RT-PCR Analysis.* The total RNA was extracted from 10 mg of the left ventricular infarction border zone tissue using the TRIzol Reagent according to the manufacturer's protocol (Invitrogen, Carlsbad, CA, USA). The total RNA (1  $\mu\text{g}$ ) was reverse transcribed into cDNA using a RT Reagent Kit (TaKaRa, Tokyo, Japan). Real-time PCR was performed with the SYBR $^{\circledR}$  Premix Ex Taq $^{\text{TM}}$  kit in a 10  $\mu\text{l}$  reaction volume (TaKaRa, Tokyo, Japan). The primers used for PCR are shown in Table 1. qRT-PCR

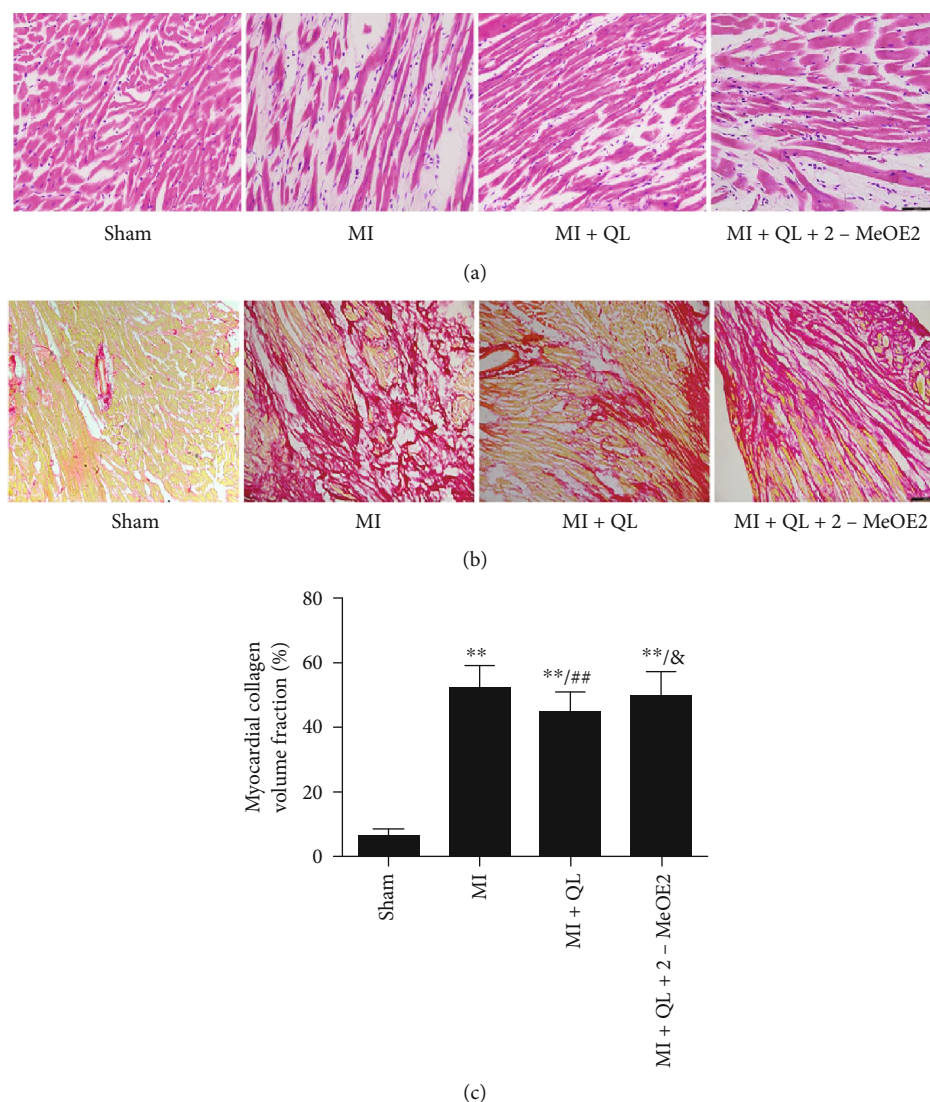
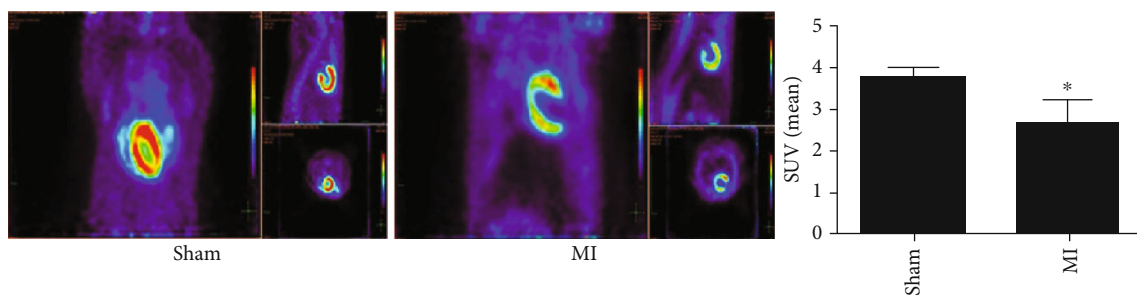


FIGURE 2: QL preserved myocardial structure and inhibited cardiac fibrosis via the HIF-1 $\alpha$ -dependent pathway. (a) QL preserved the arrangement of myocardial fibers, which were obviously irregularly arranged in the MI group (20x, scale bar = 100  $\mu$ m,  $n = 4$ /group). (b and c) QL attenuates cardiac fibrosis with decreased cardiac fibrosis compared with the MI group (10x, scale bar = 200  $\mu$ m,  $n = 4$ /group). Data are expressed as means  $\pm$  SEM. \* $p < 0.05$  and \*\* $p < 0.01$  compared with the sham group; # $p < 0.05$  and ## $p < 0.01$  compared with the MI group; & $p < 0.05$  and && $p < 0.01$  compared with the MI+QL group.

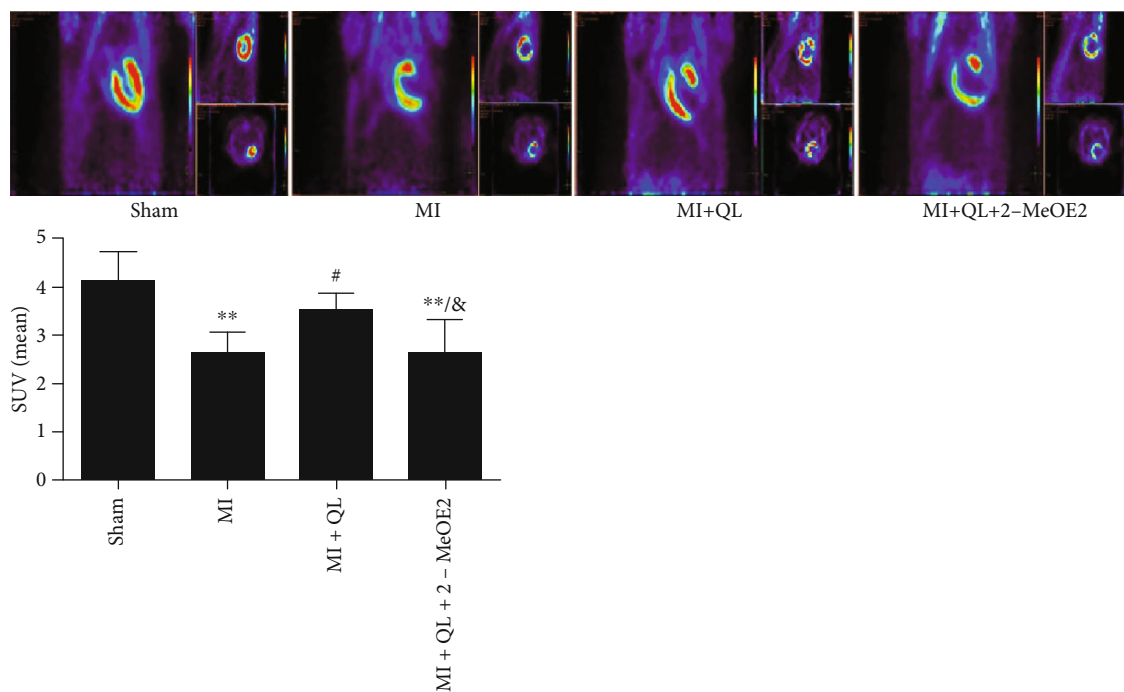
was performed on the CFX Connect™ Real-Time System (Bio-Rad Laboratories, Inc., California, USA). The standard  $2^{-\Delta\Delta Ct}$  relative quantification method was applied with  $\beta$ -actin used as the endogenous control.

**2.11. Western Blot Analysis.** Approximately 10 mg of the left ventricular border zone tissue samples was lysed and homogenized in 200  $\mu$ l of the lysis buffer on ice, which was followed by centrifugation at 12,000 g for 20 min at 4°C. Protein concentration was measured by the BCA protein assay (Beyotime Biotechnology, Shanghai, China). Aliquots of 30  $\mu$ g of the protein lysates were electrophoresed on 8%, 10%, or 12% SDS-PAGE gels and then transferred to PVDF membranes (Millipore, Billerica, MA, USA). After being blocked with 5% bovine serum albumin (BSA) for 1 hour at room temperature, the blots were incubated overnight at 4°C

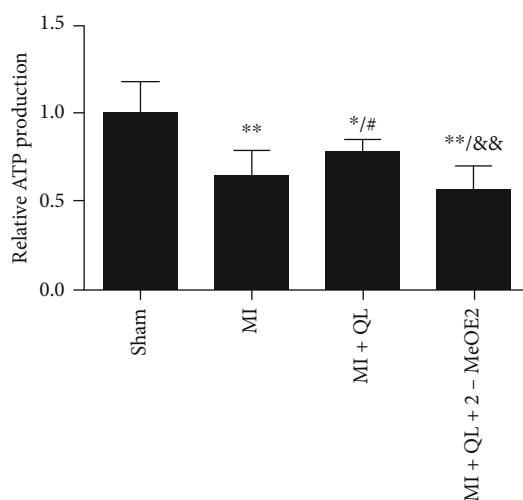
with specific rabbit/mouse anti-rat antibodies for HIF-1 $\alpha$  (Novus International Inc., USA, 1:1000), GLUT4 (Cell Signaling Technology, USA, 1:800), PKM2 (Cell Signaling Technology, USA, 1:1000), LDHA (Cell Signaling Technology, USA, 1:1000), PDH (Cell Signaling Technology, USA, 1:1000), CS (Cell Signaling Technology, USA, 1:1000), CD36 (Cell Signaling Technology, USA, 1:1000), PGC-1 $\alpha$  (Cell Signaling Technology, USA, 1:1000), VEGF (Cell Signaling Technology, USA, 1:1000), VEGFR2 (Cell Signaling Technology, USA, 1:1000), and CD31 (Santa Cruz Biotechnology, Inc., USA, 1:200). On the next day, membranes were washed with TBST three times (10 min for each) before being incubated with horseradish peroxidase- (HRP-) conjugated secondary antibodies (1:10000, Kangchen, China) for 2 hours at room temperature. The HRP-conjugated monoclonal rabbit anti-rat  $\beta$ -actin antibody (1:10000, Kangchen, China)



(a)

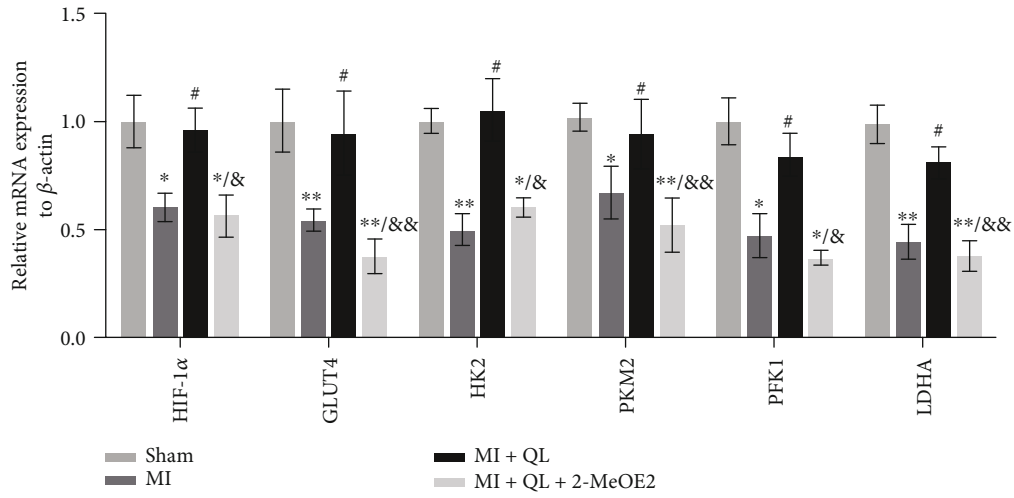


(b)



(c)

FIGURE 3: QL promoted myocardial glucose uptake and ATP production via the HIF-1 $\alpha$  signaling pathway. (a) Animals of the MI group showed a significantly lower myocardial  $^{18}\text{F}$ -FDG uptake (exhibited as SUV mean) than those of the sham group before drug intervention. After 6 weeks of treatment, the myocardial  $^{18}\text{F}$ -FDG uptake (SUV mean) (b) and ATP production (c) were significantly increased in the MI+QL group compared with the MI group, while the HIF-1 $\alpha$  inhibitor attenuated these effects ( $n = 7/\text{group}$ ). Data are expressed as means  $\pm$  SEM. \* $p < 0.05$  and \*\* $p < 0.01$  compared with the sham group; # $p < 0.05$  and ## $p < 0.01$  compared with the MI group; & $p < 0.05$  and && $p < 0.01$  compared with the MI+QL group.



(a)

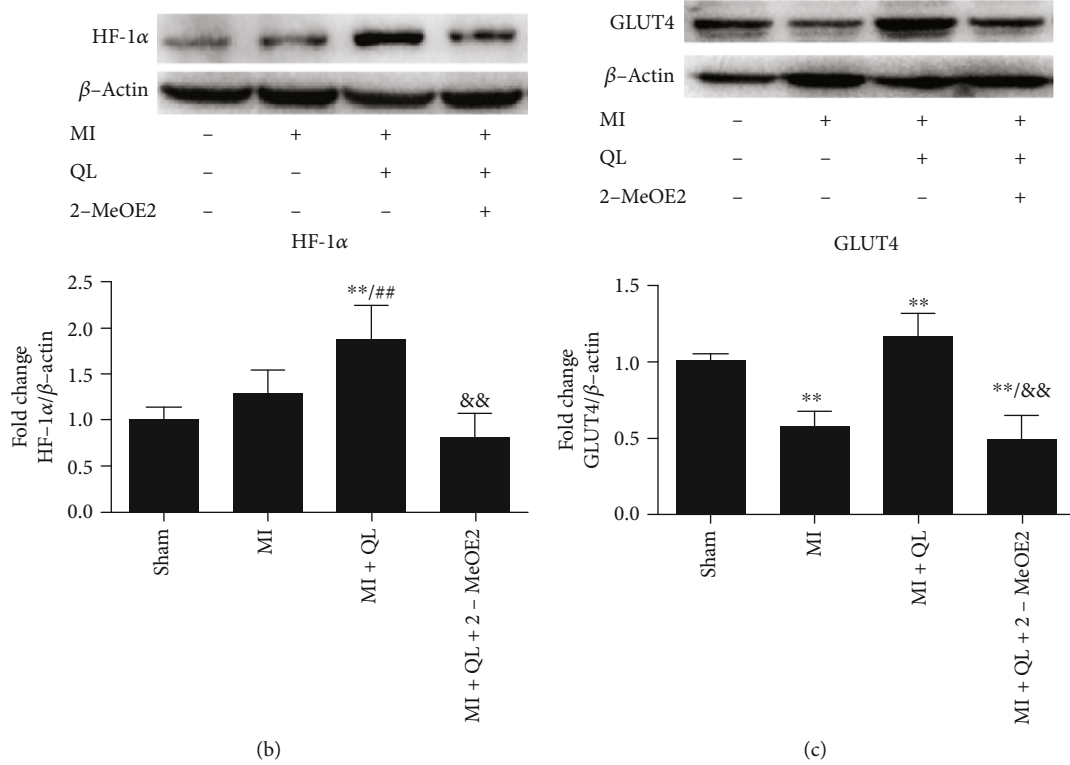


FIGURE 4: Continued.

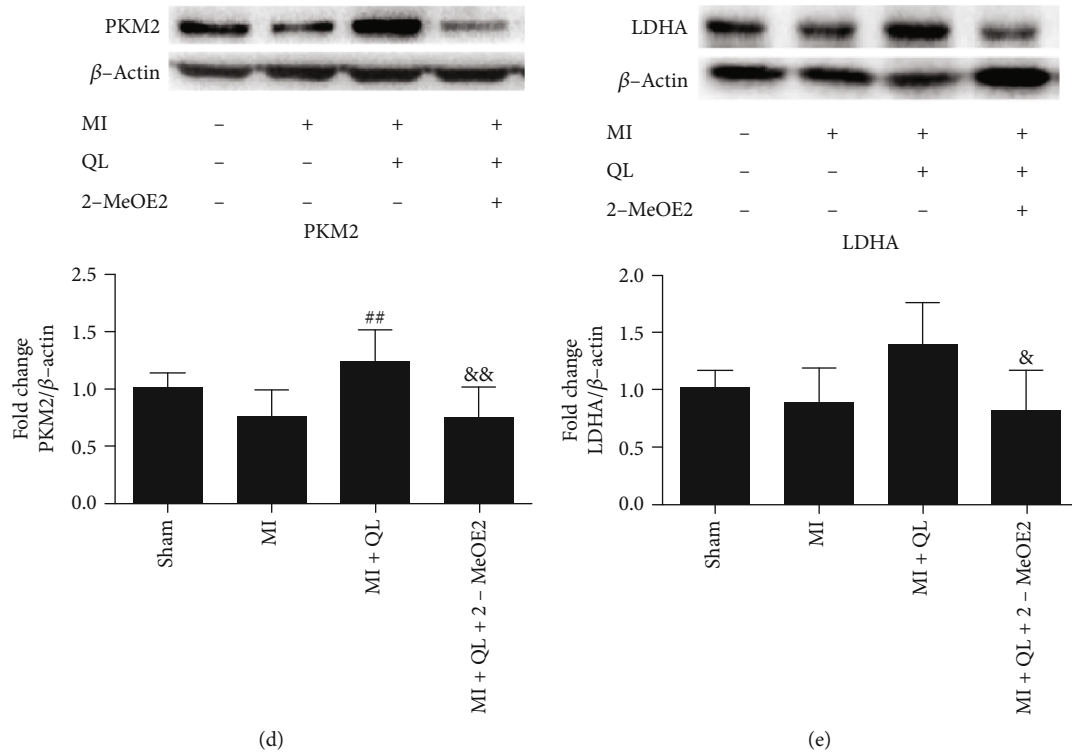


FIGURE 4: QL treatment promoted myocardial glucose uptake and glycolysis in a HIF-1 $\alpha$ -dependent manner. (a) QL upregulated mRNA expression of HIF-1 $\alpha$ , GLUT4, HK2, PKM2, PFK1, and LDHA, which were significantly abolished by 2-MeOE2 ( $n = 7/\text{group}$ ). (b-e) QL upregulated protein expressions of HIF-1 $\alpha$ , GLUT4, PKM2, and LDHA, which were also abolished by 2-MeOE2 ( $n = 7/\text{group}$ ). Data are expressed as means  $\pm$  SEM. \* $p < 0.05$  and \*\* $p < 0.01$  compared with the sham group; # $p < 0.05$  and ## $p < 0.01$  compared with the MI group; & $p < 0.05$  and && $p < 0.01$  compared with the MI+QL group.

was used to detect  $\beta$ -actin levels. Finally, the antibody complexes were visualized and quantified by the Gel Doc<sup>TM</sup> XR+ System (Bio-Rad Laboratories, Inc., California, USA) and Image Lab Software. The results were expressed as density values that were normalized to  $\beta$ -actin.

**2.12. Statistical Analyses.** Data were presented as mean  $\pm$  SEM. For the comparison between two groups, the differences in the mean values were evaluated by Student's  $t$ -test and the Mann-Whitney  $U$  test. For the comparison among three or more groups, differences were determined by one-way ANOVA with Tukey's post hoc test. A value of  $p < 0.05$  was considered to be statistically significant. All statistical analyses were performed with SPSS 17.0 software.

### 3. Results

**3.1. QL Treatment Preserved Cardiac Function and Decreased the Level of Serum NT-proBNP in MI Rats in a HIF-1 $\alpha$ -Dependent Manner.** Compared with the sham group, increased LVIDd, LVIDs, and NT-proBNP levels, in addition to decreased EF and FS were found in the MI group. QL treatment for 6 weeks significantly improved cardiac function and decreased NT-proBNP levels, while these protective effects were partly attenuated in the presence of a HIF-1 $\alpha$  inhibitor (Figures 1(a) and 1(b)).

**3.2. QL Ameliorated Myocardial Derangement and Fibrosis via a HIF-1 $\alpha$ -Dependent Pathway.** As shown in Figure 2(a), the surviving myocardial cells in the infarct border zone were obviously irregularly arranged, the myocardial cells displayed lysis and breakage of cardiac muscle fibers, while numerous infiltrated inflammatory cells were detectable, which was partially reversed by QL treatment. However, cotreatment with the HIF-1 $\alpha$  inhibitor 2-MeOE2 attenuated the beneficial effects of QL again. Myocardial fibrosis is a hallmark of cardiac remodeling after AMI. Sirius red staining revealed significantly enhanced cardiac fibrosis in the MI group compared to the sham group, while QL significantly alleviated cardiac fibrosis, and this effect could be partially blocked by treatment with 2-MeOE2 (Figures 2(b) and 2(c)).

**3.3. QL Treatment Promoted Myocardial Glucose Uptake and ATP Production via a HIF-1 $\alpha$  Signaling Pathway.** Before drug administration, we used PET to detect the cardiac glucose uptake of MI rats and sham rats. The results showed that compared with the sham group, the myocardial glucose uptake was significantly lower in MI rats (Figure 3(a)).

After 6 weeks, the results revealed significantly higher myocardial <sup>18</sup>F-FDG uptake and ATP production in the MI+QL group compared with the MI group, while treatment of the specific HIF-1 $\alpha$  inhibitor significantly blocked these effects. This suggests that the HIF-1 $\alpha$  pathway played a critical role in QL-induced metabolic improvement (Figures 3(b) and 3(c)).

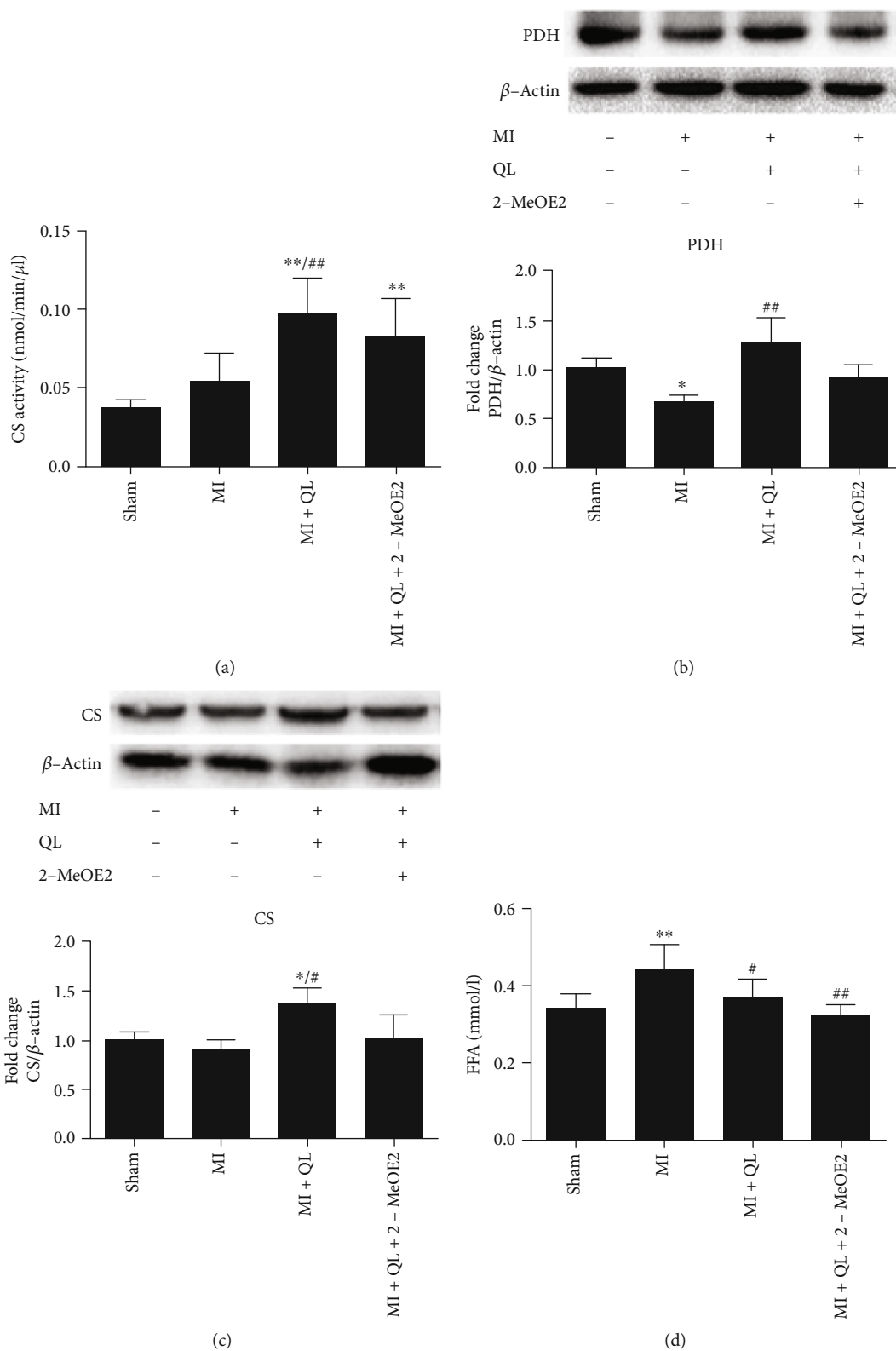


FIGURE 5: Continued.



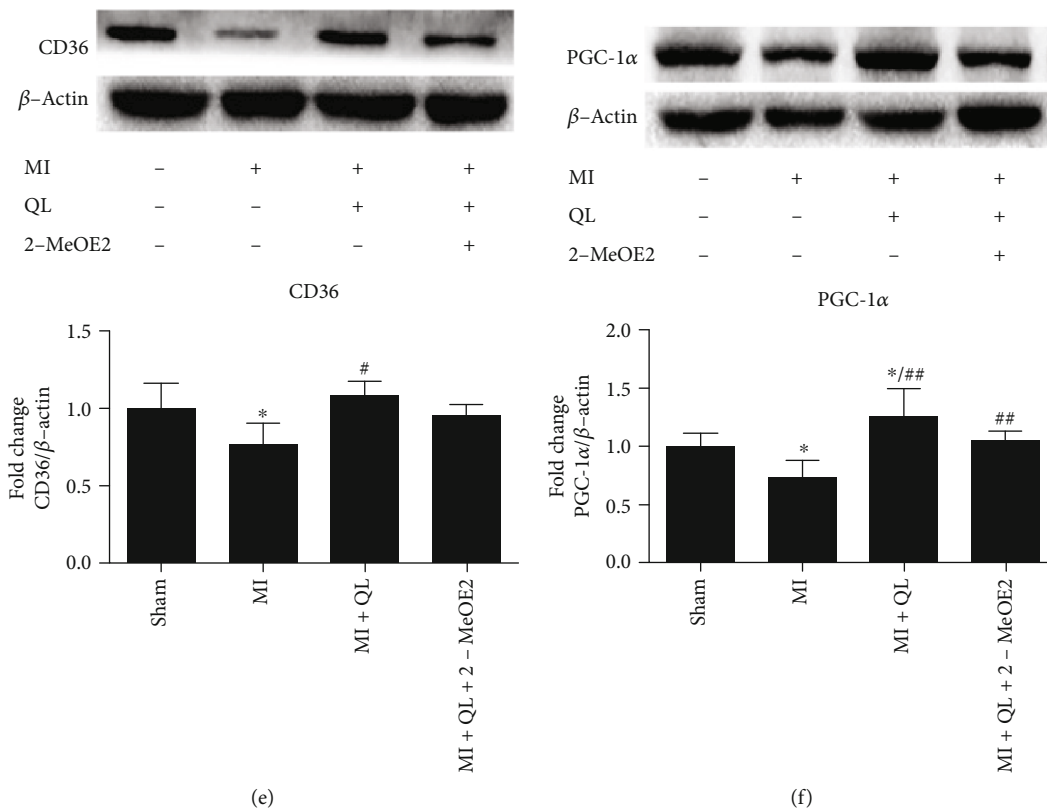


FIGURE 5: QL treatment promoted glucose oxidation and free fatty acid (FFA) uptake in a HIF-1 $\alpha$ -independent manner. (a) QL promoted CS protein activity ( $n = 7$ /group). (b and c) QL elevated PDH and CS protein expressions, while the HIF-1 $\alpha$  inhibitor did not significantly attenuate this effect ( $n = 7$ /group). (d) QL decreased serum FFA levels ( $n = 7$ /group). (e and f) QL significantly promoted FFA uptake by increasing the expressions of CD36 and PGC-1 $\alpha$ , which were downregulated in the MI group, and the HIF-1 $\alpha$  inhibitor could not reverse this effect ( $n = 7$ /group). Data are expressed as means  $\pm$  SEM. \* $p < 0.05$  and \*\* $p < 0.01$  compared with the sham group; # $p < 0.05$  and ## $p < 0.01$  compared with the MI group.

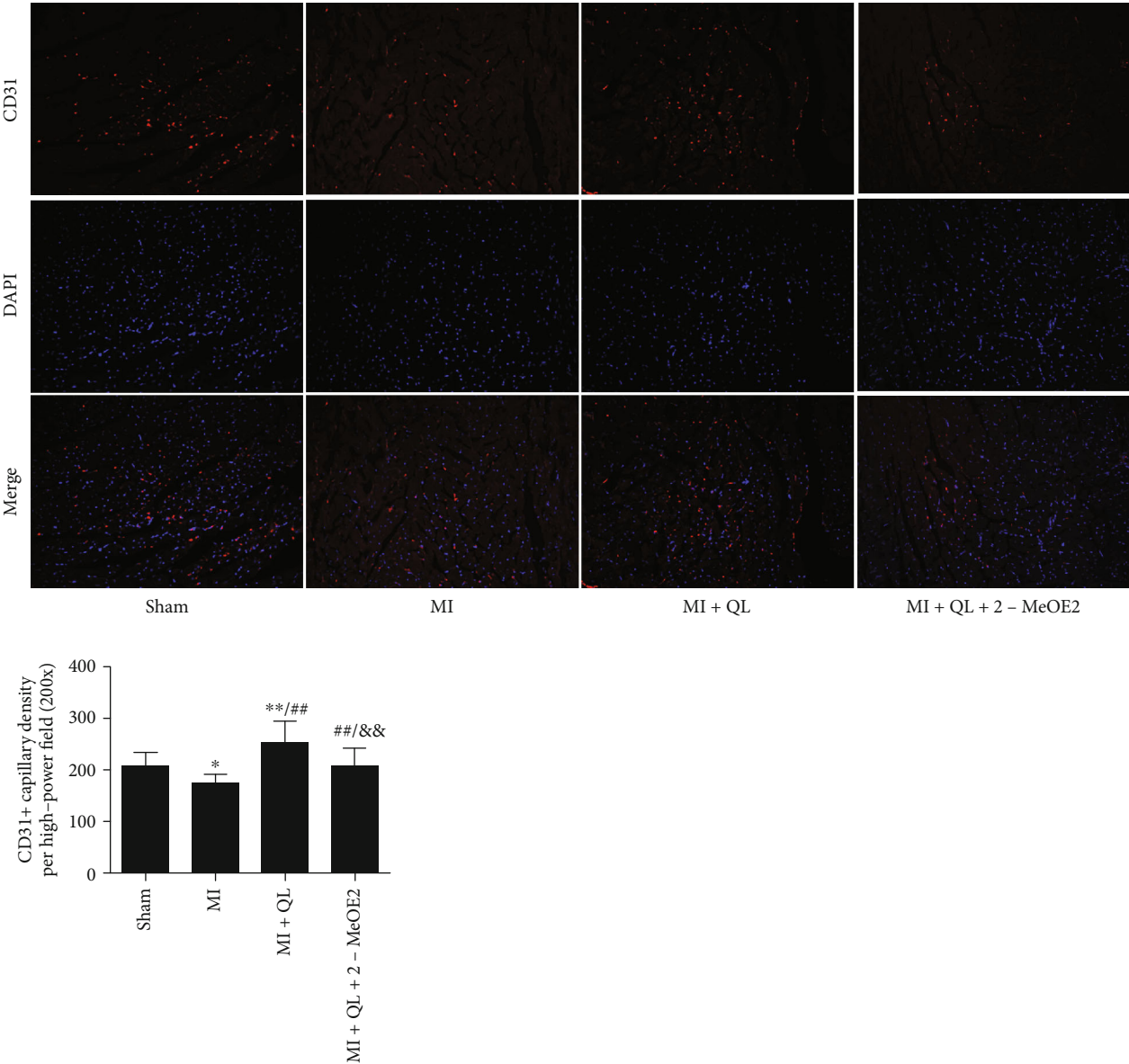
Moreover, both mRNA and/or protein expressions of HIF-1 $\alpha$ , GLUT4, HK2, PKM2, PFK1, and LDHA were upregulated in the MI+QL group compared with MI group, while the HIF-1 $\alpha$  inhibitor attenuated these effects (Figures 4(a)–4(e)). HK2, PKM2, PFK1, and LDHA are the key enzymes of glycolysis, and GLUT4 was the key glucose transporter, so these results further indicated that QL promoted myocardial glucose uptake and glycolysis via the HIF-1 $\alpha$  signaling pathway.

**3.4. QL Treatment Activated Enzyme Expression of Glucose Oxidation and Serum Fatty Acid Uptake in a HIF-1 $\alpha$ -Independent Manner.** PDH and CS are key enzymes involved in glucose aerobic oxidation. We found that protein expressions of PDH and CS, in addition to CS activity, were significantly increased after QL, while HIF-1 $\alpha$  inhibition did not significantly affect this effect (Figures 5(a)–5(c)). The present study also demonstrated significantly decreased CD36 and PGC-1 $\alpha$  protein expressions and increased serum FFA levels in the MI group compared with the sham group. QL treatment upregulated CD36 and PGC-1 $\alpha$  expressions and lowered serum FFA levels, which was not significantly affected by HIF-1 $\alpha$  inhibition (Figures 5(d)–5(f)). This indicates that QL promoted fatty acid uptake in a HIF-1 $\alpha$ -independent manner.

**3.5. QL Treatment Promoted Microvascular Angiogenesis of Myocardial Tissue via a HIF-1 $\alpha$ /VEGF Pathway.** CD31 immunofluorescence staining and Western blot analysis were performed to detect the effects of QL on myocardial microvascular density. Representative images are shown in Figure 6(a). CD31-positive endothelial cells are shown in red and nuclei in blue. Our data revealed a significantly higher CD31-positive microvascular density in the MI+QL group than in the MI group, which was significantly attenuated by treatment with 2-MeOE2. Western blot results also showed that QL could upregulate VEGF, VEGFR2, and CD31 expression, while treatment with a HIF-1 $\alpha$  inhibitor attenuated the QL-induced effect (Figures 6(b)–6(d)). Collectively, our data implied that QL treatment promoted the angiogenesis of infarcted myocardium partly via upregulating the HIF-1 $\alpha$ /VEGF pathway.

## 4. Discussion

In the present study, we observed the effects of QL on myocardial energy metabolism and explored the underlying mechanisms. The results revealed that QL reversed myocardial remodeling by promoting glycolysis via the HIF-1 $\alpha$ -dependent pathway, while QL can also increase the enzyme



(a)

FIGURE 6: Continued.

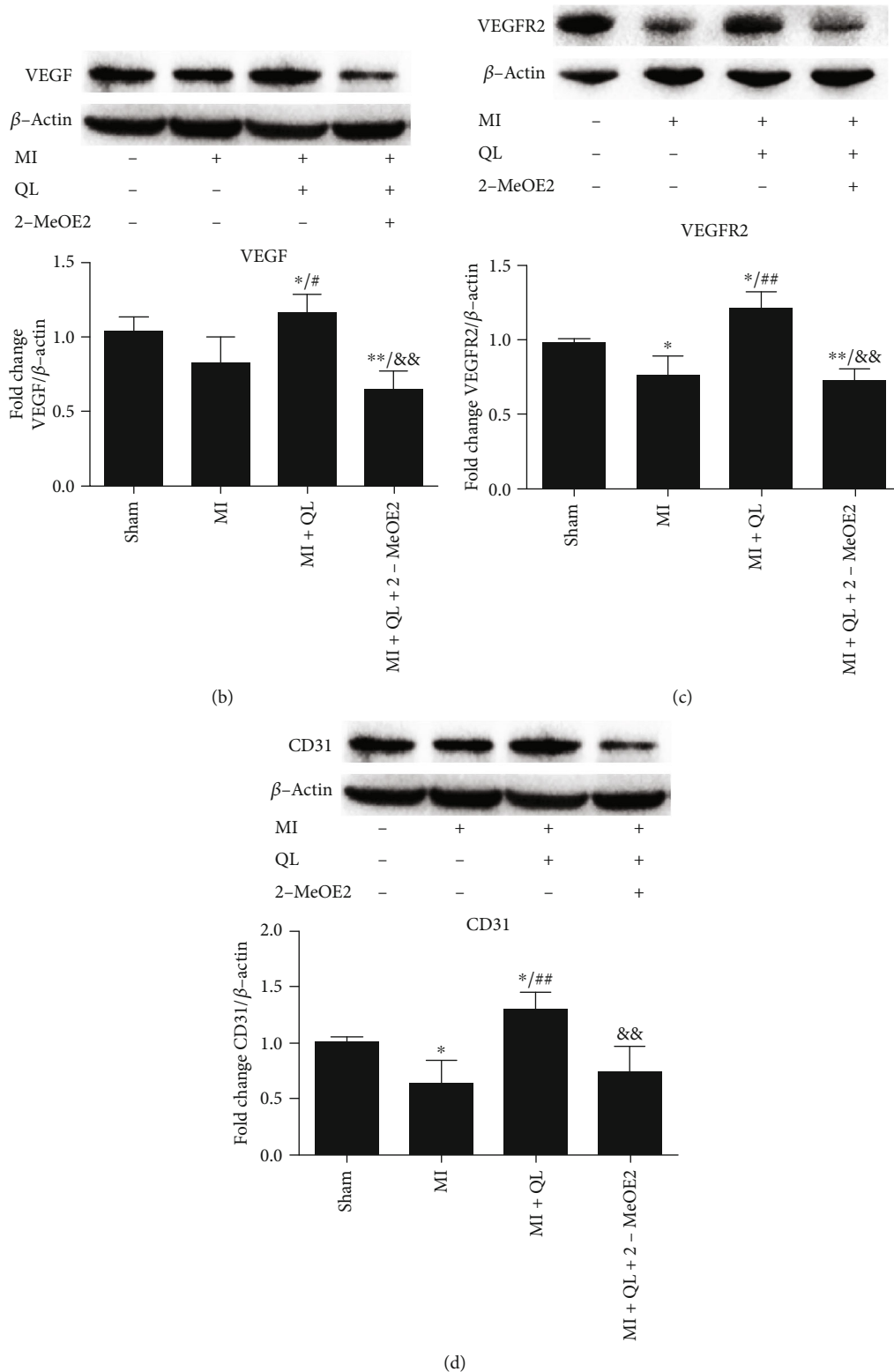


FIGURE 6: QL treatment promoted myocardial angiogenesis. (a) CD31 immunofluorescence staining (20x, scale bar = 100  $\mu$ m) showed that QL significantly increased myocardial angiogenesis, which was significantly attenuated by pretreatment with the HIF-1 $\alpha$  inhibitor. Red indicates CD31-positive signals; blue indicates DAPI nuclei. The newborn capillary density was quantified as the number per high-power field ( $n = 4$ /group). Western blot analysis showed that QL significantly upregulated myocardial VEGF (b), VEGFR2 (c), and CD31 (d) protein expressions, while pretreatment with the HIF-1 $\alpha$  inhibitor attenuated these effects ( $n = 7$ /group). Data from at least four independent experiments were calculated and expressed as means  $\pm$  SD. \* $p < 0.05$  and \*\* $p < 0.01$  compared with the sham group; # $p < 0.05$  and ## $p < 0.01$  compared with the MI group; && $p < 0.01$  compared with the MI+QL group.

expression of glucose oxidation and free fatty acid uptake via a HIF-1 $\alpha$ -independent mechanism.

The reduced substrate utilization capacity served as one important pathological mechanism of cardiac dysfunction in heart failure, which was the result of reduced substrate uptake, oxidation, or a combination of both [25]. There are conflicting results in the previous studies regarding substrate utilization in heart failure [26]. These previous studies found that glucose utilization was increased in early heart failure but substantially declined in advanced heart failure [27–30]. Results on the changes in fatty acid utilization in heart failure are also inconsistent [26], but most studies show that it remained unchanged or slightly increased early in heart failure, before having decreased in advanced heart failure [31–33]. In this study, we found that compared with the sham group, myocardial glucose uptake, oxidation, and ATP production were reduced, while the serum FFA level was elevated in MI rats. These factors might contribute to the observed cardiac dysfunction in MI rats. QL treatment significantly increased myocardial glucose uptake, glycolysis, oxidation, and ATP production; decreased serum FFA; and improved cardiac function. The upregulation of the levels of HIF-1 $\alpha$ , GLUT4, PDH, CD36, and PGC-1 $\alpha$  expression was involved in the observed beneficial effects of QL.

HIF-1 $\alpha$  is a master transcription factor that regulates many target genes (such as VEGF, VEGF receptor 1, and GLUT4), whose protein products play a critical role in improving angiogenesis and vascular remodeling, glucose metabolism, cell survival, and oxygen delivery [12, 34–38]. VEGF is a major mediator of neovascularization in physiological and pathological conditions by promoting vessel formation [39]. Significantly upregulated HIF-1 $\alpha$  and VEGF have been found in the rat ischemic myocardium 1 week after MI, while their expressions were only slightly increased compared with the sham group 2 weeks and 4 weeks after MI [40–42]. The expression levels of VEGF and HIF-1 $\alpha$  were positively related with the increasing microvessel density in the infarct area. In the present study, the protein expressions of HIF-1 $\alpha$  and VEGF were similar between the two groups. The reason may be that the initial activation of HIF-1 $\alpha$  and VEGF promotes angiogenesis and improves blood and oxygen supply, which leads to the gradual decrease of expression. QL treatment significantly upregulated their expressions and promoted neovascularization. Results from the CD31 immunofluorescence staining and Western blot assay also demonstrated that QL increased neonatal capillary density and CD31 protein expressions, while inhibition of HIF-1 $\alpha$  and VEGF activity abolished these beneficial effects of QL.

In addition to promoting angiogenesis and oxygen delivery, HIF-1 $\alpha$  also activates several downstream genes encoding transporters and enzymes related to glucose metabolism. Glucose transportation into cardiomyocytes determines the efficiency of glucose utilization. This is insulin dependent and requires the most important (quantitatively) glucose transporter expressed in the myocardium, which can be activated by HIF-1 $\alpha$ . Previous studies have shown that the myocardial expression of GLUT4 is reduced in rats with heart failure [18, 43], which leads to impaired cardiac glucose metabolism. Metabolic gene expression in the failing human

heart showed decreased GLUT1, GLUT4, and PDK2 mRNA expression [29]. Consistent with previous studies, we found that the mRNA and protein expressions of GLUT4 in the myocardium of MI rats were significantly reduced. Importantly, compared with the MI group, QL treatment significantly upregulated GLUT4 mRNA and protein expressions, which were attenuated by the HIF-1 $\alpha$  inhibitor. Furthermore, PET imaging also suggested that QL could promote myocardial glucose uptake by regulating the HIF-1 $\alpha$  signal pathway.

Apart from glucose transporters, several key enzymes including HK2 [36, 44], PFK1, and PKM2 [45] play an important role in glucose metabolism by converting glucose to pyruvate, which is also regulated by HIF-1 $\alpha$ . Pyruvate can be converted to acetyl-CoA by PDH or to lactic acid by LDHA. HIF-1 $\alpha$  can activate pyruvate dehydrogenase kinase 1 (PDK1) and LDHA expression to switch cells from aerobic metabolic to anaerobic glycolysis [46, 47], since PDH can be phosphorylated and inactivated by PDK1. In our study, we found that compared with the sham group, the mRNA expressions of HK2, PFK1, PKM2, and LDHA were reduced, but the protein expression of PKM2 and LDHA remained unchanged in the MI group; QL treatment significantly upregulated their expressions, which could be suppressed by pretreatment with the HIF-1 $\alpha$  inhibitor. These results indicated that QL could promote the myocardial glycolysis of post-MI hearts in a HIF-1 $\alpha$ -dependent manner.

Moreover, QL also increased PDH and CS activity in a HIF-1 $\alpha$ -independent manner. CS is a mitochondrial enzyme found in all cells that is capable of oxidative metabolism and is involved in lipogenesis, cholesterologenesis, and energy production. Its activity follows a circadian pattern, with the results indicating that QL could also enhance glucose aerobic metabolism. However, HIF-1 $\alpha$ -mediated induction of PDK1 has been found to prevent the entry of pyruvate into the tricarboxylic acid cycle [46], which seems contradictory to our results. Nevertheless, activated HIF-1 $\alpha$  could promote angiogenesis as well as recover blood and oxygen supply, which might favor mitochondrial respiration and aerobic metabolism. Thus, this may explain these conflicting outcomes. On the other hand, our results showed that QL promoted PDH and CS expression via HIF-1 $\alpha$ -independent pathways.

PGC-1 $\alpha$  is a powerful transcriptional coactivator and a key regulator in cardiac mitochondrial biogenesis and oxidative metabolism, which works by cooperating with numerous transcription factors (such as nuclear respiratory factor-1 or 2 and estrogen-related receptor  $\alpha$ ) to promote related genes [48]. It plays a critical role in upregulating antioxidant genes and interacting with peroxisome proliferator-activated receptors (PPARs) to increase fatty acid oxidation and angiogenesis [49]. Fatty acid translocase (FAT)/CD36 is a key protein in the translocation of fatty acids across the sarcolemmal membrane of cardiomyocytes [5]. CD36 and CPT-1 are the target genes of PPAR, which was coactivated by PGC-1 $\alpha$ . There were studies showing that QL could increase PGC-1 $\alpha$  and CPT-1 expression in rats with heart failure from pressure overload and H9C2 cardiomyocytes [18, 19]. Due to heart failure, serum FFA concentrations increased significantly, which could decrease glucose oxidation by inhibiting PDH activity [7]. On the other hand, there were studies presenting decreased

circulating FFA concentrations, which could promote glucose uptake and oxidation indirectly [9]. In accordance with a previous study, we found that QL significantly upregulated the expression of the PGC-1 $\alpha$  and CD36 protein, which may promote FFA uptake and decrease serum FFA levels in a HIF-1 $\alpha$ -independent pathway. It is important to note that decreased serum FFA concentration might further promote glucose oxidation indirectly through activating PDH expression. A previous study also showed that QL and its main chemical property (astragaloside) could improve diastolic and systolic function by promoting AMPK phosphorylation and PPAR $\gamma$ , PPAR $\alpha$ , and PGC-1 $\alpha$  expression [18, 50–54], which are key regulators of energy metabolism. So, we postulate that the AMPK, PPAR, and PGC-1 $\alpha$  pathway might be the possible mechanisms for QL to promote aerobic metabolism, and which were independent of the HIF-1 $\alpha$  pathway.

## 5. Conclusions

In summary, the present study demonstrated that QL restored the microstructure of myocardium, attenuated myocardial fibrosis, and improved cardiac function in heart failure rats post MI. In the present study, we found that the enhancement of enzyme expression of myocardial glucose and fatty acid metabolism with elevated ATP level may account for the observed beneficial effects of QL. The activation of the HIF-1 $\alpha$  signaling pathway and its downstream target genes proved to be at least partly involved in these benefits, including promoted glycolysis and ATP level. Although the effect of QL on promoting enzyme expression of glucose oxidation and FFA uptake is achieved via a HIF-1 $\alpha$ -independent pathway, the exact mechanism behind this effect requires further study. Our data provided a novel potential working mechanism of QL regarding its impact on myocardial glucose and fatty acid metabolic balance with an elevated ATP level in this rat model of heart failure after myocardial infarction.

## Data Availability

The data used to support the findings of this study are available from the corresponding author upon request.

## Conflicts of Interest

The authors declared no potential conflicts of interest with respect to the research, authorship, and/or publication of this article.

## Authors' Contributions

Yanyan Wang, Mingqiang Fu, and Jingfeng Wang contributed equally to this work.

## Acknowledgments

This study was supported by grants from the National Natural Science Foundation of China (81873123), the Program for the Outstanding Academic Leaders supported by the Shanghai Science and Technology Commission (16XD1400700), the National Basic Research Program of China (973 Program,

2012CB518605), and the Shanghai Municipal Commission of Health and Family Planning (2018JP002).

## References



- [1] D. Mozaffarian, E. J. Benjamin, A. S. Go et al., "Heart disease and stroke statistics—2015 update: a report from the American Heart Association," *Circulation*, vol. 131, no. 4, pp. e29–322, 2015.
- [2] V. L. Roger, S. A. Weston, and M. M. Redfield, "Trends in heart failure incidence and survival in a community-based population," *ACC Current Journal Review*, vol. 13, no. 12, p. 30, 2004.
- [3] D. Levy, S. Kenchaiah, M. G. Larson et al., "Long-term trends in the incidence of and survival with heart failure," *The New England Journal of Medicine*, vol. 347, no. 18, pp. 1397–1402, 2002.
- [4] J. Mori, R. Basu, B. A. McLean et al., "Agonist-induced hypertrophy and diastolic dysfunction are associated with selective reduction in glucose oxidation: a metabolic contribution to heart failure with normal ejection fraction," *Circulation Heart Failure*, vol. 5, no. 4, pp. 493–503, 2012.
- [5] G. D. Lopaschuk, J. R. Ussher, C. D. Folmes, J. S. Jaswal, and W. C. Stanley, "Myocardial fatty acid metabolism in health and disease," *Physiological Reviews*, vol. 90, no. 1, pp. 207–258, 2010.
- [6] N. Fillmore, J. Mori, and G. D. Lopaschuk, "Mitochondrial fatty acid oxidation alterations in heart failure, ischaemic heart disease and diabetic cardiomyopathy," *British Journal of Pharmacology*, vol. 171, no. 8, pp. 2080–2090, 2014.
- [7] Z. Wang, J. Ding, X. Luo et al., "Effect of allopurinol on myocardial energy metabolism in chronic heart failure rats after myocardial infarct," *International Heart Journal*, vol. 57, no. 6, pp. 753–759, 2016.
- [8] N. Quan, W. Sun, L. Wang et al., "Sestrin2 prevents age-related intolerance to ischemia and reperfusion injury by modulating substrate metabolism," *The FASEB Journal*, vol. 31, no. 9, pp. 4153–4167, 2017.
- [9] T. Kato, S. Niizuma, Y. Inuzuka et al., "Analysis of metabolic remodeling in compensated left ventricular hypertrophy and heart failure," *Circulation Heart Failure*, vol. 3, no. 3, pp. 420–430, 2010.
- [10] R. M. Bersin, C. Wolfe, M. Kwasman et al., "Improved hemodynamic function and mechanical efficiency in congestive heart failure with sodium dichloroacetate," *Journal of the American College of Cardiology*, vol. 23, no. 7, pp. 1617–1624, 1994.
- [11] X. Yue, X. Lin, T. Yang et al., "Rnd3/RhoE modulates hypoxia-inducible factor 1 $\alpha$ /vascular endothelial growth factor signaling by stabilizing hypoxia-inducible factor 1 $\alpha$  and regulates responsive cardiac angiogenesis," *Hypertension*, vol. 67, no. 3, pp. 597–605, 2016.
- [12] G. L. Semenza, "Hypoxia-inducible factor 1 and cardiovascular disease," *Annual Review of Physiology*, vol. 76, no. 1, pp. 39–56, 2014.
- [13] Y. Du, Y. Ge, Z. Xu et al., "Hypoxia-inducible factor 1 alpha (HIF-1 $\alpha$ )/vascular endothelial growth factor (VEGF) pathway participates in angiogenesis of myocardial infarction in muscone-treated mice: preliminary study," *Medical Science Monitor*, vol. 24, pp. 8870–8877, 2018.

- [14] Y. Cheng, Y. Feng, Z. Xia, X. Li, and J. Rong, " $\omega$ -Alkynyl arachidonic acid promotes anti-inflammatory macrophage M2 polarization against acute myocardial infarction via regulating the cross-talk between PKM2, HIF-1 $\alpha$  and iNOS," *Biochimica et Biophysica Acta (BBA) - Molecular and Cell Biology of Lipids*, vol. 1862, no. 12, pp. 1595–1605, 2017.
- [15] K. Sarkar, Z. Cai, R. Gupta et al., "Hypoxia-inducible factor 1 transcriptional activity in endothelial cells is required for acute phase cardioprotection induced by ischemic preconditioning," *Proceedings of the National Academy of Sciences of the United States of America*, vol. 109, no. 26, pp. 10504–10509, 2012.
- [16] J. Wang, J. Zhou, X. Ding et al., "Qiliqiangxin improves cardiac function and attenuates cardiac remodeling in rats with experimental myocardial infarction," *International Journal of Clinical and Experimental Pathology*, vol. 8, no. 6, pp. 6596–6606, 2015.
- [17] X. Li, J. Zhang, J. Huang et al., "A multicenter, randomized, double-blind, parallel-group, placebo-controlled study of the effects of qili qiangxin capsules in patients with chronic heart failure," *Journal of the American College of Cardiology*, vol. 62, no. 12, pp. 1065–1072, 2013.
- [18] J. Zhang, C. Wei, H. Wang et al., "Protective effect of qiliqiangxin capsule on energy metabolism and myocardial mitochondria in pressure overload heart failure rats," *Evidence-based Complementary and Alternative Medicine*, vol. 2013, Article ID 378298, 9 pages, 2013.
- [19] S. Lin, X. Wu, L. Tao et al., "The metabolic effects of traditional Chinese medication Qiliqiangxin on H9C2 cardiomyocytes," *Cellular Physiology and Biochemistry*, vol. 37, no. 6, pp. 2246–2256, 2015.
- [20] J. Wang, J. Zhou, Y. Wang et al., "Qiliqiangxin protects against anoxic injury in cardiac microvascular endothelial cells via NRG-1/ErbB-PI3K/Akt/mTOR pathway," *Journal of Cellular and Molecular Medicine*, vol. 21, pp. 1905–1914, 2017.
- [21] L. Yuan, L. Qiu, Y. Ye et al., "Heat-shock transcription factor 1 is critically involved in the ischaemia-induced cardiac hypertrophy via JAK2/STAT3 pathway," *Journal of Cellular and Molecular Medicine*, vol. 22, no. 9, pp. 4292–4303, 2018.
- [22] Z. Chen, Y. Li, Y. Wang et al., "Cardiomyocyte-restricted low density lipoprotein receptor-related protein 6 (LRP6) deletion leads to lethal dilated cardiomyopathy partly through Drp1 signaling," *Theranostics*, vol. 8, no. 3, pp. 627–643, 2018.
- [23] A. Sun, Y. Zou, P. Wang et al., "Mitochondrial aldehyde dehydrogenase 2 plays protective roles in heart failure after myocardial infarction via suppression of the cytosolic JNK/p53 pathway in mice," *Journal of the American Heart Association*, vol. 3, no. 5, article e000779, 2014.
- [24] S. Das, T. Aiba, M. Rosenberg et al., "Pathological role of serum- and glucocorticoid-regulated kinase 1 in adverse ventricular remodeling," *Circulation*, vol. 126, no. 18, pp. 2208–2219, 2012.
- [25] G. Heusch, P. Libby, B. Gersh et al., "Cardiovascular remodeling in coronary artery disease and heart failure," *The Lancet*, vol. 383, no. 9932, pp. 1933–1943, 2014.
- [26] S. Neubauer, "The failing heart—an engine out of fuel," *The New England Journal of Medicine*, vol. 356, no. 11, pp. 1140–1151, 2007.
- [27] A. Remondino, N. Rosenblatt-Velin, C. Montessuit et al., "Altered expression of proteins of metabolic regulation during remodeling of the left ventricle after myocardial infarction," *Journal of Molecular and Cellular Cardiology*, vol. 32, no. 11, pp. 2025–2034, 2000.
- [28] L. Nascimben, J. S. Ingwall, B. H. Lorell et al., "Mechanisms for increased glycolysis in the hypertrophied rat heart," *Hypertension*, vol. 44, no. 5, pp. 662–667, 2004.
- [29] P. Razeghi, M. E. Young, J. L. Alcorn, C. S. Moravec, O. H. Frazier, and H. Taegtmeier, "Metabolic gene expression in fetal and failing human heart," *Circulation*, vol. 104, no. 24, pp. 2923–2931, 2001.
- [30] M. Taylor, T. R. Wallhaus, T. R. Degrado et al., "An evaluation of myocardial fatty acid and glucose uptake using PET with [18F]fluoro-6-thia-heptadecanoic acid and [18F]FDG in patients with congestive heart failure," *Journal of Nuclear Medicine*, vol. 42, no. 1, pp. 55–62, 2001.
- [31] W. C. Stanley, F. A. Recchia, and G. D. Lopaschuk, "Myocardial substrate metabolism in the normal and failing heart," *Physiological Reviews*, vol. 85, no. 3, pp. 1093–1129, 2005.
- [32] J. C. Osorio, W. C. Stanley, A. Linke et al., "Impaired myocardial fatty acid oxidation and reduced protein expression of retinoid X receptor- $\alpha$  in pacing-induced heart failure," *Circulation*, vol. 106, no. 5, pp. 606–612, 2002.
- [33] M. P. Chandler, J. Kerner, H. Huang et al., "Moderate severity heart failure does not involve a downregulation of myocardial fatty acid oxidation," *American Journal of Physiology. Heart and Circulatory Physiology*, vol. 287, no. 4, pp. H1538–H1543, 2004.
- [34] L. Zhang, Z. Sun, P. Ren et al., "Localized delivery of shRNA against PHD2 protects the heart from acute myocardial infarction through ultrasound-targeted cationic microbubble destruction," *Theranostics*, vol. 7, no. 1, pp. 51–66, 2017.
- [35] F. Zhang, M. Hao, H. Jin et al., "Canonical hedgehog signalling regulates hepatic stellate cell-mediated angiogenesis in liver fibrosis," *British Journal of Pharmacology*, vol. 174, no. 5, pp. 409–423, 2017.
- [36] Y. Lu, B. Wang, Q. Shi, X. Wang, D. Wang, and L. Zhu, "Brusatol inhibits HIF-1 signaling pathway and suppresses glucose uptake under hypoxic conditions in HCT116 cells," *Scientific Reports*, vol. 6, no. 1, article 39123, 2016.
- [37] I. N. Schellinger, N. Cordasic, J. Panesar et al., "Hypoxia inducible factor stabilization improves defective ischemia-induced angiogenesis in a rodent model of chronic kidney disease," *Kidney International*, vol. 91, no. 3, pp. 616–627, 2017.
- [38] K. Dashnyam, G. Z. Jin, J. H. Kim, R. Perez, J. H. Jang, and H. W. Kim, "Promoting angiogenesis with mesoporous microcarriers through a synergistic action of delivered silicon ion and VEGF," *Biomaterials*, vol. 116, pp. 145–157, 2017.
- [39] G. Liu, L. Li, D. Huo et al., "A VEGF delivery system targeting MI improves angiogenesis and cardiac function based on the tropism of MSCs and layer-by-layer self-assembly," *Biomaterials*, vol. 127, pp. 117–131, 2017.
- [40] R. An, C. Xi, J. Xu et al., "Intramyocardial injection of recombinant adeno-associated viral vector coexpressing PR39/adrenomedullin enhances angiogenesis and reduces apoptosis in a rat myocardial infarction model," *Oxidative Medicine and Cellular Longevity*, vol. 2017, Article ID 1271670, 13 pages, 2017.
- [41] Q. L. Wang, H. J. Wang, Z. H. Li, Y. L. Wang, X. P. Wu, and Y. Z. Tan, "Mesenchymal stem cell-loaded cardiac patch promotes epicardial activation and repair of the infarcted myocardium," *Journal of Cellular and Molecular Medicine*, vol. 21, no. 9, pp. 1751–1766, 2017.
- [42] C. Cheng, P. Li, Y. G. Wang, M. H. Bi, and P. S. Wu, "Study on the expression of VEGF and HIF-1 $\alpha$  in infarct area of rats with AMI," *European Review for Medical and Pharmacological Sciences*, vol. 20, no. 1, pp. 115–119, 2016.

- [43] D. Fliegner, D. Westermann, A. Riad et al., "Up-regulation of PPAR $\gamma$  in myocardial infarction," *European Journal of Heart Failure*, vol. 10, no. 1, pp. 30–38, 2008.
- [44] H. G. Lee, H. Kim, T. Son et al., "Regulation of HK2 expression through alterations in CpG methylation of the HK2 promoter during progression of hepatocellular carcinoma," *Oncotarget*, vol. 7, no. 27, pp. 41798–41810, 2016.
- [45] R. H. de Wit, A. Mujic-Delic, J. R. van Senten, A. Fraile-Ramos, M. Siderius, and M. J. Smit, "Human cytomegalovirus encoded chemokine receptor US28 activates the HIF-1 $\alpha$ /PKM2 axis in glioblastoma cells," *Oncotarget*, vol. 7, no. 42, pp. 67966–67985, 2016.
- [46] H. Semba, N. Takeda, T. Isagawa et al., "HIF-1 $\alpha$ -PDK1 axis-induced active glycolysis plays an essential role in macrophage migratory capacity," *Nature Communications*, vol. 7, no. 1, article 11635, 2016.
- [47] X. G. Cui, Z. T. Han, S. H. He et al., "HIF1/2 $\alpha$  mediates hypoxia-induced LDHA expression in human pancreatic cancer cells," *Oncotarget*, vol. 8, no. 15, pp. 24840–24852, 2017.
- [48] S. Movafagh, S. Crook, and K. Vo, "Regulation of hypoxia-inducible factor-1 $\alpha$  by reactive oxygen species: new developments in an old debate," *Journal of Cellular Biochemistry*, vol. 116, no. 5, pp. 696–703, 2015.
- [49] K. Zhang, J. Lu, T. Mori et al., "Baicalin increases VEGF expression and angiogenesis by activating the ERR $\alpha$ /PGC-1 $\alpha$  pathway," *Cardiovascular Research*, vol. 89, no. 2, pp. 426–435, 2011.
- [50] S. Shen, H. Jiang, Y. Bei et al., "Qiliqiangxin attenuates adverse cardiac remodeling after myocardial infarction in ovariectomized mice via activation of PPAR $\gamma$ ," *Cellular Physiology and Biochemistry*, vol. 42, no. 3, pp. 876–888, 2017.
- [51] J. Wang, Z. Li, Y. Wang et al., "Qiliqiangxin enhances cardiac glucose metabolism and improves diastolic function in spontaneously hypertensive rats," *Evidence-based Complementary and Alternative Medicine*, vol. 2017, Article ID 3197320, 11 pages, 2017.
- [52] S. Zhang, F. Tang, Y. Yang et al., "Astragaloside IV protects against isoproterenol-induced cardiac hypertrophy by regulating NF- $\kappa$ B/PGC-1 $\alpha$  signaling mediated energy biosynthesis," *PLoS One*, vol. 10, no. 3, article e0118759, 2015.
- [53] Z. Dong, P. Zhao, M. Xu et al., "Astragaloside IV alleviates heart failure via activating PPAR $\alpha$  to switch glycolysis to fatty acid  $\beta$ -oxidation," *Scientific Reports*, vol. 7, no. 1, article 2691, 2017.
- [54] B. Tang, J. G. Zhang, H. Y. Tan, and X. Q. Wei, "Astragaloside IV inhibits ventricular remodeling and improves fatty acid utilization in rats with chronic heart failure," *Bioscience Reports*, vol. 38, no. 3, 2018.

## Research Article

# *Dracocephalum moldavica* L. Extracts Protect H9c2 Cardiomyocytes against H<sub>2</sub>O<sub>2</sub>-Induced Apoptosis and Oxidative Stress

Min Jin,<sup>1,2</sup> Hui Yu,<sup>3</sup> Xia Jin,<sup>4</sup> Lailai Yan,<sup>1,5,6</sup> Jingyu Wang<sup>1,5,6</sup> , and Zhanli Wang<sup>2,3</sup> 

<sup>1</sup>Department of Laboratorial Science and Technology, School of Public Health, Peking University, Beijing 100191, China

<sup>2</sup>School of Public Health, Baotou Medical College, Baotou 014060, China

<sup>3</sup>Inner Mongolia Key Laboratory of Disease-Related Biomarkers, The Second Affiliated Hospital, Baotou Medical College, Baotou 014030, China

<sup>4</sup>Inner Mongolia Autonomous Region People's Hospital, Hohhot 010010, China

<sup>5</sup>Vaccine Research Center, School of Public Health, Peking University, Beijing 100191, China

<sup>6</sup>Peking University Medical and Health Analysis Center, Peking University, Beijing 100191, China

Correspondence should be addressed to Jingyu Wang; [wjy@bjmu.edu.cn](mailto:wjy@bjmu.edu.cn) and Zhanli Wang; [wang.zhanli@hotmail.com](mailto:wang.zhanli@hotmail.com)

Received 16 December 2019; Accepted 7 March 2020; Published 5 May 2020

Guest Editor: Ayodeji F. Ajayi

Copyright © 2020 Min Jin et al. This is an open access article distributed under the Creative Commons Attribution License, which permits unrestricted use, distribution, and reproduction in any medium, provided the original work is properly cited.

**Background and Objectives.** *Dracocephalum moldavica* L. is an herbal medicine used to treat cardiovascular diseases in China. The purpose of this study was to assess the cardioprotective effect of *D. moldavica* L. extracts against H<sub>2</sub>O<sub>2</sub>-induced apoptosis and oxidative stress in H9c2 cells and to explore the mechanism behind this effect. **Materials and Methods.** The petroleum ether (petrol), dichloromethane (CH<sub>2</sub>Cl<sub>2</sub>), ethyl acetate (EtOAc), and n-butyl alcohol (n-BuOH) fractions were isolated from alcohol extracts of *D. moldavica* L. Total phenolic and flavonoid contents and *in vitro* antioxidant activities of different fractions were evaluated. H9c2 cells were then treated with *D. moldavica* L. extracts before challenging with H<sub>2</sub>O<sub>2</sub>. Cell viability was determined by colorimetric assay, and ELISA was used to measure the levels of lactate dehydrogenase (LDH), malondialdehyde (MDA), and superoxide dismutase (SOD). Apoptosis levels and mitochondrial membrane potential were measured by flow cytometry. The expressions of cell apoptosis regulatory proteins caspase-3, Bax, and Bcl-2 were determined by western blotting. **Results.** Our results demonstrated that the EtOAc fraction from *D. moldavica* L. ethanol extract, which is rich in phenolic and flavonoid active constituents, had the strongest free radical scavenging activity. Additionally, this fraction increased H<sub>2</sub>O<sub>2</sub>-induced reduction in cell viability, SOD activity, and mitochondrial membrane potential. It also reduced H<sub>2</sub>O<sub>2</sub>-induced elevation in ROS production, contents of LDH and MDA, and H9c2 apoptosis. We further found that the EtOAc fraction increased Bcl-2 expression, while it decreased caspase-3 and Bax expressions induced by H<sub>2</sub>O<sub>2</sub> in H9c2 cells. **Conclusions.** Our data revealed that the EtOAc fraction from *D. moldavica* L. ethanol extract ameliorates H<sub>2</sub>O<sub>2</sub>-induced cardiotoxicity via antiapoptotic and antioxidant mechanisms.

## 1. Introduction

Ischemic heart disease (IHD), the most common cause of death worldwide, is a chronic disease leading to myocardial ischemia, hypoxia, and necrosis [1]. The mechanisms involved in IHD are complicated. Accumulating evidence has revealed that oxidative stress plays an important role in the pathogenesis of myocardial ischemia-reperfusion (I/R)

injury [2]. Oxidative stress occurs as a consequence of a redox imbalance in cells between prooxidants and antioxidants [3]. The overproduction of reactive oxygen species (ROS) and impairment of endogenous antioxidant systems may lead to the release of inflammatory cytokines and the enhancement of reactive aldehydes such as malondialdehyde (MDA) [4]. The increase in oxidative stress may also result in mitochondrial dysfunction, eventually leading to



the activation of cardiac apoptotic signaling, further exacerbating ischemic injury [5]. The exogenous administration of antioxidants or the upregulation of endogenous antioxidants is an important approach for the prevention of I/R-induced cardiac injury [6]. Therefore, a pharmacological agent with antioxidant properties might be an effective strategy for cardioprotection. Plants often contain several potential active components which possess antioxidant properties such as phenols, flavonoids, terpenoids, and saponins [7]. Recently, several studies have revealed that herbal extracts containing antioxidant compounds exert a cardioprotective effect [8, 9].

*Dracocephalum moldavica L.* is a common perennial species that is widely used as a folk medicine for the treatment of cardiovascular diseases [10]. Several studies have shown that the extracts of *D. moldavica L.* possess high antioxidant activity [11, 12]. Previous studies also confirmed that the total flavonoid extract of *D. moldavica L.* can efficiently attenuate ischemia-induced myocardial injury, and its mechanism may be related to the improvement of myocardial oxidative stress states and regulation of the antiapoptotic signaling pathways [13, 14]. *D. moldavica L.* has been reported to contain flavonoids, glycoside, tannins, steroid, saponins, and phenolic compounds [15]. However, the antioxidant fraction and antioxidative stress mechanism of the alcohol extracts of *D. moldavica L.* have not been comprehensively described. This work is aimed at identifying the antioxidant fraction of *D. moldavica L.* extracts and at further investigating its antioxidant stress effects. Moreover, the cardioprotective effects of *D. moldavica L.* component in H9c2 cardiomyocytes under  $H_2O_2$ -induced oxidative stress and its underlying mechanisms were also investigated.

## 2. Materials and Methods

**2.1. Chemicals and Reagents.** 2,2-Diphenyl-1-picrylhydrazyl-radical (DPPH), dimethyl sulfoxide (DMSO), 2,2'-azinobis (3-ethylbenzothiazoline-6-sulfonic acid) diammonium salt (ABTS), potassium persulfate, and hydrogen peroxide ( $H_2O_2$ ) were purchased from Sigma-Aldrich (St. Louis, MO, USA). The cell culture products were purchased from Thermo Fisher Scientific Inc. (Waltham, MA, USA). The kits used to determine the MDA content and lactate dehydrogenase (LDH) and superoxide dismutase (SOD) activities were obtained from Jiancheng Bioengineering Institute (Nanjing, China). The fluorescent dye 5,5',6,6'-tetrachloro-1,1',3,3'-tetraethylbenzimidazolyl-carbocyanine iodide (JC-1) was purchased from Sigma-Aldrich (St. Louis, MO, USA), and the annexin V/propidium iodide (PI) apoptosis detection kit was obtained from Invitrogen (Eugene, OR, USA). General laboratory reagents were purchased from Sinopharm Chemical Reagent Co., Ltd. (Beijing, China). Antibodies of anti-Bax and anti-cleaved-caspase-3 were purchased from Millipore (Beverly, MA, USA), and antibodies of anti-Bcl-2, anti-pro-caspase-3, and anti- $\beta$ -actin were purchased from Sangon Biotech (Shanghai, China). All chemical reagents were at least of analytical grade.

**2.2. Plant Material and Extract Preparation.** The aerial parts of *D. moldavica L.* were collected from the county of Tongliao, Inner Mongolia, China. The plant materials were air-dried and ground into a powder. The plant powder and the solvent (1:10 v/v) were placed in the flask of a constant-speed blender with a digital display (60 W, China) for reflux extraction twice with the following conditions: ethanol and water (65:35 v/v) as the solvent, 60°C as the extraction temperature, and 120 min as the extraction time. Subsequently, the extracts were concentrated in a rotary evaporator (Yarong RE-2000A, China) under reduced pressure for ethanol removal. The obtained ethanol extracts were then separated with petroleum ether (petrol), dichloromethane ( $CH_2Cl_2$ ), ethyl acetate (EtOAc), and n-butyl alcohol (n-BuOH) using separating funnels. The resultant fractions were concentrated, dried, and stored at -20°C for further analyses.

**2.3. Quantification of the Total Phenolic and Flavonoid Contents.** The total phenolic content of each fraction was determined using the Folin-Ciocalteu method [16], whereas the total flavonoid content was measured using a spectrophotometric method as described previously [16]. Moreover, high-performance liquid chromatography (HPLC) was used for the qualitative analysis of the EtOAc fraction of *D. moldavica L.* ethanol extract with the standards (tallianine, rosmarinic acid, luteolin, apigenin, and diosmetin) as the references as described previously [17].

**2.4. In Vitro Antioxidant Activity.** The DPPH radical and ABTS radical scavenging activity was measured using the method as described previously [18]. Briefly, different dilutions of each fraction of *D. moldavica L.* ethanol extract were prepared. An aliquot of each dilution was mixed vigorously with a methanol solution of DPPH or with a water solution of ABTS. The absorbance was measured at 517 nm or 734 nm. Methanol or water was used as a blank control. The superoxide anion radical scavenging activity and the hydroxyl radical scavenging activity of each fraction were determined using a commercially available kit obtained from Jiancheng Bioengineering Institute (Nanjing, China).

**2.5. Cell Culture and Treatment.** The embryonic rat heart-derived H9c2 cell line was obtained from the Bank of the Chinese Academy of Sciences (Shanghai, China). Cells were cultivated in DMEM with 10% FBS and 100 mg/mL penicillin/streptomycin under atmospheric conditions of 95% air/5%  $CO_2$  at 37°C. H9c2 cells were then divided into three groups: control, model, and EtOAc fraction groups. The EtOAc fraction groups were pretreated with various concentrations of *D. moldavica L.* extracts (0.01, 0.05, 0.1, 0.3, 0.5, and 1.0  $\mu$ g/mL) for 24 h. No extracts were exposed to the control group and the model group. The model group and the EtOAc fraction groups were then exposed to  $H_2O_2$  (150 mM) for 4 h, and the control group was treated with DMEM medium.

**2.6. Cell Viability.** Cell viability was determined using the Cell Counting Kit-8 (DOJINDO, Tokyo, Japan) according to the manufacturer's instructions. The absorbance of the culture medium in each well was recorded at 450 nm using a

microplate reader (Bio-Rad, Hercules, CA, USA) to determine the cell viability. All experiments were repeated at least three times.

**2.7. Measurement of MDA, LDH, and SOD Levels.** The cultured supernatant and cells were collected after different treatments to determine the LDH and SOD activities as well as the MDA level using the corresponding commercially available kits obtained from Jiancheng Bioengineering Institute (Nanjing, China) following the manufacturer's instructions.

**2.8. Determination of Intracellular ROS.** The intracellular ROS levels in the H9c2 cells were measured using the fluorescent probe, 2',7'-dichlorodihydrofluorescein diacetate (DCFH-DA, Sigma-Aldrich, St. Louis, MO, USA). The cells were stained with 10 mM DCFH-DA for 20 min in the dark at 37°C. Then, fluorescence was measured using a fluorometer (U-RFLT50, OLYMPUS, Japan) at an excitation wavelength of 485 nm and an emission wavelength of 530 nm.

**2.9. Detection of Apoptosis.** Apoptosis was measured by flow cytometry using an annexin V-FITC apoptosis detection kit (Sigma-Aldrich, St. Louis, MO, USA) according to the manufacturer's instructions. Cells were incubated with 5  $\mu$ L of FITC-annexin V and 1  $\mu$ L of PI working solution (100  $\mu$ g/mL) for 15 min in the dark at room temperature. Cellular fluorescent detection and quantitative determination were then performed using a flow cytometer (Beckman Coulter, USA).

**2.10. Determination of the Mitochondrial Transmembrane Potential.** JC-1 was used to detect changes in the mitochondrial transmembrane potential. Cells were incubated with 10  $\mu$ L of 200  $\mu$ M JC-1 (final concentration, 2  $\mu$ M) for 30 min in the dark and analyzed using an SC500 flow cytometer.

**2.11. Western Blotting.** Equal amounts of protein from each sample cell were separated by SDS-PAGE and transferred to polyvinylidene difluoride membranes. The membranes were then blocked with 5% (w/v) nonfat milk powder for 2 h and incubated overnight with primary antibodies at 4°C. After washing, the membranes were incubated with horseradish peroxidase-conjugated secondary antibody for 1 h at room temperature. Finally, the protein bands were visualized using the ECL chemiluminescence detection system (Amersham, USA).

**2.12. Statistical Analysis.** Descriptive analyses were used to present the results of the chemical composition analysis and the antioxidant activity assays. The analysis of variance and Tukey's multiple range test were used to test the differences between groups, and a *P* value less than 0.05 was considered significant. The data were analyzed using SPSS 17.0 software (SPSS, Chicago, IL, USA).

### 3. Results

**3.1. Identification of the Antioxidant Fraction.** Four *in vitro* antioxidant activity assays were performed to identify the fraction of *D. moldavica* L. ethanol extract that exhibits the antioxidant activity, including DPPH, ABTS, hydroxyl, and superoxide anion radical scavenging assays. As shown in Figure 1, the EtOAc fraction of *D. moldavica* L. ethanol extract possessed the highest scavenging ability, as demonstrated by the four assays. Moreover, the highest total flavonoid content was found in the EtOAc fraction, followed by the n-BuOH, CH<sub>2</sub>Cl<sub>2</sub>, and petrol fractions. Similarly, the total phenolic contents were ranked in the order of EtOAc > n-BuOH > CH<sub>2</sub>Cl<sub>2</sub> > petrol (Table 1). Additionally, the chromatograms also showed that rosmarinic acid, tilianin, luteolin, apigenin, and disometin were found in the EtOAc fraction (Figure S1).

**3.2. The EtOAc Fraction of *D. moldavica* L. Ethanol Extract Protected H9c2 Cells against H<sub>2</sub>O<sub>2</sub>-Induced Cytotoxicity.** To assess the effects of the EtOAc fraction of *D. moldavica* L. ethanol extract on H<sub>2</sub>O<sub>2</sub>-induced cytotoxicity in H9c2 cells, the cell viability was determined. As shown in Figure 2(a), the cell viability was significantly decreased in the H<sub>2</sub>O<sub>2</sub>-treated group compared with the control group. The EtOAc fraction at the doses of 0.1, 0.3, 0.5, and 1.0  $\mu$ g/mL significantly attenuated H<sub>2</sub>O<sub>2</sub>-induced reduction in cell viability, in comparison with the model group. The results further showed that cell viability was increased in a dose-dependent manner when the EtOAc fraction concentration was increased from 0.1 to 0.5  $\mu$ g/mL. However, compared with the model group, the EtOAc fraction had no significant effect on cell viability at the doses of 0.01 and 0.05  $\mu$ g/mL. Therefore, the doses of 0.1, 0.3, and 0.5  $\mu$ g/mL of the EtOAc fraction were selected for further experiments. Moreover, cytotoxicity was studied by determining the LDH activity. The LDH activity was remarkably high in the model group as compared to control. There were significant decreases in the LDH activity after increasing the doses of the EtOAc fraction (0.1, 0.3, and 0.5  $\mu$ g/mL) in comparison with the model group (Figure 2(b)).

**3.3. The EtOAc Fraction of *D. moldavica* L. Ethanol Extract Inhibited H<sub>2</sub>O<sub>2</sub>-Induced Oxidative Damage in H9c2.** To determine whether or not the EtOAc fraction can protect H9c2 cells in response to H<sub>2</sub>O<sub>2</sub> injury, we examined H<sub>2</sub>O<sub>2</sub>-induced alterations in ROS production and MDA level in the presence of the EtOAc fraction in H9c2 cells. Our results showed that the EtOAc fraction treatment significantly reduced ROS production (Figure 3(a)). The EtOAc fraction treatment also significantly prevented the H<sub>2</sub>O<sub>2</sub>-induced MDA levels in a dose-dependent manner (Figure 3(b)). We further measured the effects of the EtOAc fraction on the expression of free radical scavenging enzymes as well as the level of total SOD. As shown in Figure 4, the EtOAc fraction treatment significantly increased the expression of CAT and HO-1 compared with the control group. Besides, the EtOAc fraction treatment restored the H<sub>2</sub>O<sub>2</sub>-induced decrease in the total SOD in a dose-dependent manner.

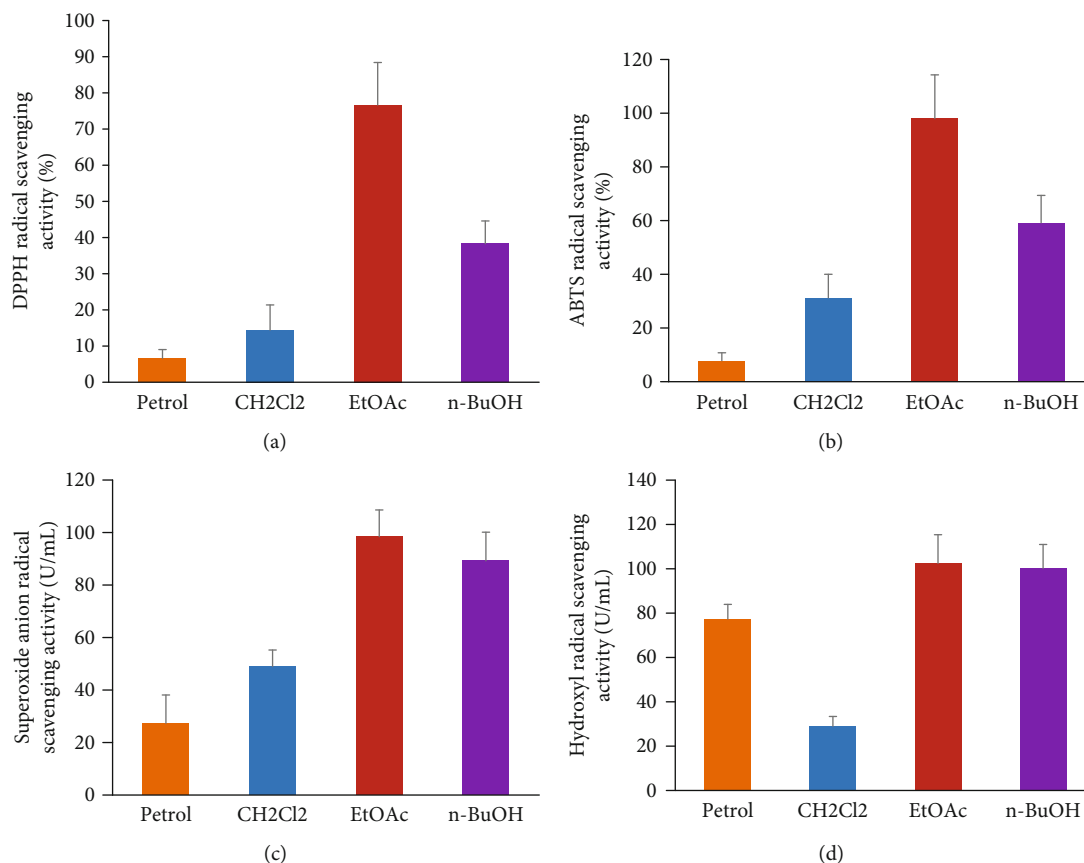


FIGURE 1: Antioxidant activity of the four obtained fractions of *D. moldavica L.* ethanol extract: (a) DPPH, (b) ABTS, (c) superoxide radical, and (d) hydroxyl radical.

TABLE 1: Total phenolic content (TFC) and total flavonoid content (TPC) of different polar fractions of *D. moldavica L.* ethanol extract<sup>a</sup>.

Fractions	Yield (mg/g)	TFC (mg RE/g)	TPC (mg GAE/g)
Petrol	8.51 ± 0.09	7.65 ± 0.26	16.49 ± 0.24
CH <sub>2</sub> Cl <sub>2</sub>	8.62 ± 0.07	19.15 ± 0.24	142.45 ± 1.52
EtOAc	9.33 ± 0.06	65.04 ± 0.57	511.05 ± 1.91
n-BuOH	19.55 ± 0.21	50.13 ± 0.32	294.38 ± 1.54

<sup>a</sup>Values are presented as the mean ± SD.

**3.4. The EtOAc Fraction of *D. moldavica L.* Ethanol Extract Inhibited H<sub>2</sub>O<sub>2</sub>-Induced Mitochondrial Damage in H9c2.** To determine whether or not the EtOAc fraction can protect mitochondria in response to H<sub>2</sub>O<sub>2</sub> injury, we examined H<sub>2</sub>O<sub>2</sub>-induced alterations in mitochondrial membrane potential in the presence of 0.5 μg/mL EtOAc fraction in H9c2 cells using JC-1 dye. We found that the EtOAc fraction prevented the H<sub>2</sub>O<sub>2</sub>-induced impairment in mitochondrial membrane potential in a dose-dependent manner (Figure 5).

**3.5. The EtOAc Fraction of *D. moldavica L.* Ethanol Extract Inhibited H<sub>2</sub>O<sub>2</sub>-Induced H9c2 Apoptosis.** To examine the effects of the EtOAc fraction on H<sub>2</sub>O<sub>2</sub>-induced H9c2 apopto-

sis, the percentage of apoptotic cells was detected by flow cytometry. The apoptotic rate was increased in the H<sub>2</sub>O<sub>2</sub> group, while the EtOAc fraction treatment decreased the apoptotic rate in a dose-dependent manner (Figure 6).

**3.6. The EtOAc Fraction of *D. moldavica L.* Ethanol Extract Regulated the Apoptosis-Related Protein Expression in H9c2.** The effects of the EtOAc fraction on apoptosis-related protein expression were also measured by western blotting. We found that the EtOAc fraction treatment significantly decreased the expression of the proapoptotic proteins caspase-3 and Bax, while it enforced the expression of antiapoptotic protein Bcl-2 in a dose-dependent manner when compared with the model group (Figure 7).

## 4. Discussion

*D. moldavica L.* is one of the most widely used medicinal herbs in traditional Chinese medicine. Previous studies demonstrated that the extracts of *D. moldavica L.* display antioxidant activities [19]. The myocardial protective function of total flavonoid extract from *D. moldavica L.* has also been reported [13, 20]. Recently, our group further demonstrated that *D. moldavica L.* attenuated cerebral ischemia-reperfusion injury in rats by inhibiting inflammation and oxidative stress [21]. To date, however, the exact molecular

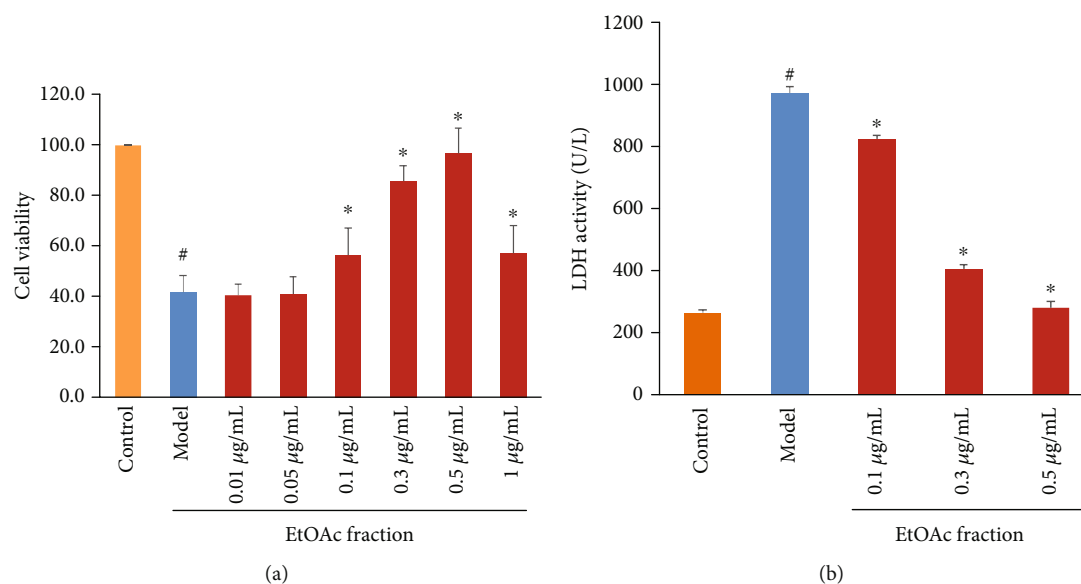


FIGURE 2: Effects of the EtOAc fraction of *D. moldavica L.* ethanol extract on cell viability and LDH activity in  $H_2O_2$ -treated H9c2 cells. (a) Cell viability. (b) LDH activity. Values are presented as the mean  $\pm$  SD. \* $P < 0.05$ , vs. the model group. # $P < 0.05$ , vs. the control group.

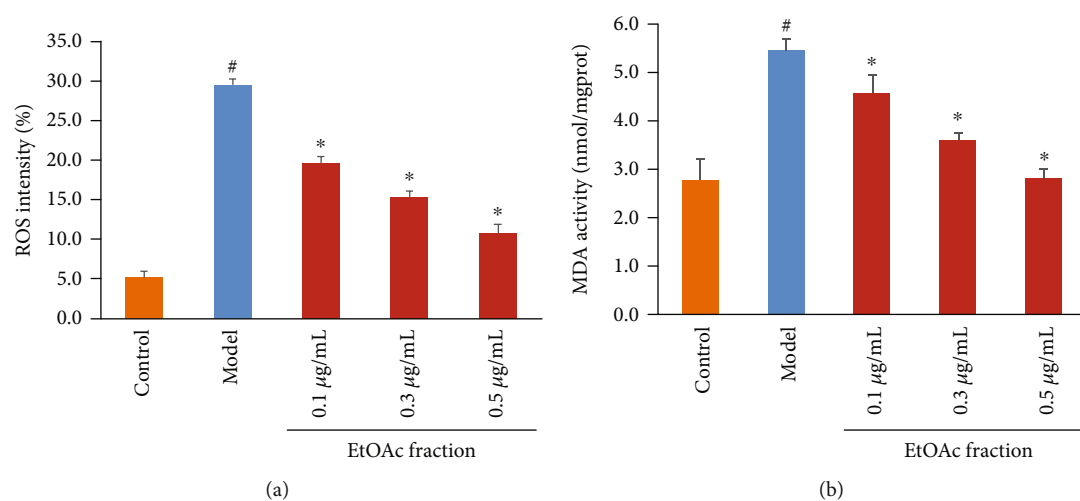


FIGURE 3: Effects of the EtOAc fraction of *D. moldavica L.* ethanol extract on ROS production and MDA level in  $H_2O_2$ -treated H9c2 cells. (a) ROS production. (b) MDA level. Values are presented as the mean  $\pm$  SD. \* $P < 0.05$ , vs. the model group. # $P < 0.05$ , vs. the control group.

mechanisms of action of *D. moldavica L.* on responses to  $H_2O_2$ -induced injury in H9c2 cells have not been clearly defined. In the study, we identified the antioxidant fraction of *D. moldavica L.* ethanol extract and investigated its cardioprotective effects and possible mechanisms.

The preliminary antioxidant activity results showed that the EtOAc fraction of *D. moldavica L.* ethanol extract exhibited the remarkable highest antioxidant activity in the four obtained fractions. Additionally, our results revealed that the EtOAc fraction contained the highest abundance of flavonoids and phenols, which are shown to have strong antioxidant activities [22, 23]. As shown in Figure S1, we further found that tilianin and rosmarinic acid were the main

compounds in the EtOAc fraction of *D. moldavica L.* ethanol extract. The presence of rosmarinic acid in *D. moldavica L.* has antioxidant potential and radical scavenging activity [24]. Tilianin from *D. moldavica L.* was proved to display anti-inflammatory activity [25]. Therefore, the antioxidant properties of the EtOAc fraction can be explained by its phytoconstituents, such as tilianin and rosmarinic acid, which were representative phenolic and flavonoid compounds of *D. moldavica L.* These results confirmed for the first time that the EtOAc fraction mediated the antioxidant properties of *D. moldavica L.*

In this study, we showed that the EtOAc fraction significantly increased the cell viability, reduced LDH release,

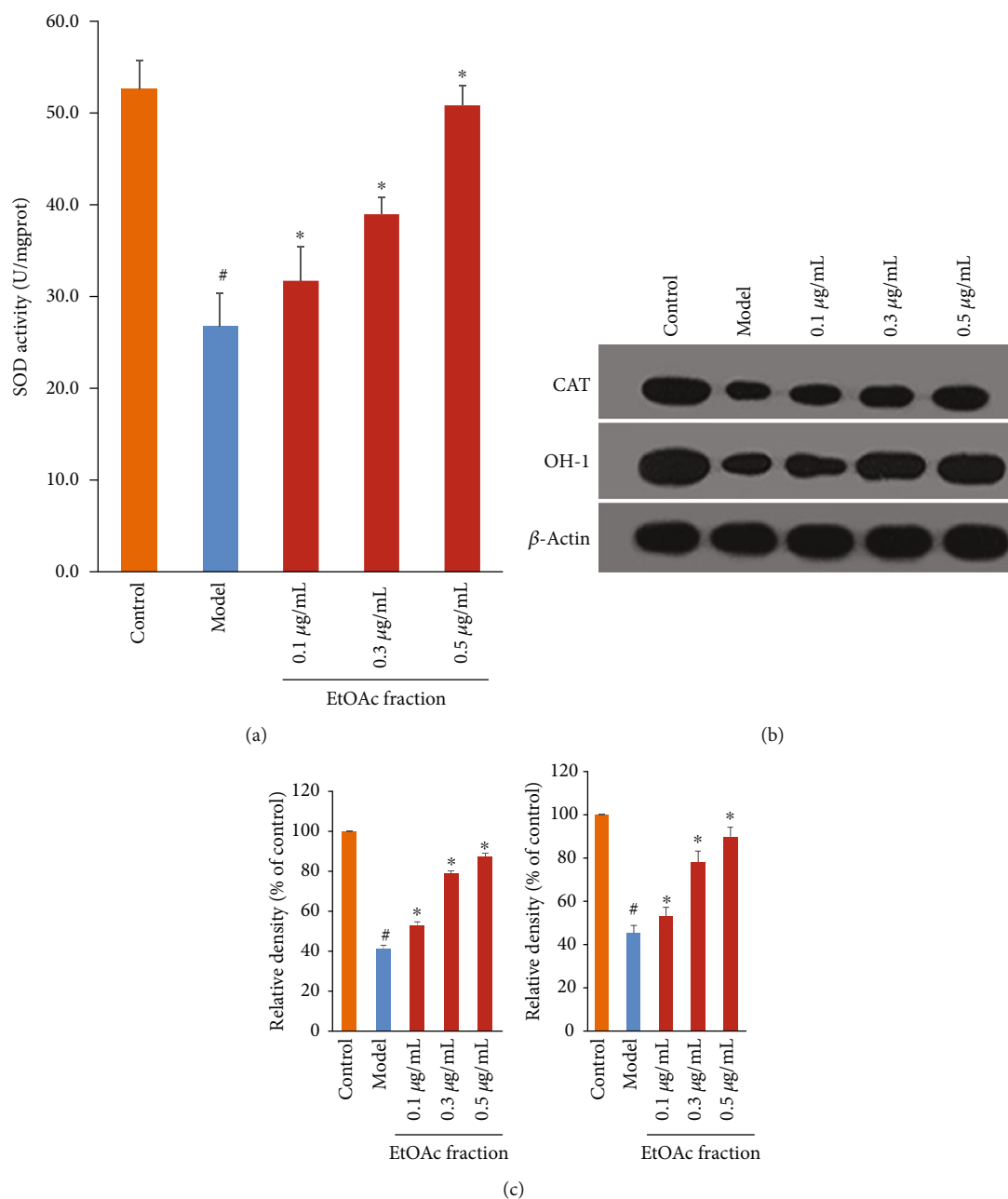


FIGURE 4: Effects of the EtOAc fraction of *D. moldavica L.* ethanol extract on the level of total SOD and the expression of CAT and HO-1 in H<sub>2</sub>O<sub>2</sub>-treated H9c2 cells. (a) The level of total SOD. (b) The expression of CAT and HO-1. (c) Densitometry analysis of CAT (left) and HO-1 (right) levels. Values are presented as the mean  $\pm$  SD. \* $P < 0.05$ , vs. the model group. # $P < 0.05$ , vs. the control group.

inhibited ROS production, and decreased MDA level in H<sub>2</sub>O<sub>2</sub>-treated H9c2 cells. Additionally, the EtOAc fraction enhanced the SOD level and the expression of CAT and HO-1. It is well-known that these critical antioxidant enzymes play a major role in ROS scavenging [26]. As already mentioned, extracts of *D. moldavica L.* could reduce the MDA level and increase the contents of SOD and CAT in diabetic rats [27]. Our results were consistent with previous findings. Overall, the results confirmed that the EtOAc fraction prevents H9c2 cells against H<sub>2</sub>O<sub>2</sub>-induced oxidative stress.

It is reported that oxidative stress-induced excess intracellular ROS can damage the mitochondrial membrane potential and result in cell apoptosis [26]. In the present study, we evaluated the effect of the EtOAc fraction on the mitochondrial membrane potential of H9c2 cells exposed to oxidative stress. We found that the EtOAc fraction maintained the mitochondrial function and inhibited the apoptosis of H9c2 cells in response to oxidative stress. Previous studies also demonstrated that total flavonoid extract from *D. moldavica L.* attenuated ischemia-reperfusion-induced myocardial apoptosis [14], which agreed well with our results.

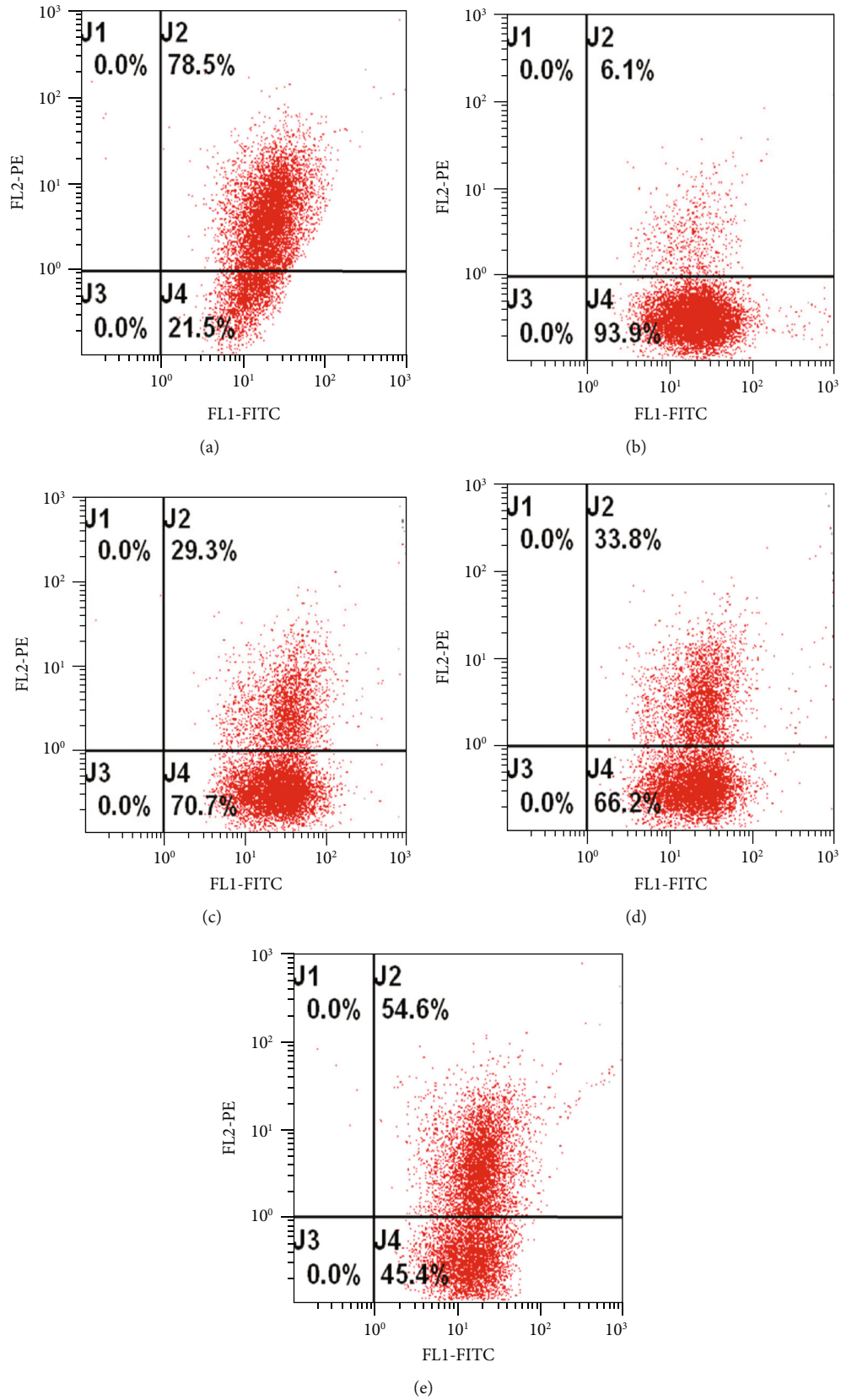


FIGURE 5: Effects of the EtOAc fraction of *D. moldavica L.* ethanol extract on the mitochondrial membrane potential in H<sub>2</sub>O<sub>2</sub>-treated H9c2 cells. (a) Control group. (b) Model group. (c) EtOAc fraction group (0.1 µg/mL). (d) EtOAc fraction group (0.3 µg/mL). (e) EtOAc fraction group (0.5 µg/mL). Values are presented as the mean ± SD. \**P* < 0.05, vs. the model group. #*P* < 0.05, vs. the control group.

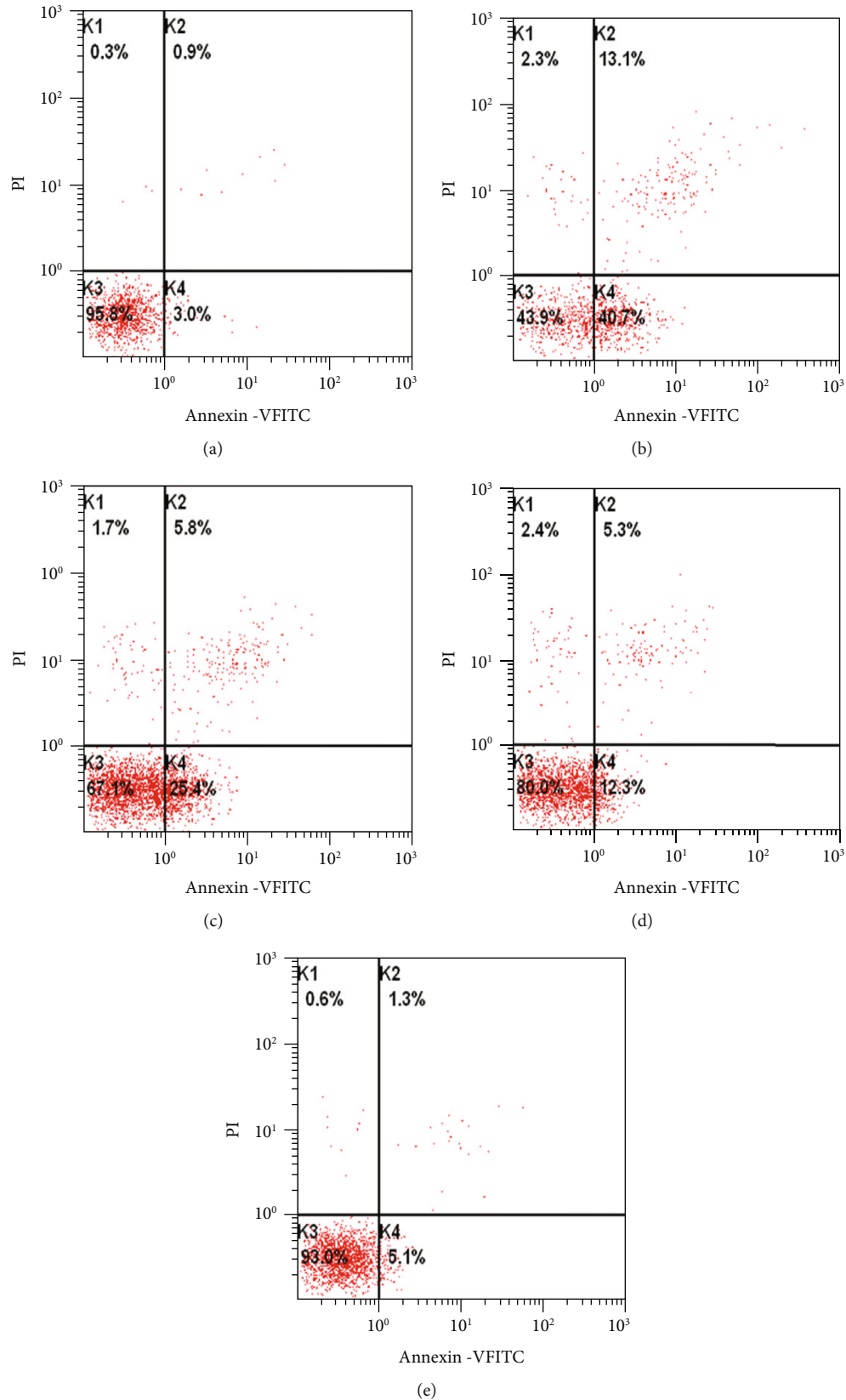


FIGURE 6: Effects of the EtOAc fraction of *D. moldavica L.* ethanol extract on apoptosis in  $\text{H}_2\text{O}_2$ -treated H9c2 cells. (a) Control group. (b) Model group. (c) EtOAc fraction group (0.1  $\mu\text{g/mL}$ ). (d) EtOAc fraction group (0.3  $\mu\text{g/mL}$ ). (e) EtOAc fraction group (0.5  $\mu\text{g/mL}$ ). Values are presented as the mean  $\pm$  SD. \* $P < 0.05$ , vs. the model group. # $P < 0.05$ , vs. the control group.

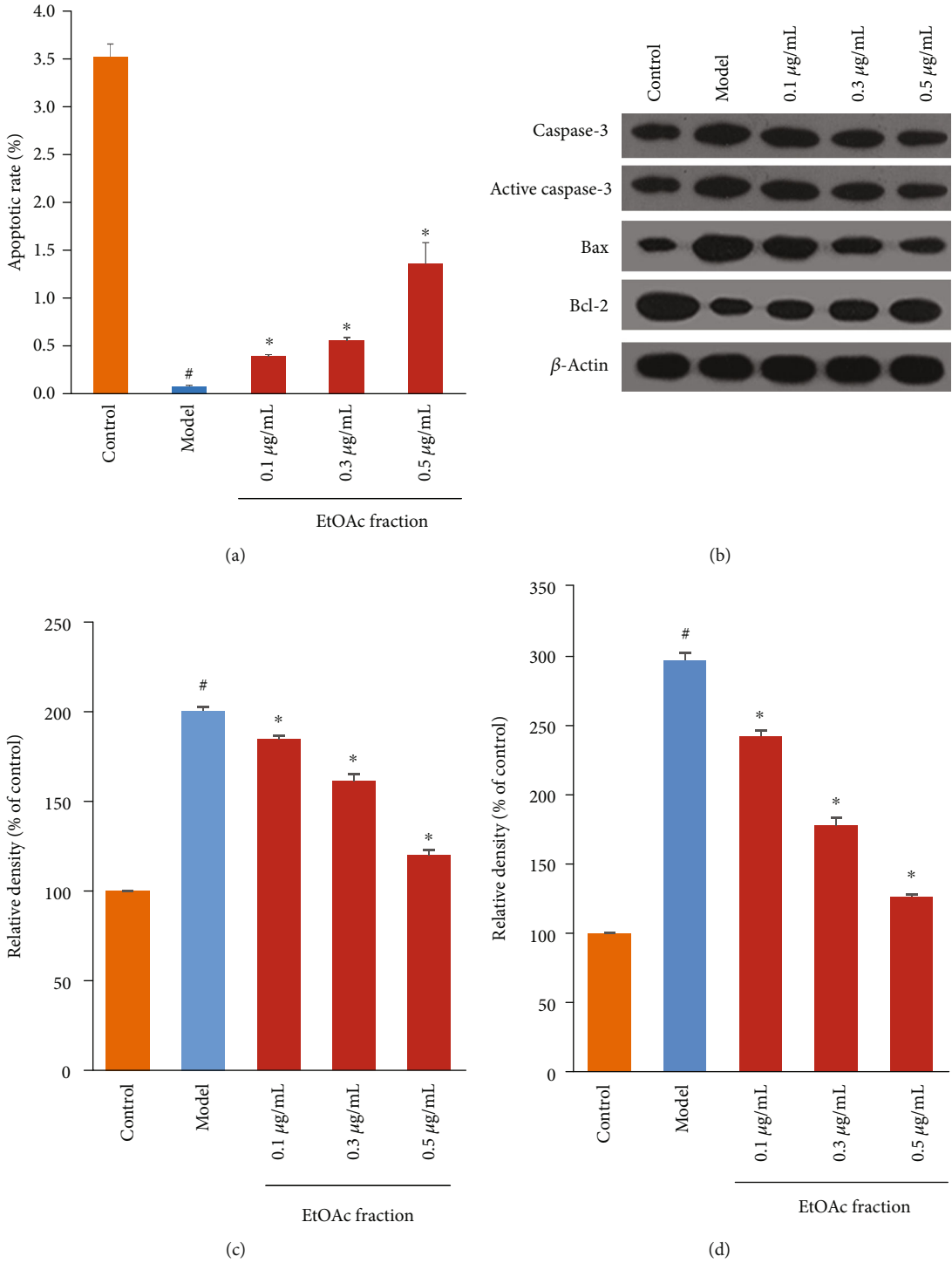


FIGURE 7: Continued.



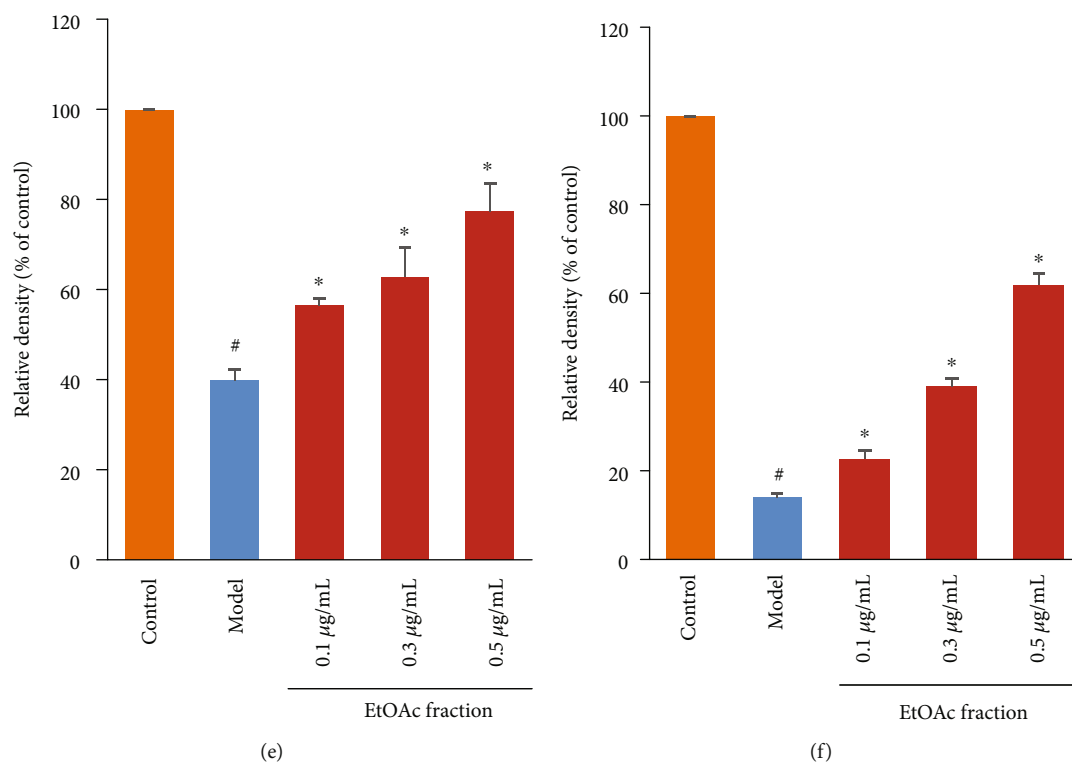


FIGURE 7: Effects of the EtOAc fraction of *D. moldavica L.* ethanol extract on the apoptotic rate and apoptosis-related protein expression in H<sub>2</sub>O<sub>2</sub>-treated H9c2 cells. (a) Effects of the EtOAc fraction of *D. moldavica L.* ethanol extract on the apoptotic rate. (b) Representative western blotting analysis of the protein expression levels of caspase-3, active caspase-3, Bax, and Bcl-2. (c–f) Densitometry analysis of caspase-3, active caspase-3, Bax, and Bcl-2 levels, respectively. Values are presented as the mean  $\pm$  SD. \* $P < 0.05$ , vs. the model group. # $P < 0.05$ , vs. the control group.

To further understand the effect of the EtOAc fraction on apoptosis, we measured the expression of apoptosis-related proteins by western blotting analysis. Our results showed that the EtOAc fraction can increase the expression of the antiapoptotic protein (Bcl-2) and inhibit the expression of proapoptotic proteins (Bax), which play crucial pathophysiological roles in cardiomyocyte apoptosis following H<sub>2</sub>O<sub>2</sub> injury. The result is in agreement with previous studies [28]. This study further revealed that the EtOAc fraction decreased H<sub>2</sub>O<sub>2</sub>-induced caspase-3 activity, which was the most important apoptotic factor [29]. These results suggested that regulation of mitochondrial function and apoptosis partially contributed to the EtOAc fraction-induced cardioprotection against oxidative stress. Further studies might be required to investigate the effect of other pathways on H<sub>2</sub>O<sub>2</sub>-induced myocardial injury.

In conclusion, the present study provided, for the first time, evidence that the EtOAc fraction of *D. moldavica L.* ethanol extract exhibited significant antioxidant activity. Meanwhile, the study revealed that the EtOAc fraction protected H9c2 cardiomyocytes against H<sub>2</sub>O<sub>2</sub>-induced cytotoxicity and oxidative stress. The underlying mechanisms are possibly associated with the preservation of the mitochondrial function and attenuation of cardiomyocyte apoptosis. However, further studies are needed to investigate other pathways involved in the cardioprotective effect of the EtOAc fraction of *D. moldavica L.* ethanol extract. These findings

provide a scientific basis for its ethnomedical use in the treatment of cardiovascular diseases.

### Data Availability

All data generated or analyzed during this study are included in this published article or available from the corresponding author upon reasonable request.

### Disclosure

The funding body had no role in the study design, data collection and analysis, or preparation of the manuscript.

### Conflicts of Interest

The authors declare that they have no competing interests.

### Authors' Contributions

MJ conducted the study, collected the data, performed the analysis of the data, and prepared the manuscript. HY conducted the study and performed the analysis of the data. XJ and LY were responsible for the data collection. JW and ZW designed and supported the study and edited the manuscript. All authors approved the final version of the manuscript.

## Acknowledgments

This research was funded by the National Natural Science Foundation of China (81760056 and 81660048), the Natural Science Foundation of Inner Mongolia Autonomous Region of China (2016MS08106), and the Scientific Research Projects of the Inner Mongolian Higher-Educational System (NJZY19194).

## Supplementary Materials

Figure S1: HPLC-DAD chromatograms of EtOAc fraction of *D. moldavica* L. ethanol extract, visualized at 330 nm. 1, rosmarinic acid; 2, tilianin; 3, luteolin; 4, an unknown compound; 5, apigenin; 6, disometin. (*Supplementary Materials*)

## References

- [1] J. A. Finegold, P. Asaria, and D. P. Francis, "Mortality from ischaemic heart disease by country, region, and age: statistics from World Health Organisation and United Nations," *International Journal of Cardiology*, vol. 168, no. 2, pp. 934–945, 2013.
- [2] D. Zhao, J. Yang, and L. Yang, "Insights for oxidative stress and mTOR signaling in myocardial ischemia/reperfusion injury under diabetes," *Oxidative Medicine and Cellular Longevity*, vol. 2017, Article ID 6437467, 12 pages, 2017.
- [3] A. Rahal, A. Kumar, V. Singh et al., "Oxidative stress, prooxidants, and antioxidants: the interplay," *BioMed Research International*, vol. 2014, Article ID 761264, 19 pages, 2014.
- [4] N. Zhu, C. Cai, A. Zhou, X. Zhao, Y. Xiang, and C. Zeng, "Schisandrin B prevents hind limb from ischemia-reperfusion-induced oxidative stress and inflammation via MAPK/NF- $\kappa$ B pathways in rats," *BioMed Research International*, vol. 2017, Article ID 4237973, 8 pages, 2017.
- [5] L. H. Huang, J. Li, J. P. Gu, M. X. Qu, J. Yu, and Z. Y. Wang, "Butorphanol attenuates myocardial ischemia reperfusion injury through inhibiting mitochondria-mediated apoptosis in mice," *European Review for Medical and Pharmacological Sciences*, vol. 22, no. 6, pp. 1819–1824, 2018.
- [6] H. Tsutsui, S. Kinugawa, and S. Matsushima, "Oxidative stress and heart failure," *American Journal of Physiology. Heart and Circulatory Physiology*, vol. 301, no. 6, pp. H2181–H2190, 2011.
- [7] J. M. Dahanayake, P. K. Perera, P. Galappatty, H. D. S. Melshandi Perera, and L. D. A. M. Arawwawala, "Comparative phytochemical analysis and antioxidant activities of *Tamalakyadi decoction* with its modified dosage forms," *Evidence-Based Complementary and Alternative Medicine*, vol. 2019, Article ID 6037137, 9 pages, 2019.
- [8] M. Guo, Y. Liu, and D. Shi, "Cardiovascular actions and therapeutic potential of Tetramethylpyrazine (active component isolated from *Rhizoma Chuanxiong*): roles and mechanisms," *BioMed Research International*, vol. 2016, Article ID 2430329, 9 pages, 2016.
- [9] I. Pérez-Torres, J. C. Torres-Narváez, V. Guarner-Lans et al., "Myocardial protection from ischemia-reperfusion damage by the antioxidant effect of *Hibiscus sabdariffa Linnaeus* on metabolic syndrome rats," *Oxidative Medicine and Cellular Longevity*, vol. 2019, Article ID 1724194, 13 pages, 2019.
- [10] B. Ibáñez, G. Heusch, M. Ovize, and F. van de Werf, "Evolving therapies for myocardial ischemia/reperfusion injury," *Journal of the American College of Cardiology*, vol. 65, no. 14, pp. 1454–1471, 2015.
- [11] K. Dastmalchi, H. J. Damien Dorman, I. Laakso, and R. Hiltunen, "Chemical composition and antioxidative activity of Moldavian balm (*Dracocephalum moldavica* L.) extracts," *LWT - Food Science and Technology*, vol. 40, no. 9, pp. 1655–1663, 2007.
- [12] A. C. Aprotosoae, C. T. Mihai, G. Vochita et al., "Antigenotoxic and antioxidant activities of a polyphenolic extract from European *Dracocephalum moldavica* L.," *Industrial Crops and Products*, vol. 79, pp. 248–257, 2016.
- [13] J. Jiang, X. Yuan, T. Wang et al., "Antioxidative and cardioprotective effects of total flavonoids extracted from *Dracocephalum moldavica* L. against acute ischemia/reperfusion-induced myocardial injury in isolated rat heart," *Cardiovascular Toxicology*, vol. 14, no. 1, pp. 74–82, 2014.
- [14] C. Zeng, W. Jiang, X. Yang, C. He, W. Wang, and J. Xing, "Pre-treatment with Total Flavonoid Extract from *Dracocephalum Moldavica* L. Attenuates Ischemia Reperfusion-induced Apoptosis," *Scientific Reports*, vol. 8, no. 1, article 17491, 2018.
- [15] Q. Li, Y. Liu, L. Han et al., "Chemical constituents and quality control of two *Dracocephalum* species based on high-performance liquid chromatographic fingerprints coupled with tandem mass spectrometry and chemometrics," *Journal of Separation Science*, vol. 39, no. 21, pp. 4071–4085, 2016.
- [16] P. Matić, M. Sabljčić, and L. Jakobek, "Validation of spectrophotometric methods for the determination of total polyphenol and total flavonoid content," *Journal of AOAC International*, vol. 100, no. 6, pp. 1795–1803, 2017.
- [17] H. Yu, M. Liu, Y. Liu, L. Qin, M. Jin, and Z. Wang, "Antimicrobial activity and mechanism of action of *Dracocephalum moldavica* L. extracts against clinical isolates of *Staphylococcus aureus*," *Frontiers in Microbiology*, vol. 10, article 1249, 2019.
- [18] F. Sersen, F. Gregan, P. Kotora et al., "Synthesis and free radical scavenging activity of new *Hydroxybenzylidene hydrazines*," *Molecules*, vol. 22, no. 6, pp. 894–905, 2017.
- [19] C. Ibarra-Alvarado, A. Rojas, S. Mendoza et al., "Vasoactive and antioxidant activities of plants used in Mexican traditional medicine for the treatment of cardiovascular diseases," *Pharmaceutical Biology*, vol. 48, no. 7, pp. 732–739, 2010.
- [20] M. E. Tan, C. H. He, W. Jiang et al., "Development of solid lipid nanoparticles containing total flavonoid extract from *Dracocephalum moldavica* L. and their therapeutic effect against myocardial ischemia–reperfusion injury in rats," *International Journal of Nanomedicine*, vol. 12, no. 1, pp. 3253–3265, 2017.
- [21] J. X. Jia, Y. Zhang, Z. L. Wang et al., "The inhibitory effects of *Dracocephalum moldavica* L. (DML) on rat cerebral ischemia reperfusion injury," *Journal of Toxicology and Environmental Health. Part A*, vol. 80, no. 22, pp. 1206–1211, 2017.
- [22] A. Shakeri, G. D'Urso, S. F. Taghizadeh et al., "LC-ESI/LTQOrbitrap/MS/MS and GC-MS profiling of *Stachys parviflora* L. and evaluation of its biological activities," *Journal of Pharmaceutical and Biomedical Analysis*, vol. 168, no. 1, pp. 209–216, 2019.
- [23] T. Sunagawa, T. Shimizu, A. Matsumoto et al., "Cardiac Electrophysiological Alterations in Heart/Muscle-Specific Manganese-Superoxide Dismutase-Deficient Mice: Prevention by a Dietary Antioxidant Polyphenol," *BioMed Research International*, vol. 2014, Article ID 704291, 12 pages, 2014.

- [24] A. Wójtowicz, A. Oniszczuk, T. Oniszczuk et al., “Application of *Moldavian dragonhead* (*Dracocephalum moldavica* L.) leaves addition as a functional component of nutritionally valuable corn snacks,” *Journal of Food Science and Technology*, vol. 54, no. 10, pp. 3218–3229, 2017.
- [25] W. Shen, G. Anwaier, Y. Cao et al., “Atheroprotective mechanisms of Tilianin by inhibiting inflammation through down-regulating NF- $\kappa$ B pathway and foam cells formation,” *Frontiers in Physiology*, vol. 10, p. 825, 2019.
- [26] L. Huang, W. Jiang, L. Zhu et al., “ $\gamma$ -Oryzanol suppresses cell apoptosis by inhibiting reactive oxygen species-mediated mitochondrial signaling pathway in H<sub>2</sub>O<sub>2</sub>-stimulated L02 cells,” *Biomedicine & Pharmacotherapy*, vol. 121, article 109554, 2020.
- [27] I. Pouraboli, S. Nazari, N. Sabet, F. Sharififar, and M. Jafari, “Antidiabetic, antioxidant, and antilipid peroxidative activities of *Dracocephalum polychaetum* shoot extract in streptozotocin-induced diabetic rats: *In vivo* and *in vitro* studies,” *Pharmaceutical Biology*, vol. 54, no. 2, pp. 272–278, 2016.
- [28] X. Zhao, M. Dou, Z. Zhang, D. Zhang, and C. Huang, “Protective effect of *Dendrobium officinale* polysaccharides on H<sub>2</sub>O<sub>2</sub>-induced injury in H9c2 cardiomyocytes,” *Biomedicine & Pharmacotherapy*, vol. 94, no. 1, pp. 72–78, 2017.
- [29] H. Koohepeyma, I. Goudarzi, M. Elahdadi Salmani, T. Lashkarbolouki, and M. Shabani, “Folic acid protects rat cerebellum against oxidative damage caused by homocysteine: the expression of Bcl-2, Bax, and Caspase-3 apoptotic genes,” *Neurotoxicity Research*, vol. 37, no. 3, pp. 564–577, 2020.

## Research Article

# Multimodal $\alpha$ -Glucosidase and $\alpha$ -Amylase Inhibition and Antioxidant Effect of the Aqueous and Methanol Extracts from the Trunk Bark of *Ceiba pentandra*

Telesphore Benoit Nguelefack , Christian Kuete Fofie, Elvine Pami Nguelefack-Mbuyo , and Adeline Kaptue Wuyt

Laboratory of Animal Physiology and Phytopharmacology, Department of Animal Biology, Faculty of Science, University of Dschang, P.O. Box 67, Dschang, Cameroon

Correspondence should be addressed to Telesphore Benoit Nguelefack; [nguelefack@yahoo.fr](mailto:nguelefack@yahoo.fr)

Received 9 December 2019; Accepted 27 March 2020; Published 21 April 2020

Guest Editor: Ayodeji F. Ajayi

Copyright © 2020 Telesphore Benoit Nguelefack et al. This is an open access article distributed under the Creative Commons Attribution License, which permits unrestricted use, distribution, and reproduction in any medium, provided the original work is properly cited.

Postprandial hyperglycemia and oxidative stress are important factors that worsen the health condition of patients with type 2 diabetes. We recently showed that extracts from *Ceiba pentandra* mitigate hyperglycemia in dexamethasone- and high diet/streptozotocin-induced diabetes. Herein, we evaluated the postprandial regulatory properties and the antioxidant effects of the aqueous (AE) and methanol (ME) extracts from the stem bark of *Ceiba pentandra*. The phytochemical analysis of AE and ME was performed using the LC-MS technique and the total phenolic and flavonoid assays. Both extracts were tested for their ability to inhibit superoxide anion ( $O_2^{\bullet-}$ ), hydrogen peroxide ( $H_2O_2$ ), protein oxidation, alpha-amylase, and alpha-glucosidase activities. The mode of enzyme inhibition was also determined in a kinetic study. AE and ME were both rich in phenolic and flavonoid compounds. ME was 2.13 and 1.91 times more concentrated than AE in phenolic and flavonoid compounds, respectively. LC-MS allowed the identification of 5 compounds in both extracts. ME and AE inhibited  $O_2^{\bullet-}$  with  $IC_{50}$  of 51.81 and 34.26  $\mu\text{g/ml}$ , respectively. On  $H_2O_2$ , they exhibited  $IC_{50}$  of 44.84 and 1.78  $\mu\text{g/ml}$ , respectively. Finally, they exhibited  $IC_{50}$  of 120.60 and 140.40  $\mu\text{g/ml}$ , respectively, in the inhibition of protein oxidation induced by  $H_2O_2$ , while showing  $IC_{50}$  of 39.26 and 97.95  $\mu\text{g/ml}$  on the protein oxidation induced by AAPH. ME and AE inhibited alpha-amylase with  $IC_{50}$  of 6.15 and 54.52  $\mu\text{g/ml}$ , respectively. These extracts also inhibited alpha-glucosidase, demonstrating  $IC_{50}$  of 76.61 and 86.49  $\mu\text{g/ml}$ . AE exhibited a mixed noncompetitive inhibition on both enzymes, whereas ME exhibited a competitive inhibition on  $\alpha$ -amylase and a pure noncompetitive inhibition on  $\alpha$ -glucosidase. These results demonstrate that ME and AE scavenge reactive oxygen species and prevent their effects on biomolecules. Besides, ME and AE inhibit carbohydrate digestive enzymes. These properties may contribute to reduce postprandial hyperglycemia and regulate glycemia in diabetic patients.

## 1. Introduction

Diabetes mellitus is becoming a serious and leading health threat in low- and middle-income countries. It is one of the largest global health emergencies of the 21st century with increasing prevalence. Approximately 463 million adults aged 20 to 79 years are currently living with diabetes, and by 2045, this will rise to 700 million. Diabetes accounted for 4.2 million deaths worldwide in 2019 [1]. Chronic hyperglycemia is a common feature in all diabetic patients. There-

fore, the main strategy in the management of diabetes is the achievement of an adequate glycemic control. Fasting glycemia is routinely measured as a determinant of glycemic control, but although necessary, it is insufficient. To achieve an effective blood glucose control, postprandial glycemia should also be taken into consideration. In fact, the loss of postprandial glycemic control has been shown to be an early step of glucose homeostasis disorder that occurs earlier than fasting glycemia impairment [2, 3]. Recent evidences have demonstrated that postprandial hyperglycemia is an independent

risk factor for both microvascular and macrovascular complications in both type 1 and type 2 diabetes mellitus [4, 5]. Micro- and macrovascular changes are a preeminent cause of diabetes-related death and disability [6].

Besides, hyperglycemia has been associated with excess free radical production [7] which results in oxidative stress (OS). OS is a key component in diabetic complications acting through various mechanisms including increased flux of the polyol pathway, advanced glycation end product formation and accumulation, overactivation of the hexosamine pathway, and protein kinase C activation [8, 9].

One current approach in the management of postprandial hyperglycemia consists in slowing down the absorption of carbohydrates using inhibitors of digestive enzymes such as acarbose, voglibose, and miglitol. Although these drugs have beneficial effects such as weight loss, they have unpleasant gastrointestinal side effects that frequently result in therapy abandonment [10]. The search for other therapeutic alternatives is therefore encouraged, especially those which can address both postprandial hyperglycemia and oxidative stress.

Plants are important sources of antioxidants. Hydroxytyrosol, for example, a phenolic compound obtained from the olive tree, is currently considered the most powerful antioxidant [11]. Among the groups of secondary metabolites most known for their antioxidant activities, polyphenols and especially flavonoids are of particular interest. Intensive literature has demonstrated their benefits and their structure-related activities [12, 13].

Previous studies performed by our research team showed that *Ceiba pentandra* (L.) Gaertn. stimulates glucose utilization and reduces glucose release by the liver [14], promotes glycogen synthesis and prevents gluconeogenesis [15], exhibits antioxidant activity against DPPH and hydroxyl radical, prevents lipid peroxidation and red blood cell hemolysis [14], and possesses antidiabetic effects on dexamethasone-treated rats [16] and on high-fat diet/streptozotocin-treated rats [17]. Based on these studies, we undertook to quantify the total phenolic and flavonoid contents in the methanol and aqueous extracts of *Ceiba pentandra* trunk bark, to characterize and compare by LC-MS the chemical composition of the aqueous and methanol extracts, to investigate their scavenging activities on other oxidant systems yet unstudied, and to evaluate the effects of these extracts on the carbohydrate digestive enzymes.

## 2. Materials and Methods

**2.1. Extract Preparation.** Fresh barks from the trunk of *Ceiba pentandra* were harvested in Yaoundé (center region of Cameroon) in 2016 by a botanist, Dr. Tsabang Nolé, and authenticated at the Cameroon National Herbarium by comparison with an existing specimen no. HNC 43623. The barks were air dried, and the dry barks were powdered using a grinder. Two hundred grams (200 g) of the obtained powder were boiled for 20 minutes in 2 l distilled water. The filtrate was freeze dried and yielded 8.86 g of aqueous extract that was stored at 2°C until use.

The methanol extract was prepared as follows: 200 grams of powder were macerated in 2 l of methanol for 48 hours. The filtrate was concentrated on a rotary evaporator. After collection, the extract was put in an oven at 40°C for 24 h to remove residual methanol. The resulting 3.9 g of pellets representing the methanol extract was stored at 2°C until use.

**2.2. Chemicals.** Folin-Ciocalteu's reagent, sodium carbonate, aluminum chloride, sodium nitrate, potassium hydroxide, methanol, gentamycin, ethylene diamine tetra-acetic acid, sodium hydroxide, gallic acid, quercetin, sodium hydrogen phosphate, sodium dihydrogen phosphate, trichloroacetic acid, nitroblue tetrazolium, Tris, nicotinamide adenine dinucleotide, phenazine methosulfate, hydrogen peroxide, ascorbic acid, bovine serum albumin (BSA), Coomassie blue, sodium chloride, 2',2'-azobis (2-methylpropionamide) dihydrochloride (AAPH), 5,5'-dithiobis (2-nitrobenzoic acid) acid, potassium cyanide,  $\alpha$ -amylase,  $\alpha$ -glucosidase, dinitrosalicylic acid, starch, p-nitrophenyl glucopyranoside, glucose, and dimethyl sulfoxide were all purchased from Sigma-Aldrich Chemical Co. (Taufkirchen, Germany).

### 2.3. Experimental Protocols

**2.3.1. Determination of Total Phenolic Content.** The amount of total phenols in the extracts was determined spectrophotometrically by the Folin-Ciocalteu reagent method [18]. Optical density was read at 750 nm. The concentration of total phenols in the extracts was determined from the gallic acid standard curve and expressed as milligrams of gallic acid equivalent per 100 g of dry mass extract (mg EAG/100 g). The experiment was done in triplicate.

**2.3.2. Determination of Total Flavonoids (TF).** Colorimetric determination of total flavonoid content in *C. pentandra* extracts was performed using aluminum chloride as described by Chang et al. [19] with quercetin as a standard. Optical density was read at 510 nm. The concentration of total flavonoids in the extracts was determined from the quercetin standard curve and expressed in milligrams of quercetin equivalent per 100 g of dry mass of extract (mg EQ/100 g). The assay was done in triplicate.

**2.3.3. LC-MS Analysis.** The following parameters were used for the LC-MS analysis: spray voltage of 4.5 kV and capillary temperature of 200°C. Nitrogen was used as sheath gas (10 l/min). The spectrometer was attached to an UltiMate 3000 UHPLC System (Thermo Fisher Scientific, USA) consisting of an LC pump, diode array detector (DAD) ( $\lambda$ : 190–600 nm), autosampler (injection volume 10  $\mu$ l), and column oven (40°C). The separations were performed using a Synergi MAX-RP 100A (50  $\times$  2 mm, 2.5  $\mu$ m particle size) with a H<sub>2</sub>O (+0.1% HCOOH) (A)/acetonitrile (+0.1% HCOOH) (B) gradient (flow rate 500  $\mu$ l/min, injection volume 10  $\mu$ l). Samples were analyzed using a gradient program as follows: 95% A isocratic for 1.5 min and linear gradient to 100% B over 6 min, and after 100% B isocratic for 2 min, the system returned to its initial condition (90% A) within 1 min and was equilibrated for 1 min. High-resolution mass spectra were obtained with a QTOF Spectrometer (Bruker,

Germany) equipped with a HESI source. The spectrometer was operated in positive mode (mass range: 100-1500, with a scan rate of 1.00 Hz) with automatic gain control to provide high-accuracy mass measurements within 0.40 ppm deviation using Na formate as calibrant.

**2.3.4. Superoxide Scavenging Test.** The radical scavenging activity of the aqueous and methanol extracts from *C. pentandra* trunk bark was assessed on superoxide anion using a method described by Robak and Gryglewski [20] with some modifications. Superoxide anions were generated in a phenazine methosulfate- (PMS-) NADH system. The reaction mixture was made of 0.5 ml test solution, 0.95 ml 0.1 M phosphate buffer (pH 7.4), 0.5 ml 20 mM PMS, 156 mM NADH, and 25 mM NBT in phosphate buffer (pH 7.4). Extracts were used at concentrations of 1, 3, 10, 30, 100, and 300  $\mu\text{g/ml}$ . Gallic acid was tested at the same concentrations and used as a reference drug. Reduction of nitroblue tetrazolium was monitored at 560 nm on a Helios Epsilon Spectrophotometer (Thermo Fisher Scientific). The test was carried out in triplicate. The percent inhibition was calculated as follows:

$$\% \text{inhibition} = 100 \times \frac{\text{OD control} - \text{OD sample}}{\text{OD control}} \quad (1)$$

**2.3.5. Hydrogen Peroxide Scavenging Activity.** A method previously described by Ruch et al. [21] was used to assess the ability of plant extracts to decompose hydrogen peroxide ( $\text{H}_2\text{O}_2$ ). Briefly, a 40 mM solution of  $\text{H}_2\text{O}_2$  prepared in phosphate buffer (pH 7.4) was mixed with graded concentrations (1-300  $\mu\text{g/ml}$ ) of extracts or ascorbic acid. After 10 min of incubation, optical densities were read at 230 nm against a blank solution made up of phosphate buffer without  $\text{H}_2\text{O}_2$ . The percentage of  $\text{H}_2\text{O}_2$  scavenging activity was calculated as in the previous test.

**2.3.6.  $\text{H}_2\text{O}_2$ - and AAPH-Induced Protein Oxidation Assay.** The effect of plant extracts against protein oxidation was evaluated according to the method of Simplicio et al. [22] with some modifications. Zero point five milliliter aliquots of BSA (30 mg/ml) prepared in phosphate buffer saline (50 mM, pH 7.4) were incubated with 0.5 ml of extracts or gallic acid. Fifteen minutes later, 0.5 ml of  $\text{H}_2\text{O}_2$  (20 mM) or AAPH (2',2'-azobis (2-methylpropionamide) dihydrochloride) solution (50 mM) in another set of experiment, was added to the reaction medium and incubated at 37°C for 30 minutes and 1 hour, respectively. Proteins were precipitated with ammonium sulfate (70%) followed by vigorous shaking and centrifugation at 3000 rpm. The pellet obtained was resuspended in 1.5 ml of PBS, and 0.2 ml of Ellman's reagent was introduced. The level of thiol groups was measured 10 minutes later at 412 nm.

**2.3.7.  $\alpha$ -Amylase Inhibitory Test.** The alpha-amylase inhibitory test was performed using a modified procedure of McCue and Shetty [23]. A volume of 250  $\mu\text{l}$  of extract or acarbose (1-300 mg/ml) was mixed with 250  $\mu\text{l}$  of 0.02 M sodium phosphate buffer (pH 6.9) containing  $\alpha$ -amylase at a concentration of 0.5 mg/ml. The mixture was preincubated at 25°C

for 10 minutes. Then, 250  $\mu\text{l}$  of 1% starch solution in 0.02 M sodium phosphate buffer (pH 6.9) was added and incubated at 25°C for another 10 minutes. The reaction was stopped by adding 500  $\mu\text{l}$  of dinitrosalicylic acid (DNS). The tubes were then incubated in a water bath at 95°C for 5 minutes and cooled at room temperature followed by dilution with 5 ml distilled water. The optical density was measured at 540 nm. The inhibitory activity on alpha-amylase was calculated as percent inhibition using the following formula:

$$\% \text{inhibition} = \left( \frac{\text{OD control} - \text{OD extracts}}{\text{OD control}} \right) \times 100. \quad (2)$$

**2.3.8. Determination of the Inhibitory Mode of Extracts on  $\alpha$ -Amylase.** To determine the mode of inhibition of the plant extracts on the activity of alpha-amylase, the kinetic of action of these extracts was evaluated using three concentrations:  $\text{IC}_{50}/2$ ,  $\text{IC}_{50}$ , and  $\text{IC}_{50} \times 2$ . The method used was a modification of that described by Ali et al. [24]. Extract solution (250  $\mu\text{l}$ ) was preincubated with 250  $\mu\text{l}$  of  $\alpha$ -amylase solution (7.5 U/ml) for 10 minutes at 25°C. Two hundred and fifty microliters (250  $\mu\text{l}$ ) of starch solution at increasing concentrations (3, 6, 9, 12, and 15 mg/ml) were added to start the reaction. The reaction mixture was incubated for 10 minutes at 25°C and then at 95°C for 5 minutes after the addition of 500  $\mu\text{l}$  DNS to stop the reaction. In control tubes, extracts were replaced by phosphate buffer (pH 6.9). Optical densities were read at 540 nm and converted into reaction rates. A double reciprocal graph ( $1/v$  versus  $1/(S)$ ), where  $v$  is the reaction rate and ( $S$ ) the concentration of the substrate, was plotted. The mode of inhibition of the extract on  $\alpha$ -amylase activity was determined using the Lineweaver-Burk curve [25].

**2.3.9.  $\alpha$ -Glucosidase Inhibitory Test.** The ability of *C. pentandra* extracts to inhibit the activity of  $\alpha$ -glucosidase was assessed according to Kim et al.'s [26] protocol. Shortly,  $\alpha$ -glucosidase (1 U/ml) from *Saccharomyces cerevisiae* was preincubated with 250  $\mu\text{l}$  extracts for 10 minutes. P-nitrophenyl glucopyranoside substrate solution (pNPG, 3 mM) prepared in 20 mM phosphate buffer (pH 6.9) containing 2 mg/ml BSA was added to start the reaction. The reaction mixture was incubated at 37°C for 20 minutes and stopped with 1 ml of  $\text{Na}_2\text{CO}_3$  (1 M).  $\alpha$ -Glucosidase activity was determined by measuring paranitrophenol released from pNPG at 405 nm. The percent inhibition was calculated as follows:

$$\% \text{inhibition} = \left( \frac{(\text{OD control} - \text{OD sample})}{\text{OD control}} \right) \times 100. \quad (3)$$

**2.3.10. Determination of the Inhibitory Mode of Extracts on  $\alpha$ -Glucosidase.** Three different concentrations of extracts, namely,  $\text{IC}_{50}/2$ ,  $\text{IC}_{50}$ , and  $\text{IC}_{50} \times 2$ , were used to determine the mode of inhibition of  $\alpha$ -glucosidase by *C. pentandra* extracts. A modified method of Ali et al. [24] in 2006 was used. Indeed, different extract concentrations at 250  $\mu\text{l}$  each were preincubated with 500  $\mu\text{l}$  of  $\alpha$ -glucosidase solution for 10

minutes at 25°C. Then, 250 µl of pNPG substrate at increasing concentrations (1.25, 2.5, 5, 10, and 20 mM) were added to the reaction mixture. This reaction mixture was further incubated for 10 minutes at 25°C, and Na<sub>2</sub>CO<sub>3</sub> was added to stop the reaction. The optical densities were measured and converted to reaction rate. The mode of inhibition was determined using the Lineweaver-Burk curve as previously described.

**3.2.11. Statistical Analyses.** Data are expressed at mean ± standard error of the mean. IC<sub>50</sub> values were obtained after logarithmic transformation of the concentration-response curve using GraphPad Prism Software 5.01. The one-way analysis of variance (ANOVA) followed by the posttest of Tukey was used to analyze the data from total phenol and flavonoid content. The nonlinear regression (curve fit) with the sigmoidal dose-response equation was used to analyze data from all the other tests except for the enzyme kinetics, and the best fit parameters (logIC<sub>50</sub> and top) were compared. Differences were considered significant when the probability threshold *p* was less than 0.05. Where necessary, the efficiency index was calculated using the following formula [14]:

$$\text{Efficiency index} = \frac{E_{\max}}{IC_{50}}. \quad (4)$$

### 3. Results

**3.1. Phenolic and Flavonoid Content in the Extracts.** The results presenting the total phenolic and flavonoid content in *C. pentandra* extracts are shown in Figure 1(a). Regardless of the type of secondary metabolite evaluated, the methanol extract was always richer than the aqueous extract. The phenolic content was 2.13 times significantly (*p* < 0.001) higher in the methanol extract (12.62 ± 0.12 EAG/100 g) than in the aqueous extract (5.88 ± 0.51 EAG/100 g). Similarly, the flavonoid content in the methanol extract (6.99 ± 0.21 EQ/100 g) was 1.91 times significantly (*p* < 0.01) higher than in the aqueous extract (3.66 ± 0.60 EQ/100 g).

**3.2. LS-MS Phytochemical Analysis.** The fingerprint of the LC presented in Figure 1(b) shows common peaks in AE and ME as well as peaks only present in each of the extracts. The combination of data from the literature and information from the MS spectra allows tentative identification of a total of five compounds presented in Figure 1(c). Compounds **1** and **3** were present in both extracts. Compound **2** was only present in AE, while compounds **4** and **5** were visible only in ME. Compound **1** appears at RT 2.3 min with [M + H]<sup>+</sup> at *m/z* 257 and was identified as 8-(formyloxy)-8a-hydroxy-4a-methyldecahydro-2-naphthalene carboxylic acid [27, 28]. Compound **2** (RT 2.6 min) showed [M + H]<sup>+</sup> at *m/z* 185 and was identified as 2,4,6-trimethoxyphenol [29, 30]. Compound **3** appears at RT 3.6 min with [M + H]<sup>+</sup> at *m/z* 345 and was identified as 5,3'-dihydroxy-7,4',5'-trimethoxyisoflavone or vavain [31, 32]. Compound **4** (RT 4.7 min) showed [M + H]<sup>+</sup> at *m/z* 295 and was identified as 17-hydroxlinoleic acid [33, 34]. Compound **5** showed a peak at 5.9 min, [M + H]<sup>+</sup> at *m/z* 413 and was identified as stigmasterol [34].

**3.3. Superoxide Anion Radical Scavenging Activity.** As depicted in Figure 2(a), both the aqueous and the methanol extracts from the trunk bark of *C. pentandra* exhibited a concentration-dependent radical scavenging activity on superoxide anion. A significant difference (*p* < 0.03) was observed between the activities of the tested substances. With respect to the efficiency index (Table 1), gallic acid was the most effective compound followed by the methanol extract and the aqueous extract.

**3.4. Hydrogen Peroxide Radical Scavenging Activity of Ceiba pentandra Extracts.** The results obtained from this test showed that only the ascorbic acid and the methanol extract were capable of scavenging H<sub>2</sub>O<sub>2</sub> (Figure 2(b)). The aqueous extract was a poor H<sub>2</sub>O<sub>2</sub> scavenger with an E<sub>max</sub> of 22.64% produced at a concentration of 10 µg/ml. Considering IC<sub>50</sub> and the efficiency index (E<sub>max</sub>/IC<sub>50</sub>), the best efficiency was attributed to ascorbic acid that was significantly (*p* < 0.005) effective than the methanol and the aqueous extracts (Table 1).

**3.5. Inhibitory Effect of Ceiba pentandra against Hydrogen Peroxide-Induced Protein Oxidation.** The ability of the extracts to prevent the oxidation of proteins induced by hydrogen peroxide is shown in Figure 2(c). It can be seen that, similar to the H<sub>2</sub>O<sub>2</sub> scavenging test, the aqueous extract exhibited almost no antioxidant activity against H<sub>2</sub>O<sub>2</sub>-induced protein oxidation. Although the methanol extract had the same maximum effect as that of gallic acid, the latter was shown to be significantly (*p* < 0.0001) and four times more potent than the methanol extract (Table 1).

**3.6. Inhibitory Effect of Ceiba pentandra against AAPH-Induced Protein Oxidation.** As depicted in Figure 2(d), all tested substances exhibited a concentration-dependent inhibitory effect against peroxy radical- (AAPH-) induced protein oxidation. The best plant extract activity was obtained with the methanol extract, which was found to be more potent (*p* < 0.0001) than gallic acid, used in this experiment as the reference drug (Table 1).

**3.7. Inhibitory Effect of Ceiba pentandra Extracts on the Activity of Alpha-Amylase.** It can be observed from Figure 3 that all tested substances substantially inhibited α-amylase activity in a concentration-dependent manner. At the highest concentrations used, inhibition percentages produced by both extracts were nearly the same as that of acarbose. Maximum inhibitions were 84%, 91%, and 88%, respectively, for acarbose, methanol extract, and aqueous extract. Considering both IC<sub>50</sub> and EI (Table 1), it appears that the methanol extract (EI = 14.93) was approximately 4 times (*p* < 0.001) more active than acarbose (EI = 4.03) and about 9 times (*p* < 0.0001) more active than the aqueous extract (EI = 1.63).

The evaluation of the mode of inhibition shows that the methanol extract exhibited a competitive inhibition (Figure 4(a)), while the aqueous extract exerted a mixed non-competitive inhibition (Figure 4(b)).

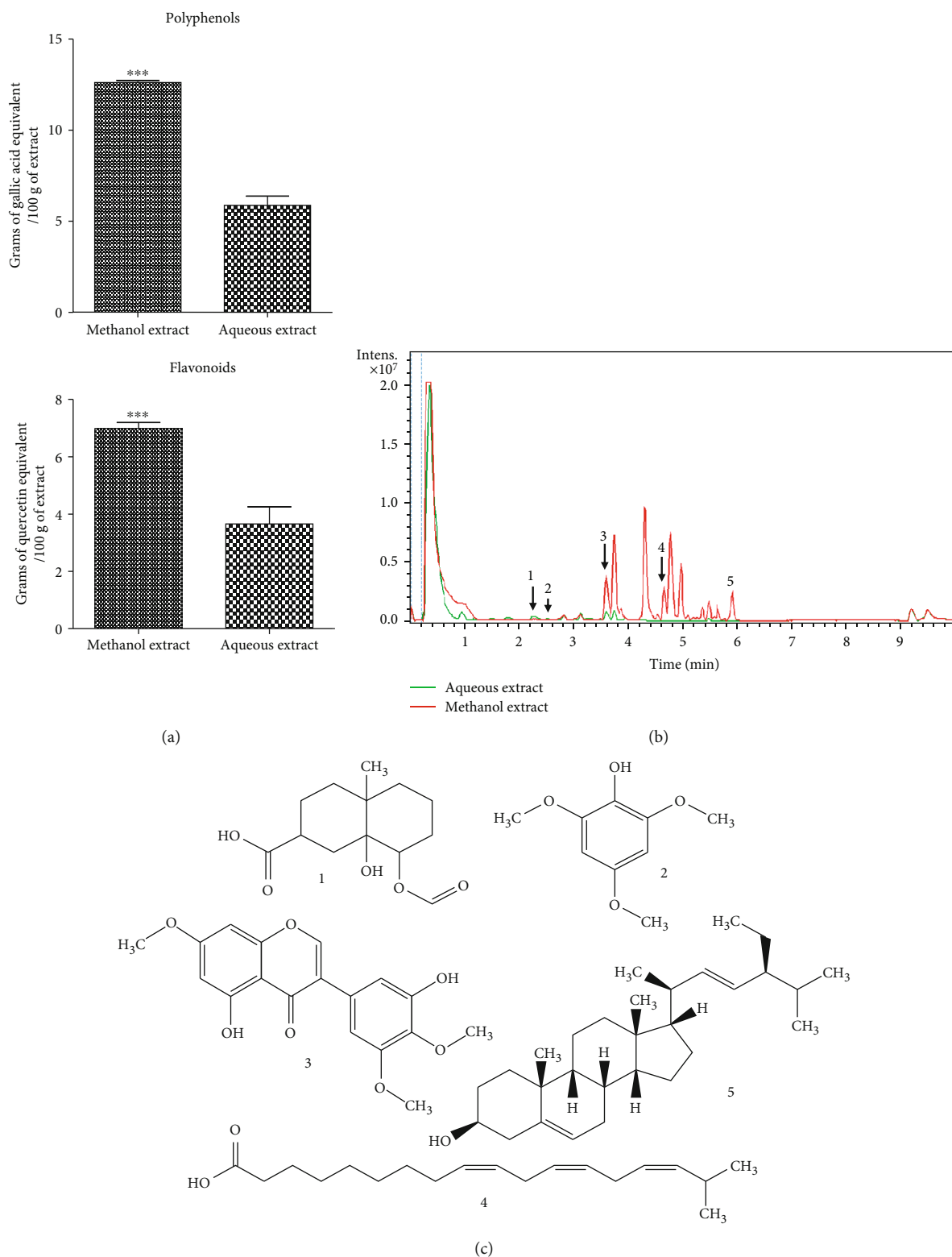
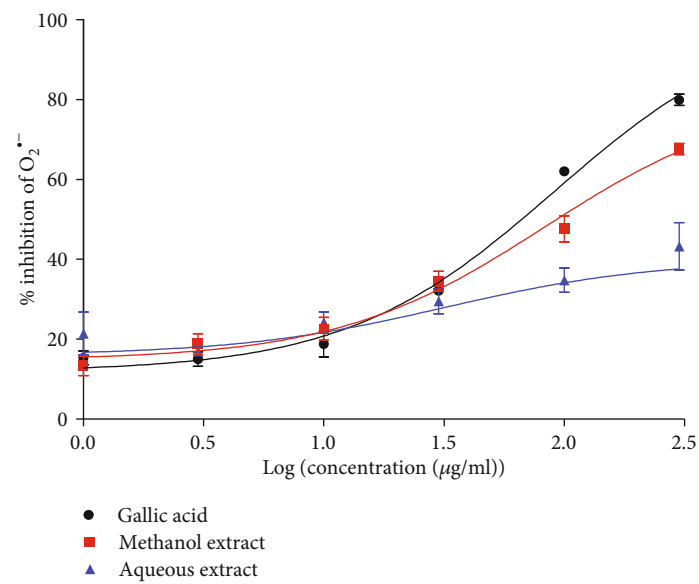
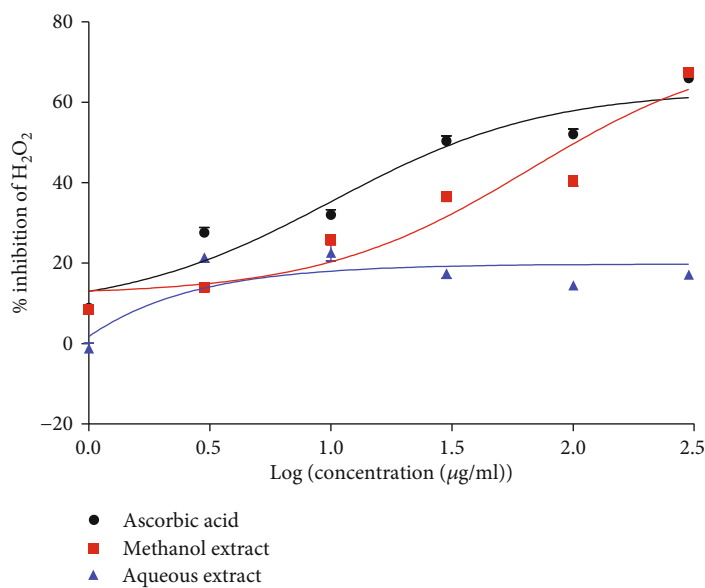


FIGURE 1: Phytochemical analysis of the aqueous and methanol extracts of the stem bark of *Ceiba pentandra*. (a) Polyphenol and flavonoid contents in the aqueous and methanol extracts of *C. pentandra* ( $n = 3$ ). (b) LC fingerprint of extracts detected with UV 190-600 nm. (c) Identified compounds (1-5) are indicated by peak numbers on the fingerprint. **1:** 8-(formyloxy)-8a-hydroxy-4a-methyldecahydro-2-naphthalene carboxylic acid; **2:** 2,4,6-trimethoxyphenol; **3:** 5,3'-dihydroxy-7,4',5'-trimethoxyisoflavone; **4:** 17-hydroxlinoleic acid; **5:** stigmasterol. \*\*\* $p < 0.001$  represents significant difference with respect to the aqueous extract.





(a)



(b)

FIGURE 2: Continued.

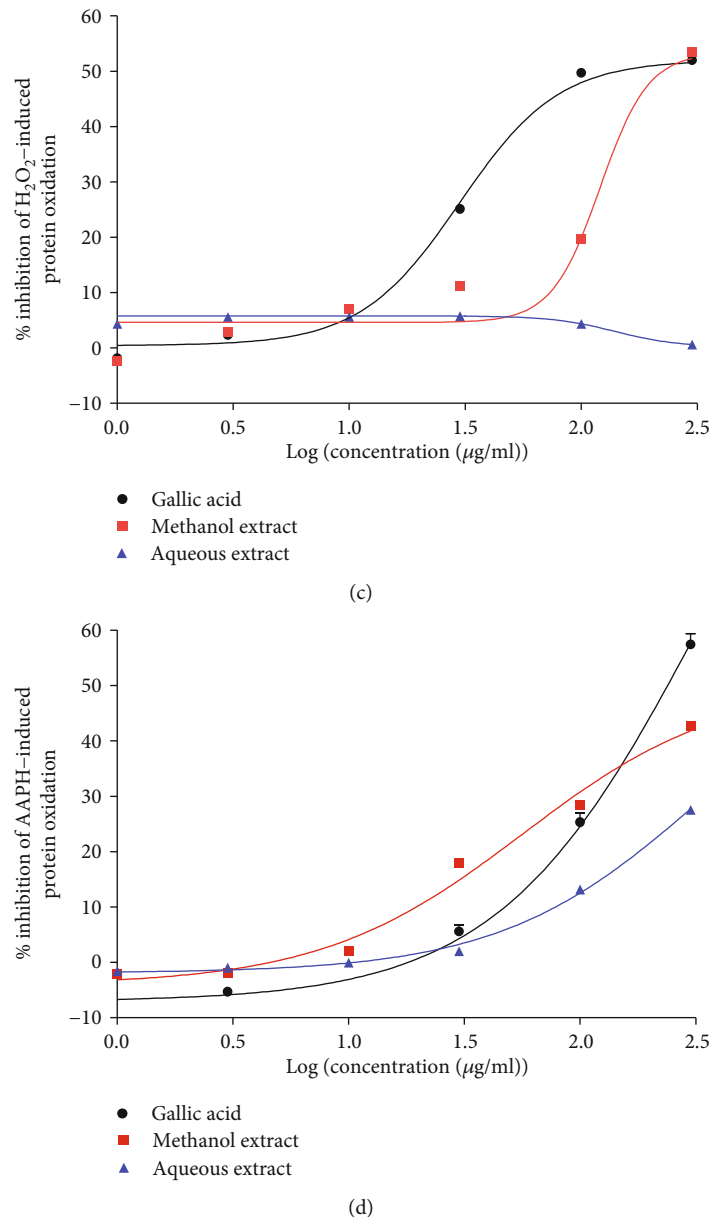


FIGURE 2: *In vitro* antioxidant effects of the aqueous and methanol extracts of the stem bark of *Ceiba pentandra*. (a) Inhibitory effect of extracts on superoxide anion. (b) Inhibitory effect of extracts on hydrogen peroxide. (c) Inhibitory effect of extracts on protein oxidation by hydrogen peroxide. (d) Inhibitory effect of extracts on protein oxidation by AAPH. Each point is the mean ± SEM of 5 repetitions.

3.8. *Inhibitory Effect of Extracts on the Activity of Alpha-Glucosidase.* The methanol extract inhibited alpha-glucosidase more effectively than the aqueous extract with a maximum effect of 87.79% at the highest concentration used (300 μg/ml) versus 63.73% for the aqueous extract (Figure 5). Nevertheless, the inhibitory effect of acarbose was ( $p < 0.0001$ ) 10 times greater than that of the methanol extract and more than 15 times the magnitude of the aqueous extract according to the efficacy index (Table 1).

The evaluation of the inhibition mode showed that the methanol extract has a pure noncompetitive (Figure 6(a)) mode of action, while the aqueous extract exhibited a mixed noncompetitive inhibition (Figure 6(b)).

#### 4. Discussion

Type 2 diabetes is a metabolic disorder culminating in the development of cardiovascular and neurological dysfunctions through the generation of oxidative stress [7]. The present study was designed to get more insight into the antioxidant mechanisms of *C. pentandra* on one hand, and to investigate its ability to prevent postprandial hyperglycemia on the other hand.

Reactive oxygen species (ROS) and mostly superoxide anion are generated from the mitochondrial respiratory chain, and their excessive production may result in oxidative stress. Although superoxide anion is a weak oxidant, it is

TABLE 1: Summary of the antioxidant and carbohydrate digestive enzyme inhibitory effects of *C. pentandra* extracts.

	Antioxidant activities								Carbohydrate digestive enzymes			
	Superoxide anion		Hydrogen peroxide		AAPH protein		H <sub>2</sub> O <sub>2</sub> protein		α-Amylase		α-Glucosidase	
	IC <sub>50</sub>	EI	IC <sub>50</sub>	EI	IC <sub>50</sub>	EI	IC <sub>50</sub>	EI	IC <sub>50</sub>	EI	IC <sub>50</sub>	EI
Methanol extract	51.81	1.3	44.84	1.5	39.26	1.09	120.6	0.44	6.15	14.93	76.61	1.14
Aqueous extract	34.26	1.26	1.78	12.07	97.95	0.28	140.4	0.04	54.52	1.62	86.49	0.78
Gallic acid	55.66	1.43			90.17	0.64	29.9	1.74				
Ascorbic acid			13.84	4.77								
Acarbose									20.97	4.03	8.49	11.76
<i>F</i>	2.77		6.13		33.65		74.23		64.54		270.40	
<i>p</i>	0.0384		0.0058		<0.0001		<0.0001		<0.0001		<0.0001	

IC<sub>50</sub>: concentration of the tested substance able to inhibit 50% of the activity; EI: efficiency index, calculated as maximal activity/IC<sub>50</sub>. The statistical analysis was performed with nonlinear regression and the best fit parameters (log IC<sub>50</sub> and top) were compared.

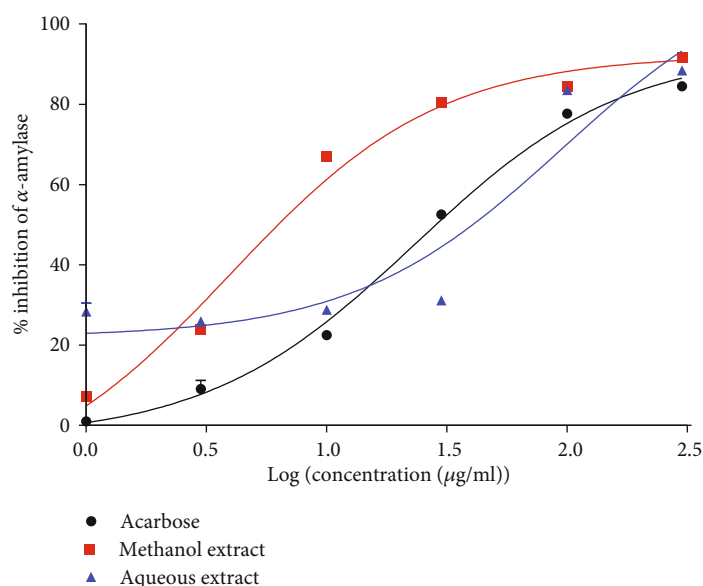


FIGURE 3: Aqueous and methanol extracts of the stem bark of *Ceiba pentandra* concentration-dependently inhibit α-amylase activity. Each point represents the mean + standard error of 5 repetitions.

known as an initial radical and plays an important role in the formation of other ROS, such as hydrogen peroxide [35]. Targeting superoxide appears to be the best way to tackle oxidative stress as this will stop the reaction cascade leading to the formation of other ROS. The present study showed that both extracts and mostly the methanol extract successfully scavenged superoxide anion, suggesting that these plant extracts could be useful tools in the fight against oxidative stress-induced tissue damages.

It is well known that superoxide can spontaneously [36] or enzymatically dismutate into H<sub>2</sub>O<sub>2</sub> [37]. In a recent study, it has been proven that H<sub>2</sub>O<sub>2</sub> mediates pathways leading to hyperglycemia via ERK and p38 MAPK in human pancreatic cancer [38]. The ability of *C. pentandra* to scavenge this molecule was evaluated, and it was observed that only the methanol extract exhibited an antioxidant activity against H<sub>2</sub>O<sub>2</sub>. This difference in activity may be due to the difference in composition of both extracts and further demonstrate that

compound **1** common to the two extracts and more abundant in the aqueous extract is not responsible for this activity.

In order to effectively verify whether these extracts were able to protect cellular components against the direct deleterious effect of hydrogen peroxide on biological molecules such as proteins, the inhibition of the oxidation of albumin was carried out. Consistent with the previous test, the aqueous extract had no effect, and the methanol extract inhibited by 53% the oxidative action of hydrogen peroxide on albumin. This result suggests that in case of oxidative stress, with overproduction of H<sub>2</sub>O<sub>2</sub> like that observed in diabetes or cardiovascular diseases, the methanol extract of *C. pentandra* would be an important asset to limit the degradation of cell molecules.

It was then evident that the aqueous extract was unable to protect proteins against oxidation induced by H<sub>2</sub>O<sub>2</sub> which is generally at the initiation phase; but whether *C. pentandra* extracts could prevent oxidation from free radicals and at

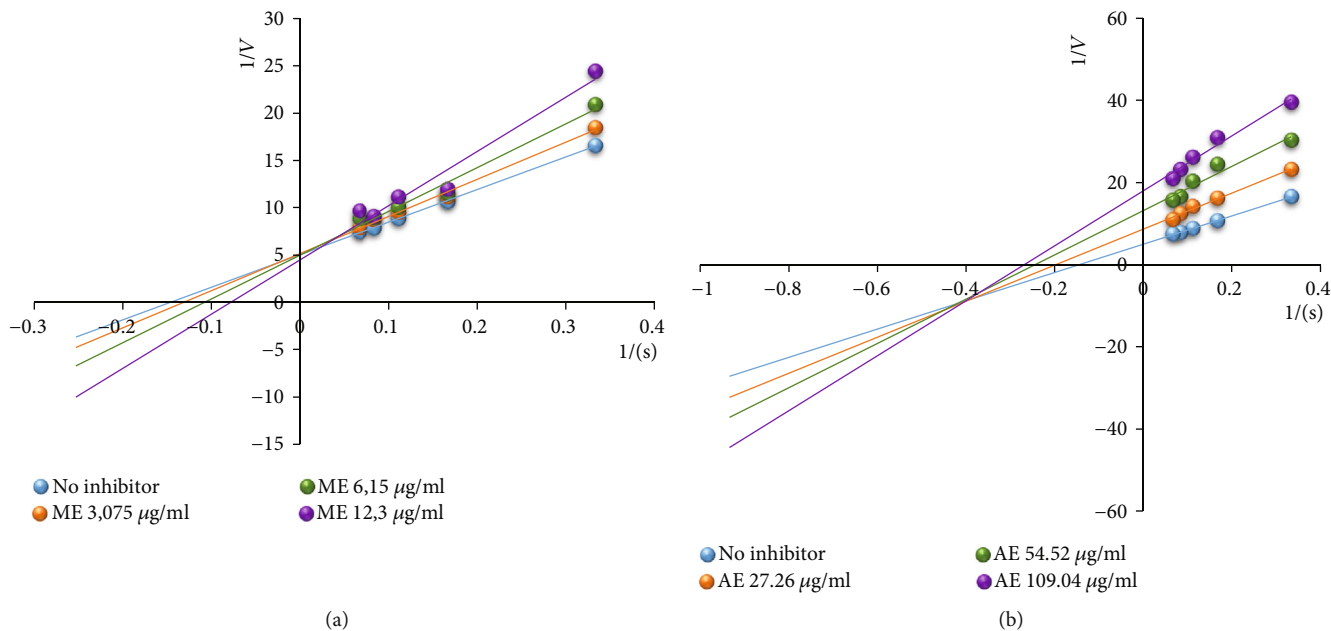


FIGURE 4: Inhibition mode of the methanol (a) and aqueous (b) extracts of *C. pentandra* on  $\alpha$ -amylase. ME: methanol extract; AE: aqueous extract. Each point represents the mean of 5 repetitions.

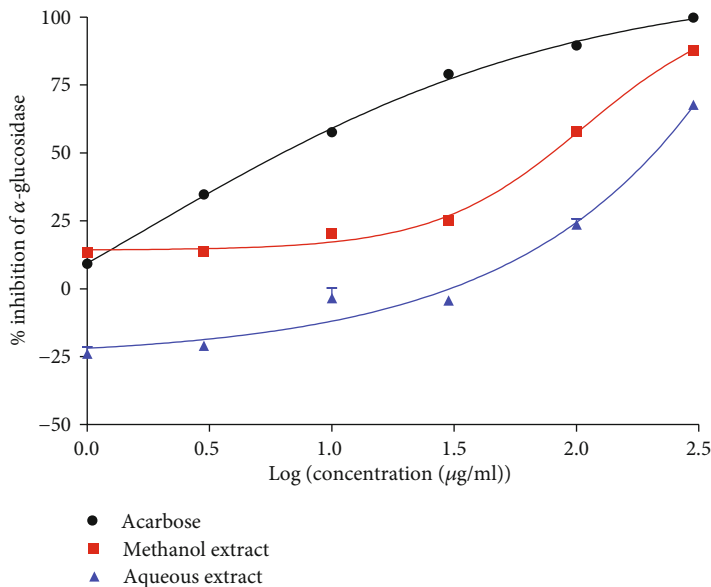


FIGURE 5: Aqueous and methanol extracts of the stem bark of *Ceiba pentandra* concentration-dependently inhibit  $\alpha$ -glucosidase activity. Each point represents the mean + standard error of 5 repetitions.

the propagation phase is still unknown. Peroxyl radicals ( $\text{ROO}^\bullet$ ) are the main oxidants responsible from the propagation phase [39] which is also called the amplification phase. Hence, the ability of the plant extracts to inhibit peroxyl radical-induced protein oxidation was investigated using AAPH. The methanol extract of *Ceiba pentandra* inhibited this oxidation by 42% and the aqueous extract by 27%. Although having a moderate activity, the methanol extract was more effective than gallic acid used as reference. This result shows that the methanol extract is an inhibitor of both initiation and propagation of peroxidation reactions, while

the aqueous extract has a moderate effect only on the propagation phase. Protein oxidation plays an important role in the etiology of diabetes and cardiovascular dysfunctions by modifying the structure and function of essential membrane proteins [40, 41] and enzymes. As a result, treatment with the methanol extract of *C. pentandra* could prevent cell dysfunctions and tissue damage associated with the oxidation of proteins.

All results obtained so far have shown that the extracts from the bark of the trunk of *Ceiba pentandra* have antioxidant properties. These effects may be attributable to the

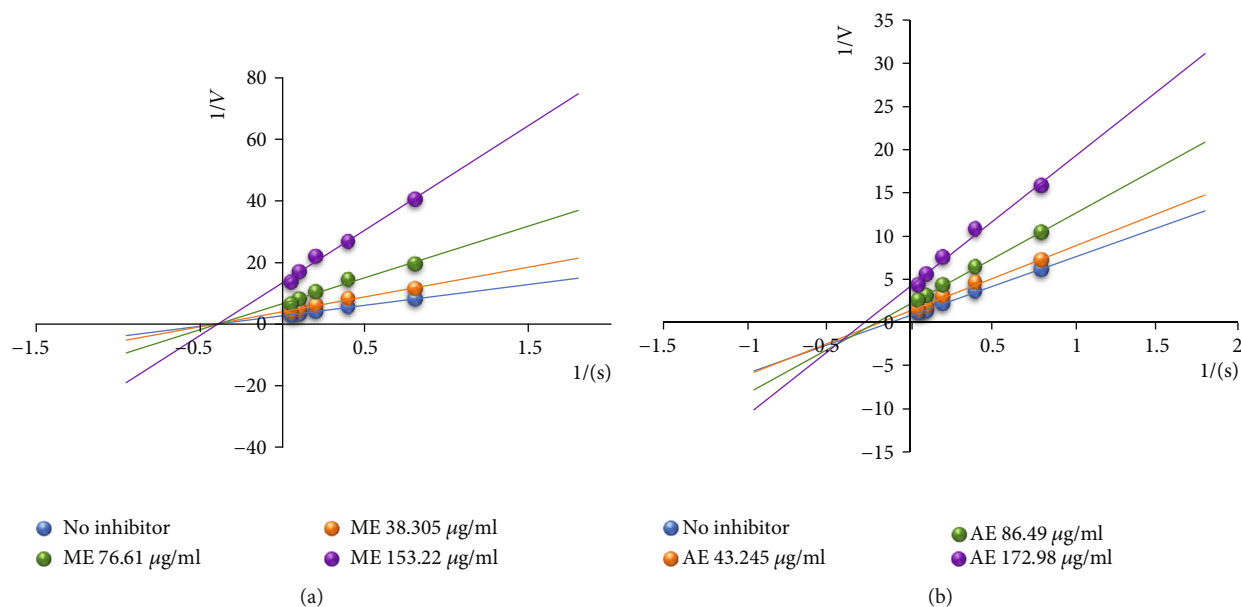


FIGURE 6: Inhibition mode of the methanol (a) and aqueous (b) extracts of *C. pentandra* on  $\alpha$ -glucosidase. ME: methanol extract; AE: aqueous extract. Each point represents the mean of 5 repetitions.

presence of certain secondary metabolites. The reason being that, polyphenols, a heterogeneous group of phenolic compounds (flavonoids, anthocyanins, phenolic acids, etc.) have an ideal chemical structure for trapping free radicals [42]. The evaluation of the polyphenol and flavonoid contents shows that the methanol extract contains nearly twice as much polyphenols and flavonoids than the aqueous extract. Besides, the LC-MS shows the presence of compounds that could enable them to be good antioxidant candidates. Although none of the identified compounds have been shown to possess antioxidant activities, their derivatives are well known antioxidants. Indeed, many isoflavones [43, 44] and trimethoxyphenol [45, 46] derivatives have exhibited antioxidant activities. The presence and the concentration of these substances in both extracts could explain, on one hand, why these extracts both have antioxidant activities, and on the other hand, why the methanol extract has a scavenging activity greater than that of the aqueous extract.

Type 2 diabetes is a progressive disease whose first step is the loss of postprandial glycemic control [47]. The resulting postprandial hyperglycemia is an independent risk factor of cardiovascular diseases and neurological dysfunctions. One of the mechanisms through which postprandial hyperglycemia induces vascular damages is oxidative stress [48]. Thus, postprandial glucose control is important not only for regulating glycemia but also for helping mitigate diabetes exacerbation and complications.

Several studies have shown that polyphenols have hypoglycemic effects at different levels: the protection of pancreatic  $\beta$ -cells against glucotoxicity, inhibition of carbohydrate digestion by inhibition of  $\alpha$ -glucosidases, inhibition of intestinal glucose uptake, inhibition of glucose production by the liver, improvement of glucose uptake in peripheral tissues, and inhibition of AGE formation [49]. Fofié et al. [14] have

shown that extracts from *Ceiba pentandra* prevent glucose production from the liver and enhance glucose consumption. Moreover, AGE formation was shown to be prevented by *C. pentandra* extracts [15]. As these mechanisms were already investigated, we further elucidated the property of these extracts to inhibit  $\alpha$ -glucosidases.

The  $\alpha$ -amylase inhibition test shows that the methanol extract was three times more effective at inhibiting this enzyme than acarbose and about 9 times more effective than the aqueous extract. The evaluation of the inhibition mode shows that the methanol extract has a competitive mode. In this case, the extract and the substrate (starch) have the same binding site on  $\alpha$ -amylase and they compete for this site. The implication of this mode of inhibition is that an excess of polysaccharide in food can significantly reduce its action. Therefore, its dose has to be calibrated depending on the quantity of food to be absorbed. As for the aqueous extract, the inhibition mode was a noncompetitive mixed one. In this case, the inhibitor found in the extract will bind to the enzyme whether or not the enzyme has already bound the starch molecules. However, this effect can be partially overcome by a high substrate concentration. Inhibition of  $\alpha$ -glucosidase shows that the methanol extract has an efficiency 1.5 times greater than that of the aqueous extract. The mode of inhibition of the methanol extract is a pure noncompetitive type meaning that the affinity of the enzyme for the inhibitor is not changed whether bound to the substrate or not. This implies that, no matter the quantity of carbohydrate absorbed, the effect of the inhibitor would not be affected. The inhibition mode of the aqueous extract is a mixed noncompetitive type. Most of the carbohydrates we eat are in the form of poly- and disaccharides. These require prior digestion into monosaccharides in order to be absorbed through the intestinal epithelium. Inhibition of this digestion

is ensured by the extracts therefore making it possible to reduce the influx of glucose and fructose into the hepatic portal vein and thus limiting the amplitude of postprandial hyperglycemic peaks and the risks of diabetes onset and its complications [50]. This inhibition of digestive enzymes by the extracts may be attributable to the presence of isoflavones as many have been shown to possess inhibitory properties on  $\alpha$ -amylase and  $\alpha$ -glucosidase activity [51, 52].

## 5. Conclusion

Results of the present work show that the aqueous and methanol extracts from the bark of *Ceiba pentandra* have scavenging properties which underlie their capacity to prevent the oxidation of biological molecules and thus maintain cell and tissue integrity. This ability is probably related to the presence of the phenolic compounds they contain. In addition, these extracts prevent postprandial hyperglycemia in part by inhibiting the activity of intestinal enzymes involved in the digestion of carbohydrates. These data thus suggest that extracts of *Ceiba pentandra* are excellent therapeutic candidates for the remediation of diabetes and its associated complications.

## Data Availability

The data used and analyzed in this study are available from the corresponding author on reasonable request.

## Conflicts of Interest

The authors declare that there are no competing interests.

## Authors' Contributions

TBN conceived the work. CKF, EPN-M, and AKW collected the data. TBN and CKF analyzed the results. CKF, EPN-M, and TBN drafted the manuscript. All the authors revised the manuscript for its intellectual content and approved the final version.

## Acknowledgments

The authors gratefully appreciate the help of Yaoundé-Bielefeld Bilateral Graduate School Natural Products with Antiparasite and Antibacterial Activities (YaBiNaPA) in phytochemical analysis. Infrastructure was provided by the University of Dschang, Cameroon to which the authors are thankful.

## References

- [1] International Diabetes Federation, *IDF Diabetes Atlas*, International Diabetes Federation, Brussels, 9th edition, 2019, March 2020 <http://www.diabetesatlas.org/resources/2019-atlas.html>.
- [2] J. Gerich, "Pathogenesis and management of postprandial hyperglycemia: role of incretin-based therapies," *International Journal of General Medicine*, vol. 6, pp. 877–895, 2013.
- [3] S. Numao, "A single bout of exercise and postprandial hyperglycemia caused by high-fat diet," *The Journal of Physical Fitness and Sports Medicine*, vol. 5, no. 2, pp. 181–185, 2016.
- [4] A. Ceriello, "Postprandial hyperglycemia and diabetes complications: is it time to treat?," *Diabetes*, vol. 54, no. 1, pp. 1–7, 2005.
- [5] É. B. Rangel, C. O. Rodrigues, and J. R. de Sá, "Micro- and macrovascular complications in diabetes mellitus: preclinical and clinical studies," *Journal Diabetes Research*, vol. 2019, article 2161085, 5 pages, 2019.
- [6] A. Chawla, R. Chawla, and S. Jaggi, "Microvascular and macrovascular complications in diabetes mellitus: distinct or continuum?," *Indian Journal of Endocrinology and Metabolism*, vol. 20, no. 4, pp. 546–551, 2016.
- [7] L. J. Yan, "Pathogenesis of chronic hyperglycemia: from reductive stress to oxidative stress," *Journal Diabetes Research*, vol. 2014, article 137919, 11 pages, 2014.
- [8] M. Brownlee, "Biochemistry and molecular cell biology of diabetic complications," *Nature*, vol. 414, no. 6865, pp. 813–820, 2001.
- [9] Y. Wu, L. Tang, and B. Chen, "Oxidative stress: implications for the development of diabetic retinopathy and antioxidant therapeutic perspectives," *Oxidative Medicine and Cellular Longevity*, vol. 2014, Article ID 752387, 12 pages, 2014.
- [10] K. Sakaguchi and M. Kasuga, "Adverse effects of alpha-glucosidase inhibitors," *Nihon Rinsho*, vol. 65, pp. 183–187, 2007.
- [11] L. Martínez, G. Ros, and G. Nieto, "Hydroxytyrosol: health benefits and use as functional ingredient in meat," *Medicine*, vol. 5, no. 1, p. 13, 2018.
- [12] K. E. Heim, A. R. Tagliaferro, and D. J. Bobilya, "Flavonoid antioxidants: chemistry, metabolism and structure-activity relationships," *The Journal of Nutritional Biochemistry*, vol. 13, no. 10, pp. 572–584, 2002.
- [13] J. B. Xiao and P. Hogger, "Dietary polyphenols and type 2 diabetes: current insights and future perspectives," *Current Medicinal Chemistry*, vol. 22, no. 1, pp. 23–38, 2015.
- [14] C. K. Fofie, S. L. Wansi, E. P. Nguielefack-Mbuyo et al., "In vitro anti-hyperglycemic and antioxidant properties of extracts from the stem bark of *Ceiba pentandra*," *Journal of Complementary and Integrative Medicine*, vol. 11, no. 3, pp. 185–193, 2014.
- [15] K. S. Fofie, K. A. Nguielefack-mbuyo, B. Kamble, N. Chauhan, V. Singh, and T. B. Nguielefack, "Insulin sensitizing effect as possible mechanism of the antidiabetic properties of the methanol and the aqueous extracts from the trunk bark of *Ceiba pentandra*," *Diabetes Updates*, vol. 5, no. 1, 2018.
- [16] C. K. Fofie, E. P. Nguielefack-Mbuyo, N. Tsabang, A. Kamanyi, and T. B. Nguielefack, "Hypoglycemic properties of the aqueous extract from the stem bark of *Ceiba pentandra* in dexamethasone-induced insulin resistant rats," *Evidence-based Complementary and Alternative Medicine*, vol. 2018, Article ID 4234981, 11 pages, 2018.
- [17] C. K. Fofie, S. Katekhaye, S. Borse et al., "Antidiabetic properties of aqueous and methanol extracts from the trunk bark of *Ceiba pentandra* in type 2 diabetic rat," *Cell Biochemistry*, vol. 120, no. 7, pp. 11573–11581, 2019.
- [18] S. McDonald, P. D. Prenzler, M. Antolovich, and K. Robards, "Phenolic content and antioxidant activity of olive extracts," *Food Chemistry*, vol. 73, no. 1, pp. 73–84, 2001.

- [19] C. C. Chang, M. H. Yang, H. M. Wen, and J. C. Chern, "Estimation of total flavonoid content in propolis by two complementary colorimetric methods," *Journal of Food and Drug Analysis*, vol. 10, no. 3, pp. 178–182, 2002.
- [20] J. Robak and R. J. Gryglewski, "Flavonoids are scavengers of superoxide anions," *Biochemical Pharmacology*, vol. 37, no. 5, pp. 837–841, 1988.
- [21] R. J. Ruch, S. J. Cheng, and J. E. Klaunig, "Prevention of cytotoxicity and inhibition of intercellular communication by antioxidant catechins isolated from Chinese green tea," *Carcinogenesis*, vol. 10, no. 6, pp. 1003–1008, 1989.
- [22] P. Di Simplicio, K. H. Cheeseman, and T. F. Slater, "The reactivity of the SH group of bovine serum albumin with free radicals," *Free Radical Research Communications*, vol. 14, no. 4, pp. 253–262, 1991.
- [23] P. P. McCue and K. Shetty, "Inhibitory effects of rosmarinic acid extracts on porcine pancreatic amylase in vitro," *Asia Pacific Journal of Clinical Nutrition*, vol. 13, no. 1, pp. 101–106, 2004.
- [24] H. Ali, P. J. Houghton, and A. Soumyanath, " $\alpha$ -Amylase inhibitory activity of some Malaysian plants used to treat diabetes; with particular reference to *Phyllanthus amarus*," *Journal of Ethnopharmacology*, vol. 107, no. 3, pp. 449–455, 2006.
- [25] A. A. Saboury, "Enzyme inhibition and activation: a general theory," *Journal of the Iranian Chemical Society*, vol. 6, no. 2, pp. 219–229, 2009.
- [26] Y. M. Kim, Y. K. Jeong, M. H. Wang, W. Y. Lee, and H. I. Rhee, "Inhibitory effect of pine extract on  $\alpha$ -glucosidase activity and postprandial hyperglycemia," *Nutrition*, vol. 21, no. 6, pp. 756–761, 2005.
- [27] K. V. Rao, K. Sreeramulu, D. Gunasekar, and D. Ramesh, "Two new sesquiterpene lactones from *Ceiba pentandra*," *Journal of Natural Products*, vol. 56, no. 12, pp. 2041–2045, 1993.
- [28] P. H. Kishore, M. V. B. Reddy, D. Gunasekar, C. Caux, and B. Bodo, "A new naphthoquinone from *Ceiba pentandra*," *Journal of Asian Natural Products Research*, vol. 5, no. 3, pp. 227–230, 2003.
- [29] S. Faizi, S. Zikr-Ur-Rehman, and M. A. Versiani, "Shamiminol: a new aromatic glycoside from the stem bark of *Bombax ceiba*," *Natural Product Communications*, vol. 6, no. 12, pp. 1897–1900, 2011.
- [30] K. R. Joshi, H. P. Devkota, and S. Yahara, "Simalin A and B: two new aromatic compounds from the stem bark of *Bombax ceiba*," *Phytochemistry Letters*, vol. 7, pp. 26–29, 2014.
- [31] M. Ueda-Wakagi, R. Mukai, N. Fuse, Y. Mizushina, and H. Ashida, "3-O-acyl-epicatechins increase glucose uptake activity and GLUT4 translocation through activation of PI3K signaling in skeletal muscle cells," *International Journal of Molecular Sciences*, vol. 16, no. 7, pp. 16288–16299, 2015.
- [32] Y. Noreen, H. el-Seedi, P. Perera, and L. Bohlin, "Two new isoflavones from *Ceiba pentandra* and their effect on cyclooxygenase-catalyzed prostaglandin biosynthesis," *Journal of Natural Products*, vol. 61, no. 1, pp. 8–12, 1998.
- [33] J. Refaat, S. Y. Desoky, M. A. Ramadan, and M. S. Kamel, "Bombacaceae: a phytochemical review," *Pharmaceutical Biology*, vol. 51, no. 1, pp. 100–130, 2013.
- [34] F. Anwar, U. Rashid, S. A. Shahid, and M. Nadeem, "Physicochemical and antioxidant characteristics of kapok (*Ceiba pentandra* Gaertn.) seed oil," *Journal of the American Oil Chemists' Society*, vol. 91, no. 6, pp. 1047–1054, 2014.
- [35] K. Pavithra and S. Vadivukkarasi, "Evaluation of free radical scavenging activity of various extracts of leaves from *Kedrostis foetidissima* (Jacq.) Cogn.," *Food Science and Human Wellness*, vol. 4, no. 1, pp. 42–46, 2015.
- [36] S. B. Nimse and D. Pal, "Free radicals, natural antioxidants, and their reaction mechanisms," *RSC Advances*, vol. 5, no. 35, pp. 27986–28006, 2015.
- [37] Y. Wang, R. Branicky, A. Noè, and S. Hekimi, "Superoxide dismutases: dual roles in controlling ROS damage and regulating ROS signaling," *The Journal of Cell Biology*, vol. 217, no. 6, pp. 1915–1928, 2018.
- [38] W. Li, Z. Wu, Q. Ma et al., "Hyperglycemia regulates TXNIP/TRX/ROS axis via p38 MAPK and ERK pathways in pancreatic cancer," *Current Cancer Drug Targets*, vol. 14, no. 4, pp. 348–356, 2014.
- [39] D. A. Pratt, K. A. Tallman, and N. A. Porter, "Free radical oxidation of polyunsaturated lipids: new mechanistic insights and the development of peroxy radical clocks," *Accounts of Chemical Research*, vol. 44, no. 6, pp. 458–467, 2011.
- [40] D. M. Niedowicz and D. L. Daleke, "The role of oxidative stress in diabetic complications," *Cell Biochemistry and Biophysics*, vol. 43, no. 2, pp. 289–330, 2005.
- [41] K. V. Ramana, S. Srivastava, and S. S. Singhal, "Lipid peroxidation products in human health and disease 2016," *Oxidative Medicine and Cellular Longevity*, vol. 2017, Article ID 2163285, 2 pages, 2017.
- [42] O. Kadiri, "A review on the status of the phenolic compounds and antioxidant capacity of the flour: effects of cereal processing," *International Journal of Food Properties*, vol. 20, pp. S798–S809, 2017.
- [43] C. E. Rüfer and S. E. Kulling, "Antioxidant activity of isoflavones and their major metabolites using different in vitro assays," *Journal of Agricultural and Food Chemistry*, vol. 54, no. 8, pp. 2926–2931, 2006.
- [44] G.-A. Yoon and S. Park, "Antioxidant action of soy isoflavones on oxidative stress and antioxidant enzyme activities in exercised rats," *Nutrition Research and Practice*, vol. 8, no. 6, pp. 618–624, 2014.
- [45] M. A. R. Matos, M. S. Miranda, and V. M. F. Morais, "3,4,5-Trimethoxyphenol: a combined experimental and theoretical thermochemical investigation of its antioxidant capacity," *The Journal of Chemical Thermodynamics*, vol. 40, no. 4, pp. 625–631, 2008.
- [46] S. Falah, T. Katayama, and T. Suzuki, "Chemical constituents from *Gmelina arborea* bark and their antioxidant activity," *Journal of Wood Science*, vol. 54, no. 6, pp. 483–489, 2008.
- [47] L. Monnier, C. Colette, G. J. Dunseath, and D. R. Owens, "The loss of postprandial glycemic control precedes stepwise deterioration of fasting with worsening diabetes," *Diabetes Care*, vol. 30, no. 2, pp. 263–269, 2007.
- [48] A. Ceriello, "Postprandial hyperglycemia and cardiovascular disease: is the HEART2D study the answer?," *Diabetes Care*, vol. 32, no. 3, pp. 521–522, 2009.
- [49] K. Hanhineva, R. Törrönen, I. Bondia-Pons et al., "Impact of dietary polyphenols on carbohydrate metabolism," *International Journal of Molecular Sciences*, vol. 11, no. 4, pp. 1365–1402, 2010.
- [50] S. Kumar, S. Narwal, V. Kumar, and O. Prakash, " $\alpha$ -Glucosidase inhibitors from plants: a natural approach to treat diabetes," *Pharmacognosy Reviews*, vol. 5, no. 9, pp. 19–29, 2011.

- [51] C. Wu, J. Shen, P. He et al., "The  $\alpha$ -glucosidase inhibiting isoflavones isolated from *Belamcanda chinensis* leaf extract," *Records of Natural Products*, vol. 6, no. 2, pp. 110–120, 2012.
- [52] D. H. Kim, W. T. Yang, K. M. Cho, and J. H. Lee, "Comparative analysis of isoflavone aglycones using microwave-assisted acid hydrolysis from soybean organs at different growth times and screening for their digestive enzyme inhibition and antioxidant properties," *Food Chemistry*, vol. 305, 2020.